

Controlling biofilm formation on dental implants: an experimental and computational study of natural compounds in Layer-by-Layer functionalised electrospun membranes

**Daisy Amber Wren Honey** 

A thesis submitted for the degree of Doctor of Philosophy

School of Engineering

October 2023

## Declaration

I certify that this thesis contains my own work, except where acknowledged, and that no part of this material has been previously submitted for a degree or any other qualification at this or any other university.

#### Abstract

Guided Bone Regeneration (GBR) after dental implant placement is at risk of failure should bacterial and biofilm growth occur around wound site. Current barrier membranes can maintain site structure, and incorporation of antibacterial components and antibiotics can provide a surface resistant to bacteria.

This PhD project assessed the utility of natural compounds (Manuka Honey 400, Manuka Honey 550+, Tea Tree Oil, and Lemon Oil) for their efficacy as antimicrobial agents and for their biocompatibility, as an alternative to antibiotics.

Two bacteria commonly associated with implant failure, *Staphylococcus aureus* NCTC 6571 and *Porphyromonas gingivalis* W50, were exposed to selected compounds to evaluate their minimum inhibitory and bactericidal concentrations. Mammalian neo-natal fibroblasts and osteoblasts hFOB1.19 were exposed to the same compounds to evaluate their cytotoxicity.

All the selected compounds inhibited bacterial growth and were cytotoxic for the mammalian cells at different concentrations. Given its better biocompatibility, Manuka Honey (MH) 550+ was selected for further tests.

This project then sought to provide a proof of concept of a physical barrier membrane, nanolayers of 20%w/v Manuka Honey 550+ were functionalised onto poly(ε-caprolactone) electrospun membranes via layer-by-layer assembly using in-house automation. Membranes were imaged, and characterised via scanning electron microscopy, Fourier transform infrared spectroscopy, and release profiles, before analysing cytotoxic and antimicrobial effects. Functionalised membranes showed good bonding up to 14 nanolayers. Inhibition of *S. aureus* and *P. gingivalis* was comparable to bare electrospun membranes, however MH membranes allowed greater proliferation of mammalian cells during initial growth period demonstrating their benefits as a therapeutic barrier membrane.

Finally, an agent-based model was developed to provide qualitative comparisons to *in vitro* results mimicking a top-down view of an agar plate during bacterial growth that agreed qualitatively to the experimental results. The mathematical model shows a framework for simulating an antimicrobial membrane with defined parameters, which can be based on experimental measurements, and can be used in the development of an ideal membrane for the oral cavity during GBR.

Acknowledgements

This body of work would not have been possible without the invaluable support of numerous

individuals and groups to which I would like to extend my thanks. Firstly, to my three

supervisors; Piergiorgio, Nick, and Dana, who have provided unending support and patience

in teaching a Physicist three very distinct fields, I hope that I did your subject proud. I'd like to

also give thanks to Camilla Gallo, Chiara Tonda-Turo, and Irene Carmagnola, who have aided in

preliminary experiments and electrospun membrane fabrication.

To the technicians and teaching staff along the way that have brought a guiding influence in

the many lab spaces I have been involved in. I also extend my gratitude to my colleagues both

inside and outside of these spaces that have been a source of inspiration, reflection, and a well

needed uplift in those trying months.

To my partner, Danielle, for giving me the drive to keep pushing on (and sometimes pushing

me to keep going). To my two year old, Fable, for the many park visits that take my mind off of

the day to day stresses. Both of you are able to give me warmth on the coldest days.

To my friends and family; the length of my thanks would rival that of this thesis, and your

contributions were vital to my success, no matter how small. I'm sorry that I can't put all your

names down here, but you know who you are, and I am grateful.

Finally, I would like to dedicate this piece to all the students who are worried that their non-

traditional background won't get them far in academia. I failed my A levels, and had to resit a

year during my undergraduate, but with a great deal of perspiration (and a little bit of luck), I

have been fortunate enough to find myself submitting my doctoral thesis. Chin up my bonny

bairn as my mam would say.

"Now go and make interesting mistakes."

Neil Gaiman

iii

## **Table of Contents**

CHAPTER 1 INTRODUCTION	1
1.1 Background	1
1.2 Impact and Novelty	3
1.3 Aims & Objectives	3
1.3.1 Project Aims	3
1.3.2 Project Objectives	4
1.4 Thesis Structure	5
CHAPTER 2 LITERATURE REVIEW	7
2.1 Periodontal anatomy and alveolar bone	7
2.2 Dental Implants	8
2.2.1 Bone Defects	9
2.2.2 Osseointegration	10
2.2.3 Bacterial infections	11
2.3 Medical requirements for the design of GBR membranes	15
2.4 Commercially available membranes	16
2.5 GBR Strategies of new membranes under preclinical evaluation	19
2.5.1 Industrialisation Process and Challenges	23
2.6 New approaches for the manufacturing of membranes for GBR	23
2.6.1 Electrospinning	24
2.6.2 Layer-by-Layer assembly nanotechnology	26
2.6.3 Alternative biomaterials for improving antibacterial action	29
2.6.4 Manuka Honey	30
2.6.5 Essential oils	32

2.6.6 Tea Tree Oil	33
2.6.7 Lemon Oil	34
2.6.8 Essential Oil Emulsification	35
2.7 Computational modelling of biofilm growth	37
2.7.1 Agent- and Individual-based modelling	40
2.7.2 Examples of model adaptation	43
2.8 Prospects of Novel GBR Techniques	45
CHAPTER 3 MATERIALS AND METHODS	47
3.1 Introduction	47
3.2 Materials	47
3.3 Electrospun membrane preparation and surface functionaliza	ition at the nanoscale 44
3.3.1 Preparation	49
3.3.2 LbL-assembly functionalisation	49
3.4 Physico-chemical characterisation	50
3.4.1 Dynamic Light Scattering and Zeta-Potential	50
3.4.2 Fourier Transformed Infrared Spectroscopy with attenuate	d total reflection (FTIR-
ATR)	50
3.4.3 X-Ray photoelectron spectroscopy (XPS)	51
3.4.4 Scanning Electron Microscopy	51
3.5.5 Manuka Honey <i>in vitro</i> release	51
3.5 In vitro bacterial tests	52
3.5.1 Bacteria culture	52
3.5.2 Zone of inhibition assays	53
3.5.3 Minimum Inhibitory and Bactericidal Concentration Assays	s of the starting
antibacterial agents	55
3.5.4 Membrane antimicrobial properties	57

3.6 In vitro cellular tests	57
3.6.1 Cell culture	57
3.6.2 Cytocompatibility tests	58
3.6.3 Osteoblast calcification assays	58
3.7 iDynoMiCs 2.0	59
3.7.1 Running a simulation	62
3.7.2 Defining environment	63
3.7.3 Populating environment	63
3.7.4 Growth Kinetics	64
3.7.5 Change orientation for top-down simulation	66
3.7.6 Modelling antibacterial membrane placement	67
3.7.7 Diffusion of antibacterial substance and inhibition of bacterial growth	68
3.7.8 Defining parameters	69
3.7.9 Positive Control 65	
3.7.10 Membrane Placement	72
3.8 Diffusivity	73
3.9 Initial Concentration	73
3.10 Multiple bacterial species	74
3.11 Statistical Analysis	75
CHAPTER 4 EVALUATION OF THE PHYSICO-CHEMICAL AND BIOLOGICAL PROPE	RTIES OF
SELECTED BIOMATERIALS	76
4.1 Introduction	76
4.2 Results	77
4.2.1 Zone of inhibition assays to identify bacterial toxicity against S. aureus	NCTC6571
and P. gingivalis W50	77
4.2.2 Minimum Inhibitory and Bactericidal Concentration assays to identify	bacterial
toxicity against S. gureus NCTC6571 and P. gingivalis W50	81

4.2.3 Cytotoxicity assays to assess toxicity against human neonatal fibroblast an	d
osteoblast (hFOB1.19) cells	87
4.2.4 Osteoblast Calcification	93
4.3 Discussion	100
CHAPTER 5 EVALUATION OF MANUKA HONEY 550+ FUNCTIONALISED ELECTROSPU	IN
MEMBRANES	106
5.1 Introduction	106
5.2 Results	107
5.2.1 Mixing and Potential	107
5.3 Functionalised membrane analysis	108
5.3.1 Fourier-transform infrared spectroscopy	108
5.3.2 XPS analysis	111
5.3.3 Scanning Electron Microscopy	115
5.3.4 Manuka Honey release	117
5.3.5 Antibacterial properties	118
5.3.6 Membrane cytotoxicity	120
5.4 Discussion	124
CHAPTER 6 MATHEMATICAL MODELLING OF BIOFILM GROWTH AND ANTIBACTERIA	
ACTIVITY	128
6.1 Introduction	128
6.2 Aims & Objectives	129
6.2.1 Objectives	129
6.3 Results	130
6.3.1 Assessing the influence of membrane placement on agent growth	131
6.3.2 Considering the influence of diffusivity in comparison to uninhibited grow	th 133
6.3.3 Influence of initial concentration on agent growth	134

6.3.4 Modelling two pacterial species in non-competitive growth in presence of	
inhibiting membrane	135
6.4 Discussion	137
CHAPTER 7 CONCLUSIONS AND RECOMMENDATIONS	142
7.1 General discussion	142
7.2 Recommendations	146
7.2.1 Computational modelling: parameters and developments	147
7.2.2 Membrane functionalisation	148
REFERENCES	137
APPENDIX 1	176

# **Table of Figures**

Figure 2.1: Cross section of tooth socket (alveolus) located across the alveolar bone,
composed of compact (cortical) bone and spongy (trabecular) bone. Figure adapted from
(Ramalingam, Sundar et al. 2020)7
Figure 2.2: Diagram of example tooth fractures. Note far right tooth has full fracture. Image
after (Bethesda (MD) and National Institute of Dental and Craniofacial Research (US) 2021).
Figure 2.3: Keyword search of published work in last 10 years using Scopus. A) Keywords
"GBR" and "polymer" publications by year. B) Citations of results in A) by year. C) Keywords
"GBR" and "ceramic", and separately "GBR" and "metal" publications by year. D) Citations of
results in C) by year. Figure adapted from (Yang, Wu et al. 2022)11
Figure 2.4: Schematic of Gram-negative and Gram-positive bacteria cells. Note different
construction of outer membrane. Image after (Pajerski, Ochonska et al. 2019)13
Figure 2.5: Anatomy of bacteria cell showing DNA and cell wall. Also shown are fimbriae,
responsible for surface adhesion, and flagella, responsible for bacteria motility15
Figure 2.6: Diagram showing how a physical barrier membrane is placed during Guided Bone
Regeneration procedure. Image after (Mount Nittany Health 2017)16
Figure 2.7: Electrospinning schematic showing how a polymer solution is ejected from the
emitter onto a collector. The potential difference applied between emitter and collector
causes the development of a Taylor Cone, which causes polymer droplets to elongate into
strands that whip and deposit across collector surface. Image adapted from (Jamnongkan,
Wattanakornsiri et al. 2012)25
Figure 2.8: Procedure diagrams of the five different categories of layer-by-layer manufacture;
Dip, Spin, Spray, Electromagnetic, and Fluidic Assembly. Image after (Richardson, Björnmalm
et al. 2015)28
Figure 2.9: Chemical structure of methylglyoxal. Image after (Alvarez-Suarez, Gasparrini et al.
2014)31
Figure 2.10: Emulsification of oil using a surfactant. Surfactants are shown by the ball and tail
representing the hydrophilic and hydrophobic ends respectively. These surfactants
encapsulate the oil, allowing for homogeneity in oil-water mixtures36

Figure 2.11: Lifecycle of bacterial culture. Six phases show; 1. Lag, 2. Acceleration, 3.
Exponential, 4. Retardation, 5. Stationary, 6. Decline. Figure adapted from (Monod 1949) 39
Figure 2.12: Graphical pseudo-code of standard time step procedure. Image adapted from
(Kreft, Booth et al. 1998, Valentina Gogulancea, González-Cabaleiro et al. 2019). Here
concentrations present in each grid are diffused into surrounding grid spaces, and variables
within growth equations are updated. If an agent is below minimum size, the cell death
occurs, and if greater than division size, then agents are divided. Both minimum and division
parameters are specified by the user
Figure 2.13: Flow chart of biomass growth and detachment under flow stresses. Figure
adapted from (Picioreanu, Loosdrecht et al. 2000)
Figure 3.1: Petri Dish layout used in Zone of Inhibition assays, showing control and reagent
placement55
Figure 3.2: Well layout for minimum inhibitory concentration assays, showing antibiotic
controls and two negative controls using inoculated and non-inoculated nutrient broth
(untreated culture and untreated broth respectively). Note tested samples were tested in
duplicate
Figure 3.3: Example of iDynoMiCs user interface during protocol run. Note at each timestep
outputs current number of agents
Figure 3.4: Example code that composites two nutrients (A and B) outputting a 2x3 matrix,
both with the same nutrient concentration
Figure 3.5: Example agent shape defined in the protocol. Note TYPE and CLASS called,
including any values that are specified where required64
Figure 3.6: Growth kinetics defined for an agent. Parameters used are for P. gingivalis with
inhibiting factor for Manuka Honey (discussed further in CHAPTER 4) 65
Figure 3.7: Java Class file determining the shift of two agents at division 66
Figure 3.8: 24-hour coccoid agent growth. Left: Typical cross-sectional biofilm growth upon
substrate. Right: Top-down, agar plate style simulation
Figure 3.9: Example code of agentKill Class File that removes agents that fall within Upper
and Lower Ranges. For a 100x100m environment, this agentKill would remove any agents in
the North-West Corner (see Figure 3.10)
Figure 3.10: Graphical representation of model, where yellow shaded area represents
membrane placement, and aligns with protocol file outlined in Figure 3.9. Note that

translucent yellow areas show Manuka Honey dispersal from membrane. Blue dots mark
bacterial agents, and white dots mark extracellular polymeric substance69
Figure 3.11: Designated region division. Each grid cell (1 - 9) denotes single membrane
placement73
Figure 4.1: S. aureus NCTC6571 growth in the presence of Manuka Honey 400 (A), Manuka
Honey 550+ (B), Tea Tree Oil (C), and Lemon Oil (D)78
Figure 4.2: Mean zone of inhibition (mm) of S. aureus NCTC6571, with standard deviation (n
= 3, R=2), measured in prescence of Manuka Honey 400 (A), Manuka Honey 550+ (B), Lemon
Oil (C), and Tea Tree Oil (D)79
Figure 4.3: P. gingivalis W50 growth in the presence of Manuka Honey 400 (A), and Manuka
Honey 550+ (B). Tea Tree Oil and Lemon Oil petri dishes not shown as zone of inhibition was
too large to measure. 1 μL antibiotic control placed on 5 mm filter disc80
Figure 4.4 Mean zone of inhibition (mm) of P. gingivalis W50, with standard deviation (n = 3,
R=2), measured in presence of Manuka Honey 400 (A), and Manuka Honey 550+ (B)80
Figure 4.5: (A) Mean absorbance, and standard deviation (n = 2, R=2), measured in well
plates (595 nm) of S. aureus NCTC6571 inoculated broth solutions, after exposure to dilution
of Manuka Honey 400 (white) and Manuka Honey 550 (black). Untreated S. aureus
NCTC6571 bacteria, uncultured broth, and Vancomycin used as control wells. (B) Second
order polynomial fit of Manuka Honey 400 (Dashed) and Manuka Honey 550 (solid), derived
using Graphpad. ( $R^2_{MH400} < 0.9$ , $R^2_{MH550} < 0.7$ )
Figure 4.6: Mean absorbance, and standard deviation (n = 2, R=2), measured in well plates
(595 nm) of S. aureus NCTC6571 inoculated broth solutions, after exposure to dilutions of Tea
Tree Oil (white) and Lemon Oil (black). Untreated S. aureus NCTC6571 bacteria, uncultured
broth, and Vancomycin used as control wells83
Figure 4.7: (A) Mean absorbance, and standard deviation (n = 2, R=2), measured in well
plates (595 nm) of P. gingivalis W50 inoculated broth solutions, after exposure to dilutions of
Manuka Honey 400 (white) and Manuka Honey 550 (black). Untreated P. gingivalis W50
bacteria, uncultured broth, and Chlorhexidine used as control wells. (B) Exponential Decay fit
of Manuka Honey 400 (Dashed) and Manuka Honey 550 (solid), derived using Graphpad.
$(R^2_{MH400} > 0.9, R^2_{MH550} > 0.95).$ 84
Figure 4.8: (A) Mean absorbance, and standard deviation (n = 2, R=2), measured in well
plates (595 nm) P. gingivalis W50 inoculated broth solutions, after exposure to dilutions of

Tea Tree Oil (white) and Lemon Oil (black). Untreated P. gingivalis W50 bacteria, uncultured
broth, and Chlorhexidine used as control wells. (B) Simple Linear Regression fit of Lemon Oil
data (R <sup>2</sup> > 0.85). Tea Tree Oil data fit not shown
Figure 4.9: Mean and standard deviation (n = 2, R=2) of enumerated Colony Forming
Units/mL of S. aureus NCTC6571, after exposure to diluted compounds. Untreated S. aureus
NCTC6571, and Vancomycin 0.16 $\mu g/mL$ used for control plates
Figure 4.10: Mean of enumerated Colony Forming Units/mL of P. gingivalis W50, after
exposure to diluted compounds (n = 3, R=2). Untreated P. gingivalis W50, and Chlorhexidine
used as control plates. Standard deviation plotted but too small to be seen. Image without
Untreated Culture found in APPENDIX 1
Figure 4.11: Normalised mean Relative Fluorescence Units, with standard deviation (n = 3,
R=2), of human neonatal fibroblast cells after exposure to dilutions of Manuka Honey 400
(white) and Manuka Honey 550 (black) in microplate well. Excitation and emission of 530nm
(bandwidth 25nm) and 590 nm (bandwidth 35nm). Untreated human neonatal fibroblast
cells and uncultured DMEM used as upper and lower ranges
Figure 4.12: Normalised mean Relative Fluorescence Units, with standard deviation (n = 3,
R=2), of human neonatal fibroblast cells after exposure to dilutions of Tea Tree Oil (white)
and Lemon Oil (black) in microplate well. Excitation and emission of 530nm (bandwidth
25nm) and 590 nm (bandwidth 35nm). Untreated human neonatal fibroblast cells and
uncultured DMEM used as upper and lower ranges
Figure 4.13: Live/Dead staining of human neonatal fibroblast cells after 48 hours of
incubation exposed to dilutions of essential oils. Imaging under 100x objective magnification
and filtered (Live: Blue, Compromised Cells: Green). Scale bar shown in lower left of figure.91
Figure 4.14: Normalised mean Relative Fluorescence Units, with standard deviation (n = 3,
R=2), of osteoblast cells (hFOB 1.19) after exposure to dilutions of Manuka Honey 400
(White) and Manuka Honey 550+ (Black) in microplate well. Excitation and emission of
530nm (bandwidth 25nm) and 590 nm (bandwidth 35nm) measured at 3 (A) and 5 days (B).
Untreated osteoblast cells (hFOB 1.19) and uncultured DMEM F-12 used as upper and lower
ranges
Figure 4.15: Normalised mean Relative Fluorescence Units, with standard deviation (n = 3,
R=2), of osteoblast cells (hFOB 1.19) after exposure to dilutions of Tea Tree Oil (White) and
Lemon Oil (Black) in microplate well. Excitation and emission of 530nm (bandwidth 25nm)

and 590 nm (bandwidth 35nm) measured at 3 (A) and 5 days (B). Untreated osteoblast cells
(hFOB 1.19) and uncultured DMEM F-12 used as upper and lower ranges93
Figure 4.16: Macroscopic images of Alizarin Red stained Osteoblast cells exposed to dilutions
of Manuka Honey after 21- and 28-days exposure. Calcium deposits are stained (purple/red)
and become a more intense shade of red with more calcium stained. Layout given in inset
figure. Untreated osteoblast (hFOB1.19) cells used as control wells95
Figure 4.17: Mean and standard deviation (n = 2, R=2) of calcium concentration calculated
following ARS Staining of osteoblasts (hFOB1.19) exposed to dilutions of Manuka Honey 400;
0 (B), 8 (C), 16 (D), and 25 (E) mg/mL. Untreated Osteoblast Cells (hFOB1.19) used as control
wells (A)96
Figure 4.18: Mean and standard deviation (n = 2, R=2) of calcium concentration calculated
following ARS Staining of osteoblasts (hFOB1.19) exposed to dilutions of Manuka Honey 400;
33 (B), 42 (C), and 50 (D) mg/mL. Untreated Osteoblast Cells (hFOB1.19) used as control
wells (A)
Figure 4.19: Mean and standard deviation (n = 2, R=2) of calcium concentration calculated
following ARS Staining of osteoblasts (hFOB1.19) exposed to dilutions of Manuka Honey
550+; 0 (B), 8 (C), 16 (D), and 25 (E) mg/mL. Calcium deposits were dissolved and quantified
by measuring absorbance at 405 nm. Untreated Osteoblast Cells (hFOB1.19) used as control
wells (A)
Figure 4.20: Mean and standard deviation (n = 2, R=2) of calcium concentration calculated
following ARS Staining of osteoblasts (hFOB1.19) exposed to dilutions of Manuka Honey
550+; 33 (B), 42 (C), and 50 (D) mg/mL. Calcium deposits were dissolved and quantified by
measuring absorbance at 405 nm. Untreated Osteoblast Cells (hFOB1.19) used as control
wells (A)99
Figure 5.1: Mean Zeta Potential measure of Manuka Honey 400 dilutions (n= 2, R=2),
adjusted to three distinct pH values108
Figure 5.2: Mean Zeta Potential measure of Manuka Honey 550+ dilutions (n= 2, R=2),
adjusted to three distinct pH values108
Figure 5.3: FTIR-ATR spectrum response from 200 mg/mL Manuka Honey 550 and
Polyallylamine hydrochloride (PAH) coated membranes in 2 (Orange), 7 (Purple), 8 (Green),
13 (Blue) and 14 (Grev) monolayers. Aminolysed PCI membranes used as control

membrane (Red). Key wavelengths are highlighted and described in Table 5.1. Inset figures
show overlapping spectra
Figure 6.1: Mean mass per agent calculated for I) t=0h, II) 6h, III) 24h, IV) 48h. Each cell
denotes where inhibiting component was applied at t=0, see Section 3.7.10 132
Figure 6.2: Inhibitor distribution at time, t=0h (left) and 48h (right) with D= $1\cdot10^{-1}$ mg/mL per
minute. Note minimal change in final concentration distribution
Figure 6.3: Cell density (Agents per unit mL) calculated for P. gingivalis agent growth in the
presence of diffusing inhibiting membrane placed in three distinct regions of the
environment. Growth performed alongside S. aureus agent growth. Control is untreated P.
gingivalis culture
Figure 6.4: Cell density (Agents per unit mL) calculated for S. aureus agent growth in the
presence of diffusing inhibiting membrane placed in three distinct regions of the
environment. Growth performed alongside P. gingivalis agent growth. Control is untreated S.
aureus culture

## **List of Tables**

Table 2.1: Membranes currently and previously on the market. Materials used are noted and
whether they are resorbable or non-resorbable18
Table 2.2: GBR membranes currently in development. Noting defected bone in patient, and
research outcomes from patient trials. Table adapted from (Wang, Feng et al. 2022)20
Table 2.3: Novel membranes currently in development, with details regarding bacteria used,
and how reagent was incorporated into membrane21
Table 3.1: Table of Reagents with negative controls
Table 3.2: Model parameters used, with value and units and, where relevant, appropriate
references71
Table 5.1: Highlighted positions and vibrators of FTIR-ATR spectra shown in Figure 5.3. Table
layout adapted from (Elzein, Nasser-Eddine et al. 2004)

## **Abbreviations**

AMR Antimicrobial Resistance

ARS Alizarin Red S

CFU Colony Forming Units

EO Essential Oil

ePTFE Expanded polytetrafluoroethylene

FBS Foetal bovine serum

GBR Guided Bone Regeneration

LbL Layer-by-Layer

LO Lemon Oil

MGO Methylglyoxal

MH Manuka Honey

MIC Minimum Inhibitory Concentration

P. gingivalis Porphyromonas gingivalis

PAH Polyallylamine hydrochloride

PB PrestoBlue

PBS Phosphate buffer saline solution

PCL Poly(ε-caprolactone)

PLA Polyactic Acid

PLGA Poly Lactic-co-Glycolic Acid

P/S Penicillin-Streptomycin

PTFE Polytetrafluoroethylene

RT Room Temperature

S. aureus Staphylococcus aureus

SEM Scanning Electron Microscope

TTO Tea Tree Oil

XPS X-ray photoelectron spectroscopy

## **CHAPTER 1 INTRODUCTION**

#### 1.1 Background

Dental implant failure leads to additional costs incurred (French, Ofec et al. 2021), as well as the challenge of replacing the failed implant at an already compromised site (Levin 2008). In addition, patients who receive dental implants often have high expectations that near natural teeth aesthetic is restored (Grey, Harcourt et al. 2012). Implant failure, therefore, can have long lasting emotional implications on patients, and can lead to detrimental general oral health. As a result of trauma, infection, or an overexertion of force, dental implant failure can be caused by bone loss through resorption (Baggi, Cappelloni et al. 2008), making future attempts at the same restoration technique difficult or impossible to achieve (Levin 2008, Tsuchida and Nakayama 2023).

In this scenario, guided bone regeneration (GBR) is used to reconstruct missing bone around dental implants that provides a strong foundation for tooth placement, without ingress of soft tissue (Budihardja 2019). During the healing period of up to six months (Cambridge University Hospitals 2021), the site is protected from external infections through the use of physical barrier membranes.

These membranes can be resorbable or non-resorbable, depending on the material used. Examples of non-resorbable membranes include titanium and expanded polytetrafluoroethylene (ePTFE) (Gentile, Chiono et al. 2011, Aprile, Letourneur et al. 2020). These types of membranes offer protection against external particulates and maintain the space required for successful regeneration of cells. However further surgery is required to remove non-resorbable membranes, which could lead to further infection, and have reported patient discomfort and greater overall cost (Gentile, Chiono et al. 2011, Aprile, Letourneur et al. 2020).

As a result, resorbable membranes offer an alternative that provide site protection, and degrades over time, removing the need for secondary surgery. Examples include a number of crosslinked collagens and polymer-based membranes such as poly(lactide-co-glycolide)

(PLGA), and poly(lactide) (PLA) (Lee and Kim 2014, Slutzkey, Kozlovsky et al. 2015), which provide different resorption rates and biocompatibility. As the name suggests, physical barrier membranes offer a physical shield against foreign bodies, including infection-causing bacteria. Dental implant rates of success are high, with most dental implant failures experienced prior to the first year of placement (2 failures occurring in of a total 86 dental implants during the first year of a seven year study) (Rosen, Sahlin et al. 2018). After this, depending on personal oral hygiene and lifestyle, dental implant failure is very low, with one recent study reporting 140 in 4247 patients experiencing dental implant failure over a 22 year period (French, Ofec et al. 2021). Follow up procedures to replace lost dental implants have high success rates; 71% of implant replacements reported successful integration after 10 to 30 months (Levin 2008).

Whilst physical barrier membranes are currently in use, bacterial infection can still occur around membranes and is the most common cause of dental implant failure (Budihardja 2019). The incorporation of antibiotics has been considered (Shahi, Albuquerque et al. 2017, Sharif, Tabassum et al. 2019), however antibiotic use should be considered with caution. Over reliance and misuse of antibiotics has seen a rise in antimicrobial resistance (AMR), where microorganisms develop resistances to previously effective treatments (The Review on Antimicrobial Resistance 2016). AMR resistance related deaths were estimated to be around 700,000 per year in 2014 (The Review on Antimicrobial Resistance 2016), rising to 4.95 million deaths globally in 2019 (Antimicrobial Resistance Collaborators 2022), and is projected to increase exponentially to 10 million by 2050 (World Health Organisation 2014).

Alternatives to antibiotics are therefore of great interest to the greater medical community, with many looking to previously anecdotal therapies for their antimicrobial properties (Lee, Sinno et al. 2011, Wińska, Mączka et al. 2019). Some have reported no development of resistance in microorganisms (Blair, Cokcetin et al. 2009, Cooper, Jenkins et al. 2010), and therefore offer a long-term solution to antibiotic reliance.

Whilst the process of validating therapies for medical use is long, the first step is establishing a proof-of-concept of a new antibacterial.

#### 1.2 Impact and Novelty

It is the intention to present a novel proof-of-concept solution to prevent bacterial formation around dental implants during the healing process. This has utilised a blend of mechanical engineering, microbiology, and computational simulations to provide a multifaceted approach to the challenges facing the field of dentistry.

Firstly, naturally occurring bioactive compounds, such as ginger, silver, or garlic, have capacity to reduce the over reliance on antibiotics by providing alternative antimicrobial benefits. Whilst these bioactive compounds have been studied previously, these were focussed on their effect on bactericidal properties, and further studies are required to quantify the effect of bioactive compounds on mammalian cells that interact with the oral microbiome.

Secondly, the process of bioactive compound membrane manufacture has been covered, however it is unclear the strength of adhesion at high layer numbers and how the bioactive compound may diffuse from the surface.

Thirdly, computational modelling in the current iteration does not accurately mimic the *in vitro* testing of membranes on agar plates. They do not fully encompass the consideration of a diffusive antibacterial agent.

Finally, whilst dental implants are used as a pilot study with the scope of this project, there are broader applications for antibacterial membranes. These applications, such as general wound healing barriers, and implant coatings, are addressed in CHAPTER 7.

## 1.3 Aims & Objectives

#### 1.3.1 Project Aims

This project addresses three broad aims. Firstly, it presents a novel use for selected antibacterial natural compounds as a substitute for antibiotics used in Guided Bone

Regeneration to prevent biofilm growth. These are characterised to identify specific batch variance.

Secondly, it intends to provide a proof of concept of a layer-by-layer (LbL) functionalised electrospun poly( $\epsilon$ -caprolactone) (PCL) membrane that has antibacterial activity, whilst maintaining biocompatibility with mammalian fibroblasts and osteoblasts, to be applied in GBR.

The final aim provides a proof in principle of an agent-based model suitable for providing a framework for hypothesis testing and experimental design. Through the modification of the agent-based modelling software package proposed by the University of Birmingham; iDynoMiCs, a novel method has been developed. This method models an inhibiting membrane, which not only prevents bacterial growth in specified areas, but models an inhibiting reagent releasing into the environment. This utilises a combination of derived parameters from both within and without of the project to establish a top-down model of an agar plate.

## 1.3.2 Project Objectives

To address the three aims mentioned above, a number of project objectives (OBJs) are considered:

OBJ1. Parameterise the inhibiting and cytotoxic potential of Lemon Oil, Tea Tree Oil, and Manuka Honey (400, and 550+) in isolation. These were exposed to bacterial strains of *S. aureus* NCTC 6571 and *P. gingivalis* W50, and mammalian fibroblasts and osteoblasts hFOB 1.19.

OBJ2. Prepare electrospun membranes functionalised with a single bioactive reagent from potential candidates. Analysis of resultant membranes were conducted via Fourier Transformed Infrared (FTIR) Spectroscopy with attenuated total reflectance and Scanning Electron Microscope (SEM) imaging to discern surface composition and fibre morphology.

OBJ3. Antibacterial and cytotoxic potential of functionalised membrane were assessed through exposure to bacterial strains of *S. aureus* NCTC 6571 and *P. gingivalis* W50, and mammalian fibroblasts and osteoblasts hFOB 1.19

OBJ4. A mathematical model framework that mimics an agar diffusion model of an inhibiting membrane has been created. This modifies an established agent-based model; iDynoMiCs, and has been tested against a number of hypotheses that will inform future design of an ideal membrane.

#### 1.4 Thesis Structure

The thesis will be split into chapters detailing the theoretical and experimental approach to providing a proof-of-concept antibacterial barrier membrane.

CHAPTER 1: An introduction to the project, briefly outlining the motivation behind the project. The reader is also provided with a summary of the project aims and objectives.

CHAPTER 2: Outline to provide the reader with the current understanding and cutting-edge research relevant to the project. This will include summaries on:

- dental Implants and how they are installed,
- the risks of bacterial infection and the current on market and in development products that are used to prevent infection,
- how biofilm models have been historically used to simulate bacterial growth and the current trends of computational augmentations,
- the current research trends surrounding specific bioactive compounds relevant to this project and their effectiveness as an antibacterial.

CHAPTER 3: Details of the materials and methodology used to parameterise and analyse bioactive compounds, their functionalisation on electrospun membranes, and their how bioactive compounds are incorporated *in silico*.

CHAPTER 4: Results that parameterise the selected bioactive compounds for their efficacy as an antibacterial and as a cytotoxin.

CHAPTER 5: Functionalise a single bioactive compound onto an electrospun membrane, identifying the morphology of a functionalised membrane such as how these have bonded to the surface and how the bioactive compound will diffuse from the membrane in vitro.

CHAPTER 6: Study on how the selected model was manipulated to tailor it for purpose. Subsequently protocols will be outlined and performed to assessed both from published works but also in qualitative comparison to the results shown in CHAPTER 4 and CHAPTER 5.

CHAPTER 7: Summary of the findings of this PhD, along with impact of research outcomes. This will also detail considerations and recommendations for future work.

## **CHAPTER 2 LITERATURE REVIEW**

#### 2.1 Periodontal anatomy and alveolar bone

The alveolar bone is the thick ridge of bone that supports teeth placement during function. A cross sectional diagram is shown in Figure 2.1. Here, the outer bone is compact (cortical bone) and is around 1.5-3 mm thick, whilst the inner bone is spongy or cancellous (trabecular bone). The roots of the bone are placed in sockets along the ridge (alveolus) and support the tooth in placement and during mechanical function (Precision Periodontics 2022, Tsuchida and Nakayama 2023). In response to the different tooth functions (incisor, canine, premolar, and molar), the cortical bone may be thicker or thinner to support the different mechanical pressures required.

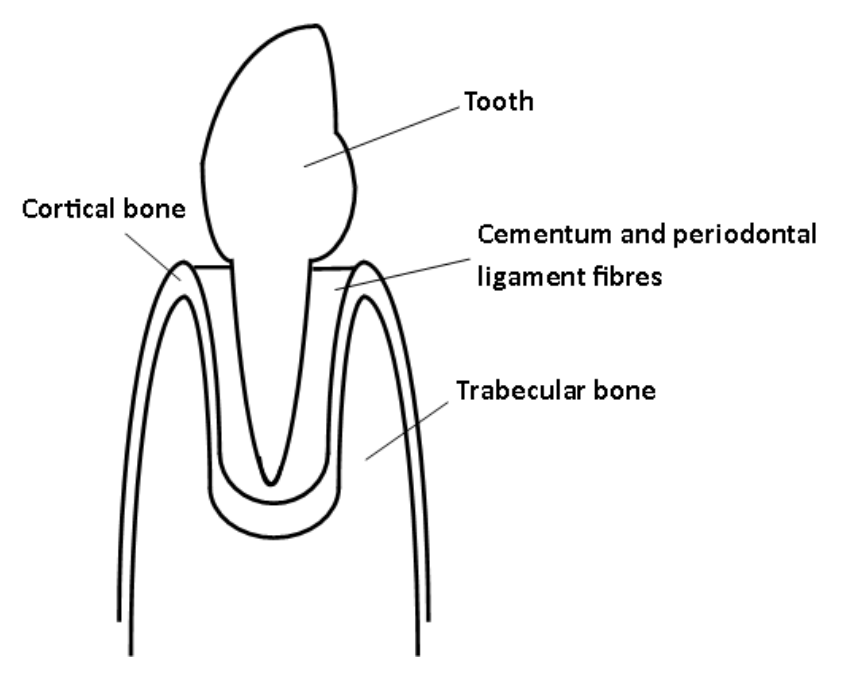


Figure 2.1: Cross section of tooth socket (alveolus) located across the alveolar bone, composed of compact (cortical) bone and spongy (trabecular) bone. Figure adapted from (Ramalingam, Sundar et al. 2020)

Maintaining good oral hygiene is important for longevity of this complex structure, however due to several external factors, tooth loss can occur. Tooth loss can have detrimental impact on patients' self-esteem, and the ability to replace teeth restores a feeling of 'normality' (Grey,

Harcourt et al. 2012, Royal College of Surgeons: Faculty of Dental Surgery and Restorative Dentistry-UK 2019). Approaches are available that are selected based on the quality of remaining tooth and bone and number of replacement teeth required. Tooth replacement or dental bridges can be used when single tooth replacement is required and, as more teeth require replacement, further options such as partial or complete dentures can be used. In the case of single tooth replacement, some procedures utilise dental implants. This procedure can also be also used for dentures where the user desires a fixed final prosthetic (Royal College of Surgeons: Faculty of Dental Surgery and Restorative Dentistry-UK 2019).

### 2.2 Dental Implants

Whilst initially expensive, dental implants offer long- and short-term health benefits that are considered a more cost-effective method of tooth replacement, costing around 81% in total when compared to fixed partial dentures (Brägger, Krenander et al. 2005, Royal College of Surgeons: Faculty of Dental Surgery and Restorative Dentistry-UK 2019). Titanium screws are placed into the jaw bone of the selected site to accept and support a manufactured false tooth/teeth (Royal College of Surgeons: Faculty of Dental Surgery and Restorative Dentistry-UK 2019, Cambridge University Hospitals 2021).

On average, the healing period for the GBR procedure is between three and six months (Cambridge University Hospitals 2021). Following this, implants are ready to accept push fit prothesis, which have designs informed by steady evolution in technology and dentistry (Gaviria, Salcido et al. 2014). One year after implant placement, implants should be stable for at least 10 years, and cumulative success rates are high at 92–98% (Royal College of Surgeons: Faculty of Dental Surgery and Restorative Dentistry-UK 2019). In periods up to 22 years, rate of dental implant failure (for example, due to infection of breakages) does not increase beyond 8%, where 140 in 4247 patients reported dental implant failure, with multiple dental implants increasing likelihood of failure (French, Ofec et al. 2021).

Over the years, design principles have been informed by research. For example, compressive stresses on the artificial tooth are of significant concern when reducing the risk of mechanical fracture. Stresses at the site occurred in a high volume localised below the connector point of

the implant in the gum, with improved stress distribution increasing with implant length and diameter (Baggi, Cappelloni et al. 2008).

Improved implant-tissue interface and bacterial resistance can be gained by altering coatings and geometry (Gaviria, Salcido et al. 2014), however if not protected, bacteria can still accumulate in and around the peri-implant tissue (soft tissue, and bone that surrounds the implant), which places dental implants at risk (Mombelli and Décaillet 2011).

During maxillofacial surgery, a loss of bone can occur during excision of previous tooth and root to make site suitable for dental implant placement. Due to this, the surrounding bone is required to regenerate, a process which has aided surgical and non-surgical treatment for bone loss within and without dentistry.

#### 2.2.1 Bone Defects

The causes of bone defects (the absence of bone) range from small fractures to larger lesions caused by, for example, trauma, disease, or sepsis, the larger of which generally requiring surgical interventions (Iglesias-Urraca 2014, Vidal, Layrolle et al. 2020). A few examples of fractures and bone loss in teeth are shown in Figure 2.2.

Bone regenerates via a complex set of processes. After defect occurs, the blood vessels around the site commence clotting and inflammation, creating a scaffold for new bone formation. Following this, a series of bone remodelling is performed by osteoblasts; responsible for new bone production through calcium deposits, and osteoclasts; responsible for bone resorption. This causes gradual calcification of scaffolds which, dependent upon fracture size, lead to recovery of full structure and mechanical strength (Sela and Bab 2012, Bigham-Sadegh and Oryan 2015). In cases where defects are too large for bone regeneration to occur, external composites are required to assist healing. This critical defect size varies, but is defined when the length of the defect is twice the diameter of the bone (Sela and Bab 2012).



Figure 2.2: Diagram of example tooth fractures. Note far right tooth has full fracture. Image after (Bethesda (MD) and National Institute of Dental and Craniofacial Research (US) 2021).

## 2.2.2 Osseointegration

The healing process in which the living bone connects with the artificial implant is referred to as osseointegration. Several factors such as biocompatibility, implant surface design, and whether the site is left undisturbed during the healing process can have implications on the quality and longevity of integration (Parithimarkalaignan and Padmanabhan 2013).

During surgery, it may be required to build up on existing bone to provide a suitable bed for implantation. Guided Bone Regeneration is a procedure that replaces the missing volume of bone in patients with particulate autogenous bone (using bone scrapings from elsewhere in the patient) and/or osteoconductive material (using synthetic, donor, or animal bone grafts). This maintains the previous structure of the wound site, whilst preventing the ingress of soft tissue (Budihardja 2019). The composite is accepted by the surrounding bone as an osteogenic cell scaffold and near-bone like matrix, the resultant strength of which depends on a number of factors such as level of tissue lost, or required surgical site (Sela and Bab 2012).

There is an increasing body of research conducted into the field of GBR, alongside the barrier membranes that are sometimes used to protect the surgical site. The previous decades research is presented in Figure 2.3, showing the ever increasing number of works published on GBR and membranes, specifically the more frequent results from polymer GBR (Figure 2.3B) versus metal or ceramic GBR (Figure 2.3D).

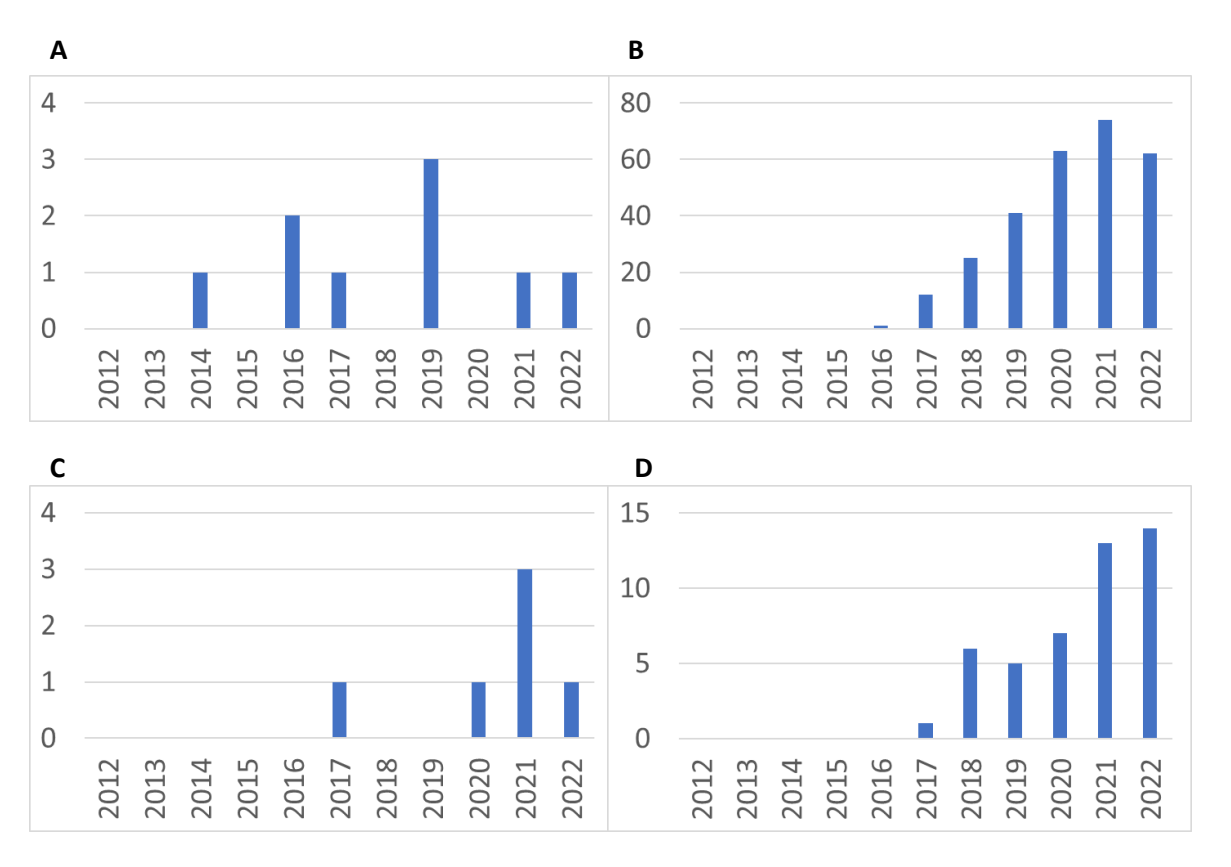


Figure 2.3: Keyword search of published work in last 10 years using Scopus. A) Keywords "GBR" and "polymer" publications by year. B) Citations of results in A) by year. C) Keywords "GBR" and "ceramic", and separately "GBR" and "metal" publications by year. D) Citations of results in C) by year. Figure adapted from (Yang, Wu et al. 2022).

#### 2.2.3 Bacterial infections

Dental implant survival rates are currently high at between 92 and 98% (Royal College of Surgeons: Faculty of Dental Surgery and Restorative Dentistry-UK 2019), which are higher when used in combination with GBR (French, Ofec et al. 2021). However, whilst systematic and individual failures of dental implant can occur (e.g. incorrect placement, or patient diet respectively) (Esposito, Hirsch et al. 1998), the most common cause of dental implant failure is due to bacterial infection at the wound site (Budihardja 2019).

Following implantation, coccoid bacteria was present in 86% of dental implants within 3 months of placement (Quirynen and Steenberghe 1993, Oh, Yoon et al. 2002). Bacterial infection can also be present after the dental implant healing period, for example peri-

implantitis (infection of the soft tissue around an implant) was also noted in 0.3 to 0.7% of complete dentures and single tooth replacements (Tabanella, Nowzari et al. 2009) which are caused by *P. gingivalis*, *Streptoccocal* bacteria, and *Fusobacterium* (Hashimoto, Okada et al. 2022). Periodontal infection (infection of the gum tissue) is caused by the same peri-implantitis causing bacteria, which can lead to inflammation of the site and an imbalance between bone resorption and bone formation. This imbalance means that new bone cannot be formed at the same speed bone is lost and this bone loss causes implant failure (Tsuchida and Nakayama 2023).

Bacterial colonisation of any site first begins when a bacterial cell attaches to a surface (primary colonisers) and begins feeding from the surrounding nutrients. This feeding causes cell growth and division. As the bacteria colony grows, other species of bacteria may opportunistically attach to the initial colony (secondary colonisers), expanding the community of bacteria, which further feed and divide. A community of bacteria like this is known as a biofilm. Bacterial biofilms have higher resistance to antibiotics, disinfectants, phagocytosis, and other components of the host immune and inflammatory defences (Esposito, Hirsch et al. 1998, Hall-Stoodley, Stoodley et al. 2012, World Health Organisation 2014).

Within the scope of interest, the bacteria have been separated into two categories of defining parameters; whether they are aerobic or anaerobic, and whether they are Gram-positive or Gram-negative. Gram-positive and Gram-negative differ in their cell structure (Figure 2.4); the outer wall of Gram-negative bacteria are thin layers of peptidoglycan and an outer membrane which results in a cell wall more resistant to penetration. In contrast, Gram-positive bacteria do not have an outer membrane, but instead thick layers of the peptidoglycan found in Gram-negative bacteria (Silhavy, Kahne et al. 2010).

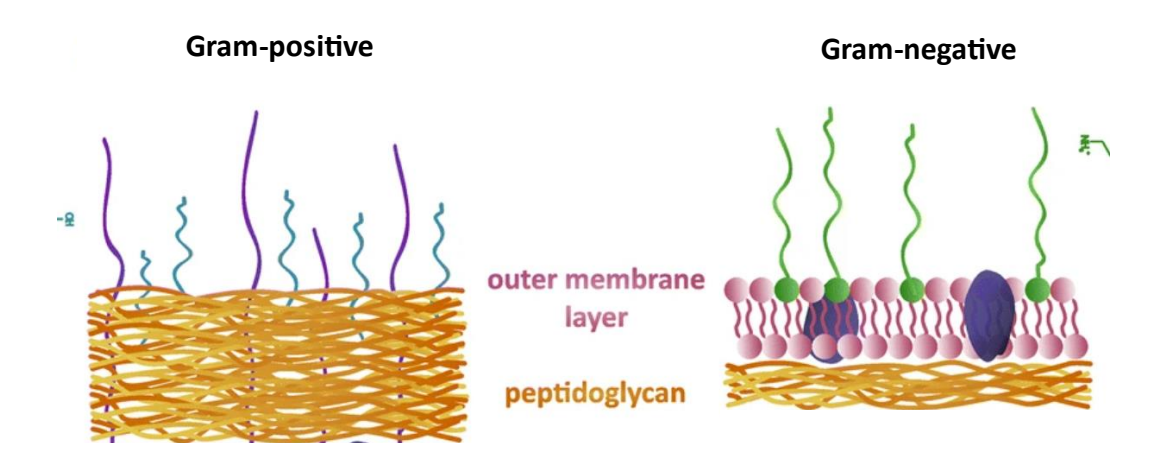


Figure 2.4: Schematic of Gram-negative and Gram-positive bacteria cells. Note different construction of outer membrane. Image after (Pajerski, Ochonska et al. 2019).

With this defined, an example of bacteria involved in dental infection is *Staphylococcus aureus* (P. Andrew Norowski and Bumgardner 2009, Hall-Stoodley, Stoodley et al. 2012), an aerobic Gram-positive primary coloniser. It is a quick growing species that is commonly found in wound infections (Henriques, Jenkins et al. 2010), and has associations with peri-implantitis (Lee and Wang 2010). An increasing concern regarding the treatment of infection is antibiotic resistance, and methicillin-resistant *S. aureus* (MRSA), is known to be resistant to multiple antibiotics. When *S. aureus* biofilms are formed, the bacteria enclosed within are provided protection from antibiotics *in vivo* (Esposito, Hirsch et al. 1998).

Furthermore, *Porphyromonas gingivalis* is an example of an anaerobic Gram-negative secondary coloniser. This bacterium utilises the iron within blood in heme which promotes growth (Olczak, Simpson et al. 2005). Once *P. gingivalis* enters the bloodstream can lead to inflammation (see above) of the bone and tissue. *P. gingivalis* is considered an important organism in the development of chronic periodontitis (infection of the soft tissue around the tooth) (How, Song et al. 2016), and during GBR, infection can lead to complications and failures of the dental implant (Gaviria, Salcido et al. 2014). *P. gingivalis* is more resistant when included as part of a biofilm (Safii, Tompkins et al. 2017), and therefore the prevention of biofilm growth is paramount to ensure stable healing during GBR.

Bacterial removal predominantly consists of mechanical removal (e.g. brushing or flossing) (Socransky and Haffajee 2002). However, whilst brushing is advised during GBR, the recommendations prefer softer bristled or low motor powered brushes, or substituted completely with chemical use such as chlorhexidine (Gulati, Govila et al. 2014). Personal care also varies between patients because of either differing interpretations of guidance, fear of causing further harm, or neglecting wound site, all of which lead to further infections. This can lead to too little, or too much, force applied during brushing, causing biofilm build up, or dental implant loss as a result (Gulati, Govila et al. 2014). Alternatives that offer consistent bacterial resistance would increase the rate of implant success, whilst also alleviating potential patient fears regarding their dental implant care during healing.

## 2.2.4 Anatomy of a bacterial cell

Bacterial cells are self replicating organisms in the 0.2 to 10 micrometre ( $\mu$ m) scale. This self replication is encoded in the DNA contained inside the cell nucleus and also determines the genetic traits of the bacterium (Holmes and Jobling 1996). A generic anatomy of the bacterial cell is given in Figure 2.5.

Although grouped by the cell envelope (Gram-positive and Gram-negative noted in Section 2.2.3), they may also be characterised by the genus (group of related species, e.g. *Streptoccocus*), shape (for example rod-like or spherical/cocci), and whether they are motile (capable of movement) (Salton and Kim 1996).

The bacteria motility is defined by the inclusion of the flagella, which moves back and forth, displacing the liquid of the environment, causing motion of the cell. When bacteria comes into surface contact with a host (e.g. soft tissue), small hairs on the exterior (fimbriae) of the cell allow adhesion (Salton and Kim 1996).

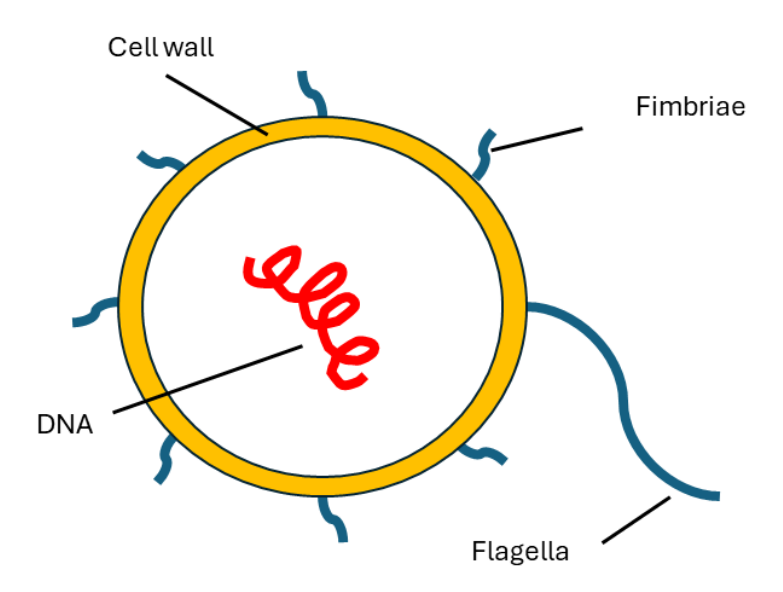


Figure 2.5: Anatomy of bacteria cell showing DNA and cell wall. Also shown are fimbriae, responsible for surface adhesion, and flagella, responsible for bacteria motility.

### 2.3 Medical requirements for the design of GBR membranes

Currently available solutions during GBR are physical barriers that shield the implant site from bacterial infection. Of these, some require subsequent removal (e.g. non-resorbable membranes (Guazzo, Gardin et al. 2018, Tahriri, Monico et al. 2019)), which could reopen wound site, allowing for further infection. The second are biodegradable or resorbable, offering eventual breakdown in the body and no need for further surgeries (P. Andrew Norowski and Bumgardner 2009). It is shown that healing during GBR is improved with either non-resorbable or resorbable membrane (Dimitriou, Mataliotakis et al. 2012)

When considering a protective covering for a wound site, such as the membrane used in GBR (see Figure 2.6), a suitable membrane must meet certain criteria. At least, membranes are required to be biocompatible and not toxic or immunogenic, be able to maintain the wound site integrity and protect wound site cells. Membranes are either resorbable or non-resorbable membranes, the former is able to degrade, and is required to biodegrade at a rate proportional to the bone regeneration within the oral wound site of around 6 months (Cambridge University Hospitals 2021), their non-resorbable counterparts require later

surgical intervention to remove, and risk further bacterial infection as wounds are reopened (Gentile, Chiono et al. 2011).



Figure 2.6: Diagram showing how a physical barrier membrane is placed during Guided Bone Regeneration procedure. Image after (Mount Nittany Health 2017).

Of the materials used in membranes, synthetic polymers such PLA or PLGA are appreciated for their biocompatible and degradable properties, although this is believed to be poorer than their collagen-based alternatives. Collagen based membranes have inherently shorter degradation times and are supplemented with compounds where longer degradation times are required (Gentile, Chiono et al. 2011, Lee and Kim 2014).

Although offering a physical barrier, however, bacterial biofilm build up can still occur upon, or around, the membrane site, and in some examples of commercial available membranes, promote bacterial growth (Slutzkey, Kozlovsky et al. 2015). Therefore, membranes that are inherently fabricated, or coated, with antimicrobial reagents would further reduce to rate of bacterial build up and lower the risk of infection during healing. In theory, as these membranes degrade, any antibacterial reagents would diffuse into the surrounding area as the saliva breaks down the polymeric fibres. As the reagent is mixed with the saliva, the surrounding area would inherit a degree of antibacterial action.

## 2.4 Commercially available membranes

Wound healing membrane designs vary depending on application. Internally applied membranes commonly used in oral GBR are biodegradable or resorbable animal-derived collagen membranes, preferred over their non-resorbable alternative, which requires further

removal between 6 and 8 weeks after surgery (Cambridge University Hospitals 2021), risking further bacterial infection as the wound site risks being reopened. A summary of a selection of commercially available membranes can be found in Table 2.1.

Commercially available membranes provide physical barriers to bacterial ingress, however, do not provide therapeutics benefits. In some cases of non-resorbable membrane, such as ePTFE, due to the stiffness of the material, this can cause splitting of soft tissue and still lead to bacterial infection of the site (Aprile, Letourneur et al. 2020). Therefore, continual protection from bacterial growth cannot rely solely on a physical barrier and there is clear need for antimicrobial properties to be considered as part of membrane manufacture.

Chemical and biological reagents have been used in combination with the above physical barriers to provide antibacterial coatings. Among the natural sources, Manuka Honey, for example, reduces inflammation and bacteria present during wound healing (Mandal and Mandal 2011), and has been used to soak or cover externally applied dressing pads in plasters. In clinical settings, medical grade honey (i.e. honey that has been sterilised and processed to be safe for clinical use) has been prescribed for patients during healing times either as part of a dressing or as a salve (Oxford Health NHS Foundation Trust 2015). Another additive, silver, has shown antibacterial properties for centuries and is currently readily used in plasters, offering antibacterial protection of wound sites, whilst also reporting no cytotoxic potential (P. Andrew Norowski and Bumgardner 2009, Nešporová, Pavlík et al. 2020). However cytotoxic responses in fibroblasts were noted for silver impregnated dressings (Acticoat, Smith & Nephew), causing 40% cell failure, which was not seen in 30% concentration Manuka Honey coated dressings (L-Mesitran Hydro, Triticum, the Netherlands), and caused an initial boost in cell proliferation (H&R Healthcare, Du Toit and Page 2009). Suggesting that potential discrepancies occur either as a result of processing silver dressings, or of additional toxic compounds found in certain products.

Table 2.1: Membranes currently and previously on the market. Materials used are noted and whether they are resorbable or non-resorbable.

	Product	Material	Comments	Source
Resorbable	Bio-Gide, Geistlich, Manchester	Collagen	Biodegradable, includes porcine collagen.	(Slutzkey, Kozlovsky et al. 2015)
	BioMend, Zimmer Biomet, Indiana	Collagen	Resorbable	(Gentile, Chiono et al. 2011)
	Osseoguard, Zimmer Biomet, Indiana	Collagen	Resorbable. Studies report potential to promote bacterial growth	(Slutzkey, Kozlovsky et al. 2015)
	EZ Cure, Biomatlante, Loire Atlantique	Collagen	Resorbable, porcine based	(Lee and Kim 2014)
	Biofix, Biocon, Finland	Polyglycolic Acid	Resorbable, high strength (14 MPa), breaks down after 4 weeks.	(Bottinoa, Thomasb et al. 2012)
	Atrisorb	Poly-DL-Lactide	Resorbable, applied as a liquid	(Kim, Kang et al. 2011)
Non-resorbable	GORE-TEX, W. L. Gore & Associates, Arizona	Expanded polytetrafluoroethylene (ePTFE)	Non resorbable, <b>discontinued</b>	(Gentile, Chiono et al. 2011)
	Neogen, Neoss, Harrogate	ePTFE	Non resorbable, dual textured	(Aprile, Letourneur et al. 2020)
	FRIOS BoneShields, Dentsply Sirona, North Carolina	Titanium	Non resorbable, laser perforated	(Aprile, Letourneur et al. 2020)

## 2.5 GBR Strategies and new membranes under preclinical evaluation

Commercially available membranes are not universal in their aid of GBR, and tailored solutions to specific problems have been developed at the current research and development level. Table 2.2 shows selected examples of materials currently under development in patient trials, detailing materials used and outcomes.

These materials exhibit limited antibacterial properties and would benefit greatly from a number of materials currently being developed for general healthcare, solutions, and food industry applications. Table 2.3 gives a selection of these materials alongside novel utilisation of antibiotics.

Antibiotic loaded membranes have been reported previously with positive results. Tetracycline containing fibres inhibited complete biofilm formation of *Porphyromonas gingivalis*, *Fusobacterium nucleatum*, *Prevotella intermedia*, and *Aggregatibacter actinomycetemcomitans* (Shahi, Albuquerque et al. 2017). Other antibiotics have been readily incorporated into electrospun fiber membranes with broad release profiles. One of the major concerns when formulating membrane is a release profile that is sufficient for the duration of the wound healing process (Gizaw, Thompson et al. 2018).

Emerging biological compounds are also of interest in membrane fabrication to curtail rising costs of manufacture. One such material is moth silk, that has previously been used as a suture material, and was successfully utilised as an electrospun membrane with positive biocompatibility and strength, making it suitable for GBR (Lee and Kim 2014). Spider silk has also been investigated as a biodegradable alternative membrane, of interest for spider silks' inherent mechanical strength. Manufactured self-assembled spider silk membranes were found to have high tensile strength, be permeable to protein transfer, and support the growth of human keratinocyte cells (Gustafsson, Tasiopoulos et al. 2020).

Table 2.2: GBR membranes currently in development. Noting defected bone in patient, and research outcomes from patient trials. Table adapted from (Wang, Feng et al. 2022).

Material	<b>Defected Bone</b>	Graft materials and coverings	Comments
Platelet-rich fibrin membrane	Staged lateral bone block	Grafted with autogenous bone combined with bovine bone mineral	Promotes proliferation and migration of cells
Injectable form of platelet rich fibrin (PRF)	Horizontal bone defects	Grafted with mixture of particulate autogenous and exogenous and covering with collagen membrane and leukocyte PRF membrane	Permitted sufficient bone gain to allow dental implant placement
Three-dimensional performed titanium mesh	Non-contained horizontal defects	Covering crosslinking collagen membrane	Mean hard tissue gain of 84% after 6 months
Digital customized titanium mesh	Horizontal, vertical or combined defects	Grafted with heterologous bone and autologous bone (50:50) Covering collagen membrane	Induces new bone formation
Titanium membrane	Alveolar ridge augmentation	Grafted with sulfate powder with normal saline, covering autogenous bone grafts	Hard and soft tissue stable after 1 year
Ti-reinforced PTFE membranes	Vertical defects during dental implantation	Dental Implants	After healing, no further bone augmentation required.
Ribose cross-linked collagen membranes	Contained and Non contained extraction sockets	For contained sockets, RCLC membranes were positioned across extraction sockets and for non-contained sockets, bones substitute was used to support the membrane	Provides scaffold can hold growth factors to accelerate tissue regeneration

Table 2.3: Novel membranes currently in development, with details regarding bacteria used, and how reagent was incorporated into membrane.

Reagent	Composition	Bacteria	Notes	Source
Tetracycline	Antibiotic contained in electrospun	P. gingivalis	Inhibited all bacterial colonies tested.	(Shahi,
	fibres	F. nucleatum		Albuquerque
		P. intermedia		et al. 2017)
		A. actinomycetemcomitans		
Cefixime	Antibiotic loaded electospun	S. aureus	Inhibited growth comparable to isolated	(Sharif,
	scaffolds		antibiotic. Improved results when	Tabassum et
			combined with $\beta$ -cyclodextrin.	al. 2019)
Lemon Oil	250 mg/mL edible films	S. aureus	Agar Diffusion inhibited growth, effect	(Srikandace,
		E. coli	more pronounced in <i>E. coli</i>	Indrarti et al.
				2018)
Thyme Oil	2, 4, and 6% w/v nano emulsions	E. coli	Nano emulsion had greater effect than	(Zhang, Liu
	and coarse emulsions as layer-by-		Coarse emulsion, however no inhibiting	et al. 2021)
	layer assembled food packaging		effect at concentrations below 6 %w/v	
Honey	200 ug/mL incorporated copper	E. faecalis	Well assay, honey had negative impact on	(Ismaila,
•	nanoparticles	E. coli	antibacterial properties of copper.	Shamelia et
			•	al. 2019)

Where membranes are polymer chains across a plane (see Section 2.3), hydrogels and cryogels are a three-dimensional polymer structure that swells or contracts in size when exposed to water due to the inherent hydrophilicity. Less common than membranes, gels are an emerging product that is still finding utility in wound treatment. These gels have been incorporated with antibacterials and antibiotics as a method of drug delivery, and as a mediator for other sterilisation techniques. Hydrogel successfully mediated the use of photodynamic inactivation against bacterial strains of *A. actinomycetemcomitans* and *P. gingivalis*. (Chi, Qi et al. 2019, Hixon, Bogner et al. 2019).

In the field of the regenerative medicine, electrospun membranes are a robust and efficient fabrication method that offers versatility in its applications. Electrospun fibres are able to be formulated such that a tailored drug release upon a wound site is achievable, with the long term goals of such an endeavour pointed towards wound dressings that are tailored in their application in both their mechanical and chemical properties (Gizaw, Thompson et al. 2018). Encapsulation of regeneration promoting peptides, via surface functionalisation, has shown to enhance the functionality of GBR membranes (Gentile, Ferreira et al. 2017).

Currently, one of the challenges to performing *in vivo* or clinical trials are the ethical concerns regarding naturally derived reagents such as extracts, or animal by-products (Berkovitch, Toume et al. 2016). And, whilst in depth proof-of-concept and *in vitro* studies are required to alleviate these ethical concerns, membranes in isolation, and with the inclusion of synthetic or chemical compounds, have shown their utility in small clinical studies.

Antibiotic doping membranes have found mixed outcomes when performing *in vivo* studies, where doxycycline - doping is an effective form of bacterial infection in a study of 24 patients, (Chaturvedi, Gill et al. 2008), however no distinction was found in tetracycline coated collagen membrane in double blind trials, although the sample size was very small as noted by the author (Baglivo 2011).

*In vivo* studies have considered the inclusion of silver-hydroxyapatite nanocomposites. These have shown improved biocompatibility than ePTFE membranes in rat groups (Zhang, Xu et al. 2010).

## 2.5.1 Industrialisation Process and Challenges

It is the aim to develop a novel therapeutic membrane that will provide antibacterial properties, without causing cytotoxic effects. Through the development of this membrane, it will need to conform to a number of standards to be considered market ready. One of the greater challenges should any GBR antibacterial resorbable barrier membrane be considered for market is the translation from research bench to commercial hubs. In the UK, new medical technologies are assessed via the Medicines and Healthcare products Regulatory Agency (MHRA) and National Institute for Health and Care Excellence (NICE) and must meet a series of criteria, such as robustness and transparency of data (Medicines and Healthcare products Regulatory Agency , National Institute for Health and Care Excellence 2022). One of the concerns relevant to this project is consistency of output from medical devices.

As discussed above, many bioactive reagents have inherent batch variation both when extracted and during storage, and questions arise regarding synthesis of compounds as there is clear overlapping effectiveness and inter-dependency on compounds. Whilst some types of honey have been approved by NICE, essential oils (EOs) are still considered alternative therapies by governing bodies (NHS England 2022).

In theory, one could overcome this challenge should one be able to fully synthesise components, whether through compound derivation or fully synthetic manufacture. Synthetic reagents can be fully manipulated, extracting antibacterial components from various bioactive reagents, and tailoring a specific bactericidal component. Alternatively, should EOs be recategorised by NICE, this allows the opportunity to use the broad utility of EOs without need for synthesis. This would require the proof of concept that EOs can be antibacterial without risk to cell proliferation.

## 2.6 New approaches for the manufacturing of membranes for GBR

It is the intention to utilise membranes to offer a delivery system of an antibacterial reagent. To select appropriate membranes for GBR, they should be fit for purpose (see Section 2.3).

Secondary factors require the membrane to absorb inhibiting reagents and release them within a suitable time frame to provide bacterial resistance throughout healing time (Gentile, Chiono et al. 2011, Dimitriou, Mataliotakis et al. 2012).

## 2.6.1 Electrospinning

Electrospun membranes are thin sheets of interlocking polymer strands which provide an inert and porous surface as a base. These offer utility in a delivery method for agents such as antibiotics (Chi, Qi et al. 2019). The electrospinning process is shown schematically in Figure 2.7, and in brief performed as follow:

- the solution is prepared by dissolving desired polymer (e.g. poly(ε-caprolactone)) in a solvent, mainly acids. Stirring with the addition of heat can be applied to ensure homogenous mix (Shahi, Albuquerque et al. 2017);
- polymer solution is loaded into a syringe with needle point (emitter) and set up 10 to 30 cm above a metal plate (collector) (Mailley, Hebraud et al. 2021);
- 3. a potential difference up to 20-30 V, is applied between the emitter and collector;
- 4. as the solution is slowly ejected from the emitter, a high enough electric field will cause droplets to form into thin strands in a conical shape (Taylor Cone) which rapidly move and deposit across collector (Mailley, Hebraud et al. 2021);
- final membranes were either left at room temperature or placed in a desiccator to ensure solvent evaporation and membrane solidification (Shahi, Albuquerque et al. 2017);
- 6. electrospun membranes can subsequently be removed from the collector.

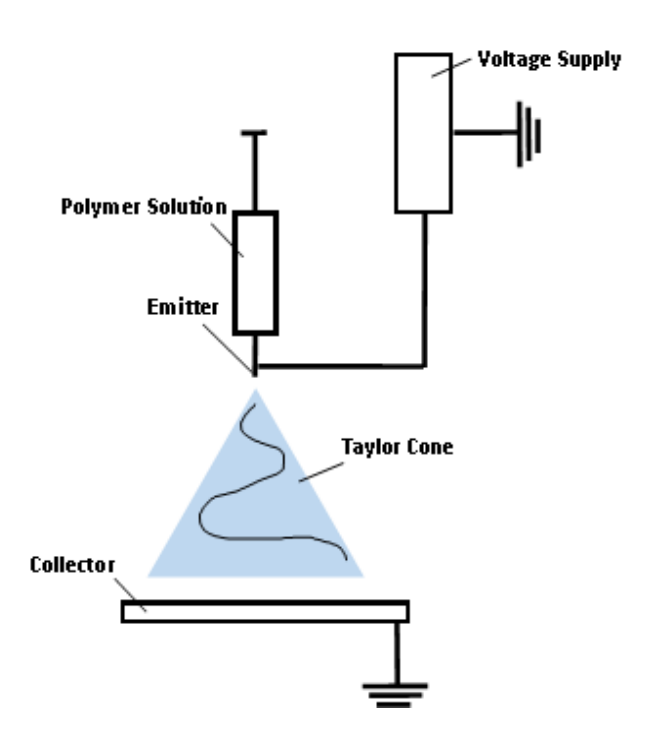


Figure 2.7: Electrospinning schematic showing how a polymer solution is ejected from the emitter onto a collector. The potential difference applied between emitter and collector causes the development of a Taylor Cone, which causes polymer droplets to elongate into strands that whip and deposit across collector surface. Image adapted from (Jamnongkan, Wattanakornsiri et al. 2012).

There is still outstanding research required to parameterise an 'ideal' membrane for improving the tissue healing and, moreover, an ideal membrane is location specific. For example, a long bone defect takes longer to heal than shorter bone defects, therefore requiring a longer degradation time (Dimitriou, Mataliotakis et al. 2012). The scope of this project lies within a specific healing time, and therefore the parameters are well defined at three to six months (Cambridge University Hospitals 2021), and should therefore a barrier membrane should degrade comparably.

For an oral environment, studies have incorporated antibiotic drug delivery systems that are capable of reducing viability in complex multi-species biofilms. Further, improved studies of biodegradability of polymer matrices can tailor degradation time of membranes. Antibiotic delivery systems are still heavily relied upon. There is a major risk of rising AMR, concerns have arisen as a result of potentially uncontrolled distribution of antibiotic. As a result, other

antibiotic-free systems require further investigation (Chi, Qi et al. 2019, Abtahi, Chen et al. 2023).

## 2.6.2 Layer-by-Layer assembly techniques

The inherent properties of barrier membranes can be augmented with additional functionalisation. Whilst the solutions used to fabricate membranes can be augmented as detailed previously (Section 2.6.1), surfaces of membranes can also be functionalised with solutions that, for example: change mechanical strength, alter hydrophobicity/hydrophilicity, and alter surface charge. These are micro- or nano-particles suspended in solutes which are deposited onto the surface in thin layers (Iler 1966). Depending on the properties of materials used, correct techniques are required for successful application (Richardson, Björnmalm et al. 2015).

Different methods have been developed that apply surface coatings to membranes, categorised as dip/immersive (Gentile, Frongia et al. 2015, Javaid, Mahmood et al. 2022), spin (Vozar, Poh et al. 2009), spray (Nogueira, Banerjee et al. 2011), electromagnetic (Junqi, G. et al. 2001), and fluidic assembly (Picart, Lavalle et al. 2001, Richardson, Björnmalm et al. 2015). An overview of these techniques is given graphically in Figure 2.8, however the general theory is similar whereby these techniques utilise the electrostatic interactions between the membrane and the molecules present in the solution.

In brief, a charged substrate is exposed to positively and negatively charged solutions containing highly charged polymer chains (polyelectrolytes) (Gentile, Frongia et al. 2015, Campbell and Vikulina 2020). These polymer chains are bound to the surface and withstand a rinsing step in buffer solution, or centrifugation to remove unadhered surface particles. This step can be repeated until a desired final product is formed (Campbell and Vikulina 2020).

The strength of surface-solution bonding is determined by the charge of the solution and membrane. For a solutions charge, this is primarily influenced by the inherent pH, which can change both the magnitude and polarity of the resultant solution (Güzey and McClements 2006).

The final product is a series of thin layers which can be accurately controlled. This level of control over thickness, high loading potential, and membrane stability are a few of the benefits available to LbL membranes that are useful in a range of biomedical applications (Gentile, Ferreira et al. 2017, Campbell and Vikulina 2020).

Dip coating has been selected for this project for its consideration as the gold standard with which all other techniques are compared (Richardson, Björnmalm et al. 2015). In addition, Newcastle University has developed an in-house automated dip coating system that allows for consistent application of nanolayers (WO2021/079106).

In brief, the process uses a series of solutions with opposing charges, which are interlaced and absorbed onto the surface through immersion of membrane. Between each of these immersive steps, a rinsing and sometimes centrifugal techniques are employed to remove un absorbed particles (Iler 1966, Richardson, Björnmalm et al. 2015). Where the inherent charge the of the membrane is not strong enough, the membrane must first be chemically altered through aminolysis; submerging the membrane in a solution which reacts with surface polymers introducing amines (e.g. NH<sub>2</sub> groups) (Kasoju, Nguyen et al. 2018). This binding of the surface caused the membrane to be positively charged, allowing for the further binding of charged aqueous solutions.

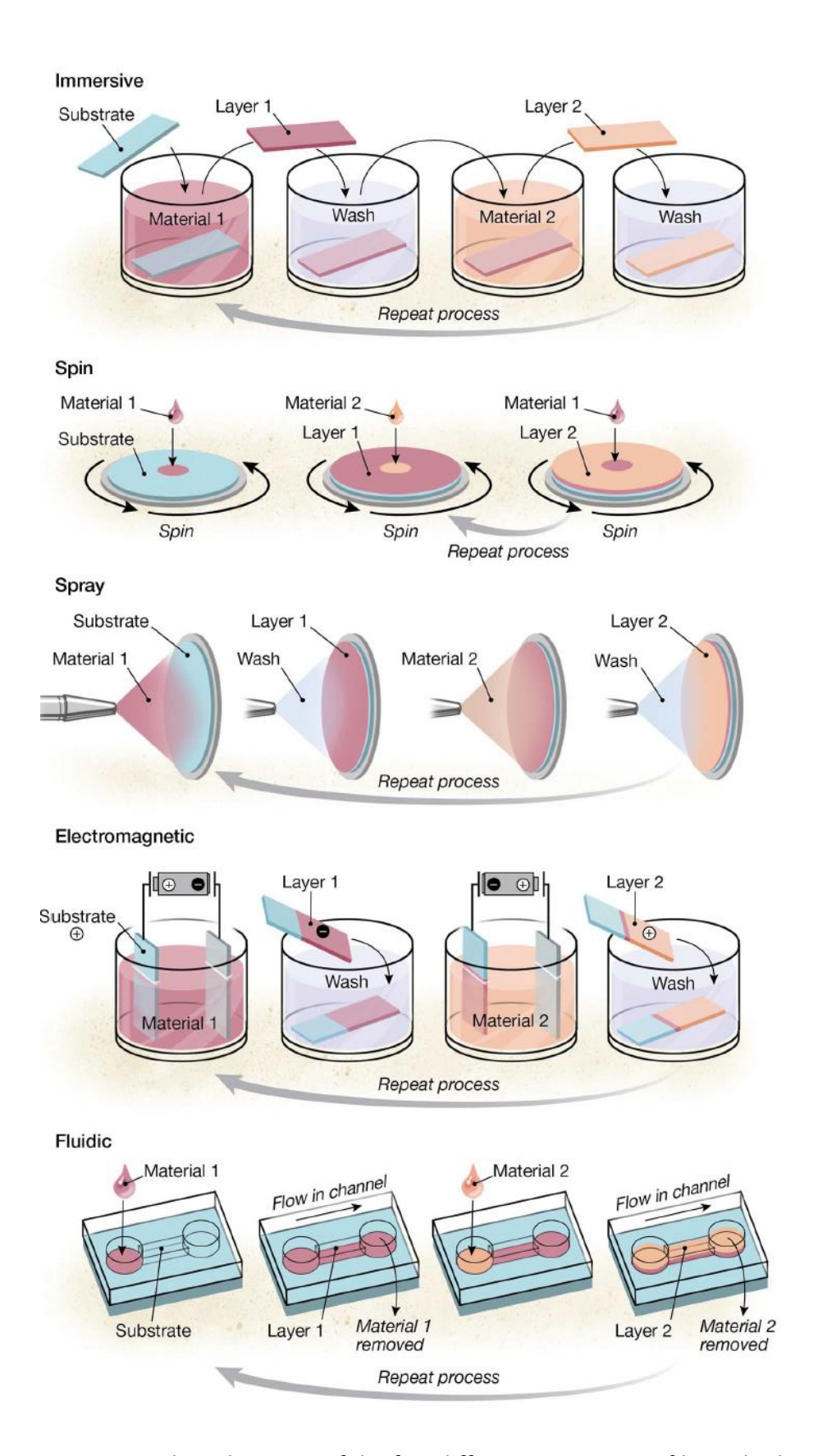


Figure 2.8: Procedure diagrams of the five different categories of layer-by-layer manufacture; Dip, Spin, Spray, Electromagnetic, and Fluidic Assembly. Image after (Richardson, Björnmalm et al. 2015).

## 2.6.3 Alternative bioactive compounds for improving antibacterial action

The composition of artificial membranes can be tailored to fit a range of medical applications. In an oral cavity during the healing process, this would offer a protective covering to prevent infection.

However, antibiotics should be used with caution, as the increasing rate of antimicrobial resistance poses a global health threat (World Health Organisation 2014). In addition, reduced blood flow in the oral tissue would limit the dispersal of any antibiotics applied that require entry into the bloodstream (P. Andrew Norowski and Bumgardner 2009). To this end, surface dispersing alternative bioactive reagents have been considered at the forefront of research as a topical agent (i.e. applied to surface). In addition, previous studies have shown they are able to offer antibacterial resistance without promoting resistance (Blair, Cokcetin et al. 2009, Cooper, Jenkins et al. 2010).

The range of potential reagents is vast, and the following reviews only three of these. Manuka Honey is the first discussed, distinct from other honeys due to its methylglyoxal content (MGO). Improved antibacterial effects have been previously attributed to this MGO content (Johnston, McBride et al. 2018). Secondly two essential oils are discussed: Tea Tree Oil (TTO) and Lemon Oil (LO). Both of which exhibit antibacterial properties (Mancuso, Catalfamo et al. 2019, Rajeshnidhi and Mahesh 2019), but contain different active components (terpinene-4-ol and 1,8-cineole for TTO, and d-limonene and  $\gamma$ -terpinene for LO). All of which offer soothing properties that aid curbing an inflammatory response and preventing periodontitis (Gokhale and Padhye 2013).

It is the intention to formulate an electrospun membrane that will be functionalised with a selected bioactive compound via dip coating. Electrospun scaffolds were shown to provide a rapid release profile, leading to quick bacterial clearance (Hixon, Bogner et al. 2019). Further, there is indication that an initial burst release occurs, followed by a steady release over 14 days, stopping at 28 days (Mancuso, Tonda-Turo et al. 2019). This highlights a concern whether, since standard healing time of dental implants is three to six months (Cambridge University Hospitals 2021), repeat replacement of the membrane is required, or whether it is possible to

provide the patient with a suitable oral rinse to replenish the lost reagents present in the membrane.

## 2.6.4 Manuka Honey

Honey is an ancient remedy, used primarily as a salve for wound treatment, that is currently undergoing a revival of interest for its anti-inflammatory and promoting of tissue repair within wounds (Mandal and Mandal 2011). Alternative external uses show honey as a chewable format that could reduce gingival scores (English, Pack et al. 2004).

Medical Grade Honey has been gamma irradiated and is deemed safe for medical applications (Kwakman and Zaat 2012). Medical Grade Honey has been used in wound dressings, with good cytocompatibility when manufactured dressings (L-Mesitran Hydro, Triticum, the Netherlands) when exposed to keratinocytes and fibroblasts (Du Toit and Page 2009). Medical Grade Honey has also seen improved healing when applied directly during oral surgery in randomised trials (Al-Khanati and Al-Moudallal 2019).

Honey varies within brands, each having a slightly different composition, which is a result of the climate and flora in the environment surrounding where the honey is produced. Manuka Honey, for example, is unique in its possession of methylglyoxal (MGO) (Chemical structure shown in Figure 2.9); a reagent that has been shown to increase antibacterial activity with increasing MGO content (Johnston, McBride et al. 2018). However, there is also clear evidence of antibacterial properties in non-MGO honeys (Kuncic, Jaklic et al. 2012, Ahmed and Othman 2013, Brudzynski and Sjaarda 2014), and there is a clear indication of synergistic mechanisms not solely dependent on MGO content (Kwakman, Velde et al. 2010).

Figure 2.9: Chemical structure of methylglyoxal. Image after (Alvarez-Suarez, Gasparrini et al. 2014).

Cryogels incorporated with 5% Manuka Honey effectively acted as a bacterial inhibitor for chronic bone infections and below this concentration inhibited *S. aureus* and *E. coli* growth (Hixon, Carletta et al. 2019). The mechanism of MGO upon bacterial cells results in fimbriae and flagella loss (see Section 2.2.4), which are responsible for bacterial motor function and adhesion between cells and to surfaces (Rabie, Serem et al. 2016), however Manuka Honey as a whole compound exhibits different physiological effects on bacterial strains, for example disrupting their metabolic activity, or blocking efflux pumps within cells (Combarros-Fuertes, Estevinho et al. 2019). Other components that are primary bactericidal reagents are hydrogen peroxide and bee defensin-1, both of which have shown to contribute to the overall antibacterial properties of honey (Kwakman, Velde et al. 2010), and it has been recently shown that one of the phytochemicals; leptosperin, has reported to contribute to the anti-inflammatory properties of MH (Kato, Kawai et al. 2019). Regarding AMR, medical-grade honey promoted no significant mutations in *S. aureus* and *P. aeruginosa* that would suggest development of AMR (Cooper, Jenkins et al. 2010).

Whilst the benefits of Manuka Honey are documented, concentrations greater than 50% produced inflammation and cytotoxicity in human tissue (Minden-Birkenmaier and Bowlin 2018). For this reason, the levels of honey present in a membrane, should be sufficient to cause bacterial cell death, whilst low enough to not oversaturate the environment in honey, resulting in worsening of the wound site.

In addition, most cytotoxicity assays utilise live and dead cell staining, which stains intact cell walls. However, whilst Manuka Honey has been tested against various mammalian cell types, to date, little is known regarding the impact of the bone-regenerating activity of osteoblasts.

It would be pertinent, therefore, to consider the function of human cells, specifically osteoblasts which are responsible for the release of calcium used in bone regeneration (see Section 2.2.1), when exposed to variable concentrations of bioactive reagents.

#### 2.6.5 Essential oils

Derived from a variety of plants, essential oils have shown a range of therapeutic uses (How, Song et al. 2016). Their similar history of soothing remedies is shared with honey, and now critical work is currently being conducted, bringing essential oils to the forefront of research into antibacterial alternatives.

Standard agar disc diffusion, or dilution tests to assess minimum inhibitory concentration, are commonly used to parameterise essential oils (Lang and Buchbauer 2012). However, due to the hydrophobicity of oils, these are only able to be diluted in small volumes (Carson, Hammer et al. 2006), and therefore additional measures such as emulsification, and droplet imaging, may be required when conducting an appraisal of results.

It is often difficult to perform antimicrobial tests with oils due to their high volatility (Lang and Buchbauer 2012). Depending on the atmosphere or environment the oils are placed in, this can severely affect the results. Further, a hydrophobic reagent may also be difficult to assess *in vitro* as most cells are suspended in a water-based solution and therefore inherently immiscible unless a surfactant is used. The addition of a surfactant may have further complications as this may subtly alter the properties of a resultant emulsion. It could therefore be theorised that there is no way to fully assess essential oils above soluble volumes.

One parameter used when assessing antibacterial properties is Minimum Inhibitory Concentration (MIC). The minimum inhibitory concentration of a compound is the lowest concentration that visibly inhibits the growth of bacteria whether in broth dilutions or on agar plates, and are unique to each bacteria (European Committee for Antimicrobial Susceptibility Testing 2000).

As mentioned previously, a large range of essential oils exist that have shown positive responses *in vitro*, however the below covers two pertinent to the scope of the project, chosen for their distinct active components.

#### 2.6.6 Tea Tree Oil

Tea Tree Oil (*Melaleuca alternifolia*, TTO) is derived from the paper bark tree, found in Australia (Soukoulis and Hirsch 2004). It is the component of many topical remedies and first used by Indigenous Australians for antifungal and antibacterial activity (Lassak and McCarthy 1997). This has been considered anecdotal in modern medicine much like honey has been in Ancient Rome, however since 1990, more robust research has been conducted on the material which has shown some antibacterial properties (Carson, Hammer et al. 2006). As a topical agent, TTO was shown to reduce acne, decolonise methicillin-resistant and methicillin-susceptible *Staphylococcus aureus* (MRSA and MSSA), inhibit Coagulase-negative staphylococcal (CoNs) growth, and shown to effectively treat fungal infection (Thomsen, Hammer et al. 2013). It has also shown antitumour activity without causing cytotoxic effects (Assmanna, Cadonáb et al. 2018). It should be noted, however, that in all cases, TTO is 100 times less effective than antibiotic controls, hence why it is used primarily in alternative therapy.

TTO has shown to be effective at concentrations around 2% v/v at inhibiting bacteria (MIC), and 50% lethal dose in rats is 1.9 to 2.6 mL/kg (Carson, Hammer et al. 2006), therefore care must be taken when developing an oral membrane as seen with Manuka Honey. The penetrative effects of TTO may be cause for its toxicity, as may also allow the ingress of other potentially toxic reagents (Yadav, Kumar et al. 2017). Irritation and allergic reactions have also been shown at concentrations of 5-10% (Yadav, Kumar et al. 2017), although susceptibility to irritation is not considered as a part of population.

The individual and synergistic effect of Tea Tree Oil in conjunction with other essential oils (e.g. Thyme, Peppermint) has been shown against bacterial strains of *S. aureus* and *K. pneumoniae*. Whilst in some cases, the minimum inhibitory concentration of the oils may be above the concentration that causes cytotoxicity, when combined with other essential oils or antibiotics,

the authors suggested could lower the Minimum Inhibitory Concentration (MIC) value below a toxic threshold and become safe for use (Vuuren, Suliman et al. 2009).

TTO containing gel (2.5% concentration) was compared to 0.2% chlorhexidine gel in double blind trials on a total of 49 individuals over an 8 week period (Soukoulis and Hirsch 2004). The TTO-gel appeared to reduce Papillary Bleeding Index; whether the gum bleeds during gentle probing, and Gingival Index; the assessed severity of gingivitis. This is expected given that 1,8-cineole and terpinene-4-ol are active ingredients (5.1% and 40.1% concentration respectively (Carson, Hammer et al. 2006)) in TTO that possess anti-inflammatory properties, the latter of which also possess antimicrobial properties (Carson, Hammer et al. 2006). However, no reduction was initially seen in the Plaque Surface Score; the amount of plaque present on a tooth surface, which increased at latter stages of the study. Whilst terpinene-4-ol was found to be greater in antimicrobial efficacy in isolation (Loughlin, Gilmore et al. 2008), the inclusion within TTO may reduce risk of bacterial resistance development (Carson, Hammer et al. 2006, Loughlin, Gilmore et al. 2008).

Whilst a range of studies involving TTO have been established both in isolation and as part of a delivery system, much of the current literature is suggested to be of "low quality and heterogeneity", which suggest new and better studies are required (Deyno, Mtewa et al. 2019). As there is no standard for oil based antibacterial assays, conflicting protocols and therefore MIC values can often occur, leading to the conflicting outcomes to some attempts to parameterise oil-based materials.

## 2.6.7 Lemon Oil

Lemon Oil (*Citrus Limonum*, LO) is part of the citrus family of essential oils, extracted from lemon peel. The earliest use of lemons or their oils in modern medicine, was in the treatment of scurvy in the  $18^{th}$  Century (Lind 1753). Their active components are d-limonene and  $\gamma$ -terpinene, shared by other citrus oils, are responsible for their antibacterial, and antioxidant properties. Lemon Oil offers benefits over Tea Tree Oil as it is already well established as being safe for food use (Frassinetti, Caltavuturo et al. 2011). Whilst its antifungal effects have been

reported, when compared to other essential oils such as Sage or Thyme, Lemon Oil is far less effective (Císarová, Tančinová et al. 2016).

In simple solutions in DMSO, Lemon Oil has shown strong inhibition against both Grampositive (Staphylococcus aureus and Enterococcus faecalis) and Gram-negative bacteria (Xanthomonas campestris pv. Citri , Escherichia coli, Salmonella cholerasuis, Pseudomonas aeruginosa, and Enterobacter aerogenes), with minimum inhibitory concentrations (MIC) between 15-200 µg/mL (0.015-0.2 mg/mL) (Frassinetti, Caltavuturo et al. 2011). Lemon Oil incorporated into edible films were shown to have a larger MIC of 250 mg/mL against *E. coli* and *S. aureus* (Srikandace, Indrarti et al. 2018). This large between MIC values may be as a result of how the solution is functionalised and may require higher initial concentrations in the edible films to release LO in quantities similar to those seen in DMSO solutions.

Lemon Oil when screened amongst many EO and terpinenes including strains of *S. epidermidis*, *Klebsiella*, *E. hermanii*, *E.coli*, and *Candida spp.*, showed good inhibition in most strains. No inhibition was seen in *E.coli*, *Klebsiella*, and *E. hermanii*. Effectiveness against strains differed between other studies, which was attributed to the origin, climate and the season where the EO was produced leading to batch variation (Mancuso, Catalfamo et al. 2019).

#### 2.6.8 Essential Oil Emulsification

Due to the hydrophobic and volatile nature of essential oils, volumes over a very small threshold are not soluble in water and are often difficult to incorporate into delivery systems such as membranes (Carson, Hammer et al. 2006, Wulansari, Jufri et al. 2017, Yadav, Kumar et al. 2017), therefore an emulsification process is required to allow for the utilisation of larger quantities. Emulsions are suspensions of oil in water using a surfactant, which lowers the boundary tension between two previously immiscible substances (Mason, Bibette et al. 1995).

Surfactants in this case are molecules made of hydrophilic and hydrophobic ends, best represented by a ball and tail respectively (for graphical representation, see Figure 2.10). Hydrophobic substances easily bind to the hydrophobic oils, encapsulating the oil droplets.

The exterior of these droplets are now hydrophilic, allowing oil and water to be mixed to homogeneity.

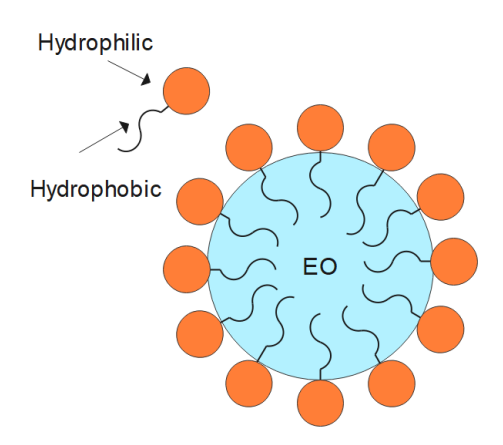


Figure 2.10: Emulsification of oil using a surfactant. Surfactants are shown by the ball and tail representing the hydrophilic and hydrophobic ends respectively. These surfactants encapsulate the oil, allowing for homogeneity in oil-water mixtures.

A number of surfactants have been studied for their emulsifying capacity in conjunction with EOs. Attempts to optimise protocols of Citral and surfactants Brij 97, and Span 85, and ethylene glycol as a cosolvent were developed to create nanoemulsions. These were first homogenised, then sonicated in a water bath, and the average resultant droplet size of the EO in water was between 10 and 100nm (Lu, Huang et al. 2018).

Citrus peel derived pectin was also used as a surfactant in a similar manner seen previously, by first creating a coarser emulsion using a stirrer, then homogeniser, then sonicated the solution in a water bath to form nano droplets of corn oil in water. These showed similar droplet size values around 50nm in size. It was also observed that charges were pH dependent in both oil-water solution, and surfactant in isolation, which lead to phase separation when pH reached 7, as both solution and surfactant became negatively charged (Güzey and McClements 2006).

Tween 80 was also used in a similar protocol as the above with Thyme oil up to 6% w/v concentrations, and was shown that the nanoemulsions improved antibacterial activity against

E. coli when droplet size was smaller (Zhang, Liu et al. 2021). Nanoemulsion gels of 5,7, and 9% Tea Tree Oil by combining with Tween-80 30% w/v and distilled water, which was mixed at 500 rpm to create a coarse emulsion, before adding propylene glycerol 15% w/v and homogenising at 2,000 rpm for 15 minutes. To create a gel, Carbopol 940 (1% w/v) was mixed with distilled water before being homogenised with triethanolamine (0.1% w/v/) at 100 rpm, which was then slowly combined with the nanoemulsion to form a nanoemulsion gel (20% w/v gel base). The resultant emulsion showed droplet size ranging from 166 to 188 nm (nano range 100-500 nm), which increased with TTO concentration, and a zeta potential ranging from -24 to -19 mV, which decreased with rising TTO concentration. Droplet size increased over an 8-week period, suggesting recombination of oil droplets, and additionally at temperatures of 40°C phase separation occurred in 9% w/v TTO gels, however this was remedied with mild agitation. This emulsion was effective at treating P. acnes strains, likely attributed to the active ingredient terpinene-4-ol (Wulansari, Jufri et al. 2017).

There is strong indication that a nanoemulsion is not only stable when an appropriate surfactant is used, but also exhibits stronger antibacterial properties in comparison to their coarser solutions. They have also shown to be readily accepted into layer-by-layer deposition, and therefore are of clear utility when considering possible alternative bioactive compounds for GBR membranes.

## 2.7 Computational modelling of biofilm growth

The utilisation of mathematical modelling to investigate the growth of bacteria is well established and broad in its applications (Swimberghe, Coenye et al. 2019, Styles, Brown et al. 2021). Early forms of modelling growth are given by cellular automata; a binary grid array system that displays either an agent, 1, or no agent, 0 (Wolfram 1984). Whilst mathematically concise, it finds utility in population dynamics (Mattei, Frunzo et al. 2018), however does not consider agent-agent interactions.

One of the earliest mathematical expressions of bacterial growth; the Monod kinetics, aims to describe the six phases of a bacterial development: 1. Lag, 2. Acceleration, 3. Exponential, 4.

Retardation, 5. Stationary, 6. Decline (see Figure 2.11) (Monod 1949). Monod kinetics provides insight into the dynamics of bacterial growth function of nutrient availability and is currently in widespread use throughout the microbiology and computational science community (Esser, Leveau et al. 2015, Mattei, Frunzo et al. 2018). Monod kinetics can be applied to single or multiple species' growth on different substrates (Galinha, Sanches et al. 2018).

Bacterial cultures growth can be modelled in suspension (Ofiţeru, Bellucci et al. 2014) or attached to a substrate (Verotta, Haagensen et al. 2017). Within the scope of this thesis, the area of interest is bacterial growth around the dental implant during healing. The growth of bacteria around this wound site focuses specifically on bacteria incident on and around the implant surface, and therefore further consideration is given to biomass growth upon substrates (as biofilm).

Kinetic models have improved over the years by utilising high-speed computing power to increase the simulation time and considering complex geometries. In current computational bacterial growth modelling, it is typical to use individual- or agent-based modelling. Individual-based computes the movement and interactions of each organism (Hellweger, Clegg et al. 2016), whereas agent-based is more holistic and considers a grouping of entities or organisms and considers the whole system (Gorochowski, Matyjaszkiewicz et al. 2012). Whilst both approaches are interchangeable, there difference is apparent in the level of detail of the resultant growth (see Section 2.2.3) (Kreft, Picioreanu et al. 2001).

Current iterations of biofilm models are tailored to their use in specific applications such as food safety (Le Marc, Valík et al. 2009), wastewater treatment (Ofiţeru, Bellucci et al. 2014), and cleaning of polluted sites (bioremediation) (Esser, Leveau et al. 2015). The use of simulations can reduce time spent in the lab, rapidly test hypotheses, and offer innovative solutions for biofilm control (Dzianach, Dykes et al. 2019).

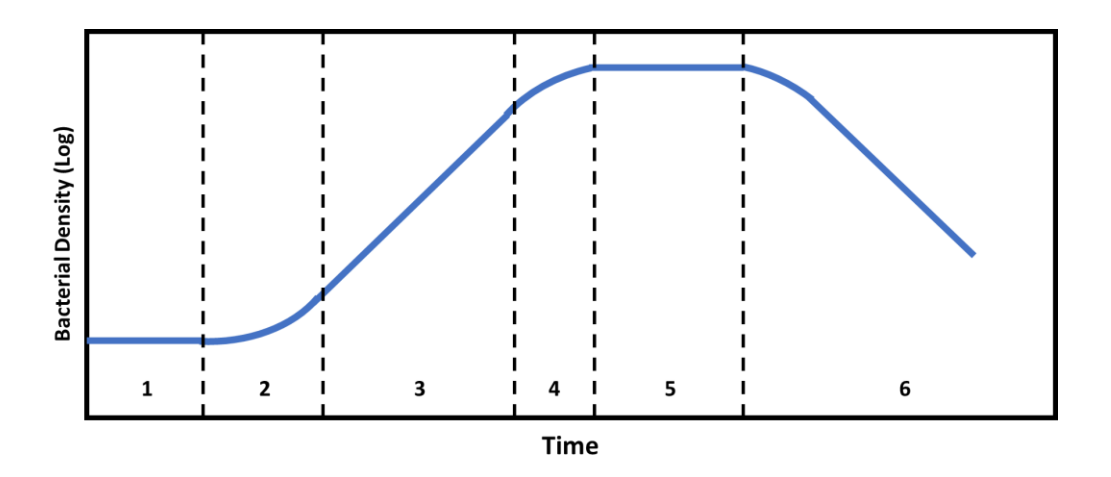


Figure 2.11: Lifecycle of bacterial culture. Six phases show; 1. Lag, 2. Acceleration, 3. Exponential, 4. Retardation, 5. Stationary, 6. Decline. Figure adapted from (Monod 1949).

The lifecycle of bacterial culture is broken into six stages (Figure 2.11). At each of these phases, the organism (X) consumes nutrient from environment (S) and performs growth, given by

$$substrate(S) + cells(X) \rightarrow extracellular\ products(P) + cells(nX)$$
 Eq 2.1

where growth leads to extracellular products (P) and a change in cell number given by the factor n. The extracellular products encompass a wide range of waste chemicals (e.g.  $CO_2$ ), polymers (e.g. polysaccharides), and networks of proteins known as the extracellular matrix, whose physical barrier is linked to the increase resistance of biofilms (Shuler and Kargi 2002, Mattei, Frunzo et al. 2018). For a batch process, the biomass changes over time, given by

$$\mu_{net} = \frac{1}{X} \frac{dX}{dt}$$
 Eq 2.2

where  $\mu_{net}$  (minute<sup>-1</sup>) is the net growth of the biomass (i.e. the difference between the rate of cell growth, new cells added, and the rate of cell death, dead cells removed;  $\mu_{net} = \mu_g - \mu_d$ ), X is the concentration of biomass (pg/ $\mu$ m<sup>3</sup>), and t is time (minute). Depending on the phases, the net growth rate is either positive, negative, or zero. The specific growth rate is dependent on the substrate concentration (S, pg/ $\mu$ m<sup>3</sup>) and is given by

$$\mu = \mu_{max} \frac{S}{K_S + S}$$
 Eq 2.3

where  $\mu$  is the specific growth rate,  $\mu_{max}$  is the maximum specific growth rate, and  $K_S$  (pg  $\mu m^{-3}$ ) is the value of S when  $\mu$  is equal to half of  $\mu_{max}$  ( $K_S = S(\mu = 0.5 \cdot \mu_{max})$ ). These kinetic expressions can be adapted to include additional factors influencing the growth. Of interest to this project is a non-competitive inhibition factor, which represents the inhibiting effect of bioactive compounds (Han and Levenspiel 1988, Shuler and Kargi 2002). This is given by

$$\mu = \mu_{max} \frac{S}{K_S + S} \cdot \frac{I}{I + K_I}$$
 Eq 2.4

where I (pg/ $\mu$ m<sup>3</sup>) is the concentration of inhibiting reagent, and K<sub>I</sub> is the inhibition constant, equal to half the minimum inhibition concentration, K<sub>I</sub> = 0.5·MIC.

Considering the growth rate expression, Equation 2.2 then becomes:

$$\frac{dX}{dt} = \mu_{max} \frac{S}{K_S + S} \cdot X$$
 Eq 2.5

which calculates the change in biomass concentration over time. Similarly, one can substitute

Equation

Eq 2.4 to give

$$\frac{dX}{dt} = \mu_{max} \frac{S}{K_S + S} \cdot \frac{I}{I + K_I} \cdot X$$
 Eq 2.6

## 2.7.1 Agent- and Individual-based modelling

Agent-based models (AbM) defines a collection of individuals with shared parameters (Esser, Leveau et al. 2015). This allows users to model large environments and finds utility in population studies (Picioreanu, Loosdrecht et al. 2000).

Whilst biofilm based or agent based models consider full or partial biomass growth (Esser, Leveau et al. 2015), modelling based on population produces often noise dominated outputs (Gregory, Vlachos et al. 2005). A more accurate, but time consuming, model considers each individual bacterial cell (or agent); known as individual-based modelling (IbM). IbM finds utility when rare organisms, events, or species variability are considered (Kreft, Picioreanu et al. 2001).

When considering individual bacterial agents, further parameters can be considered, such as individual mechanics or agent rate of division. A representation of a time step during an AbM is given by Figure 2.12. Specifically noted here, after growth is considered, the agents that have reached critical mass, divide into two agents of halved mass. The division causes mechanical stresses that push agents around the simulation space.

Once growth and division are calculated, considerations are given to the mechanical stresses the biofilm undergoes both from agents acting upon each other, and external environmental flow. If these stresses are greater than the binding strength of the biofilm, cells can be removed from the biofilm surface in either small (erosion) or large chunks (sloughing) (see Figure 2.13 for flow chart of this process). This detachment could lead to re-attachment to the substrate elsewhere, or removal from the area of interest via nutrient flow (Picioreanu, Loosdrecht et al. 2000).

Individual based modelling can consider growth in a multi species, multi substrate environment (Kreft, Booth et al. 1998, Kreft, Picioreanu et al. 2001, Gregory, Vlachos et al. 2005). IbM is capable of modelling complex environments, including growth in porous media (Tiwari and Bowers 2001), inhibiting substrates (Dzianach, Dykes et al. 2019), and the biofilm response to mechanical stresses (Li, Taniguchi et al. 2019).

When more complex environments and biological systems are required, novel solutions are provided using a blend of multiple software packages (Ofiţeru, Bellucci et al. 2014).

However, as more demanding and complex scenarios are proposed, errors can be introduced into the system as the ideal model deviates from the real world results, noticed on scales larger

than 400  $\mu$ m (Hellweger, Clegg et al. 2016). In addition, due to the high volume of cell interactions (either with other cells or the environment), modelling can be a lengthy process, with more complex bacterial interactions taking around one week to simulate two days of movement, rendering it unsuitable for rapid device development (Gregory, Vlachos et al. 2005). Assumptions can be made which simplify model mathematics, however these introduce their own inherent systemic errors.

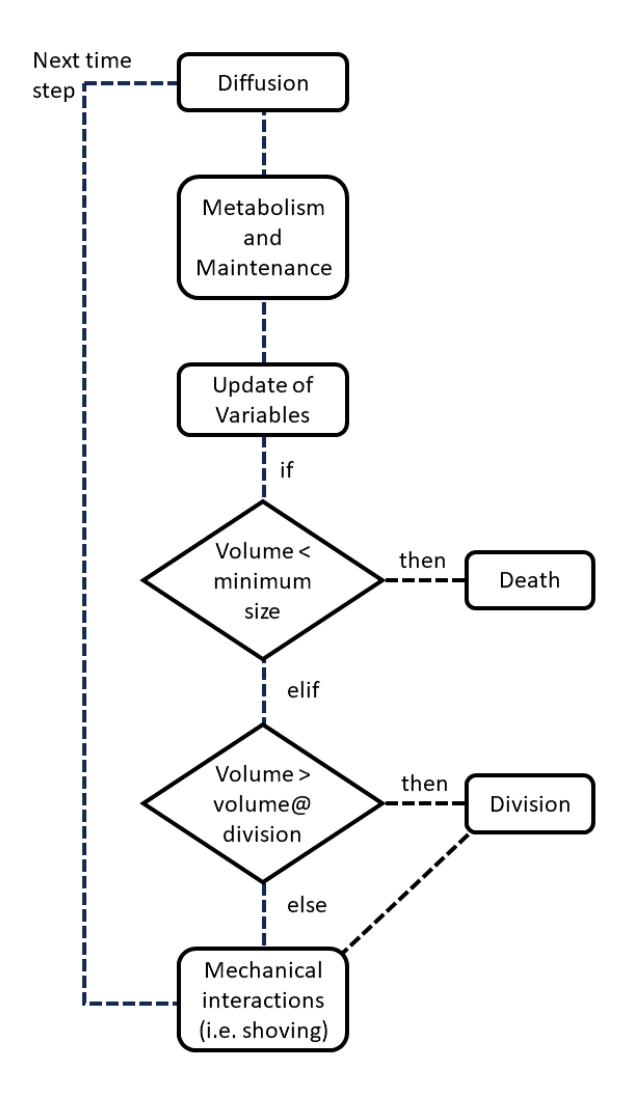


Figure 2.12: Graphical pseudo-code of standard time step procedure. Image adapted from (Kreft, Booth et al. 1998, Valentina Gogulancea, González-Cabaleiro et al. 2019). Here concentrations present in each grid are diffused into surrounding grid spaces, and variables within growth equations are updated. If an agent is below minimum size, the cell death occurs, and if greater than division size, then agents are divided. Both minimum and division parameters are specified by the user.

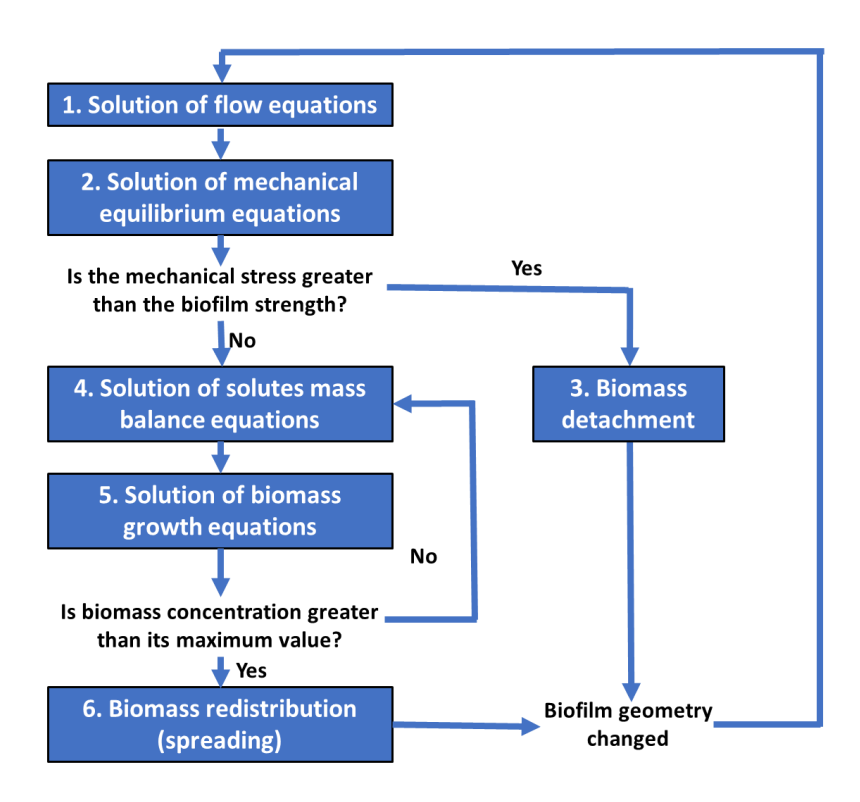


Figure 2.13: Flow chart of biomass growth and detachment under flow stresses. Figure adapted from (Picioreanu, Loosdrecht et al. 2000).

Although a range of applications exist in literature, a particular package, iDynoMiCs, was selected for the availability and customisability (Kreft Group 2015). This Java-based application is readily accepting of multiple species and capable of tailoring an environment composed of specific nutrients. In the current form, whilst it is able to accept inhibiting kinetic equations, it does not consider the removal of agents when in contact with an antibacterial and would therefore require modification to be fit for purpose.

## 2.7.2 Examples of model adaptation

Models can adapt and evolve to be fit for purpose, and a few examples are outlined here. For instance, the exponential growth phase was replaced with expressions for population growth (Logistics, Gompertz, and Bertalanffy), and were found to compare well with experimental data (Verotta, Haagensen et al. 2017). Further from this, the action of a bacteria limiting agent was considered, finding that the number of dead cells follows closely to experimental results,

which is promising, even considering the large variability of live/dead cells within the data (Verotta, Haagensen et al. 2017).

Biofilm growth models were initially developed to simulate the growth of one bacterial species, however various groups have considered multiple species within the environment. Even interactions between two species can become lengthy processes as the number of interactions increases. For example spatial organisation, how the metabolic activities of multiple species interact, and the synergistic and antagonist effect of competing species is at the forefront of interest within growth modelling (Liu, Sørensen et al. 2016). Two competing bacterial populations of supragingival plaque that were distinct in nature have previously been modelled (Martin, Tamanai-Shacoori et al. 2017). The two species are pathogenic and non-pathogenic, both competing for the sole glucose source, but express dominant growth at different time periods (early, or late). These were not labelled as specific bacteria, but rather varied within given parameters of threshold of cell division, width of daughter cell mass ratio, etc. (Head, Marsh et al. 2014). Taking primary colonisers and pathogens of *S. gordonii* and *P. gingivalis* respectively, the mathematical agent-based model and experimental results showed qualitative agreement (Martin, Tamanai-Shacoori et al. 2017).

More complex interactions between the species have also been simulated through quorum sensing (QS) (inter-bacteria communication). The implementation of QS allows bacteria to follow nutrient rich areas of the simulation, whilst avoiding more toxic areas (Niu, Wang et al. 2013).

In specific relation to the oral environment, the growth of bacteria can be affected by individual diet. For example, an increase or decrease of specific sugars could, in theory, affect the growth of glucose consuming bacteria such as *P. gingivalis* (Koshy-Chenthittayil, Archambault et al. 2021). Further, an introduction of inhibitory reagents could inadvertently provide nutrients for bacterial growth and should therefore be modelled appropriately.

Current mathematical models lack the capacity to describe the biofilm-surface interaction (Verotta, Haagensen et al. 2017). Previous studies have considered substrates that are both inhibitory and nutrient sources (Andrews 1968), or simply inhibitory (Esser, Leveau et al. 2015).

However, these studies did not suitably model a diffusing inhibitory source such as an antibacterial membrane.

Multiple species biofilm models have been reported previously (Gregory, Vlachos et al. 2005, Martin, Tamanai-Shacoori et al. 2017), but their representation in a top-down orientation in the presence of a diffusing inhibiting reagent is lacking. This would offer the possibility to simulate the growth of bacterial strains with different growth conditions (e.g., *S. aureus* and *P. gingivalis*, which need aerobic and anaerobic conditions, respectively), which are difficult to cultivate together in the lab.

## 2.8 Prospects of Novel GBR Techniques

The use of an interdisciplinary approach allows for a multifaceted solution to the challenges facing potential dental implant failure. An alternative to antibiotic use has been of recent interest, and there is clear need to parameterise potential biomaterials as due to the lack of consistency between studies (Deyno, Mtewa et al. 2019). There is also a lack of studies on the interaction of bioactive compounds with cells responsible for regeneration (e.g. osteoblasts) (Wang, Feng et al. 2022), which would directly impact the length and quality of healing.

The mechanics of how bioactive compounds would adhere to a barrier membrane surface via LbL has broadly been considered previously (Yassin, German et al. 2016), however the utilisation of this proof of concept has not been undertaken. Specifically, how this antibacterial membrane would interact with bacterial strains and mammalian cells, and how bioactive compounds who diffuse from the membrane over time has not been considered.

Experimentation is a labour-intensive effort and is lacking a clear hypothesis testing capability when considering inhibiting or bactericidal reagents. Current iterations perform multiple bacterial species (Head, Marsh et al. 2014, Martin, Tamanai-Shacoori et al. 2017), and inhibiting agents (Verotta, Haagensen et al. 2017), however a diffusing membrane in a top down orientation that mimics membrane placement onto an agar plate has not been studied. The introduction of a computational element that could consider a novel approach to agent-

based modelling with the inclusion of an inhibiting membrane would allow a user to provide an ideal membrane composition *in silico* with minimal input from *in vitro* experimentation. These approaches provide multiple novel insights into the process of bioactive compound selection, *in vitro* and *in silico* analysis. The result of which seeks to provide a framework for deriving an ideal membrane for use in the oral cavity during the healing time following GBR surgery.

## CHAPTER 3 MATERIALS AND METHODS

#### 3.1 Introduction

This chapter presents the primary methodologies employed in this PhD thesis. Specifically, this chapters details the broad range of protocols used in the three distinct areas and will be referred to for concision throughout this project. In brief, the topics covered here are protocols on:

- bacterial and tissue cultures to identify how selected compounds would interact with the environment when placed in an oral cavity,
- engineering techniques employed when fabricating electrospun membranes and functionalising via layer-by-layer assembly,
- the series of protocols used to simulate agent-based models that would inform the design of an ideal membrane.

#### 3.2 Materials

Tea tree essential and castor oils were purchased from Holland & Barrett; Lemon Essential Oils was purchased from Jade Bloom; Pectin (from citrus peel), Polycaprolactone (PCL, Molecular weight = 80 kDa), Hexamethylenediamine 98% and Polyallylamine hydrochloride (PAH, Molecular weight = 50 kDa), sodium acetate buffer and sodium chloride (NaCl) were provided by Sigma-Aldrich, UK. Manuka Honey (MGO 400 and 550+) was purchased from Manuka Health, US. MGO 400 and 550+ are a measure of the methylglyoxal content present in the Manuka Honey, measured in mg/kg. All solvents were of analytical grade and used with no further purification. They were all purchased from Sigma Aldrich, UK.

Where mammalian cell response is analysed, human neonatal fibroblasts (passage 10, supplied by ThermoFisher, UK), and osteoblasts (hFOB1.19, passage 3) (obtained as a gift from Dr John Taylor, Newcastle) were fit for purpose as these were responsible for tissue and bone growth during oral cavity wound healing and would allow a reflection of proliferation *in vitro* (Tsuchida and Nakayama 2023).

For bacteria, *Staphylococcus aureus* (*S. aureus* NCTC6571) and *Porphyromonas gingivalis* (*P. gingivalis* W50) are used to analyse a broad range of bacterial types, each offering distinct Gram-stain responses, and anaerobic and aerobic growth conditions (both bacterial strains derived from stock provided by Ekaterina Kozhevnikova at Translational Oral Biosciences, Newcastle University). They are also appropriate for the proposed oral environment as *S. aureus* is found in 43% of peri-implantitis cases (Persson and Renvert 2014), and *P. gingivalis* has associations with periodontitis (How, Song et al. 2016).

**Manuka Honey:** Manuka Honey 400 and 550+ were mixed with distilled water into a concentration of 30% wt/v (300 mg/mL, Methyglyoxal content, MGO<sub>400</sub>: 120 mg/kg, MGO<sub>550+</sub>: 165 mg/kg), this was then serially diluted further to create concentrations of 25%, 20%, 15%, 10%, and 5% wt/v. When added to well assays, the working concentrations would be 5.0% (50 mg/mL, MGO<sub>400</sub>: 20 mg/kg, MGO<sub>550+</sub>: 27.5 mg/kg), 4.2% (42 mg/mL, MGO<sub>400</sub>: 16.8 mg/kg, MGO<sub>550+</sub>: 23.1 mg/kg), 3.3% (33 mg/mL, MGO<sub>400</sub>: 13.2 mg/kg, MGO<sub>550+</sub>: 18.15 mg/kg), 2.5% (25 mg/mL, MGO<sub>400</sub>: 10 mg/kg, MGO<sub>550+</sub>: 13.75 mg/kg), 1.6% (16 mg/mL, MGO<sub>400</sub>: 6.4 mg/kg, MGO<sub>550+</sub>: 8.8 mg/kg), and 0.8% wt/v (80 mg/mL, MGO<sub>400</sub>: 3.2 mg/kg, MGO<sub>550+</sub>: 4.4 mg/kg). The upper limit of these working concentrations were chosen as cyrogels containing 5% Manuka Honey were sufficient in inhibiting bacteria (Hixon, Bogner et al. 2019).

Each concentration was mixed on an IKA C-MAG HS7 magnetic stirrer (Sigma-Aldrich, UK) for 10 minutes at 45°C and adjusted with 1.0M HCl and NaOH from a pH of between 3 and 4, to a pH of 5.5. A pH of 5.5 was used in this case as it has been reported previously that low acidic solutions promote wound healing and increase the antibacterial activity (Nagoba, Suryawanshi et al. 2015).

**Essential Oils:** Both Tea Tree and Lemon Oils were mixed at low concentrations in distilled water to a final concentration range of 1.0, 0.5, 0.25, 0.1, 0.05, and 0.01 % wt/v and vortexed for 5 minutes. When added to well assays, the working concentrations would be 0.167% (1670  $\mu$ g/mL), 0.083% (830  $\mu$ g/mL), 0.042% (420  $\mu$ g/mL), 0.017% (170  $\mu$ g/mL), 0.008% (80  $\mu$ g/mL), and 0.002% wt/v (20  $\mu$ g/mL). These are chosen to cover the range of inhibitory concentrations

seen in previous studies, noted between 0.02% wt/v (200 μg/mL) (Frassinetti, Caltavuturo et al. 2011) and 0.22% wt/v (2200 μg/mL) (Shapiro, Meier et al. 1994).

Where a change in pH was required (e.g. Zeta Potential analysis), solutions were adjusted using hydrochloric acid (HCl) and sodium hydroxide (NaOH). These were added dropwise using a glass pipette, and continually monitored using a pH Meter F20 (Mettler Toledo, Switzerland).

## 3.3 Electrospun membrane preparation and surface functionalisation at the nanoscale

## 3.3.1 Preparation

Polycaprolactone electrospun membranes were fabricated utilising a protocol refined by Camilla Gallo, visiting MSc student from Politecnico di Torino, Italy. A 17.5% wt/v PCL solution was prepared by dissolving PCL in a 1:1 mixture of acetic acid and formic acid. The solution was mixed on an IKA C-MAG HS7 magnetic stirrer (Sigma-Aldrich, UK) overnight in a fume hood.

The PCL solution was loaded into a syringe and placed into the Spinbox platform and syringe feeding system (Bioinicia, Spain), and dispersed onto the collector surface charged at 16 kV at a rate 600  $\mu$ l/hour from a nozzle-collector distance of 12 cm. Solution was extruded out of nozzle and electrospun for 2 h, the resultant membrane was left to set overnight in a fume cupboard. Then, the membrane was removed from collector plate using tweezers. To avoid contamination from bacteria or alteration of the mechanical properties of the membranes, each were stored in a dark, low moisture area until further use.

## 3.3.2 LbL- assembly functionalisation

The electrospun membranes were chemically functionalised by aminolysis following the protocol reported by Ferreira et al. (Ferreira, Gentile et al. 2016) to positively pre-charge the surface to allow the further LbL assembly functionalisation (see Section 2.6.2). Briefly, the membranes were submerged in 0.05 M Hexamethylenediamine (dissolved in isopropanol) for 15 minutes and rinsed in distilled water 3 times before being left to dry overnight.

The aminolysed electrospun membranes were dip-coated using the layer-by-layer machine developed at Newcastle University (Patent WO 2021/079106) (Newcastle University 2021). Dip coating was utilised here as it is considered the gold standard of layer-by-layer coating (Richardson, Björnmalm et al. 2015). The membranes were clamped and lowered into a polyanionic solution (a solution containing negatively charged groups) containing 20% wt/v (200 mg/mL) Manuka Honey 550+ dissolved in sodium acetate buffer for 10 minutes (forming the first coating nanolayer), followed by a 5-minute dip rinse in sodium acetate buffer used as washing solution. Then, the membranes were immersed in a polycation solution containing 1% wt/v PAH for 10 minutes (forming the second nanolayer) and rinsed in the sodium acetate buffer for 5 minutes. This was repeated as desired up to 14 monolayers and left to dry overnight. All the polyelectrolyte solutions were adjusted to a final pH of 5 to stabilise their charge as reported in literature (Mancuso, Tonda-Turo et al. 2019) The membranes were then left to dry overnight, and then cut with a scalpel to 1 cm x 1 cm for further testing. Membranes were stored as noted in Section 3.3.1 until required.

## 3.4 Physico-chemical characterisation

#### 3.4.1 Zeta-Potential

The zeta-potential of all polyelectrolyte solutions (e.g. Manuka Honey solutions) were analysed using the Litesizer 500 (Anton Paar) device. The measurements were carried out in 1 mL cuvettes, where the set parameters were an equilibration time of 120s, 15 runs at room temperature (25°C) and scattering angle of 173°. All the measurements were repeated three times.

# 3.4.2 Fourier Transformed Infrared Spectroscopy with attenuated total reflectance (FTIR-ATR)

FTIR-ATR analysis was conducted to investigate the functional groups on the surface of the samples. Measurements were obtained with a Spectrum Two PE instrument equipped with a horizontal attenuated total reflectance (ATR) diamond crystal (PerkinElmer Inc., USA). Data were collected in Absorbance mode, with wavenumber values ranging from 4000 cm<sup>-1</sup> to 550 cm<sup>-1</sup> considering 16 scans for each spectrum (resolution 2 cm<sup>-1</sup>).

## 3.4.3 X-Ray photoelectron spectroscopy (XPS)

X-ray photoelectron spectroscopy is a quantitative technique that allows measuring the elemental composition at the surface of a material, and also it is useful to determine the binding states between the elements (carbon, nitrogen, and oxygen specifically).

The samples were examined by a scanning microprobe Kratos Axis Ultra-DLD XPS spectrometer (EPSRC Harwell XPS Service Cardiff, UK), equipped with a monochromatised AIK $\alpha$  X-ray radiation source. The base pressure in analysis chamber was  $10^{-9}$  m bar. Samples were analysed in High Power mode with an X-ray take-off angle of 45° (scanned size~1400 × 200  $\mu$ m). For each specimen, survey scans (Fixed Analyser Transmission mode, binding energy (BE) range 0–1200 eV, pass energy 117.4 eV) and high-resolution spectra (FAT mode, pass energy 29.35 eV) were acquired of C1s. Atomic concentration (measured in At.%) on the survey scan were performed using the built-in CasaXPS software package. Subsequently, in order to detect the Binding Energy (BE) representing the chemical binding states of the each elements within the films, the XPS spectra for the chemical elements detected from the films were subjected to peak deconvolution using the same software.

## 3.4.4 Scanning Electron Microscopy

Functionalised LbL membranes were imaged under Scanning Electron Microscope. Membranes were mounted onto stands and sputter coated with gold. These were subsequently loaded into the JSM-IT510 SEM microscope (JEOL Ltd., Tokyo), and imaged at four magnifications (13000x, 7500x, 5000x, and 2500x) at random positions across membrane surface. Diameter of fibres were measured using ImageJ, taking at least 20 measurements at three magnifications.

## 3.4.5 Manuka Honey in vitro release

To understand how the Manuka Honey is released over time, functionalised membranes were placed in 3 mL Phosphate buffer saline solution (PBS) in 12 well plates. These were kept at

37°C. At intervals of up to 21 days, 1 mL of PBS was collected and retained, and fresh 1 mL of PBS was added to the well. These samples were tested for MGO content as these could provide correlation to the quantity of manuka honey released, using an ab241006 MGO Assay Kit (Abcam, UK).

For methylglyoxal content, the contents of the MGO Assay kit were prepared as stated to create a suitable Reaction Mix,  $80~\mu L$  of which was added to each well. A Background Mix was prepared as stated and added to background control wells of PBS buffer only and were incubated at room temperature for 2 hours. Absorbance was then measured using a Synergy HT microplate reader (Biotek Instruments, Vermont) at 450 nm and MGO content calculated via standard MGO curve (see

$$Sample\ MGO\ content = \frac{MGO\ Content\ in\ Standard\ Curve}{Sample\ volume\ added\ to\ reaction\ well} \cdot Dilution\ Factor$$

## 3.5 In vitro bacterial tests

## 3.5.1 Bacteria culture

*S. aureus* was routinely cultured in Brain-Heart Infusion (BHI) broth containing 38 g/L BHI powder (Melford, UK), dissolved in distilled water with stirring. BHI agar was created by adding 15 g/L Bacto-Agar (Melford, UK) to the broth. Growth media were sterilised by autoclaving at 121 °C 15 psi. 20 mL of liquid agar were added to polystyrene petri dishes (Fisher Scientific, UK) and allowed to set inside a laminar flow hood. To create a Yeast Extract variant (BHI(Ye)), 5g/L Yeast Extract (Formedium, Hunstanton) was added to the BHI broth. Broth solutions were aliquoted into 20 mL glass universal bottles and autoclaved.

For routine culture of *P. gingivalis*, Fastidious Anaerobic Broth (FAB) was prepared containing 29.7 g/L dissolved Fastidious Anaerobe Broth powder (Neogen, Ayr), aliquoted into 20 mL universal glass bottles and autoclaved at 121 °C. To create Fastidious Anaerobic Agar (FAA), 15 g/L Bacto-Agar (Melford, Ipswich) was added to FAB prior to autoclave. Once autoclaved at 121 °C, liquid agar was cooled in a water bath to 50 °C to prevent coagulation before adding

25 mL/L of defibrinated horse blood (TCS Biosciences, Buckingham) and mixed well. 20 mL of this liquid agar were poured into polystyrene petri dishes and allowed to cool inside laminar flow hood.

*S. aureus* was grown at 37 °C in a Genlab incubator (Genlab, UK) for 12-18 hours, and *P. gingivalis* was grown at 37 °C in a Whitley DG 250 incubator (Don Whitley Scientific, Bingley) for 3-5 days. Antibiotic controls used for *S. aureus* NCTC6571 were vancomycin at concentrations of 0.01% wt/v (0.1 mg/mL) while for *P. gingivalis* W50 chlorhexidine at concentrations of 0.2% v/v (2 mg/mL) was used.

## 3.5.2 Zone of inhibition assays

Solutions containing Manuka Honey and Essential Oils were prepared accordingly;

 Manuka Honey: Manuka Honey 400 and 550+ (Holland & Barrett, UK) were mixed with distilled water on an IKA C-MAG HS7 magnetic stirrer (Sigma-Aldrich, UK) into a final concentration of 30% wt/v, this was then serially diluted further to create concentrations of 25, 20, 15, 10, and 5% wt/v.

Each concentration was mixed on a magnetic plate stirrer for 10 minutes at 45°C and titrated with 1.0M HCl and NaOH to a pH of 5.5.

Essential Oils: Both Tea Tree Oils (Holland & Barrett, UK) and Lemon Oils (Jade Bloom, Utah) were mixed at low concentrations in distilled water on an IKA C-MAG HS7 magnetic stirrer (Sigma-Aldrich, UK) to a final concentration range of 1.0, 0.5, 0.25, 0.1, 0.05, and 0.01% wt/v and vortexed on a Whirlimixer vortex mixer (Fisher Scientific, UK) for 5 minutes.

In all cases, where a change in pH was required, solutions were titrated using hydrochloric acid (HCl) or sodium hydroxide (NaOH). These were added drop-wise using a glass pipette, and continually monitored using a pH Meter F20 (Mettler Toledo, Switzerland).

Overnight cultures of bacteria were adjusted to 0.5 OD<sub>595</sub> via broth dilution using the Spectrophotometer Biochrom Libra S11 (Biochrom Ltd., UK). OD<sub>595</sub> here is the optical density of a solution measured at a wavelength of 595 nm. Optical density is used to estimate the amount of bacterial colony forming units/mL present in a solution. 0.5 OD<sub>595</sub> here is roughly 4 x 108 CFU/mL (Couto, Chen et al. 2018). 100 μL of the bacterial broth were placed onto agar plates and spread evenly using a sterile L-shaped spreader. Plates were left to dry for up to 30 minutes and divided into 4 quarters. Autoclaved 8 mm cork borers were used to bore wells into 2 quarters of the agar to allow for reagents and negative controls (see Table 3.1). Sterilised 5 mm diameter Whatman filter paper discs (Sigma-Aldrich, St. Louis) were placed onto the third quarter, to allow placement of 1 µL of positive controls; Vancomycin 0.01% wt/v was used for S. aureus, and Chlorhexidine 0.2% v/v was used for P. gingivalis. For negative controls, sugar solutions were used for Manuka Honey with comparable sugar concentration. This was to assess the effect of the high sugar content of the solutions on the bacterial colonies. The fourth quarter was left blank to confirm homogenous plate growth. See Figure 3.1 for layout. Where Essential Oils were used, glass petri dishes (Sigma-Aldrich, UK) were substituted in place of polystyrene, as preliminary studies saw essential oils dissolving polystyrene plates. Castor Oil was used as negative controls for EOs as this has been used as a medium in Tea Tree Oil dilutions previously and has no apparent effect on the antimicrobial efficacy (Thomsen, Hammer et al. 2013).

Table 3.1: Table of Reagents with negative controls.

Reagent	Negative Control
Manuka Honey 400, Manuka Honey 550+	Sugar equivalent (% wt/v) sugar solution;
	Concentration <sub>MH 400</sub> = $0.821$
	Concentration <sub>MH 550</sub> = $0.8$
Tea Tree Oil	Castor Oil (Undiluted)
Lemon Oil	Castor Oil (Undiluted)

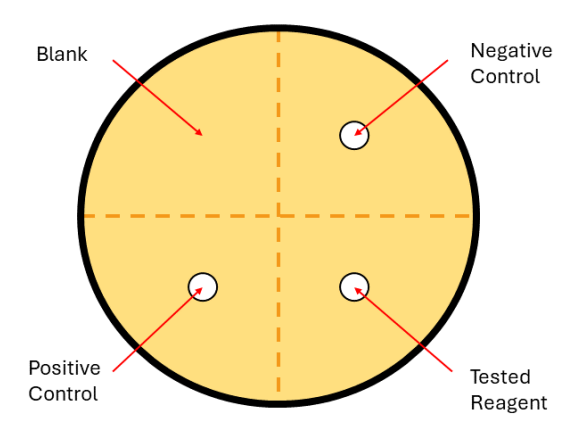


Figure 3.1: Petri Dish layout used in Zone of Inhibition assays, showing control and reagent placement.

The plates were incubated at 37 °C as reported in Section 3.6.1. Resultant zones of inhibition were measured across their diameter at their widest point, where an even circle could be traced.

# 3.5.3 Minimum Inhibitory and Bactericidal Concentration Assays of the starting antibacterial agents

Methods used were adapted minimum inhibitory concentration assays detailed by Li et al. (Li, Cai et al. 2019) and in ISO 20776-1:2019 (British Standards Institution 2020). In a 24 well plate,  $100~\mu L$  of  $0.5~OD_{595}$  cultured bacteria were added to  $400~\mu L$  of nutrient broth in each well.  $100~\mu L$  of tested samples were added to these wells and mixed, leading to a final bacterial concentration of  $0.08~OD_{595}$  (approximately  $10^7~CFU/mL$ ). Antibiotic controls used for *S. aureus* NCTC6571 were vancomycin at concentrations of 0.01%~wt/v while for *P. gingivalis* W50 chlorhexidine at concentrations of 0.2%~v/v were used.  $500~\mu L$  of nutrient broth was placed in separate well, defined as uncultured broth, and untreated culture were negative control wells (see Figure 3.2). Wells were incubated at parameters according to Section 3.2. Following incubation,  $100~\mu L$  of each sample were transferred in triplicate to a 96-well plate and the

optical density was measured at 595 nm in a microplate reader (Synergy HT; BioTek, Vermont). After subtracting absorbance values from uncultured broth well (i.e. growth medium), minimum inhibitory concentrations were identified as the lowest concentrations of tested samples that inhibited bacterial growth, defined when the measured optical density was significantly lower than untreated bacterial growth wells.

To identify minimum bactericidal concentrations (MBC), a serial dilution of wells that were identified as Minimum Inhibitory Concentrations were taken. 10  $\mu$ l droplets of serial dilutions from  $10^{-2}$  to  $10^{-7}$  were plated in triplicate and incubated (see Section 3.5 for suitable agar plate composition and incubation conditions). These colonies could then be counted and extrapolated to CFU/mL and compared to control plates. Samples were considered bactericidal should they reduce the CFU/mL by >99.9% of negative control well (Clinical and Laboratory Standards Institute 1999).

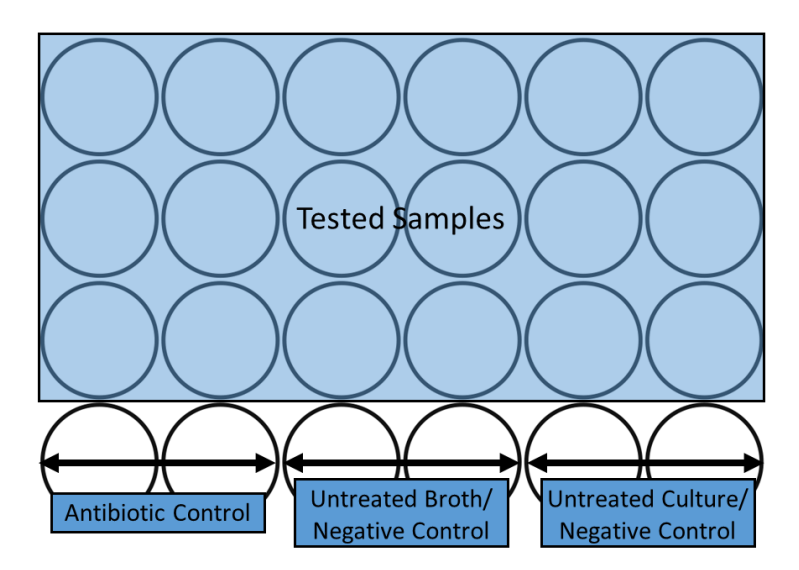


Figure 3.2: Well layout for minimum inhibitory concentration assays, showing antibiotic controls and two negative controls using inoculated and non-inoculated nutrient broth (untreated culture and untreated broth respectively). Note tested samples were tested in duplicate.

# 3.5.4 Membrane antimicrobial properties

LbL-functionalised and PCL membranes were loaded into a 24 well plate with 100  $\mu$ l of 0.5 OD<sub>595</sub> cultured bacteria. Nutrient broth was added to a total of 500  $\mu$ l/well and incubated according to appropriate parameters (see Section 3.5).

Membranes were removed and rinsed briefly in PBS to remove nutrient broth and scraped using a cell scraper. The resultant mixture was resuspended in 500  $\mu$ L of nutrient broth before performing serial dilution. 10  $\mu$ l droplets of serial dilutions from 10<sup>-2</sup> to 10<sup>-7</sup> were plated in triplicate and incubated further according to Section 3.5. These colonies could then be counted and extrapolated to CFU/biofilm and compared to control plates. Membranes were considered antimicrobial when they significantly reduced the CFU/biofilm in comparison to untreated bacterial growth wells.

#### 3.6 In vitro cellular tests

#### 3.6.1 Cell culture

Fibroblasts and osteoblasts play a key role in the wound healing process (e.g. extra cellular matrix production and bone deposition), and for this reason were used to understand the effect of the bioactive compounds during the wound healing process.

The neonatal human dermal fibroblasts were cultured using Dulbecco's Modified Eagle Medium (DMEM) containing 1 g/L glucose (Scientific Laboratory Supplies Limited, UK), supplemented with a 0.2  $\mu$ m filter sterilised solution of 1% v/v Penicillin-Streptomycin (P/S), 1% v/v L-glutamine, and 10% v/v of foetal bovine serum (FBS). The cells were grown at 37 °C in an MCO-18M incubator (Sanyo Electric Biomedical, Tokyo) overnight to 80% confluency.

The osteoblasts were cultured in F12 HAM Dulbecco's Modified Eagle's Medium containing 2.5 mM L-glutamine (Sigma, St. Louis), supplemented with 10% v/v FBS, and 5 % v/v P/S. The cells were grown at 37 °C in a Class II Safety Cabinet, Bioair SafeFlow 1.2 (VWR, Pennsylvania) for up to 5 days until 80% confluency reached.

# 3.6.2 Cytocompatibility tests

In brief, fibroblasts were exposed to Manuka Honey and Essential Oil dilutions in 24 well plates at concentrations of 1 x  $10^5$  cells/mL in appropriate cell culture media. Then, PrestoBlue (PB) assay was used to assess cell viability and proliferation; the reagent changes colour based on the metabolic activity of the cells becoming fluorescent. These assays were carried out at specific time points. PB solution was filtered into DMEM media 1:10% v/v and vortexing. The media was removed from the wells and washed with sterile PBS and then PB solution was added to cover well base (200  $\mu$ L). A control of PB solution was added to separate well as a blank. The multi-well plates were incubated at 37 °C for 2h covered with foil. Triplicates were taken from each sample and each time point (24 and 48 hours for fibroblasts, 3 and 5 days for osteoblasts). The results were analysed using the FLUOstar Omega MicroPlate Reader (BMG Labtech), measuring the fluorescence (560 nm excitation and 590 nm emission). After the measurements, the PB solution was completely removed from the wells, the wells were washed two times with PBS, then fresh media was added, and the culture proceeded until the following time point.

Furthermore, Live/Dead® Assays were performed at specific time points. This assay allows the discrimination of the cell population thanks to a simultaneously stain of the viable cells (blue) and the dead cells (green). The solution was prepared according to the manufacturer instructions. Briefly, 10  $\mu$ L of calcein-AM (acetoxymethyl) solution and 5  $\mu$ L of propidium iodide solution were added into 5mL of PBS and vortexed. The final solution was put onto the wells in a thin layer. The wells were incubated for 30 minutes and then the results were read using fluorescence microscopy (EVOS M5000, Thermo Fisher).

# 3.6.3 Osteoblast calcification assay

To establish osteoblast functionality, a modified method of those used by Korbut et al. was provided by Jamie Coulter, Newcastle University (Korbut, Włodarczyk et al. 2021). Osteoblasts at concentration of 1 x  $10^5$  cells/mL were added to 24 well plates, and Osteoblast Mineralisation Medium (Sigma-Aldrich, UK) was added and used as a growth medium to a total volume of 500  $\mu$ l before being incubated in a Class II Safety Cabinet, Bioair SafeFlow 1.2

(VWR, UK) for 1-2 hours to allow acclimatisation of cells to growth medium. Afterward, 100  $\mu$ L of 5-30 % w/v Manuka Honey dilutions were added to each well and incubated for 7, 14, 21, and 28 days, with media change occurring every 3 days. At relevant time points, nutrient broth was aspirated from well assays and rinsed with PBS, and subsequent alizarin red staining was conducted to dye calcium deposits left by osteoblasts (see Section 2.2.1). Alizarin red staining (Sigma-Aldrich, UK) and quantification was achieved as follows.

Cells were fixed with 200  $\mu$ L Paraformaldehyde (4 %) and incubated at 37 °C, 5% CO<sub>2</sub> for 30 minutes in a Multi Purpose Benchtop Incubator (Genlab, UK). These were subsequently removed and gently washed with distilled water. Well plates were stored at 3-5 °C until needed for up to 28 days if 100  $\mu$ L PBS was added wells. When required, PBS was removed completely and 500  $\mu$ L of Alizarin Red Staining Solution was added. Wells were incubated at in the dark at room temperature for 60 minutes with gentle shaking. The dying solution was removed and washed 4 times with distilled water. An extended 10-minute wash of PBS solution was also applied and completely removed. These well plates were then imaged macro- and microscopically. These was stored for up to 28 days at -20 °C prior to dye extraction for quantification purposes.

To quantify calcium deposits, 200  $\mu$ L acetic acid (10 %) was added to each well and incubate at room temperature for 30 minutes with shaking. Each well was then scraped to collect the cells and transferred with solution into 2.0 mL Eppendorf tubes. Samples were vortexed briefly and then heated to 85 °C for 10 minutes and cool on ice. Then, Eppendorfs were centrifuged in a SLS Eppendorf micro centrifuge (Eppendorf, Germany) at 20,000 rpm for 15 minutes and supernatant was transferred to new Eppendorf. The pH was adjusted to between 4.1 and 4.5 before being placed into 96-well plate in triplicate for absorbance measurement (405nm).

#### 3.7 iDynoMiCs 2.0

iDynoMiCs 2.0 is the second iteration of the iDynoMiCs software package that uses agent-based modelling to calculate growth kinetics of bacteria. Within this PhD thesis, it has been manipulated to provide a framework for the design of an ideal membrane.

IDynoMiCs is capable of accepting multiple species within an environment of varied nutrients. However the kinetics calculations used can become exponentially complex. For this reason, the following parameters and assumptions were defined in order to mimic the oral environment whilst limiting computing time.

- 1. *P. gingivalis* and *S. aureus* parameters (e.g. growth rate and cell size) were used in order to better qualitatively compare any output *in silico* and *in vitro*. Whilst the cell size was used, all bacteria cells were assumed to be spherical.
- 2. At initialisation, all cells are deposited evenly across surface.
- 3. Only the agent growth, division and spreading are considered.
- 4. Spreading can only occur through the physical interaction of surrounding agents as each agent is assumed to be immobile.
- 5. When splitting occurs, the mass of the two subsequent agents are equal (Kreft, Picioreanu et al. 2001).
- 6. When multiple bacteria were used, these were non-competitive and did not share nutrients in the environment.
- 7. The environment is boundaried and two-dimensional.
- 8. The initial concentration of nutrients is similar to that seen on an agar plate.
- 9. When multiple nutrients and antibacterial concentrations are used, these do not interact.
- 10. Where variable parameters were used, the upper and lower range bound the expected parameter evenly.

General modelling design is discussed in CHAPTER 2, however an iDynoMiCs specific description is given here. It is the intention to model agent growth in the presence of a diffusing membrane. Agents will grow consuming the surrounding nutrient (S, pg/ $\mu$ m<sup>3</sup>), however their growth will be inhibited according to the concentration of inhibitor (I, pg/ $\mu$ m<sup>3</sup>).

At each time step the growth is given by

$$substrate(S) + cells(X) \rightarrow extracellular\ products(P) + cells(nX)$$
 Eq 3.2

this reaction is balanced using the yield ratio

$$Y = \frac{dX}{dS} = \frac{Biomass\ produced}{Substrate\ consumed}$$
 Eq 3.3

where Y is the yield. At each time step the modified growth rate (in an inhibiting environment) is given by

$$\mu = \mu_{max} \frac{S}{K_S + S} \cdot \frac{I}{I + K_I}$$
 Eq 3.4

where  $\mu$  is the growth rate (minute<sup>-1</sup>),  $\mu_{max}$  is the maximum growth rate (minute<sup>-1</sup>), S is the substrate concentration,  $K_S$  is the half saturation coefficient for the substrate (pg  $\mu$ m<sup>-3</sup>), I is the inhibitor concentration, and  $K_I$  is the half saturation coefficient for the inhibitor.

At each time step, the component concentrations diffuse in simulation space. For each component, *i*, the diffusion-reaction equation is given by

$$\frac{\partial C_i}{\partial t} = D_i \left( \frac{\partial^2 C_i}{\partial x^2} + \frac{\partial^2 C_i}{\partial z^2} \right) + r_i$$
 Eq 3.5

where  $C_i$  is the concentration at incremental time step  $\partial t$  (minute), at grid cell coordinates given by x and z.  $D_i$  is the diffusion coefficient of the component ( $\mu m^2$ /minute), and  $r_i$  is the reaction rate (Kreft, Picioreanu et al. 2001). This differential equation is solved with a numerical method (Rosenbrock).

The following section details specific operation of the iDynoMiCs module and modification of the software package.

#### 3.7.1 Running a simulation

iDynoMiCs was initiated in Eclipse IDE for Java Developers (Version: 2022-06 (4.24.0)) as both a running platform, and as a modification toolset.

iDynoMiCs utilises a library of class files to create and populate and environment in tandem with input parameters from individual protocol files. At initialisation, the software will look for specific classes and their tags and define associated user inputs accordingly. And then will run procedurally according to the graphical representation given in Figure 2.12.

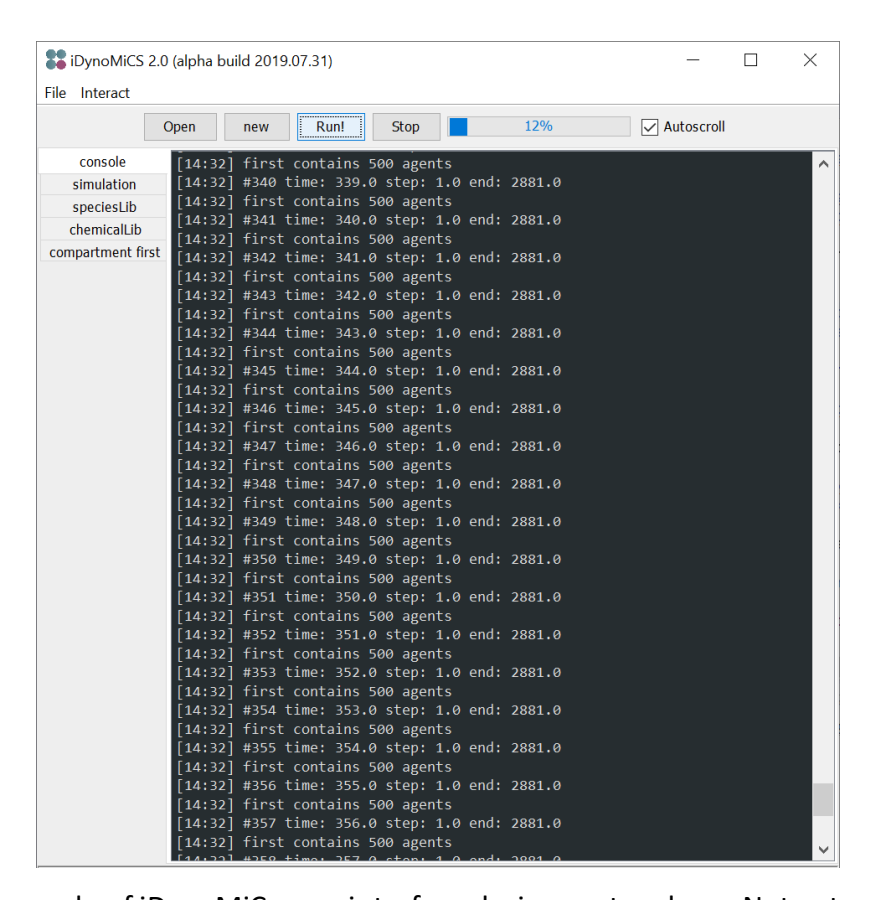


Figure 3.3: Example of iDynoMiCs user interface during protocol run. Note at each timestep outputs current number of agents.

# 3.7.2 Defining environment

Calling upon protocol files, environments are populated as defined by user, with specified environment size, dimension, and initial nutrient composition. It is possible to define multiple nutrient concentrations dependent on agent(s) present. For example, a two-agent system that requires four different nutrients for growth can be placed in an environment with four unique nutrients distinguished using different name tags. In addition, should any number of agents share nutrients, these can also be stipulated by repeat name tags.

Although a single value input is determined to be every grid cell (i.e. initial homogenous environment), it can be specified for each grid cell by inputting an array for concentration (see Figure 3.4 for example). A MATLAB function was developed to create a specific matrix of nutrient composition.

Figure 3.4: Example code that composites two nutrients (A and B) outputting a 2x3 matrix, both with the same nutrient concentration.

# 3.7.3 Populating environment

The grid cells are populated by randomly assigning each bacterium (hereafter referred to as "agent") to a free space within a defined area. For example, in a 100  $\mu$ m<sup>2</sup> area, the user could define 100 agents distributed randomly in a specified region.

The agents have defined mass (pg) and shape (e.g. coccoid) that has specified parameters, or parameters that are calculated internally (see Figure 3.5).

```
<species name="coccoid">
    <!-- pg / um^3-->
                                      type="PRIMARY"
    <aspect name="density"</pre>
                                                                                                  value="1.1" />
                                                               class="Double"
     <aspect name="#isLocated"</pre>
                                      type="PRIMARY"
                                                               class="Boolean"
                                                                                                  value="true" />
     <aspect name="surfaces"
                                       type="CALCULATED" class="AgentSurfaces"
                                      type="PRIMARY"
     <aspect name="morphology"
                                                               class="String"
                                                                                                  value="coccoid" />
                                      type="CALCULATED" class="String"
type="CALCULATED" class="SimpleVolumeState"
type="CALCULATED" class="CoccoidRadius"
    <aspect name="volume"
     <aspect name="radius"
    <aspect name="divide"
                                      type="EVENT"
                                                               class="CoccoidDivision"
    <!-- pg -->
    <aspect name="divisionMass" class="Double"
<aspect name="updateBody" type="EVENT"
<aspect name="evaluatePull" type="EVENT"</pre>
                                                               value="2.2"
                                                               class="UpdateBody"
                                                               class="ResolveInteractionDistance"
     <!-- µm -->
    <aspect name="searchDist" type="PRIMARY"</pre>
                                                                                                  value="0.1" />
```

Figure 3.5: Example agent shape defined in the protocol. Note TYPE and CLASS called, including any values that are specified where required.

#### 3.7.4 Growth Kinetics

Agent growth kinetics are defined in protocol files and are given an expression and associated yield of mass per nutrient consumed (

Eq 3.3), the type of growth that occurs, and their rate of decay (see Figure 3.6). At each time step (1 minute), individual agents grow at a rate dependent on the concentration of nutrient present. For each unit of mass, the agent grows, nutrients are consumed as specified. When an agent reaches a specific mass (see **DivisionMass** in Figure 3.5), the agent splits into two equal masses (defined as mother and daughter agents), and are shifted in randomly defined, opposite directions determined within a uniform range equal to or less than half the mother agent's radius (see Figure 3.7).

```
<species name="AOB typeA">
   <aspect name="pigment" type="PRIMARY" class="String" value="RED" />
   <speciesModule name="coccoid" />
   <speciesModule name="producer" />
    <aspect name="reactions" type="PRIMARY" class="InstantiableList">
       <list class="RegularReaction" nodeLabel="reaction"</pre>
       entryClass="RegularReaction" keyClass="String" keyLabel="name">
           <reaction name="growth">
           <!-- Testing inputting P gingivalis constants. -->
               <expression value="mass * mumax *</pre>
                      ( nutrient / ( nutrient + Kp ) )*(Ki/(inhibitor + Ki))">
                   <!-- pg/µm3 -->
                   <!-- Kp value taken from Martin et al. 2017 PLoS One, 12 (3)-->
                   <constant name="Kp" value="6.1609e-3" />
                   <!-- Ki is 0.5* MIC value, Manuka Honey MIC is 5e-3-->
                   <constant name="Ki"</pre>
                                        value="2.5e-3" />
                   <!-- per minute -->
                   <!-- mumax value taken from Martin et al. 2017 PLoS One, 12 (3)-->
                   <constant name="mumax" value="397.2e-5" />
               </expression>
               <stoichiometric component="mass"</pre>
               <stoichiometric component="inhibitor" coefficient="0" />
           <reaction name="decay">
               <expression value="mass * decay">
                   <constant name="decay" value="1.4e-4" />
               </expression>
               <stoichiometric component="mass" coefficient="-1.0" />
           </reaction>
       </list>
   </aspect>
</species>
```

Figure 3.6: Growth kinetics defined for an agent. Parameters used are for *P. gingivalis* with inhibiting factor for Manuka Honey (discussed further in CHAPTER 4).

Spherical agents were chosen for all bacterium. This assumption aimed to simplify the simulation. In addition, when comparing multiple bacteria agent compositions, qualitative comparisons could be made if each agent has the same initial mass, density, and division mass.

A number of requirements are demanded of the model to appropriately simulate *in vitro* work and offer qualitative comparisons. In all cases, care should be taken to appropriately match units. Where no specific units are given, these are inferred given the context or linked files with units, or advised units given in each protocol file.

Figure 3.7: Java Class file determining the shift of two agents at division.

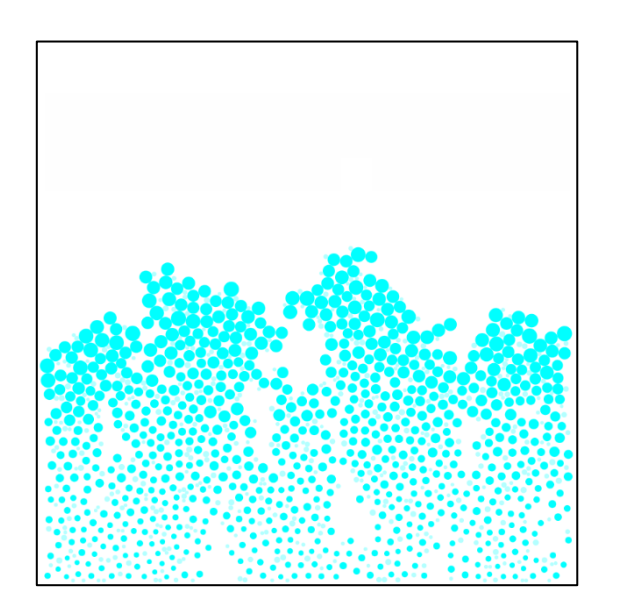
# 3.7.5 Change orientation for top-down simulation

In typical biofilm modelling software, the area of interest is often a cross sectional view to analyse how the biofilm grows upon the surface of a substrate.

However, to align with experimental work on agar plates, where a limited 2-dimensional lawn of bacteria is seen, the simulation had to reflect this appropriately. This orientation has similarities with a cellular automata system, which uses a grid array with that displays agent growth in a binary system (e.g. 0 = No agent, 1 = agent) (Wolfram 1984, Mattei, Frunzo et al. 2018), however this does not consider the agent-agent interaction required of agent based models.

To mimic this orientation, the substrate upon which the agents were populated was removed, allowing for agent placement across entire simulation environment. However, a Java Class file removes any "detached" agents from the simulation. These would be agents that are not connected to the previously seen substrate biofilm. Additionally, there is a constant influx of nutrients from the upper edge of the simulation. Both class files were removed. This means that no agent is removed from the simulation, and no influx of nutrients occurs at any border.

To this end, a simulation is created that appropriately models an agar plate with bacterial lawn (Figure 3.8).



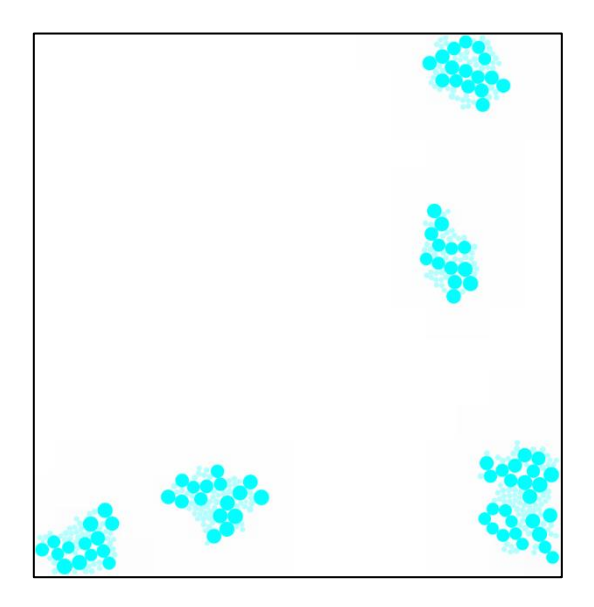


Figure 3.8: 24-hour coccoid agent growth. Left: Typical cross-sectional biofilm growth upon substrate. Right: Top-down, agar plate style simulation.

# 3.7.6 Modelling antibacterial membrane placement

A standard size of membrane is used in all experiments to allow for quantitative comparisons; however an introduction of a simulated membrane would be able to identify optimal membrane size and placement upon an agar plate.

To simulate this, using the assumption that directly underneath any membrane placement would cause instant agent death, an additional class file was created that would remove any agent within a given region. The additional class file; **agentKill**, cycles through all agents present in simulation and identifies their co-ordinate system, and whether this falls within the range of the membrane placement which is defined in the protocol files. A snapshot of a protocol file including an agentKill process is given in Figure 3.9.

Figure 3.9: Example code of agentKill Class File that removes agents that fall within Upper and Lower Ranges. For a 100x100m environment, this agentKill would remove any agents in the North-West Corner (see Figure 3.10).

#### 3.7.7 Diffusion of antibacterial substance and inhibition of bacterial growth

When inputting concentrations, iDynoMiCs first assesses the shape of the value, if it is a matrix, it inputs this appropriately (see Section 3.7.2). This has therefore been exploited this by creating Matlab function that writes an array of size  $i \times j$  with a user prompt for concentration, and membrane size. The output is a protocol compatible string of the form " $c_{11}$ ;  $c_{12}$ ; ...;  $c_{1n}$ % $c_{21}$ ; $c_{22}$ ;... $c_{2n}$ %...; $c_{nm}$ " where % and ; are delimiters.

After initial placement, the concentration will, at each time step, diffuse homogenously outward according to diffusion parameters (Figure 3.10). The diffusion step occurs under **Process Manager> ProcessDiffusion**.java, and the solver utilised is **SolveDiffusionTransient** which extends **ProcessDiffusion**.

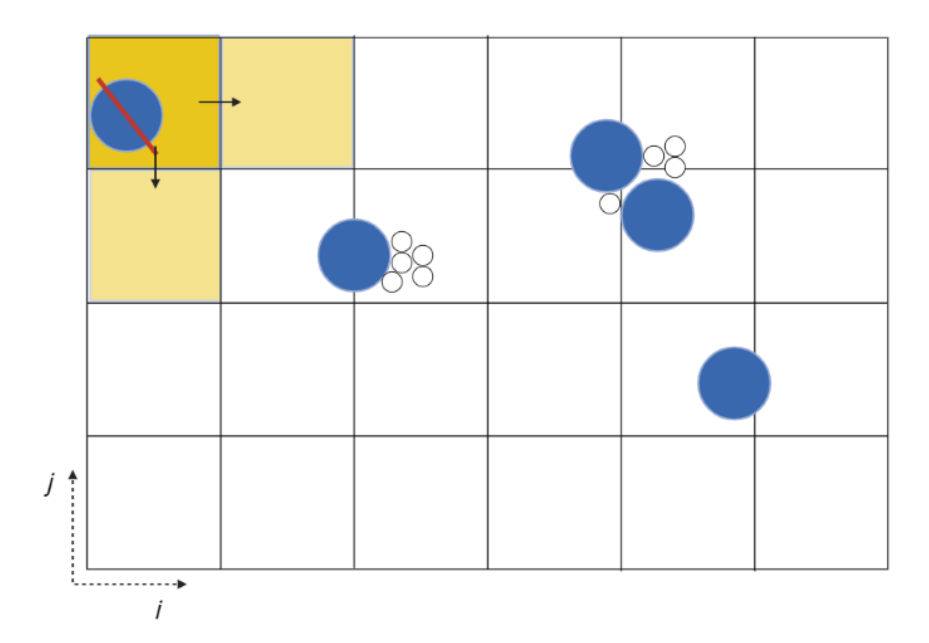


Figure 3.10: Graphical representation of model, where yellow shaded area represents membrane placement, and aligns with protocol file outlined in Figure 3.9. Note that translucent yellow areas show Manuka Honey dispersal from membrane. Blue dots mark bacterial agents, and white dots mark extracellular polymeric substance.

# 3.7.8 Defining parameters

Before outlining methodology, it is first appropriate to discuss how surrounding parameters of the simulation were derived or calculated that are used throughout the remainder of this Section. A summary of these parameters is given in Table 3.2

The diffusion coefficient of the nutrients or inhibitors thorough the simulations is 15-25% lower than that of diffusivity when measured in water (Golmohamadi, Clark et al. 2013). For this reason, when values for diffusivity are used, their corresponding biofilm diffusivity is used as 80% of the original value. Whilst no reference to the units are present in the software package, based on surrounding evidence (units of simulation time step size, and any measurements of distance), the units of diffusivity were inferred as  $\mu m^2/minute$ .

The diffusion of nutrients is assumed to flow from higher to lower grid elements, and agents grow as long as nutrients are present (Horn and Morgenroth 2006, Martin, Picioreanu et al. 2013).

The diffusion coefficient of each batch of Manuka Honey studied was not measured in this thesis and therefore was not compared to literature. However, sugar solutions were found to have diffusion of magnitude of  $10^{-9}$  m<sup>2</sup>/s which, converting to simulation parameters, is  $10^{-4}$   $\mu$ m<sup>2</sup>/minute (Kruk, Masiewicz et al. 2022).

Published work on attempts to model *S. aureus* growth show a magnitude for maximum growth rate of  $10^{-1}$  h<sup>-1</sup> when strains are grown in milk and on rice cake (Le Marc, Valík et al. 2009, Wang, Koseki et al. 2017), which is in agreement with the preliminary results included in APPENDIX 1. Other Staphylococci bacteria, specifically *S. carnosus*, found a value of  $K_s = 34 \times 10^{-3}$  g/L (Maldonado, J Krull et al. 2019), which is of a similar magnitude. Therefore, as the results published were temperature dependent, a nominal value of 82 x  $10^{-2}$  h<sup>-1</sup> at 37°C was selected.

Table 3.2: Model parameters used, with value and units and, where relevant, appropriate references.

Parameter	Value	Comments	
Domain Size	100 μm³		
Number of agents	500	Equivalent to 5 x 10 <sup>8</sup> agents/mL	
Substrate Concentration	56.26 pg/μm <sup>3</sup>	Calculated concentration of 20 mL	
		BHI active nutrients in agar plate	
Initial Manuka Honey	$10^{-1}  \text{pg/} \mu \text{m}^3$	(Mancuso, Tonda-Turo et al. 2019)	
concentration			
Initial agent mass	0.8 x 10 <sup>-3</sup> pg	Assumed via iDynoMiCs software	
Division Mass	2.2 pg	Average mass of bacterium is 1.1 pg	
		(Siu 2003)	
Diffusivity	$1 \times 10^{-4}  \mu m^3$ /minute	(Kruk, Masiewicz et al. 2022)	
P. gingivalis maximum	397.2 x 10 <sup>-5</sup> minute <sup>-1</sup>	(Martin, Tamanai-Shacoori et al.	
growth rate, $\mu_{\text{max}}$		2017)	
P. gingivalis Yield, Y <sub>XS</sub>	0.18	(Martin, Tamanai-Shacoori et al.	
		2017)	
Half saturation coefficient	$6.1609 \text{ x } 10^{-3} \text{ pg } \mu\text{m}^{-3}$	(Martin, Tamanai-Shacoori et al.	
for <i>P. gingivalis,</i> K <sub>S</sub>		2017)	
S. aureus maximum growth	137 x 10 <sup>-4</sup> minute <sup>-1</sup>	Adapted from (Le Marc, Valík et al.	
rate, μ <sub>max</sub>		2009, Wang, Koseki et al. 2017)	
S. aureus Yield, Y <sub>XS</sub>	0.315	(Maldonado, J Krull et al. 2019)	
Half saturation coefficient	$34 \times 10^{-6} \text{ pg } \mu\text{m}^{-3}$	Used half saturation coefficient for	
for <i>S. aureus</i> , K <sub>S</sub>		S. carnosus (Maldonado, J Krull et al.	
		2019)	
Half saturation coefficient	$2.5 \times 10^{-3}  pg  \mu m^{-3}$	Half MIC value, using MIC = 0.5%	
for Manuka Honey inhibitor,		wt/v rounded from CHAPTER 4.	
Kı			

The parameters for agents during growth require half saturation coefficient;  $K_S$ , and maximum growth rate;  $\mu_{max}$ . For *S. aureus*, these were not readily available in published literature. In a preliminary growth study (included in APPENDIX 1), a value of  $K_S$  was found for *S. aureus* to be

#### 3.7.9 Simulation Control Group

A control group using bacterial species without the presence of inhibiting reagents allowed for the qualitative comparisons. This would also give an indication that the parameters for the agents are working as expected.

This was achieved by removing the AgentKill addressed in Section 3.7.6, and the inclusion of inhibiting concentrations detailed at initilisation in Section 3.7.2.

#### 3.7.10 Membrane Placement

Whilst the reagent concentration is an indication of when the appropriate concentration has a measurable outcome, the placement of the membrane would define the 'reach' of the inhibiting solute. As an additional proof-of-concept, membrane placement would indicate whether effective spots maximised inhibiting range greater than mathematical artefacts of the simulation.

To fully realise this, the spatial grid was divided into 9 equally sized regions (see Figure 3.11). For each protocol file, one of these regions was selected as a membrane placement. This would imply that any agents present within the region would be removed ("killed") and the diffusion of the inhibiting reagent would occur from this region. After full simulation run (t = 10080 s), the number of final agents was recorded as the mean over 3 runs.

7	8	9
4	5	6
1	2	3

Figure 3.11: Designated region division. Each grid cell (1 - 9) denotes single membrane placement.

# 3.7.11 Diffusivity

It was hypothesised that a more diffuse reagent would provide greater inhibition of agent growth. To this end, the range of diffusivity was extended to a very diffuse medium;  $0.1~\mu m^3$  per minute, which would encompass the magnitude of saliva diffusivity ( $10^{-2}~pg/\mu m^3$  per minute (Corea-Téllez, Bustamante-Montes et al. 2008)). Saliva here was used to mimic the effect of fully dissolved bioactive compound in the oral cavity.

After 48 hours, the mass per agent was calculated and would give an indication of the impact of diffusion when present at the oral surgical site.

# 3.7.12 Initial Concentration

When considering experimental set up, systemic failures could be avoided by preliminarily checking whether the concentration of reagents present in membrane exhibit a measurable response. At the initialisation of the simulation, the concentrations present in the environment are input. Here this can be akin to the concentration at time t=0, that has diffused into the agar plate. The assumption is made that all inhibiting material is diffused at

once. As time progresses, the inhibiting material will diffuse into the surrounding environment according to Fick's Law of Diffusion.

Whilst a concentration of 0.2 pg/ $\mu$ m<sup>3</sup> was used elsewhere in this simulation, this is a nominal value assumed from the 20 % wt/v Manuka Honey nanolayers. It has been reported that, over 14 days, a measured MGO content was recorded of between 171.5 to 1.9 mg/mL (Mancuso, Tonda-Turo et al. 2019). Although these also report a plateau of concentration after 21 days, the area of interest occurs over a short period of time that can still be considered linear. For this reason, this value was readily translated to a 2-day simulation, and a total concentration of between 24.5 and 0.27 mg/mL (2.5 x  $10^{-2}$  and 2 x  $10^{-4}$  pg/ $\mu$ m<sup>3</sup>) was calculated.

Ten-fold quantities around these two total concentrations were taken;  $2 \times 10^{-2} \text{ pg/}\mu\text{m}^3 \le x \le 2 \times 10^{-6} \text{ pg/}\mu\text{m}^3$ . As the diffusivity was nominal here, it was set to  $10^{-1} \text{ pg/}\mu\text{m}^3$  to highlight any differences more prominently.

# 3.7.13 Multiple bacterial species

The chosen bacterial candidates of *P. gingivalis* and *S. aureus* were used to study the broad range of bacterium parameters such as Gram- positive or negative, and anaerobic or aerobic growth conditions. In experimental situations this ranges from the simple challenges, such as competing Gram-negative and Gram-positive bacteria, to complex experimental challenges, such as anaerobic and aerobic bacteria. In the complex environment of the oral cavity, different bacterial species are able to proliferate. Work using two species biofilm growth has been conducted previously (Martin, Tamanai-Shacoori et al. 2017), however thesis presents the use of two species growth *in vitro* on an agar plate.

An additional bacterial species was added to the *P. gingivalis* agent in previous sections, that mimics the magnitude of a *Staphylococci* bacteria. Where they differ from previous agents, a nominal value for half-saturation coefficient and maximum growth rate were designated as follows;

- $K = 34 \times 10^{-6} \text{ pg/}\mu\text{m}^3$
- $\mu_{\text{max}} = 137 \times 10^{-4} \text{ min}^{-1}$

based on previously preliminary results and published values (see Section 3.7.8) (Maldonado, J Krull et al. 2019). The nutrient concentration is unchanged; however, these are not competing bacteria. A noticeable difference is the limited space available to agents which may benefit a quicker growing bacterium in the short term. This section offers a proof of concept for wider scope outside of the project, and the ability to perform experiments that are difficult or impossible to achieve in a lab space.

# 3.8 Statistical Analysis

Where analysis was conducted on all experimental output, a brief of the analysis was as follows.

Graphs were created using GraphPad Prism version 9.5.0 for Windows (GraphPad Software, San Diego, California USA), and Matlab version R2017a 9.2.0 (MathWorks, California USA). Where image analysis was required ImageJ version 1.53c (Wayne Rasband, National Institutes of Health, USA) was used.

For each protocol, the number of samples (n) were between 2 and 3, and each protocol was repeated a minimum of 2 times (R) where possible. For each data set, when deriving statistical significance between results, after normal distribution is determined, two-way ANOVA was used to confirm statistical significance of results. Where comparisons were required between samples, Tukey's comparison test was used. Both of these statistical tests were calculated using the in-built software in GraphPad Prism version 9.5.0 for Windows (GraphPad Software, San Diego, California USA). Where p-values are cited, statistical significance is noted;  $P \le 0.05$ , \*,  $P \le 0.01$ , \*\*,  $P \le 0.001$ , \*\*\*,  $P \le 0.0001$ , \*\*\*,  $P \le 0.0001$ , \*\*\*.

# CHAPTER 4 EVALUATION OF THE PHYSICO-CHEMICAL AND BIOLOGICAL PROPERTIES OF SELECTED BIOMATERIALS

#### 4.1 Introduction

A number of natural compounds have been identified for their potential as an antimicrobial. Specifically, Manuka Honey (Section 2.6.4), Tea Tree Oil (Section 2.6.6), and Lemon Oil (Section 2.6.7) were all noted to have a broad range of therapeutic properties. Over time, the preparation techniques employed to extract these selected bioactive compounds has improved, increasing consistency between batches (Sarkar, Ghosh et al. 2018).

However, variance can still occur between selected compounds (Mancuso, Catalfamo et al. 2019): Manuka Honey 400 and 550+, Tea Tree Oil, and Lemon Oil. As a result, natural compounds require parameterisation in isolation (i.e. neat and serial dilutions) when exposed to bacteria and mammalian cells to clarify bactericidal and cytotoxic potential.

This chapter seeks to determine whether selected compounds, Manuka Honey MGO 400 and 550+, Tea Tree Oil, and Lemon Oil, are suitable for use in the oral cavity when considered in isolation. This will be achieved by testing their bactericidal and cytotoxic potential, with comparison to published results where possible. Where dilution occurs, distilled water was used as to limit the external factors. A decision will then be reached regarding candidates which are incorporated into electrospun membranes in CHAPTER 5.

Three broad objectives will be addressed:

- Identify Minimum Inhibitory and Bactericidal Concentrations of Manuka Honey 400 and 550+, Tea Tree Oil, and Lemon Oil serial dilutions in water against *S. aureus* NCTC6571 and *P. gingivalis* W50.
- 2. Identify cytotoxicity of above compounds when exposed to mammalian neo-natal fibroblasts, and osteoblasts (hFOB1.19).
- 3. Establish Manuka Honey 400 and 550+ on the ability of osteoblast to deposit calcium.

#### 4.2 Results

# 4.2.1 Zone of inhibition assays to identify bacterial toxicity against *S. aureus* NCTC6571 and *P. gingivalis* W50

Following incubation (24 hours), the diameters of each zone of inhibition were taken using a scale placed on the workbench and read through the agar (n = 3). For some compounds, a circumference of visually distinct *S. aureus* NCTC6571 growth was seen (Figure 4.1). These were measured separately and are plotted alongside the additional outputs in Figure 4.2, made distinct by use of asterisk (\*).

Manuka Honey 400 and 550+, and both Tea Tree and Lemon Oil had similar antimicrobial activity to 0.1 mg/mL antibiotic controls (vancomycin: 16.4±1.1 mm, MH400: 16.9±1.3 mm, MH550+: 19.0±0.7 mm, TTO: 26.2±2.0 mm, and LO: 21.4±2.9 mm). Manuka Honeys exhibited greater inhibition than comparable sugar solutions, and essential oils showed greater inhibition than castor oil.

Manuka Honey 400, Manuka Honey 550+, and two essential oils (Tea Tree and Lemon) were exposed to P. gingivalis W50 and assessed in a similar manner as shown above (see CHAPTER 3). Volumes of selected compounds were added to 8 mm holes bored into agar plate inoculated with P. gingivalis W50. 1  $\mu$ L of 2 mg/mL chlorhexidine was added to 5 mm filter paper discs and used as antibiotic control, castor oil was used as negative control (see Figure 4.3). Following incubation (72 hours), the diameters of each zone of inhibition were taken, with mean and standard deviation (n = 3) plotted in Figure 4.4.

Zones of inhibition greater than 19 mm were observed when Manuka Honey (400 and 550+) was exposed to *P. gingivalis W50* in comparison to 2 mg/mL chlorhexidine solution (chlorhexidine: 8.1±1.2 mm, MH400: 29.1±1.6 mm, and MH550+: 31.3±2.5 mm). Tea Tree and Lemon Oil data not shown as zone of inhibition too large to measure. Further protocols were conducted allowing for a full plate for each replicate, however, this was insufficient in size to quantify any zone of inhibition (>80 mm).

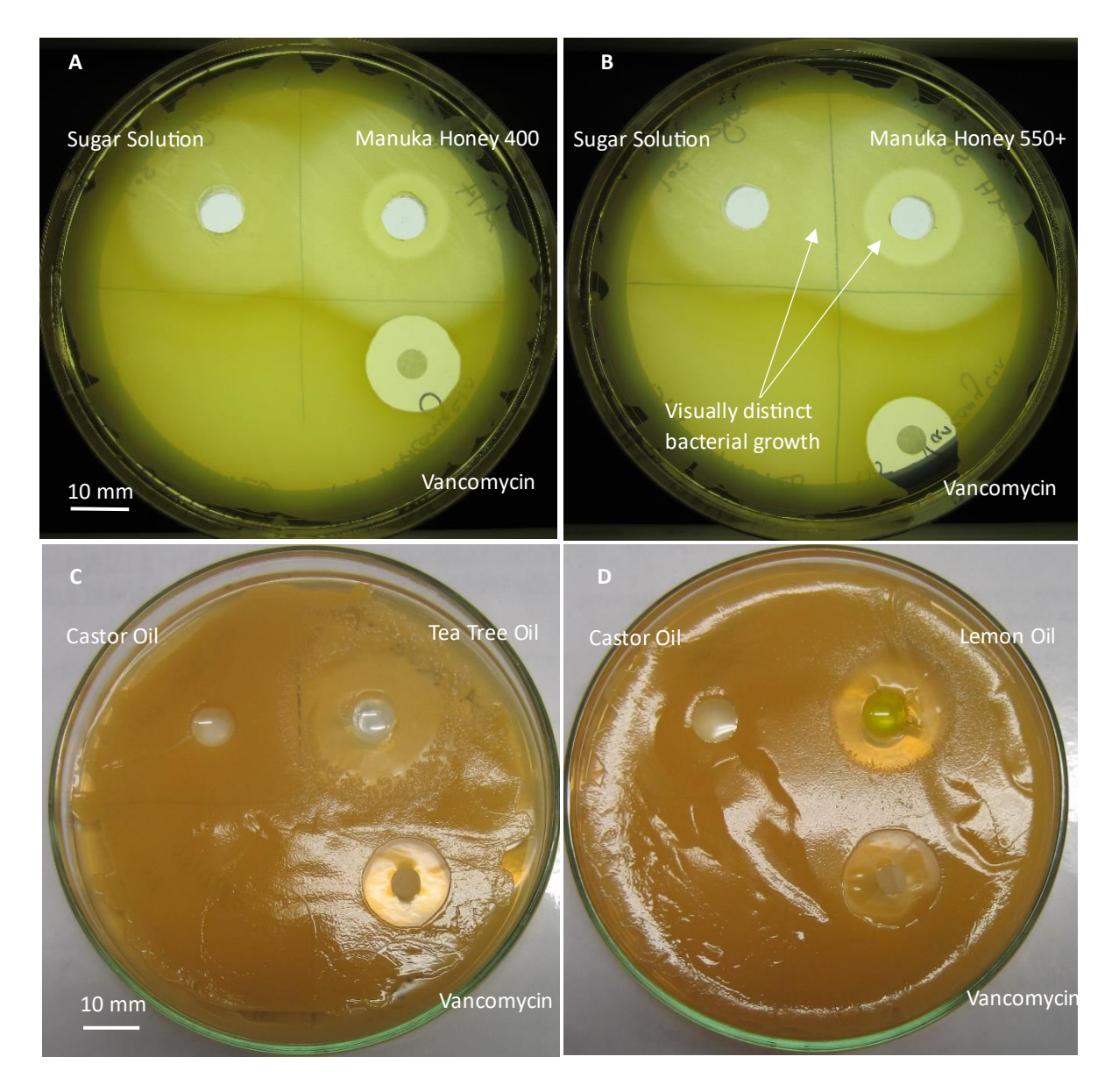


Figure 4.1: *S. aureus* NCTC6571 growth in the presence of Manuka Honey 400 (A), Manuka Honey 550+ (B), Tea Tree Oil (C), and Lemon Oil (D).

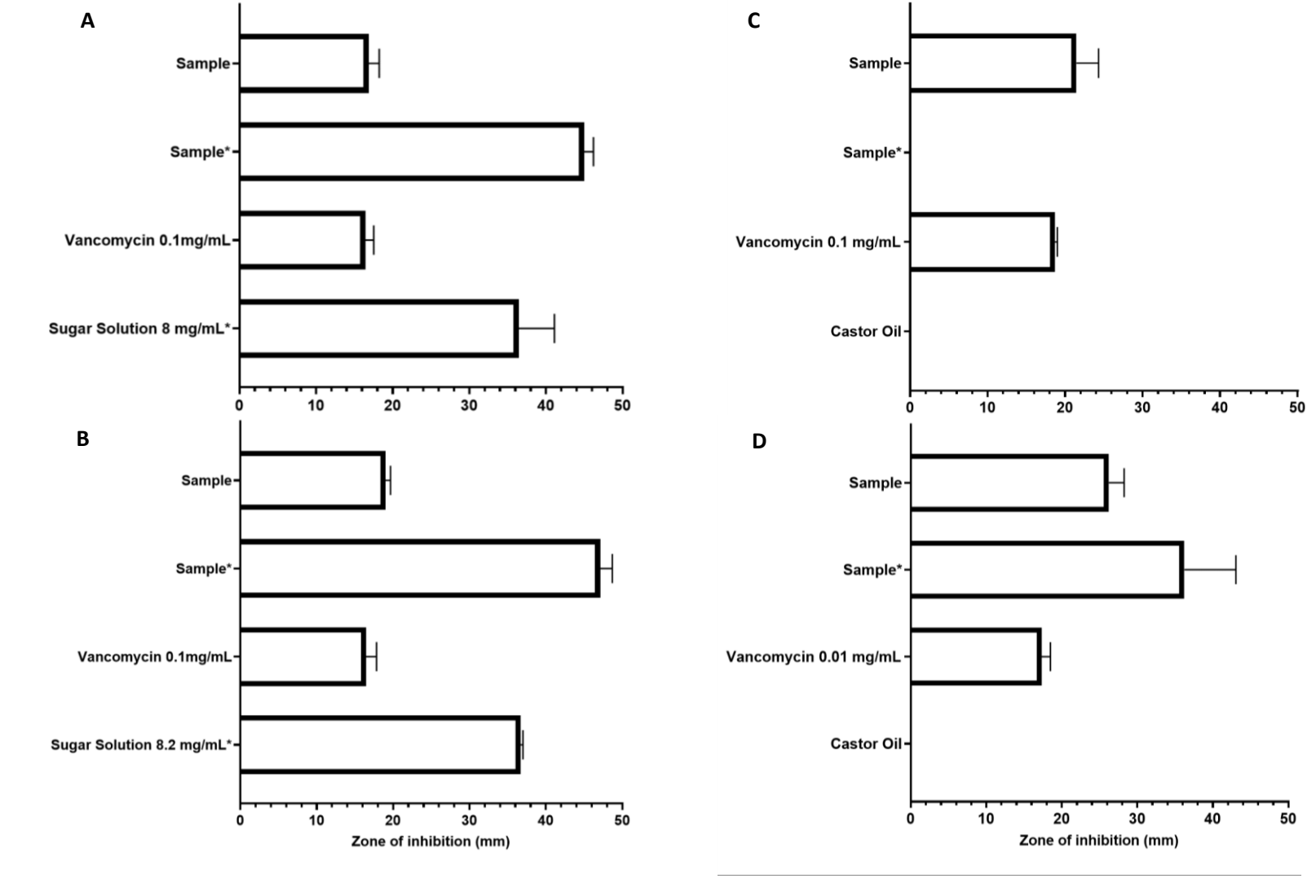


Figure 4.2: Mean zone of inhibition (mm) of *S. aureus* NCTC6571, with standard deviation (n = 3, R=2), measured in prescence of Manuka Honey 400 (A), Manuka Honey 550+ (B), Lemon Oil (C), and Tea Tree Oil (D).

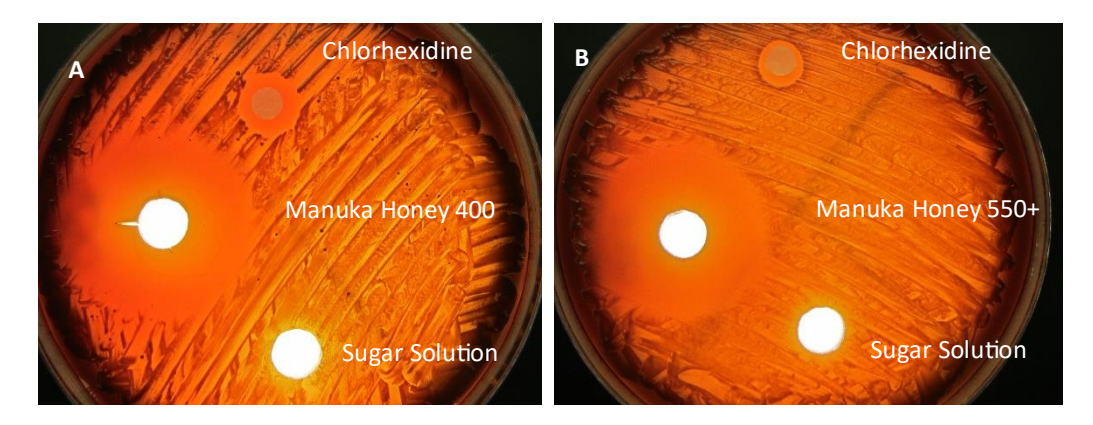


Figure 4.3: *P. gingivalis* W50 growth in the presence of Manuka Honey 400 (A), and Manuka Honey 550+ (B). Tea Tree Oil and Lemon Oil petri dishes not shown as zone of inhibition was too large to measure. 1 µL antibiotic control placed on 5 mm filter disc.

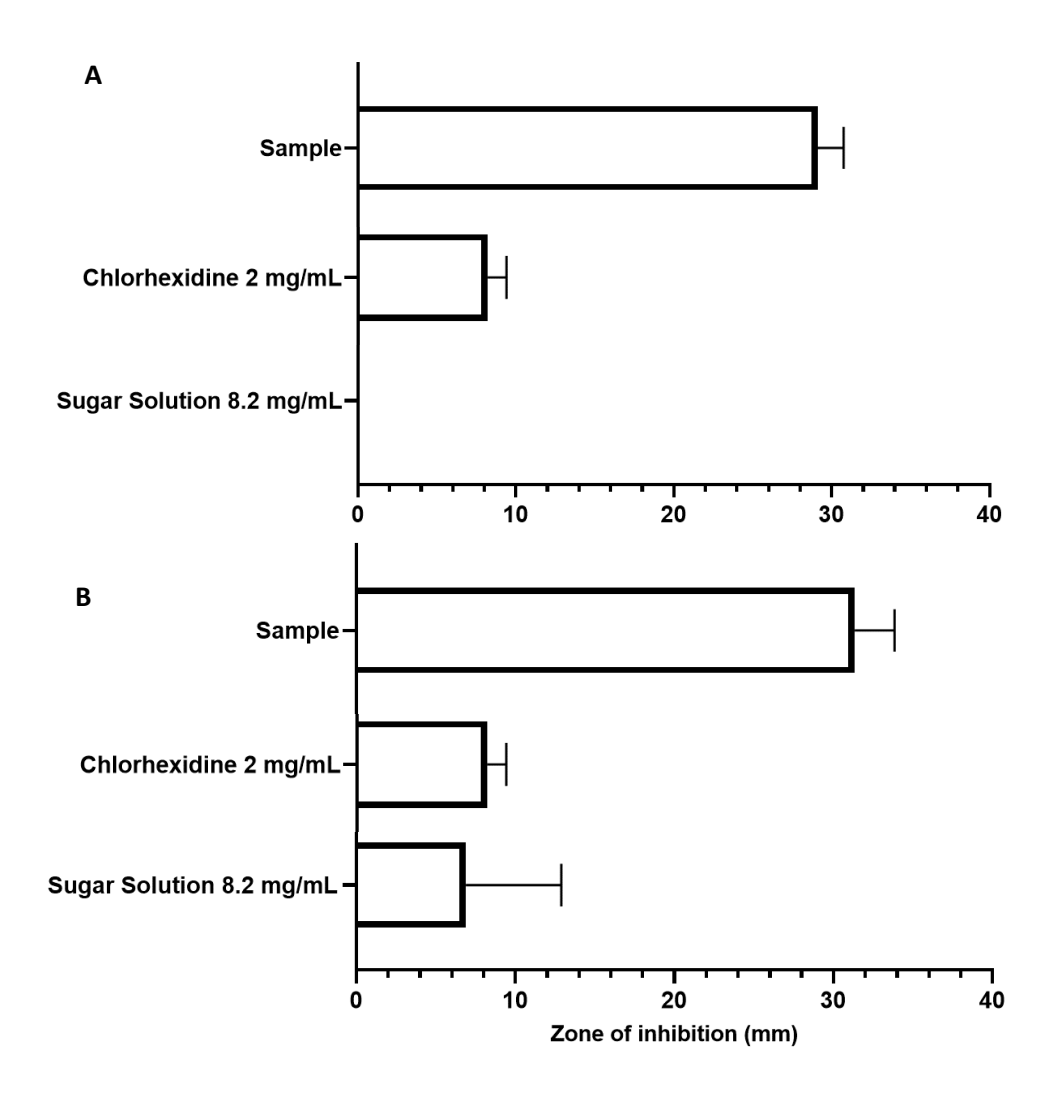


Figure 4.4 Mean zone of inhibition (mm) of *P. gingivalis* W50, with standard deviation (n = 3, R=2), measured in presence of Manuka Honey 400 (A), and Manuka Honey 550+ (B).

# 4.2.2 Minimum Inhibitory and Bactericidal Concentration assays to identify bacterial toxicity against *S. aureus* NCTC6571 and *P. gingivalis* W50

Following incubation (24 hours), the absorbance of wells was measured at a wavelength of 595 nm, with mean and standard deviation (n = 2) plotted in Figure 4.5A. The control wells show absorbance of wells;

- cultured with S. aureus, but no sample present (Untreated Culture),
- uncultured with S. aureus and no sample present (Uncultured Broth), and
- Vancomycin 0.16 μg/mL

Figure 4.5A shows inhibition of *S. aureus* NCTC6571 by Manuka Honey 400 and 550+ in white and black respectively. Both Manuka Honeys showed statistically significant inhibition of *S. aureus* NCTC6571 at minimum concentrations of 8 mg/mL (MH400:  $P \le 0.05$ , \*; MH550+:  $P \le 0.01$ , \*\*).

An increase in bacterial growth was seen at 50 mg/mL in both Manuka Honey compounds, showing a non-linear trend of bacterial inhibition. A second order polynomial curve was fitted to measured absorbance (Figure 4.5B), showing lowest inhibition between 25 and 33 mg/mL.

Tea Tree Oil and Lemon Oil dilutions were also assessed, in a manner as outlined in CHAPTER 3. Following incubation (24 hours), the absorbance of wells was measured at a wavelength of 595 nm, with mean and standard deviation (n = 2) plotted in Figure 4.6.

For both essential oils, a plateau was seen around 0.083 mg/mL, which increased to a level comparable to untreated *S. aureus* NCTC6571 control wells (Untreated culture). Tea Tree Oil showed statistical inhibition of *S. aureus* NCTC6571 at a minimum concentration of 0.008 mg/mL ( $P \le 0.05$ , \*), with parabolic-like activity seen over range measured.

Lemon Oil also exhibited an inhibitory response, albeit greater, whose concentration trendline is parabolic-like. Lemon Oil showed statistically significant inhibition of *S. aureus* NCTC6571 was seen at a minimum concentration of 0.002 mg/mL ( $P \le 0.05$ , \*)

MIC assays were also performed in identical dilutions of selected compounds and exposed to  $P.\ gingivalis$  W50 for 48 hours in well plate assays (see CHAPTER 3). 3.2 µg/mL chlorhexidine was used as antibiotic control, untreated cells  $P.\ gingivalis$  W50 bacteria, and uncultured broth were used as additional controls. Following incubation, the absorbance of wells was measured at a wavelength of 595 nm, with mean and standard deviation (n = 2) plotted in Figure 4.7A.

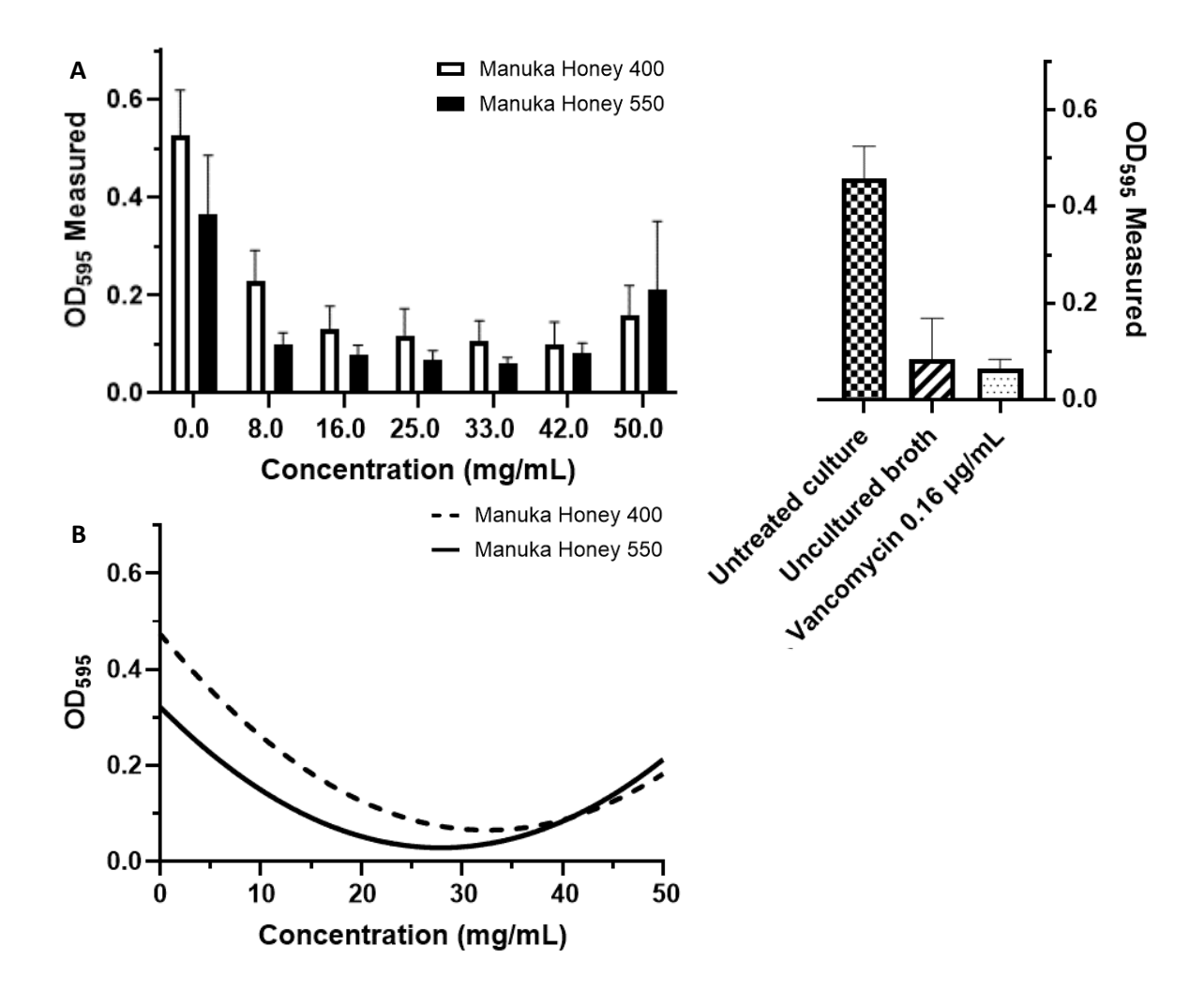


Figure 4.5: (A) Mean absorbance, and standard deviation (n = 2, R=2), measured in well plates (595 nm) of *S. aureus* NCTC6571 inoculated broth solutions, after exposure to dilution of Manuka Honey 400 (white) and Manuka Honey 550 (black). Untreated *S. aureus* NCTC6571 bacteria, uncultured broth, and Vancomycin used as control wells. (B) Second order polynomial fit of Manuka Honey 400 (Dashed) and Manuka Honey 550 (solid), derived using Graphpad. ( $R^2_{MH400} < 0.9$ ,  $R^2_{MH550} < 0.7$ )

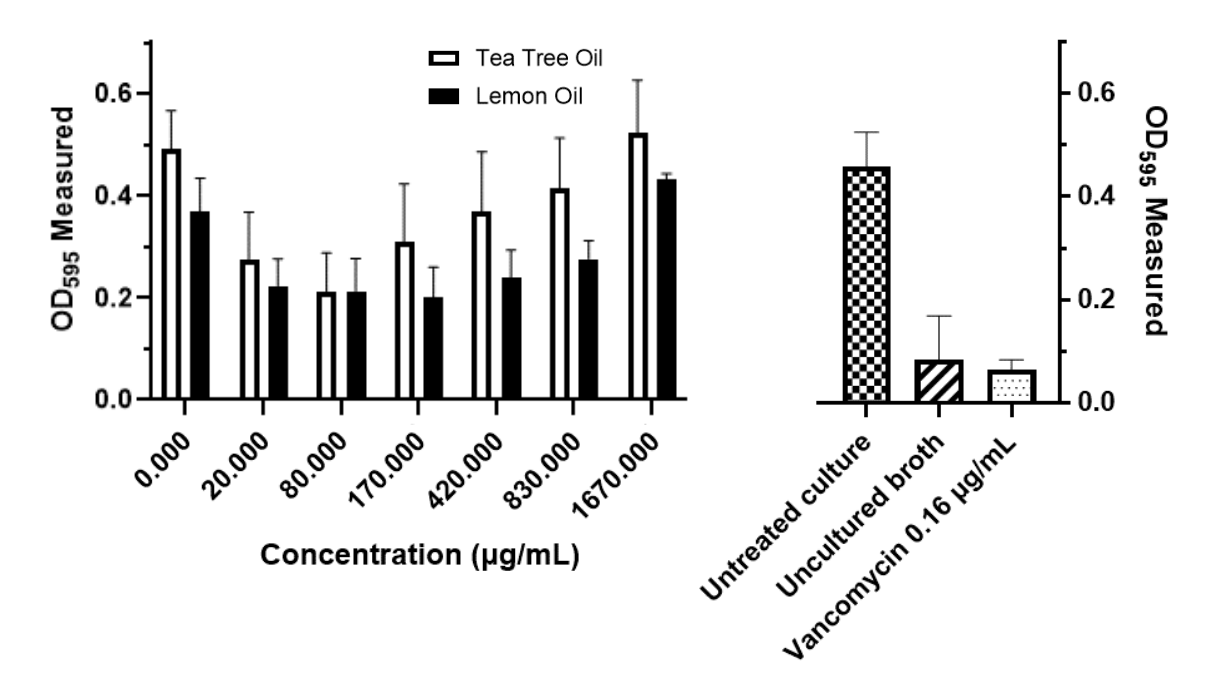


Figure 4.6: Mean absorbance, and standard deviation (n = 2, R=2), measured in well plates (595 nm) of *S. aureus* NCTC6571 inoculated broth solutions, after exposure to dilutions of Tea Tree Oil (white) and Lemon Oil (black). Untreated *S. aureus* NCTC6571 bacteria, uncultured broth, and Vancomycin used as control wells.

As shown in Figure 4.7A, both Manuka Honey types (400 and 550+) show significant inhibition of *P. gingivalis* W50 at a minimum concentration of 8 mg/mL ( $P \le 0.05$ , \*). An exponential decay fit was added (Figure 4.7B), showing strong correlation ( $R^2_{MH400} > 0.9$ ,  $R^2_{MH550} > 0.95$ ), with inhibition of 80% at concentrations of 5 mg/mL for both MH400 and MH550+

Tea Tree Oil and Lemon Oil were exposed to *P. gingivalis* W50 in a manner as mentioned previously. Following incubation (48 hours), the absorbance of wells was measured at a wavelength of 595 nm, with mean and standard deviation (n = 2) plotted in Figure 4.8A. The control wells show absorbance of wells;

- cultured with P. gingivalis, but no sample present (Untreated Culture),
- uncultured with P. gingivalis and no sample present (Uncultured Broth), and
- Chlorhexidine 3.2 μg/mL

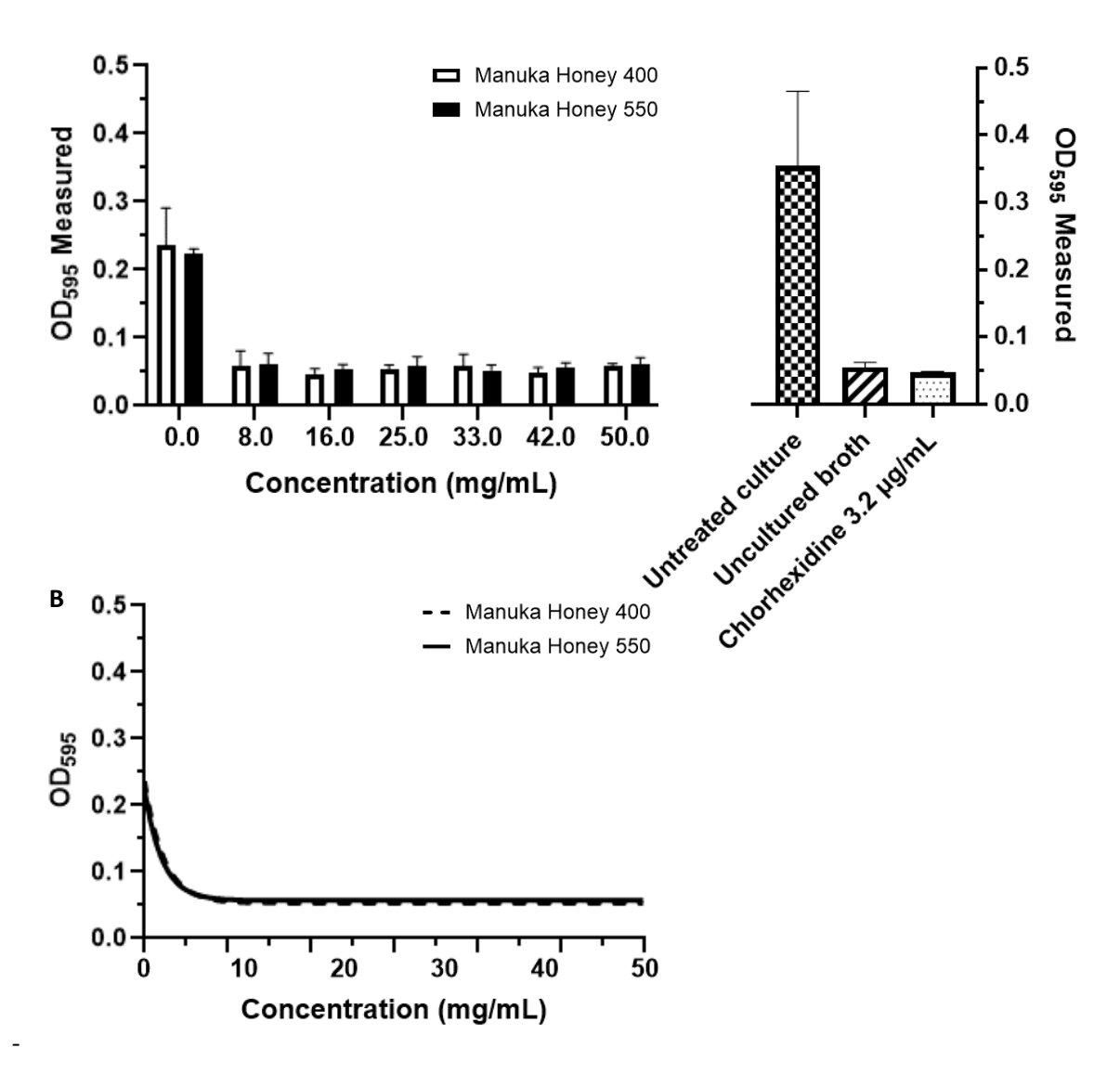


Figure 4.7: (A) Mean absorbance, and standard deviation (n = 2, R=2), measured in well plates (595 nm) of *P. gingivalis* W50 inoculated broth solutions, after exposure to dilutions of Manuka Honey 400 (white) and Manuka Honey 550 (black). Untreated *P. gingivalis* W50 bacteria, uncultured broth, and Chlorhexidine used as control wells. (B) Exponential Decay fit of Manuka Honey 400 (Dashed) and Manuka Honey 550 (solid), derived using Graphpad. ( $R^2_{MH400} > 0.9$ ,  $R^2_{MH550} > 0.95$ ).

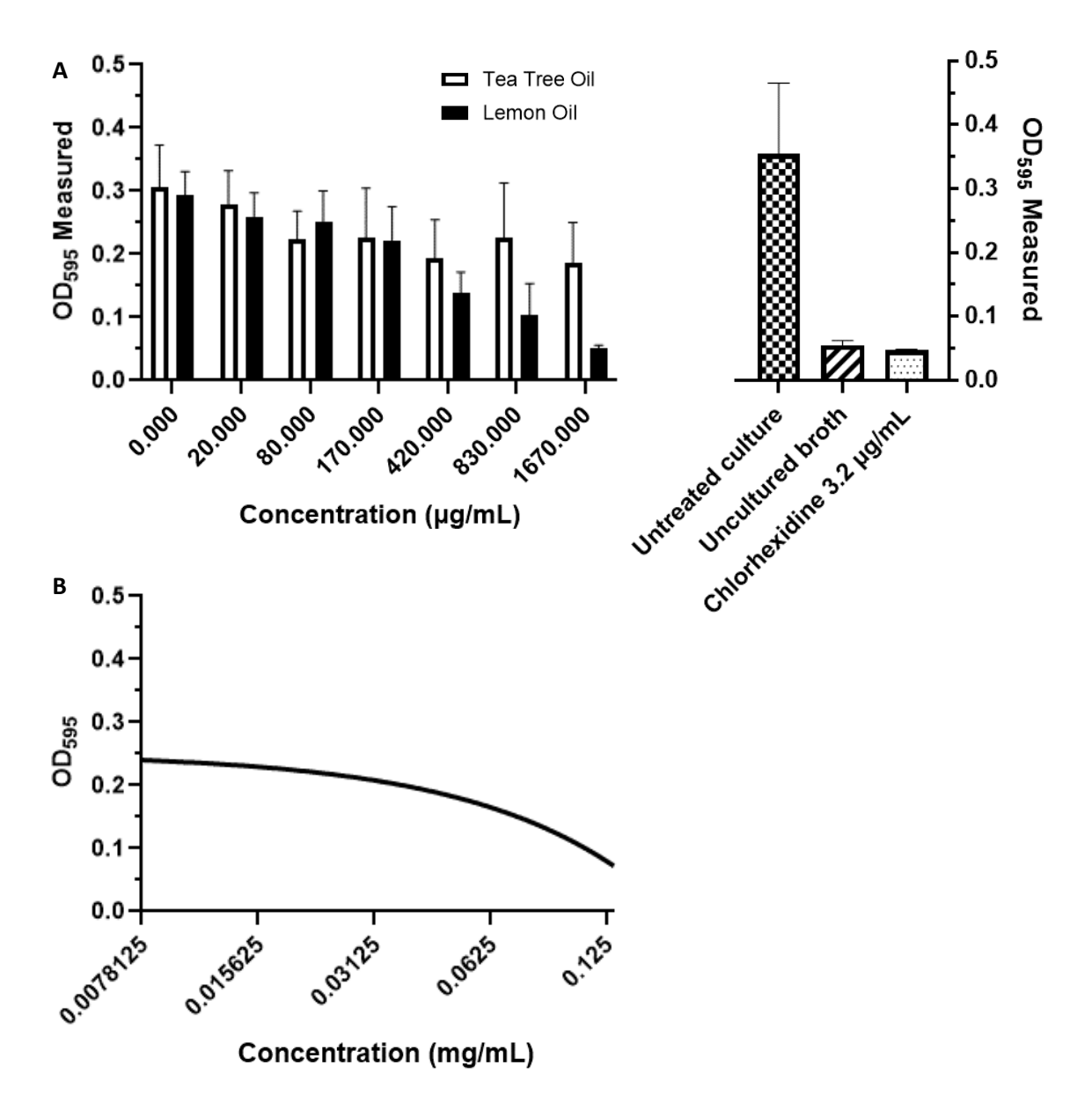


Figure 4.8: (A) Mean absorbance, and standard deviation (n = 2, R=2), measured in well plates (595 nm) P. gingivalis W50 inoculated broth solutions, after exposure to dilutions of Tea Tree Oil (white) and Lemon Oil (black). Untreated P. gingivalis W50 bacteria, uncultured broth, and Chlorhexidine used as control wells. (B) Simple Linear Regression fit of Lemon Oil data ( $R^2 > 0.85$ ). Tea Tree Oil data fit not shown.

Whilst a decrease can be seen in *P. gingivalis* W50 growth (Figure 4.8A), only marginal significance is seen at Lemon Oil concentrations of 1670 mg/mL ( $P \approx 0.055$ ). Curve fitting was utilised for Lemon Oil, which showed good fit ( $R^2 > 0.85$ ). Although initially having no effect, after a threshold is reached, inhibition begins to increase. Interpolating these values, Lemon Oil is hypothesised to provide 85% reduction in comparison to Untreated Culture at

concentrations of between 1100 and 1600 mg/mL. Curve fitting was applied to Tea Tree Oil but results not statistically significant ( $R^2 < 0.45$ ).

Where wells exhibited first signs of inhibitory effects, Colony Forming Units were enumerated via serial dilution onto agar plates (see CHAPTER 3). Following incubation (24 hours), the mean CFU/mL and standard deviation (n = 2) for *S. aureus* NCTC6571 are shown in Figure 4.9, with Untreated Culture and Vancomycin 0.16 µg/mL used as control plates.

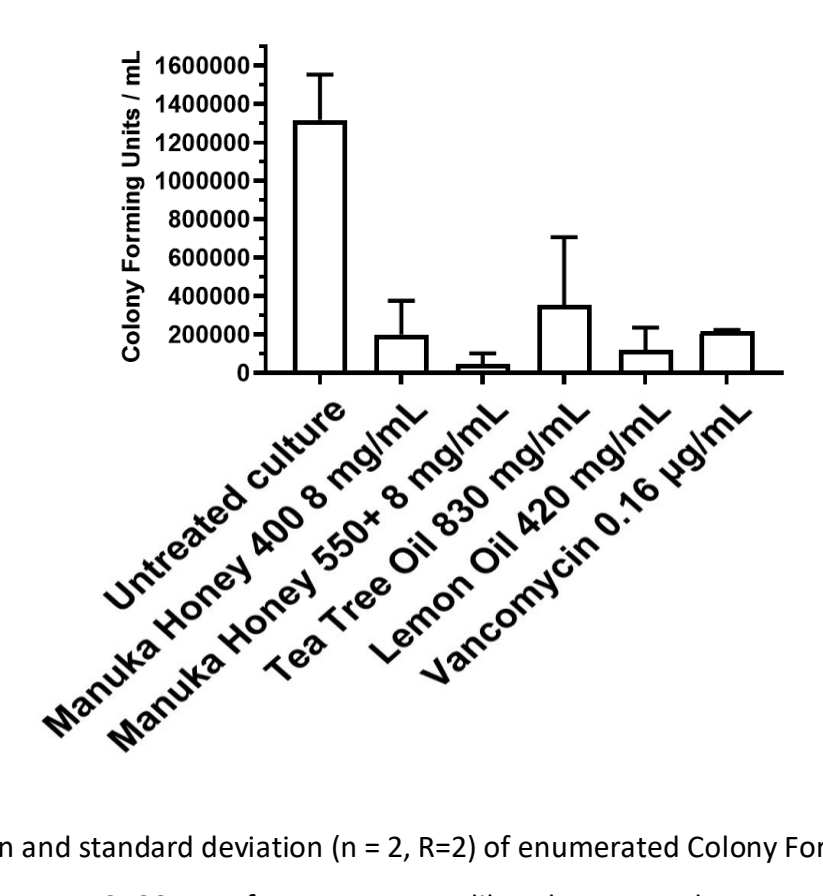


Figure 4.9: Mean and standard deviation (n = 2, R=2) of enumerated Colony Forming Units/mL of *S. aureus* NCTC6571, after exposure to diluted compounds. Untreated *S. aureus* NCTC6571, and Vancomycin 0.16  $\mu$ g/mL used for control plates.

For *S. aureus* NCTC6571, significant reduction in CFU/mL can be seen at minimum inhibitory concentrations. Enumerated CFU/mL in Manuka Honey 400 and Lemon Oil were comparable to antibiotic control, which reduced bacterial growth by 85%.

*P. gingivalis* W50 Colony Forming Units were enumerated in the same manner as outlined above (see CHAPTER 3). Following incubation (72 hours), the mean CFU/mL and standard

deviation (n = 2) was plotted in Figure 4.10. Untreated Culture and Chlorhexidine 3.2  $\mu$ g/mL were used as control plates. It was noted that all compounds at concentrations, were considered bactericidal (bacteria CFU/mL reduced by >99% (Clinical and Laboratory Standards Institute 1999)).

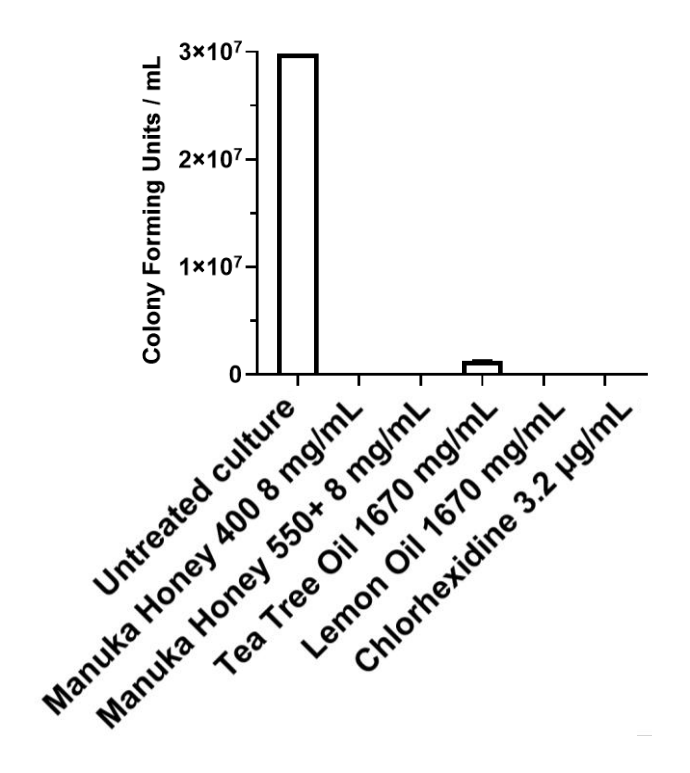


Figure 4.10: Mean of enumerated Colony Forming Units/mL of *P. gingivalis* W50, after exposure to diluted compounds (n = 3, R=2). Untreated *P. gingivalis* W50, and Chlorhexidine used as control plates. Standard deviation plotted but too small to be seen. Image without Untreated Culture found in APPENDIX 1.

# 4.2.3 Cytotoxicity assays to assess toxicity against human neonatal fibroblasts and osteoblasts (hFOB1.19) cells

Cytotoxic assays were conducted on human neonatal fibroblast cells after exposure to Manuka Honey 400 and 550+. Following exposure and incubation (2 hours), resultant solutions were loaded in triplicate into a 96 well plate and measured at an excitation and emission of 530 nm (bandwidth 25nm) and 590 nm (bandwidth 35nm) under fluorescence. Mean and standard deviation (n = 3) of relative fluorescence units (RFU) were plotted in Figure 4.11. Each mean was normalised with untreated human neonatal fibroblast cells and uncultured DMEM used as upper and lower limits respectively.

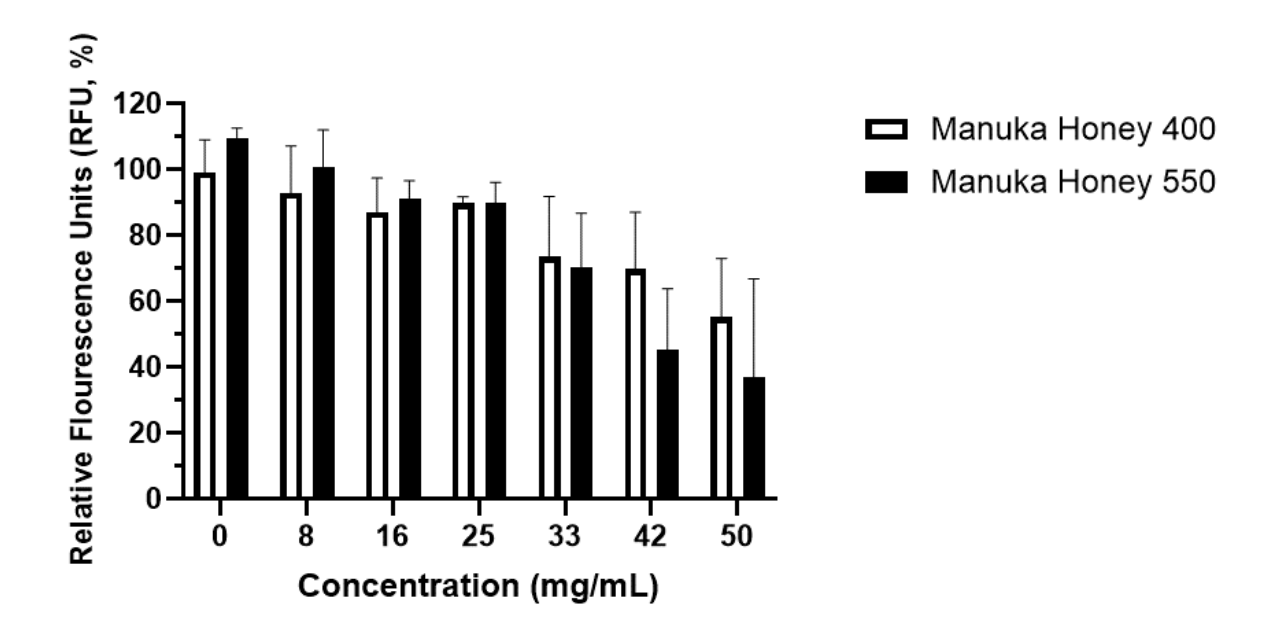


Figure 4.11: Normalised mean Relative Fluorescence Units, with standard deviation (n = 3, R=2), of human neonatal fibroblast cells after exposure to dilutions of Manuka Honey 400 (white) and Manuka Honey 550 (black) in microplate well. Excitation and emission of 530nm (bandwidth 25nm) and 590 nm (bandwidth 35nm). Untreated human neonatal fibroblast cells and uncultured DMEM used as upper and lower ranges.

Manuka Honey 400 showed statistically significant toxicity at 50 mg/mL (RFU =  $2.70\pm0.54 \times 10^5$ ) (P  $\leq 0.01$ , \*\*) in comparison to untreated cells (RFU =  $4.04\pm0.60 \times 10^5$ ). Manuka Honey 550+ had increased toxicity seen at 42 mg/mL (RFU =  $2.40\pm0.55 \times 10^{-5}$ , P  $\leq 0.01$ , \*\*) and 50 mg/mL (RFU =  $2.14\pm0.90 \times 10^5$ , P  $\leq 0.001$ , \*\*\*).

Cytotoxic assays were also conducted on human neonatal fibroblast cells after exposure to Tea Tree Oil and Lemon Oil. Normalised mean and standard deviation (n = 3) Relative Fluorescence Units (RFU) were plotted in Figure 4.12.

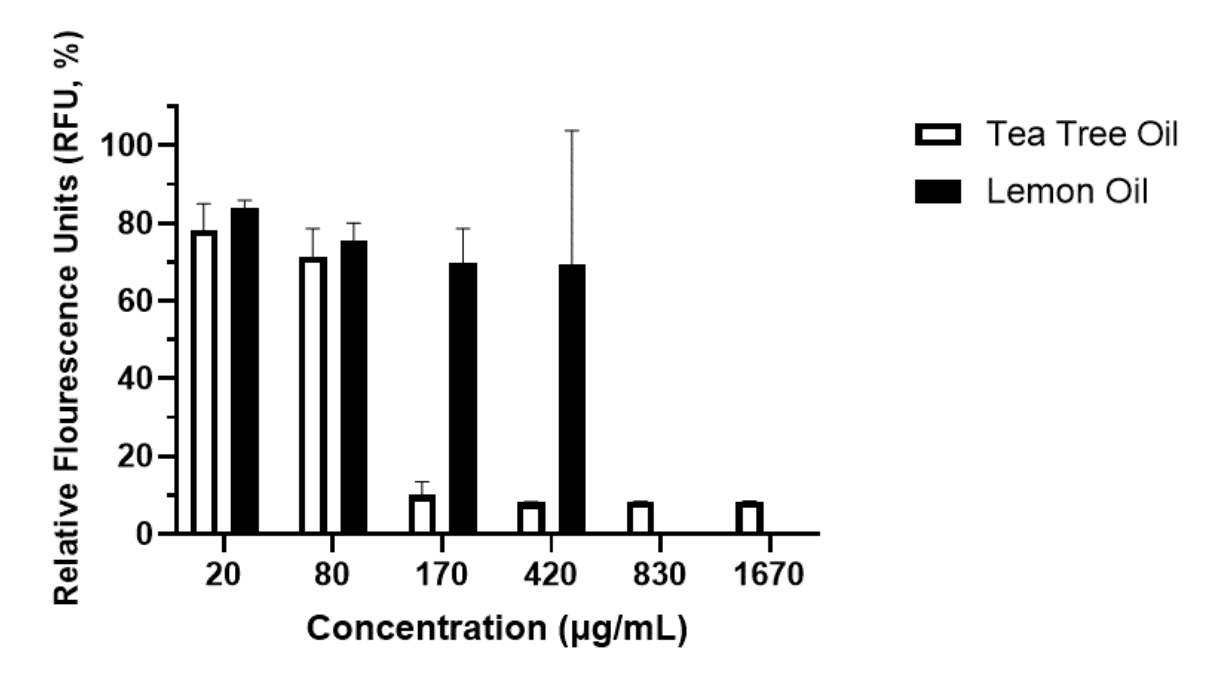


Figure 4.12: Normalised mean Relative Fluorescence Units, with standard deviation (n = 3, R=2), of human neonatal fibroblast cells after exposure to dilutions of Tea Tree Oil (white) and Lemon Oil (black) in microplate well. Excitation and emission of 530nm (bandwidth 25nm) and 590 nm (bandwidth 35nm). Untreated human neonatal fibroblast cells and uncultured DMEM used as upper and lower ranges.

Mean RFU measurements reduced to a rate comparable to uncultured DMEM (RFU =  $3.27\pm0.02 \times 10^4$ ) in 170 µg/mL Tea Tree Oil (RFU =  $5.18\pm0.65 \times 10^4$ , P  $\leq$  0.01, \*\*) and 830 µg/mL Lemon Oil (RFU =  $3.29\pm0.02 \times 10^4$ , P  $\leq$  0.01, \*\*).

After 48 hours incubation time, human neonatal fibroblast cells were imaged using Live/Dead® Assay staining solution (see CHAPTER 3). Viable cells (blue) and compromised cells (green) are shown in Figure 4.13. It can be qualitatively assessed that there is agreement regarding the greater toxicity of TTO over LO in samples, with total cell death occurring in all cases by 830 µg/mL. The Live/Dead assay could not be used for cells incubated with Manuka Honey 400 and 550+ as their autofluorescence obscured any imaging used.

The metabolic activity of osteoblast cells (hFOB 1.19) was evaluated after exposure to Manuka Honey 400 and 550+ after 3 and 5 days (see CHAPTER 3). Following exposure and incubation

(2 hours), resultant solutions were loaded in triplicate into a 96 well plate and measured at an excitation and emission of 530 nm (bandwidth 25nm) and 590 nm (bandwidth 35nm) under fluorescence. Mean and standard deviation (n = 3) relative fluorescence units (RFU) were plotted Figure 4.14. Each mean was normalised with untreated human osteoblast cells (hFOB 1.19) and uncultured DMEM F-12 used as upper and lower limits respectively.

At 3 days, no significant reduction in metabolic activity was seen at concentrations above 0 mg/mL when compared to untreated osteoblast cells (hFOB 1.19) (RFU =  $3.46\pm0.91 \times 10^3$ ) for Manuka Honey 400 (50 mg/mL RFU =  $1.85\pm0.37 \times 10^3$ , ns), and Manuka Honey 550+ (50 mg/mL RFU =  $1.94\pm0.36 \times 10^3$ , ns). Although visually distinct at higher concentrations, no statistically significant change was seen by Day 5, when compared to untreated osteoblast cells (hFOB 1.19) (RFU =  $4.09\pm1.59 \times 10^3$ ) for Manuka Honey 400 (50 mg/mL RFU =  $2.07\pm0.23 \times 10^3$ , ns), and Manuka Honey 550+ (50 mg/mL RFU =  $2.05\pm0.25 \times 10^3$ , ns).

The metabolic activity of osteoblast cells (hFOB 1.19) was evaluated after exposure to Tea Tree Oil and Lemon Oil as noted previously at 3 and 5 days. Normalised mean and standard deviation (n = 3) relative fluorescence units (RFU) were plotted in Figure 4.15.

At 3 days, 1670 µg/mL Tea Tree Oil solutions (RFU =  $2.19\pm0.47 \times 10^3$ ) did significantly reduce RFU in comparison to untreated osteoblast cells (hFOB 1.19) (RFU =  $3.46\pm0.91 \times 10^3$ , ns). 1670 µg/mL Lemon Oil solutions did show significant reduction (RFU =  $7.32\pm4.25 \times 10^2$ , P  $\leq 0.05$ , \*) in comparison to untreated osteoblast cells (hFOB 1.19). At 5 days, effect of 1670 µg/mL concentrations did not significantly reduce measured RFU in comparison to untreated osteoblast cells (hFOB 1.19) (RFU =  $4.09\pm1.57 \times 10^3$ ) for Tea Tree Oil (RFU =  $1.90\pm0.36 \times 10^3$ , ns) and Lemon Oil (RFU =  $8.26\pm3.57 \times 10^2$ , ns).

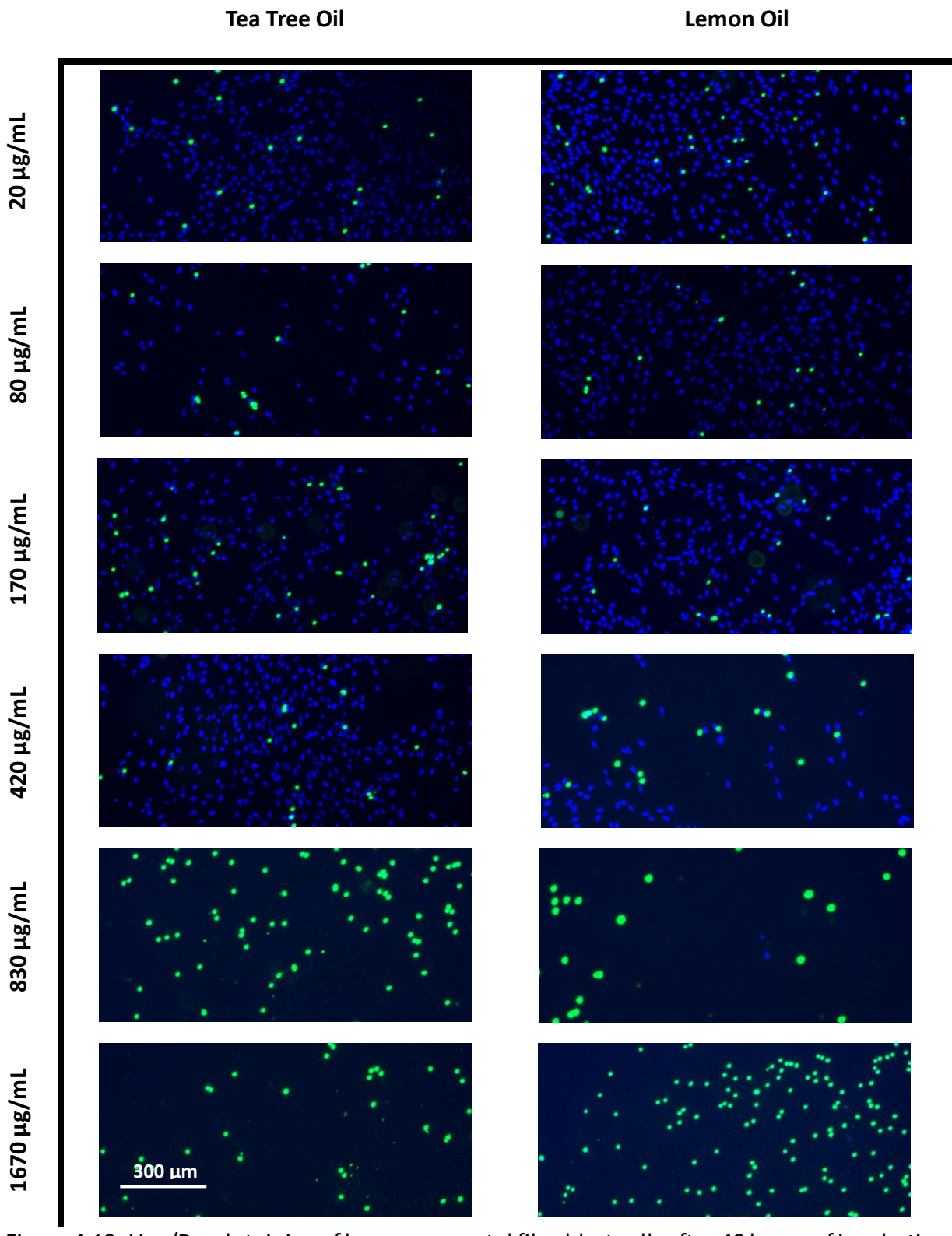


Figure 4.13: Live/Dead staining of human neonatal fibroblast cells after 48 hours of incubation exposed to dilutions of essential oils. Imaging under 100x objective magnification and filtered (Live: Blue, Compromised Cells: Green). Scale bar shown in lower left of figure.

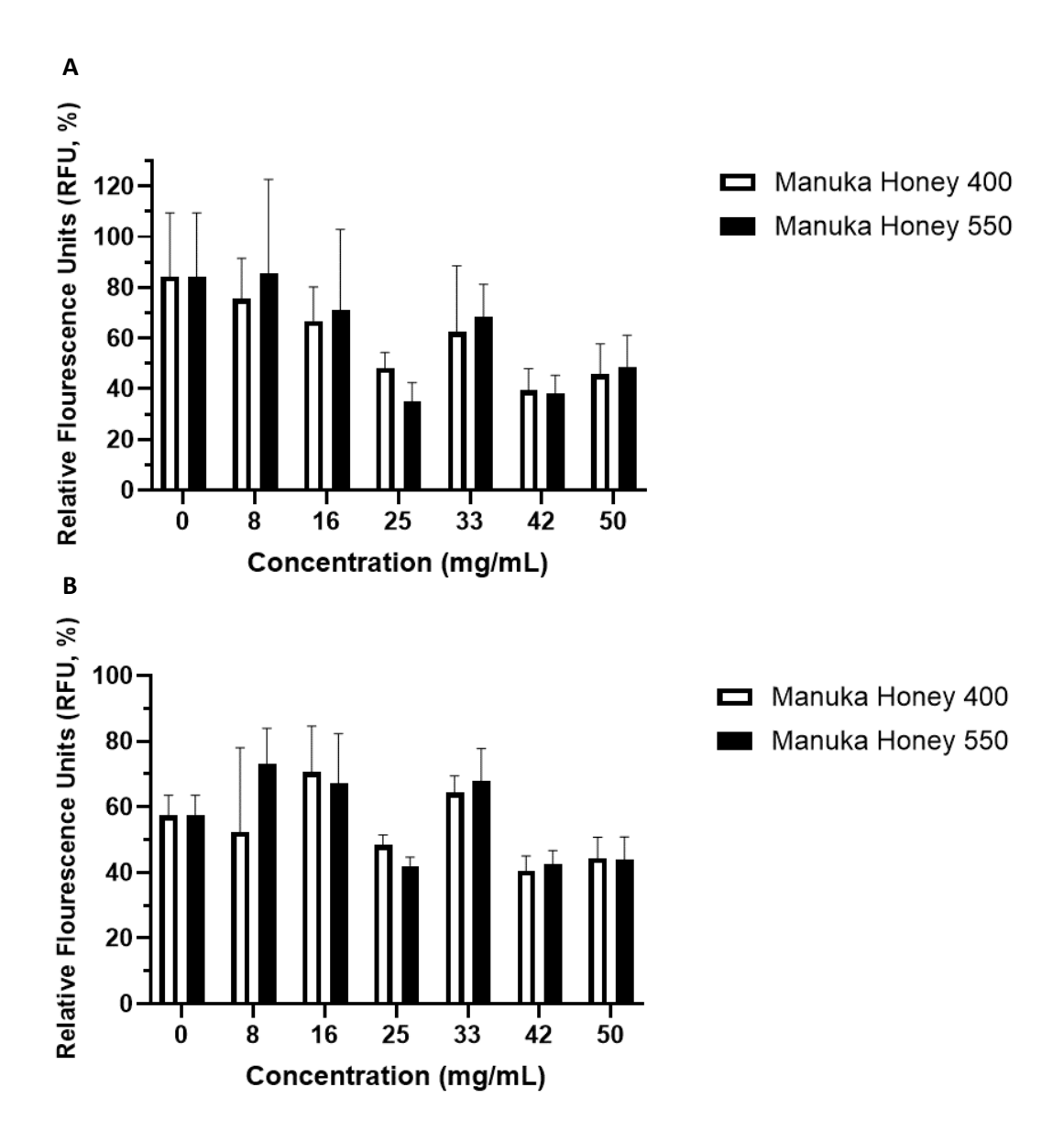


Figure 4.14: Normalised mean Relative Fluorescence Units, with standard deviation (n = 3, R=2), of osteoblast cells (hFOB 1.19) after exposure to dilutions of Manuka Honey 400 (White) and Manuka Honey 550+ (Black) in microplate well. Excitation and emission of 530nm (bandwidth 25nm) and 590 nm (bandwidth 35nm) measured at 3 (A) and 5 days (B). Untreated osteoblast cells (hFOB 1.19) and uncultured DMEM F-12 used as upper and lower ranges.

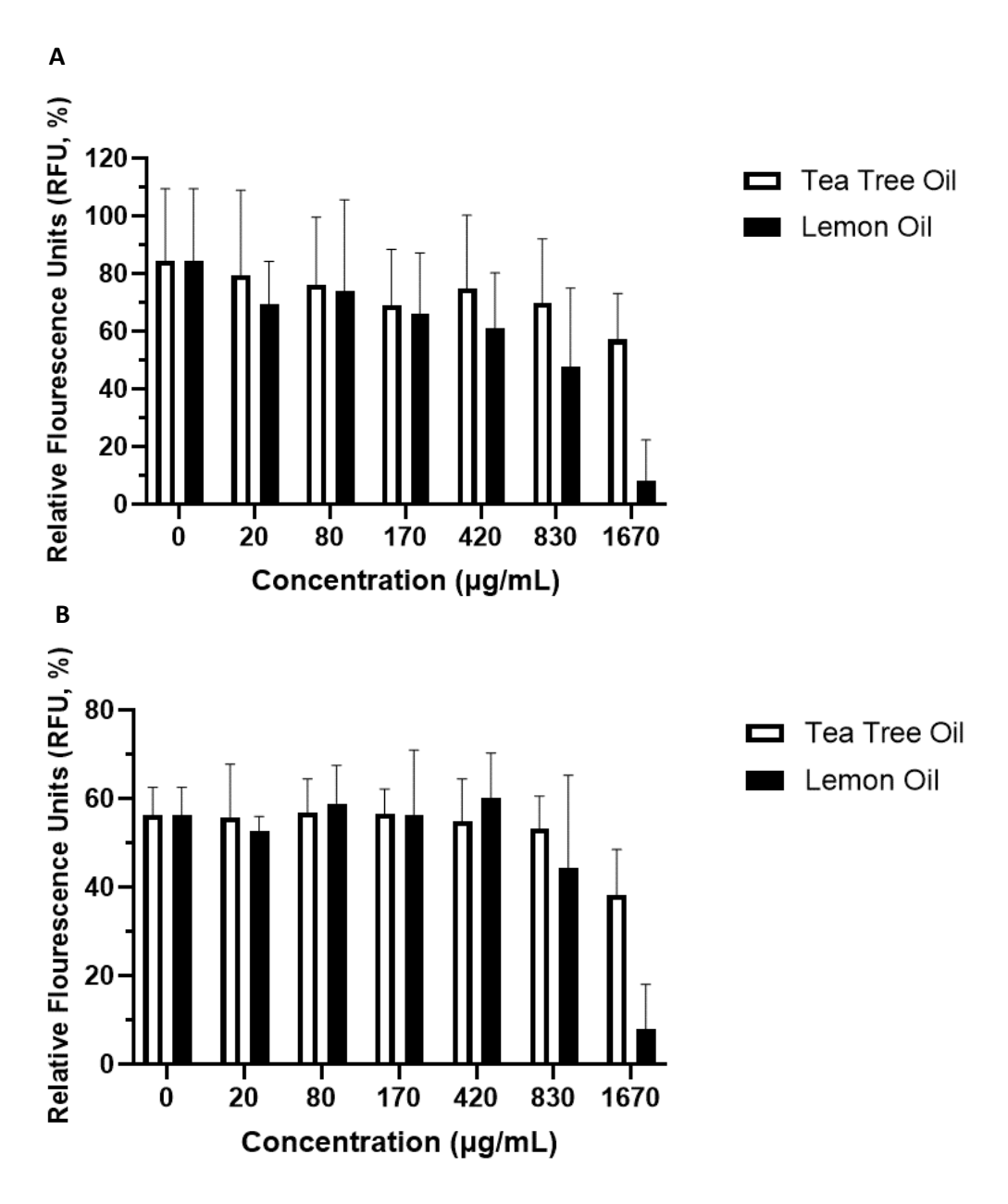


Figure 4.15: Normalised mean Relative Fluorescence Units, with standard deviation (n = 3, R=2), of osteoblast cells (hFOB 1.19) after exposure to dilutions of Tea Tree Oil (White) and Lemon Oil (Black) in microplate well. Excitation and emission of 530nm (bandwidth 25nm) and 590 nm (bandwidth 35nm) measured at 3 (A) and 5 days (B). Untreated osteoblast cells (hFOB 1.19) and uncultured DMEM F-12 used as upper and lower ranges.

## 4.2.4 Osteoblast Calcification

The mineralisation of osteoblast cells (hFOB 1.19) was assessed after exposure to Manuka Honey 400 and Manuka Honey 550+ at 21 and 28 days (see CHAPTER 3). Following staining,

wells showed visual staining of calcium nodules, shown in Figure 4.16. Untreated osteoblast cells (hFOB 1.19) were used as control wells. In 0 mg/mL, 8 mg/mL, and 16 mg/mL wells, calcium nodules are clearly seen for both Manuka Honey 400 and 550+.

Calcium deposits were assessed quantitatively (see CHAPTER 3). The supernatant was transferred to a 96 well plate, measuring the absorbance at a wavelength of 405 nm. Untreated osteoblast cells (hFOB 1.19) were used as control wells. Manuka Honey 400 dilutions from 0 to 50 mg/mL are shown in Figure 4.17 and Figure 4.18.

By 21 days, significant changes could be seen between dilutions measured and control wells (Untreated osteoblast cells (hFOB 1.19):  $0.062\pm0.192$  mM, 8 mg/mL:  $0.503\pm0.092$  mM, P  $\leq$  0.0001, \*\*\*\*), with increasing significance at all concentrations at 28 days (Untreated osteoblast cells (hFOB 1.19):  $0.900\pm0.050$  mM, 0 mg/mL:  $0.070\pm0.115$  mM, 8 mg/mL:  $0.118\pm0.073$  mM, 16 mg/mL:  $-0.018\pm0.001$  mM, 25 mg/mL:  $-0.079\pm0.000$  mM, 33 mg/mL:  $-0.047\pm0.002$  mM, 42 mg/mL:  $-0.024\pm0.000$  mM, 50 mg/mL:  $-0.031\pm0.000$  mM, P  $\leq$  0.0001, \*\*\*\*).

The same method was applied to quantitatively assess calcium deposits following exposure to Manuka Honey 550+, shown in Figure 4.19 and Figure 4.20. By 21 days, significant changes could be seen between dilutions measured and control wells (Untreated osteoblast cells (hFOB 1.19):  $0.062\pm0.192$  mM, 8 mg/mL:  $0.341\pm0.088$  mM,  $P \le 0.0001$ , \*\*\*\*), with increasing significance at all concentrations at 28 days (Untreated osteoblast cells (hFOB 1.19):  $0.900\pm0.050$  mM, 0 mg/mL:  $0.033\pm0.080$  mM, 8 mg/mL:  $0.239\pm0.146$  mM, 16 mg/mL:  $0.046\pm0.071$  mM, 25 mg/mL:  $-0.061\pm0.001$  mM, 33 mg/mL:  $-0.041\pm0.001$  mM, 42 mg/mL:  $0.002\pm0.001$  mM, 50 mg/mL:  $-0.021\pm0.001$  mM,  $P \le 0.0001$ , \*\*\*\*).

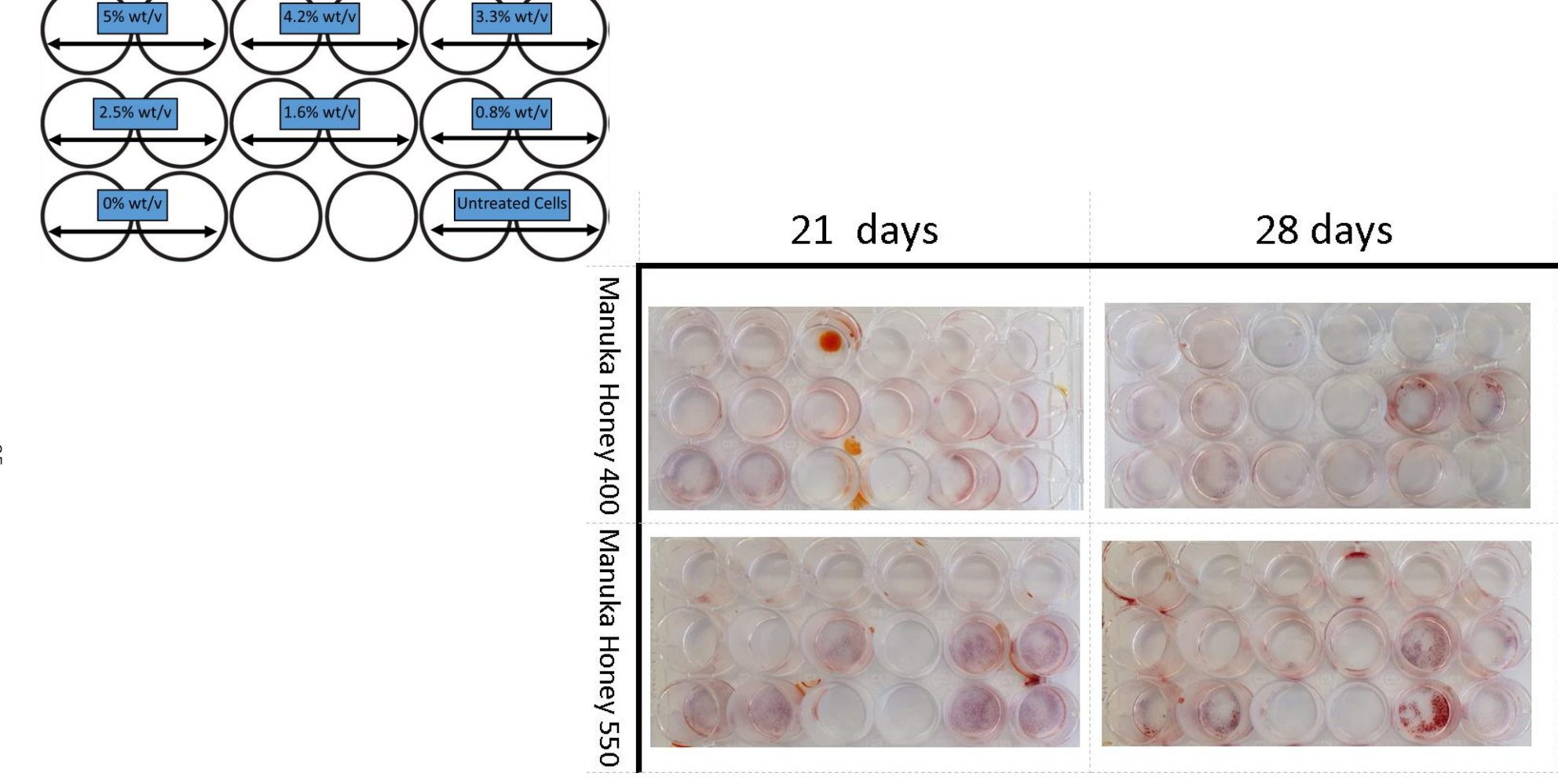


Figure 4.16: Macroscopic images of Alizarin Red stained Osteoblast cells exposed to dilutions of Manuka Honey after 21- and 28-days exposure.

Calcium deposits are stained (purple/red) and become a more intense shade of red with more calcium stained. Layout given in inset figure.

Untreated osteoblast (hFOB1.19) cells used as control wells.



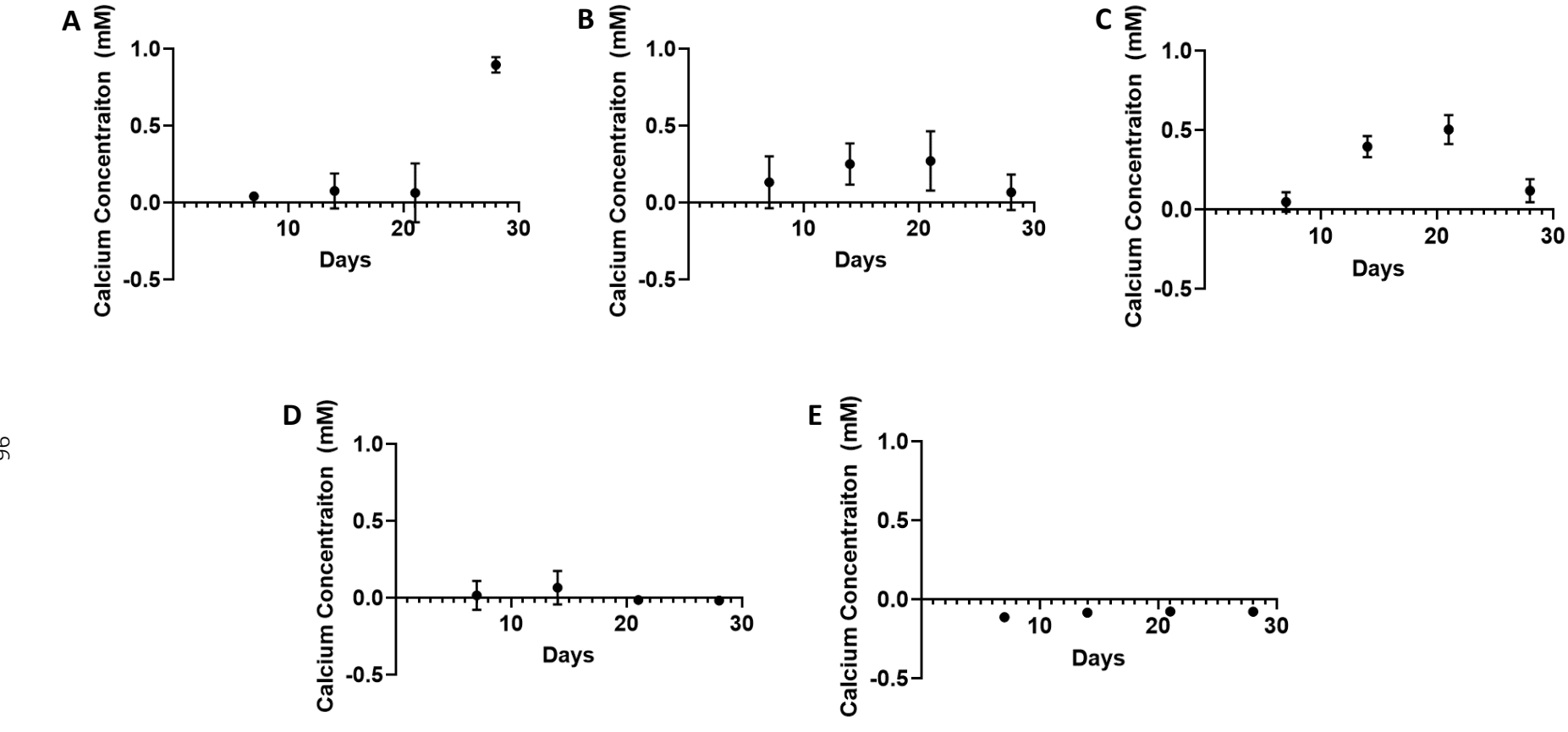


Figure 4.17: Mean and standard deviation (n = 2, R=2) of calcium concentration calculated following ARS Staining of osteoblasts (hFOB1.19) exposed to dilutions of Manuka Honey 400; 0 (B), 8 (C), 16 (D), and 25 (E) mg/mL. Untreated Osteoblast Cells (hFOB1.19) used as control wells (A).

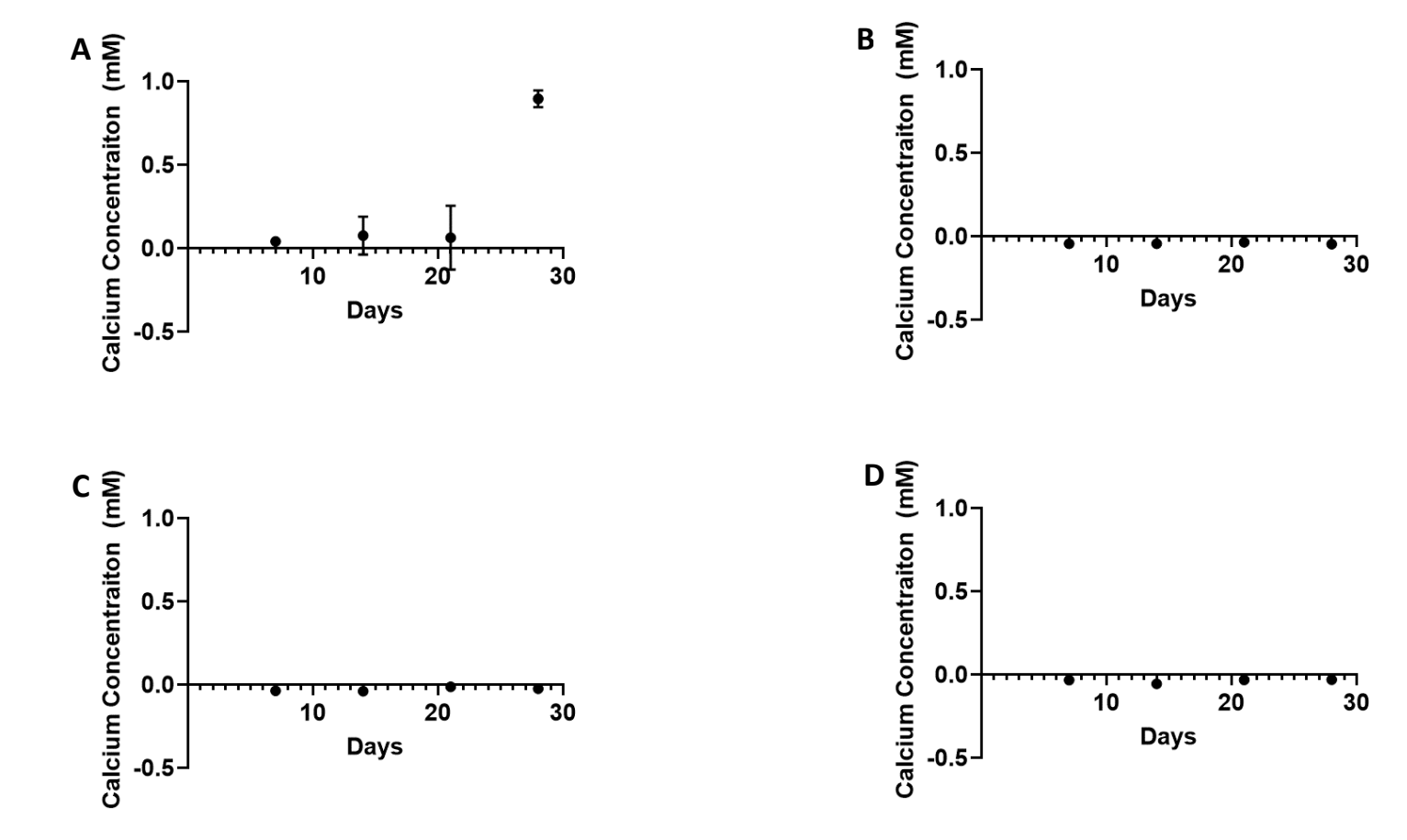


Figure 4.18: Mean and standard deviation (n = 2, R=2) of calcium concentration calculated following ARS Staining of osteoblasts (hFOB1.19) exposed to dilutions of Manuka Honey 400; 33 (B), 42 (C), and 50 (D) mg/mL. Untreated Osteoblast Cells (hFOB1.19) used as control wells (A).

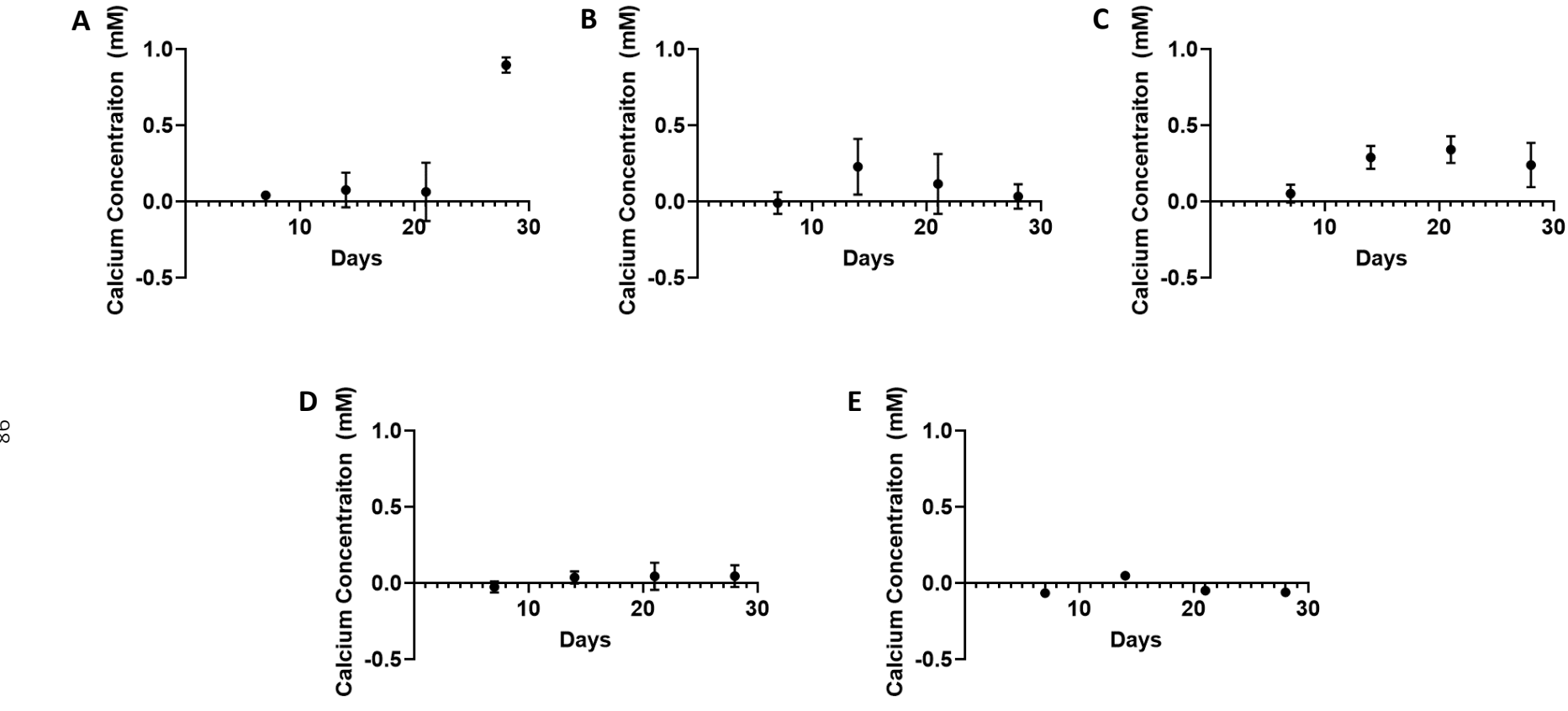


Figure 4.19: Mean and standard deviation (n = 2, R=2) of calcium concentration calculated following ARS Staining of osteoblasts (hFOB1.19) exposed to dilutions of Manuka Honey 550+; 0 (B), 8 (C), 16 (D), and 25 (E) mg/mL. Calcium deposits were dissolved and quantified by measuring absorbance at 405 nm. Untreated Osteoblast Cells (hFOB1.19) used as control wells (A).



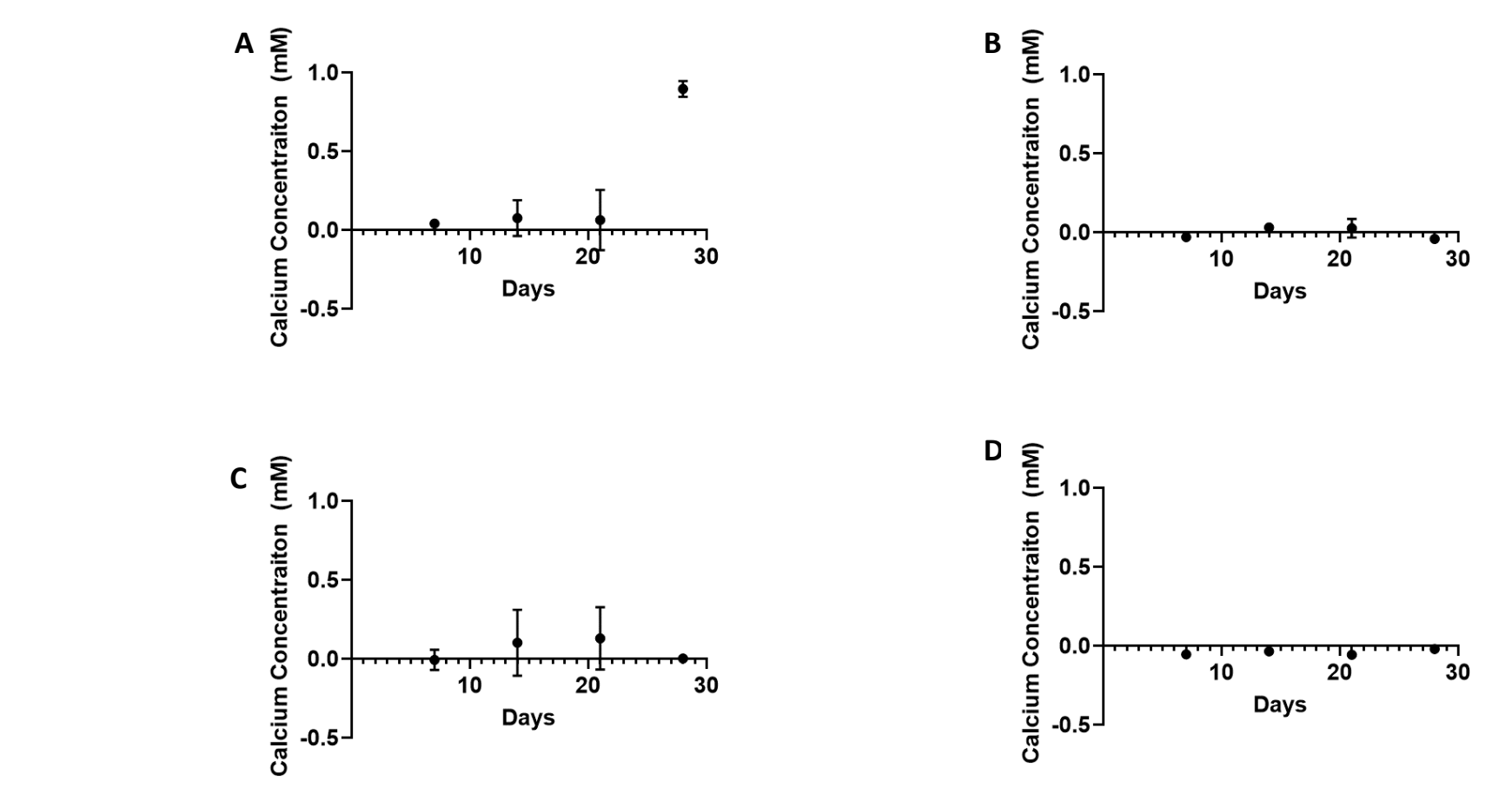


Figure 4.20: Mean and standard deviation (n = 2, R=2) of calcium concentration calculated following ARS Staining of osteoblasts (hFOB1.19) exposed to dilutions of Manuka Honey 550+; 33 (B), 42 (C), and 50 (D) mg/mL. Calcium deposits were dissolved and quantified by measuring absorbance at 405 nm. Untreated Osteoblast Cells (hFOB1.19) used as control wells (A).

#### 4.3 Discussion

Manuka Honey 400 and 550+, Tea Tree Oil, and Lemon Oil were assessed for their bactericidal and cytocompatibility. In neat concentrations, zone of inhibitions for Manuka Honey 400 were found to be 16.9±1.3 mm for *S. aureus* NCTC6571 and 29.1±1.6 mm for *P. gingivalis* W50. Manuka Honey 550+ showed an inhibition zone of 19.0±0.7 mm for *S. aureus* NCTC6571 and 31.3±2.5 mm for *P. gingivalis* W50. Tea Tree Oil showed zones of inhibition of 26.2±2.0 mm for *S. aureus* NCTC6571. Lemon Oil was noted to have zones of inhibition of 21.4±2.9 mm for *S. aureus* NCTC6571 and. However, zones of inhibition of Tea Tree Oil and Lemon Oil against were >80 mm for *P. gingivalis* W50.

Minimum inhibitory concentrations of Manuka Honey 400 were found to be 8 mg/mL for S. aureus NCTC6571 and P. gingivalis W50. Manuka Honey 550+ also showed inhibitory concentrations at 8 mg/mL for S. aureus NCTC6571 and P. gingivalis W50. Tea Tree Oil became inhibitory at concentrations of 80  $\mu$ g/mL for S. aureus NCTC6571 and >1670  $\mu$ g/mL P. gingivalis W50. Lemon Oil was noted to be inhibitory at concentrations of 20  $\mu$ g/mL for S. aureus NCTC6571 and 1670  $\mu$ g/mL P. gingivalis W50.

Metabolic activity of human neonatal fibroblast and osteoblast (hFOB1.19) cells were assessed after exposure to selected natural compounds. For human neonatal fibroblast cells, natural compounds became toxic after 24 hours at concentrations of 50 mg/mL for Manuka Honey 400, 42 mg/mL for Manuka Honey 550+, 170  $\mu$ g/mL for Tea Tree Oil, and 830  $\mu$ g/mL for Lemon Oil. For osteoblast cells (hFOB1.19), all natural compounds were cytocompatible at highest concentrations used after 5 days.

Osteoblast mineralisation was assessed after exposure of osteoblast cells (hFOB1.19) to dilutions of Manuka Honey 400 and 550+. It was noted for both Manuka Honey 400 and 550+, significant reduction in calcification occurred at dilutions of 8 mg/mL by 21 days. At 28 days, all dilutions of honey significantly reduced calcification in comparison to untreated wells.

Where available, zone of inhibitions measured here are in agreement with previous data (e.g. Lemon Oil inhibiting *S. aureus* (Mancuso, Catalfamo et al. 2019), and large inhibition zones greater than 38 mm noted in previous studies of the effect of TTO on anaerobic bacteria (Wulansari, Jufri et al. 2017)). When considered as part of dilutions, some results outlined here do not align with published works. However, as several authors have previously noted (Subramanian, Umesh Hebbar et al. 2007, Frassinetti, Caltavuturo et al. 2011), variation can occur between amongst batches of natural compounds, which means direct quantitative comparisons should always consider this.

In some cases, visually distinct bacterial growth was seen in response to tested samples (see Figure 4.1). This could be caused by some components of the tested sample diffusing into the agar quicker than others, therefore having a limited impact on bacterial growth. Alternatively, the sample may have inhibited the production of colouring pigment in the bacteria (Agarwal, Bajpai et al. 2023), which may be part of the mechanism of inhibition. Due to the scope of the project, however, this could not be investigated further.

From literature, Manuka Honey has proven to have a better antimicrobial activity than non-methylglyoxal containing honeys (e.g. West Australian or United Kingdom Honeys) (Boateng and Diunase 2015, Farkasovska, Bugarova et al. 2019), with some honeys such as Tualang Honey reported to be slight more effective at treating certain bacterial stains than Manuka Honey (Ahmed and Othman 2013).

Manuka Honey has been reported to be inhibitory around 5-20% wt/v (50-200 mg/mL) against gram positive and negative bacterial strains (Henriques, Jenkins et al. 2010, Mandal and Mandal 2011, Johnston, McBride et al. 2018). Previous studies on a range of honeys show a minimum inhibitory concentrations of between 10-16% wt/v (100-160 mg/mL) when exposed to *S. aureus* ATCC 25923 (Roshan, Rippers et al. 2017), whilst studies of other *S. aureus* strains, and honey types, exhibit MIC and MBC values of between 8-15% wt/v (80-150 mg/mL) (Cooper, Jenkins et al. 2010, Nolan, Harrison et al. 2020). When assessing bactericidal potential of MH against *P. gingivalis*, published work shows higher concentrations greater than 6% wt/v (60 mg/mL) (Ahmed and Othman 2013, Safii, Tompkins et al. 2017). Manuka Honey NPA 25+ (≈MGO 1200+) showed MIC of *P. gingivalis* OMZ 925 at 1:10 dilutions

(Schmidlin, English et al. 2014), which is higher than shown here and at two fold methylglyoxal concentrations.

The MIC values calculated in Section 4.2.2 were significantly lower than seen in most of the accessed literature. In contrast, high concentrations Manuka Honey was found to provide sufficient nutrients for bacterial growth. In addition, some early assessments, Manuka Honey at concentrations lower than 8 mg/mL saw higher *S. aureus* growth than positive controls, suggestive that this concentration is too low to inhibit bacterial growth, but provide sufficient sugar content to promote growth as reported elsewhere (Mizzi, Maniscalco et al. 2020). Extrapolated values for show a dilution of around 64 mg/mL for both Manuka Honey types would promote bacterial growth to an extent comparable to positive control wells. Fit curve has low accuracy ( $R^2_{MH400} < 0.9$ ,  $R^2_{MH550} < 0.7$ ), however, and would benefit from greater incremental data. All of this indicates that the concentration of Manuka Honey (or other compounds that contain potential bacterial nutrients) sits at a very small range that could either inhibit, or promote, bacterial growth. This is of great importance when considering the gradual diffusion of any natural compound around a wound site during the healing process.

It was indicated previously that a synergistic affect occurred between the compounds present in Manuka Honey (Kwakman, Velde et al. 2010). The MGO content in 8 mg/mL Manuka Honey 550+ is calculated to be 0.006 mM, which is an order of magnitude smaller than MIC for MGO alone, which has been recorded at 1.2mM for *S. aureus* U3300 (Rabie, Serem et al. 2016). Confirming, therefore, that the extent of bactericidal properties is due to several contributing components and properties.

When comparing minimum inhibitory concentrations of essential oils calculated in Section 4.2.2, other authors utilise a co-solvent or surfactant was used to aid in EOs miscibility in water, and there is little work achieved on this distinction between emulsions and non-emulsions. Whilst some MIC values of citrus oils agree with the output here, such as at 200  $\mu$ g/mL (Frassinetti, Caltavuturo et al. 2011), and MIC values for TTO are greater than 0.11% wt/v (1100  $\mu$ g/mL) for *P. gingivalis* when diluted in a 9% ethanol solution (Shapiro, Meier et al. 1994), some published work notes higher MIC values, ranging from 0.25-0.035% v/v (2500-350  $\mu$ g/mL) (Carson, Hammer et al. 2006, Thomsen, Hammer et al. 2013).

Some published work suggests far smaller MIC values, such as 10  $\mu$ g/mL TTO when dissolved in 10% DMSO solution (Kokina, Salević et al. 2019). However, at an incubation time of greater than 24 hours, 5 – 10% DMSO concentrations are unsuitable as a co-solvent of hydrophobic oils, with ideal experimentation times up to 3.5 hours, as the DMSO could alter the toxicity of tested reagents (Modrzyński, Jan H. Christensen et al. 2019). For this reason, the inclusion of solvents may artificially alter the perceived inhibitory or bactericidal action of compounds (Kate Summer, Browne et al. 2022). As is established here, certain essential oils dilutions do not require emulsification or dissolution within potentially harmful compounds such as DMSO to be considered effective antibacterials and would provide a more accurate reflection of tested compounds.

To find the minimum inhibitory and bactericidal concentrations, standards were used and modified to be fit for purpose (British Standards Institution 2020). Explicitly, as no guidelines for essential oil dilution are provided, suitable diluents are required. Published sources conflict in their use of diluent (Vuuren, Suliman et al. 2009, Frassinetti, Caltavuturo et al. 2011, Thomsen, Hammer et al. 2013); therefore for convenience, and to reduce the potential interference of additional components in assays as addressed above, distilled water was used as a diluent as this showed results without interference in cytotoxicity assays. Additionally, standards stipulate a serial dilution ranging from 512 to 0.125mg/L. Whilst this is appropriate for established inhibitory agents (e.g. antibiotics), greater concentrations were required in order to establish antibacterial and biocompatible response from EO and MH.

When assessing cytocompatibility in Section 4.2.3, Manuka Honey shows good compatibility with fibroblast and osteoblast cells, agreeing with previous work noting cytotoxic responses between 5 and 12 % v/v (50-120 mg/mL) (Minden-Birkenmaier and Bowlin 2018). For TTO, cytotoxic responses sit within the range of published results, with some noting no toxicity up to 1% v/v (10 mg/mL), or slight toxicity at around 10  $\mu$ g/mL (Loughlin, Gilmore et al. 2008), and other work agreeing with those outlined here, with toxicity against fibroblasts to be at 0.1% wt/v (1mg/mL) (Assmanna, Cadonáb et al. 2018). When considered *in vivo*, the threshold of toxicity is much lower than 10% patch tests that exhibited no oral irritation in patients

(Carson, Hammer et al. 2006), which may be a result of how the compounds are administered (i.e. direct and indirect exposure to cells).

Little study has been achieved on the topic of Lemon Oil cytotoxicity; however it is noted to be strongly cytotoxic against various cancer cell lines (Manjunath and Mahurkar 2021), and that it acts as a strong anti-inflammatory response for acute cases (Brah, Armah et al. 2023). As a potential antibacterial agent, Lemon Oil possesses significant inhibitory responses and coupled with the response of fibroblasts, appears non-cytotoxic within these concentrations. Lemon Oil also offers, as shown in previous studies, anti-inflammatory properties (Miguel 2010), and could be of great utility as a therapeutic aid.

There are not currently any direct studies on osteoblast cytotoxicity, however essential oils are known antioxidants (Miguel 2010), and therefore these results are in keeping with expectations as the antioxidant potential promotes cell metabolic activity (Chircov, Miclea et al. 2021). During GBR, osteoblasts are responsible for depositing calcium to the site, and whilst this addresses the viability of cells after exposure (i.e. whether the cell is healthy), this would not necessarily suggest that cells are functional. In the case of osteoblasts during GBR, this would be evidenced by whether they are able to deposit calcium during proliferation. Currently, whilst studies consider how an artificial scaffold (such as an electrospun membrane, or hydrogels) could allow for cellular adhesion and proliferation, or contain compounds that react positively to mineralisation soaking (Hixon, Bogner et al. 2019, Hixon, Carletta et al. 2019), there is unclear understanding of whether natural compounds are promoting or inhibiting osteoblast functionality.

Other studies found that Manuka Honey limited the production of calcium in cryogels *in vivo*. (Robertson, Hixon et al. 2023). Distilled water only saw significant changes to control calcification at 28 days (Untreated cells: 0.900±0.050 mM, Manuka Honey 400, 0 mg/mL: 0.070±0.115 mM, Manuka Honey 550+, 0 mg/mL: 0.033±0.080 mM), suggesting that the limited production of calcium is not entirely caused by Manuka Honey. Slowed proliferation in the initial stages may lead to cell death, causing the limited utilisation of the calcification media causing this discrepancy. Highest calcium concentrations are measured at 0.5 mM up to up to 1.6% wt/v Manuka Honey regardless of MGO content, seen at 21 days exposure

time. The highest calcium concentration measured in untreated osteoblast cells (hFOB1.19) was 0.896±0.0501 mM. It was previously reported that Manuka Honey could demineralise hard tissue, and this implied cause bone loss, which was greater at smaller concentrations (Safii, Tompkins et al. 2017). However, at Manuka Honey concentrations of 0.8% wt/v, by 21 days exposure, Manuka Honey 400 and 550+ promote greater proliferation in comparison to control wells (Untreated cells: 0.063±0.192 mM, Manuka Honey 400 0.8% wt/v: 0.503±0.092 mM, Manuka Honey 550+ 0.8% wt/v: 0.341±0.088 mM). This indicates that for short periods (0 to 21 days), Manuka Honeys could be utilised to promote proliferation in osteoblast mineralisation.

When considering the toxicity of reagents, direct exposure would always be considered more toxic than when considered as part of a membrane. For example, silver has noted to be cytotoxic when considering in direct cell exposure *in vitro*, however silver is readily incorporated into wound dressings (Nešporová, Pavlík et al. 2020). This indicates that how a compound is incorporated into any wound dressing affects the toxicity. In addition, cultured blood cells finds cytotoxic responses at much lower concentrations (Assmanna, Cadonáb et al. 2018).

As shown in Section 4.2, Manuka Honey showed consistent inhibition of *S. aureus* NCTC6571 and P. gingivalis W50 whilst still providing good cytocompatibility. Whilst Tea Tree Oil and Lemon Oil offer utility as a potential therapeutic, some cytotoxic responses were deemed significant enough that they were not considered in the functionalisation of membranes in CHAPTER 5.

# CHAPTER 5 EVALUATION OF MANUKA HONEY 550+ FUNCTIONALISED ELECTROSPUN MEMBRANES

#### 5.1 Introduction

Resorbable and non-resorbable membranes are used during the healing time of GBR that maintains site integrity and protects site cells. The inclusion of either membrane improves healing during the 6 months healing period (Dimitriou, Mataliotakis et al. 2012, Cambridge University Hospitals 2021), however non-resorbable membranes require additional surgery to remove, which could reopen wound site and lead to infection (Guazzo, Gardin et al. 2018).

Of interest within the scope of this project are the use of electrospun membranes composed of resorbable PCL, which have previously been used as a delivery method for antibiotics (Chi, Qi et al. 2019). However the over reliance on antibiotics should be considered with caution due to the increasing rise in AMR related deaths (Antimicrobial Resistance Collaborators 2022). It is the intention to show the utility of Manuka Honey 550+ which was parameterised in CHAPTER 4, noting how the morphology of electrospun membranes changes when functionalised with selected natural compound, and the bactericidal and cytotoxic potential.

When considering the functionalisation of a solution onto a membrane, solutions are required to have sufficient polarity and charge magnitude in order to appropriately bind to membrane surface, for which the measurement of zeta potential is used (Campbell and Vikulina 2020). The zeta potential of the solutions is also indicative of the stability of resultant solutions and how prone they are to phase separation, as high absolute zeta potential are more stable to very low or zero potential (Hanaor, Michelazzi et al. 2012, Ngouémazong, Christiaens et al. 2015).

This chapter seeks to determine whether Manuka Honey 550+, when functionalised onto electrospun PCL membranes via layer-by-layer assembly, is a suitable bactericidal component without causing cytotoxic response from neonatal dermal fibroblasts and osteoblasts. It also

seeks to establish whether good functionality has been applied to membrane surface using digital imaging techniques and monitoring release profile.

Four broad objectives will be addressed here:

- 1. Outline stability of solutes by analysing zeta potential of resultant solutions.
- 2. Image functionalised membranes via FTIR and SEM imaging.
- 3. Identify bactericidal and cytotoxic effect of functionalised membrane when exposed to *S. aureus* NCTC6571, *P. gingivalis* W50, mammalian neo-natal fibroblasts, and osteoblasts (hFOB1.19).

### 5.2 Results

# 5.2.1 Mixing and Potential

Manuka Honey 550+ and 400 solutions were analysed for their zeta potential. These provide an indication on their binding potential when applied in dip coating in layer-by-layer assembly, as well as their stability over time (Ngouémazong, Christiaens et al. 2015).

The inherent pH of both Manuka Honeys tested was between 3 and 3.5 before adjustment. Three pH values were assessed to understand zeta potential when Manuka Honey solutions become more acidic. Manuka Honey 400 (Figure 5.1) shows that the reagent changed the polarity behaviour from polycationic to a polyanionic charge (for 300 mg/mL,  $ZP=-1.16\pm0.09$  at pH 5.5 and  $-7.17\pm0.29$  at pH 8)

Similarly, Manuka Honey 550+ showed a linear decrease in zeta potential (for 300 mg/mL, ZP= -1.39±0.15 at pH 5.5 and -10.4±0.3 at pH 8), as solution rose in pH (Figure 5.2). There is some agreement with previous results that report Manuka Honey dilutions would have negative charges, however the zeta potential reported here is much smaller in size (Mancuso, Tonda-Turo et al. 2019). Whilst a higher potential would be beneficial to surface binding, the use of pH 5.5 is used here as, in layer-by-layer manufacture, a zeta potential from ±5mV is a suitable value for starting the electrostatic interaction with a different range of polyelectrolytes. In addition, a slightly acidic environment has demonstrated benefits in promoting wound healing and increasing antibacterial activity (Nagoba, Suryawanshi et al. 2015).

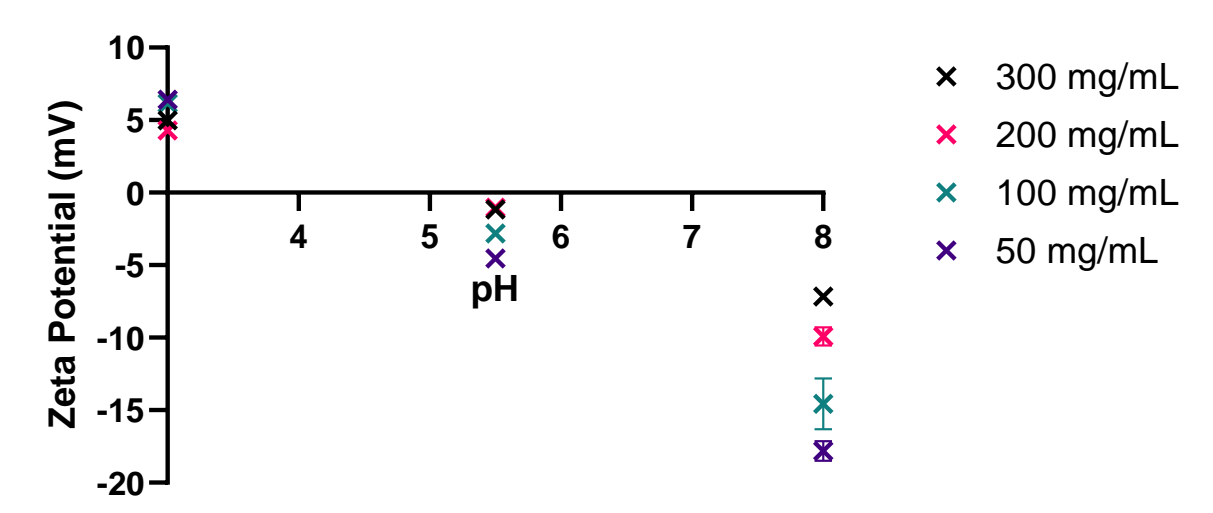


Figure 5.1: Mean Zeta Potential measure of Manuka Honey 400 dilutions (n= 2, R=2), adjusted to three distinct pH values.

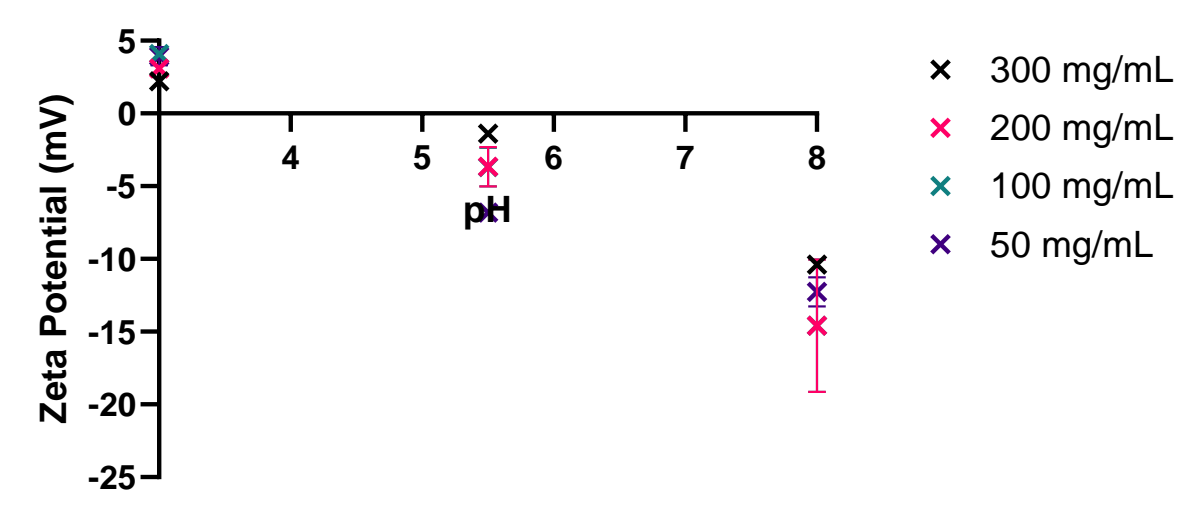


Figure 5.2: Mean Zeta Potential measure of Manuka Honey 550+ dilutions (n= 2, R=2), adjusted to three distinct pH values.

# 5.3 Functionalised membrane analysis

# 5.3.1 Fourier-transform infrared spectroscopy

A spectral profile will provide an indication of the surface composition. Qualitative comparisons can be made to untreated PCL membranes to identify where prominent peaks occur and therefore indicate whether surface binding has occurred.

Spectra of membranes are shown in Figure 5.3, with a summary of key locations provided in Table 5.1. Untreated membranes (red) show distinctive peaks expected of PCL, for example; 1727 cm<sup>-1</sup> measured during (C=O) stretching (Elzein, Nasser-Eddine et al. 2004). When Manuka Honey and PAH are applied, distinctive Manuka Honey peaks can be seen at 3384 cm<sup>-1</sup> (O–H), 2936 cm<sup>-1</sup> (C–H), 1637 cm<sup>-1</sup> (C=O), and 1057 cm<sup>-1</sup> (C–O) (Anjos, G. et al. 2015). Similarly, PAH peaks were noted at 1330 cm<sup>-1</sup> (N–H), 1481 cm<sup>-1</sup> (C–H), and 1570 cm<sup>-1</sup> (N-H) (Gentile, Ferreira et al. 2017). The range of 1500 cm<sup>-1</sup> to 750 cm<sup>-1</sup> is the most sensitive absorption region for major components in honey such as sugars, which compose up to 75%, and organic acids, which are more visible at high concentrations (Tang, Lan et al. 2019).

The resultant peaks do not linearly increase with layer number, and are shown through other layers (e.g. Manuka Honey spectra peaks can be seen where PAH is topmost layer). It is worth noting also that the distinctive peaks of Manuka Honey, PCL, and PAH do overlap.

Table 5.1: Highlighted positions and vibrators of FTIR-ATR spectra shown in Figure 5.3. Table layout adapted from (Elzein, Nasser-Eddine et al. 2004)

Position	Stretching Vibration
3384 cm <sup>-1</sup>	O-H
2936 cm <sup>-1</sup>	C–H
1727 cm <sup>-1</sup>	C=O
1637 cm <sup>-1</sup>	C=O
1570 cm <sup>-1</sup>	N-H
1481 cm <sup>-1</sup>	C–H
1330 cm <sup>-1</sup>	N-H
1057 cm <sup>-1</sup>	C–O

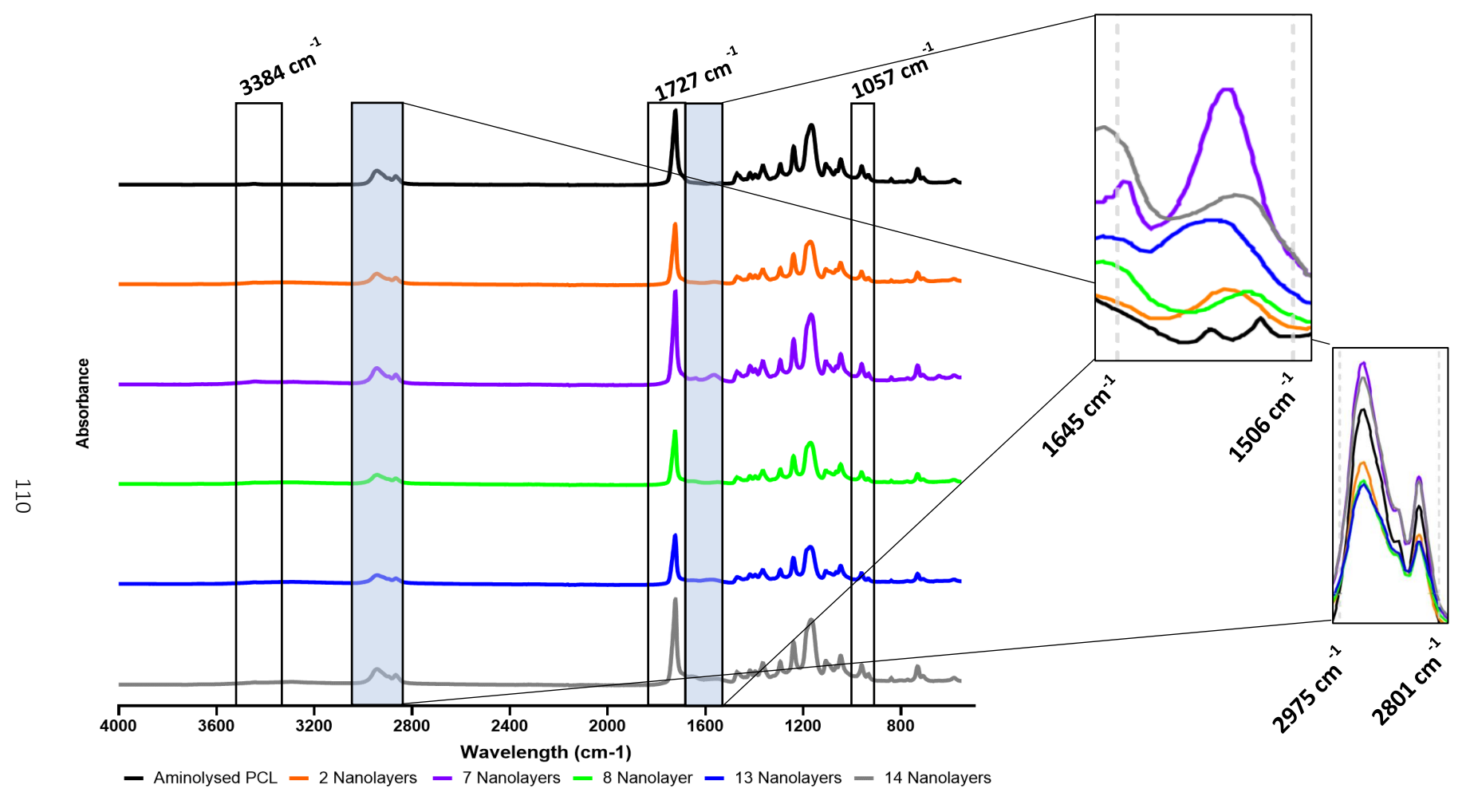


Figure 5.3: FTIR-ATR spectrum response from 200 mg/mL Manuka Honey 550 and Polyallylamine hydrochloride (PAH) coated membranes in 2 (Orange), 7 (Purple), 8 (Green), 13 (Blue), and 14 (Grey) monolayers.. Aminolysed PCL membranes used as control membrane (Red). Key wavelengths are highlighted and described in Table 5.1. Insert figures show overlapping spectra.

# 5.3.2 XPS analysis

The surface chemical composition of the membranes was examined using X-Ray Photoelectron Spectroscopy (see CHAPTER 3). The survey spectra of the samples before and after layer-by-layer assembly are shown in Figure 5.5, and the atomic percentages of the elements detected by the analysis are summarised in Table 5.2.

In all the samples, carbon (C1s) at 285 eV and oxygen (O1s) at 532 eV were observed, which is expected as these elements are fundamental components of both the substrate and coating materials. In the case of the uncoated PCL sample, nitrogen (N1s) at 399 eV was also identified. This presence can be attributed to the aminolysis treatment applied during the functionalisation process of the membranes. Subsequently, in the samples functionalized with one and two layers, N1s was not detected, indicating the successful formation of the initial layer, with Manuka honey effectively bonding to the substrate. Notably, Manuka honey lacks nitrogen atoms, and the layer's thickness might have obscured the detection of aminolysed groups, given that the analysis depth is around 5 nm (Gawek, Madkour et al. 2021). PAH contains nitrogen atoms in its chemical structure, which should have been present in the second layer. Its absence may be attributed to inadequate interaction or complete removal during the rinsing step.

From the eighth layer onwards, the nitrogen peak became significantly more pronounced, confirming the presence of PAH as a positively charged polyelectrolyte. Additionally, sodium (Na1s), a primary component of the buffer solution used to solubilize the polyelectrolytes, was identified at 1070 eV. A small amount of silicon (Si2p) was detected at 102 eV, predominantly in the 1L sample, likely due to the silicon-based tape used during the analysis.

To gain a deeper insight into the upward and downward trends in atomic percentages, high-resolution XPS analysis on C1s followed by spectra deconvolution for further examination was conducted (see CHAPTER 3). The spectra are shown in Figure 5.5. The high-resolution C1s spectra, combined with curve fitting, revealed the presence of three peaks corresponding to different carbon oxidation states: (1) 284.7–285.0 eV, attributed to –C–H or –C–C– bonds, (2) 286.8–287.0 eV, associated with –C–O– bonds, and (3) 288.5–289 eV, indicative of –C=O

groups (Mancuso, Tonda-Turo et al. 2019). These components exhibited significant variation as the layers were formed. The concentration of C=O decreased during dip coating, as it is a characteristic feature of the PCL chemical structure. In contrast, the component corresponding to C-N bonds increased, suggesting the presence of the polyelectrolytes coating.

Table 5.2: Atomic percentage of the elements detected by XPS analysis. Not detected is noted with "n.d".

Sample	Atomic %			
	O1s	C1s	N1s	Na1s
Aminolysed PCL	28.57	68.05	1.63	n.d.
Layer 1	18.57	74.83	n.d.	n.d.
Layer 2	18.16	80.76	n.d.	n.d.
Layer 8	22.26	72.10	3.18	1.1
Layer 13	22.49	71.44	2.97	1.47
Layer 14	25.19	69.84	2.85	0.68

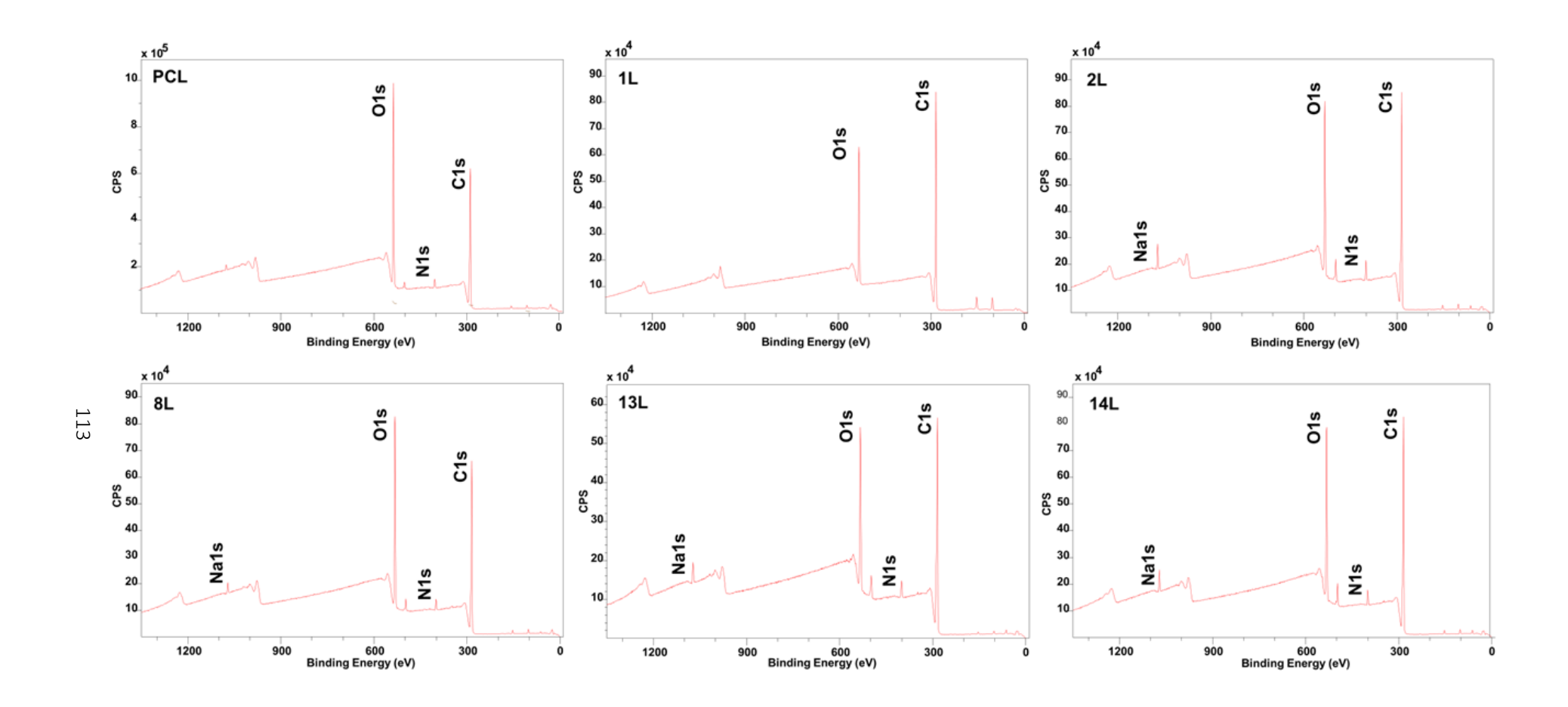


Figure 5.5: XPS survey spectra of the analysed samples before and after dip coating Layer-by-Layer assembly.

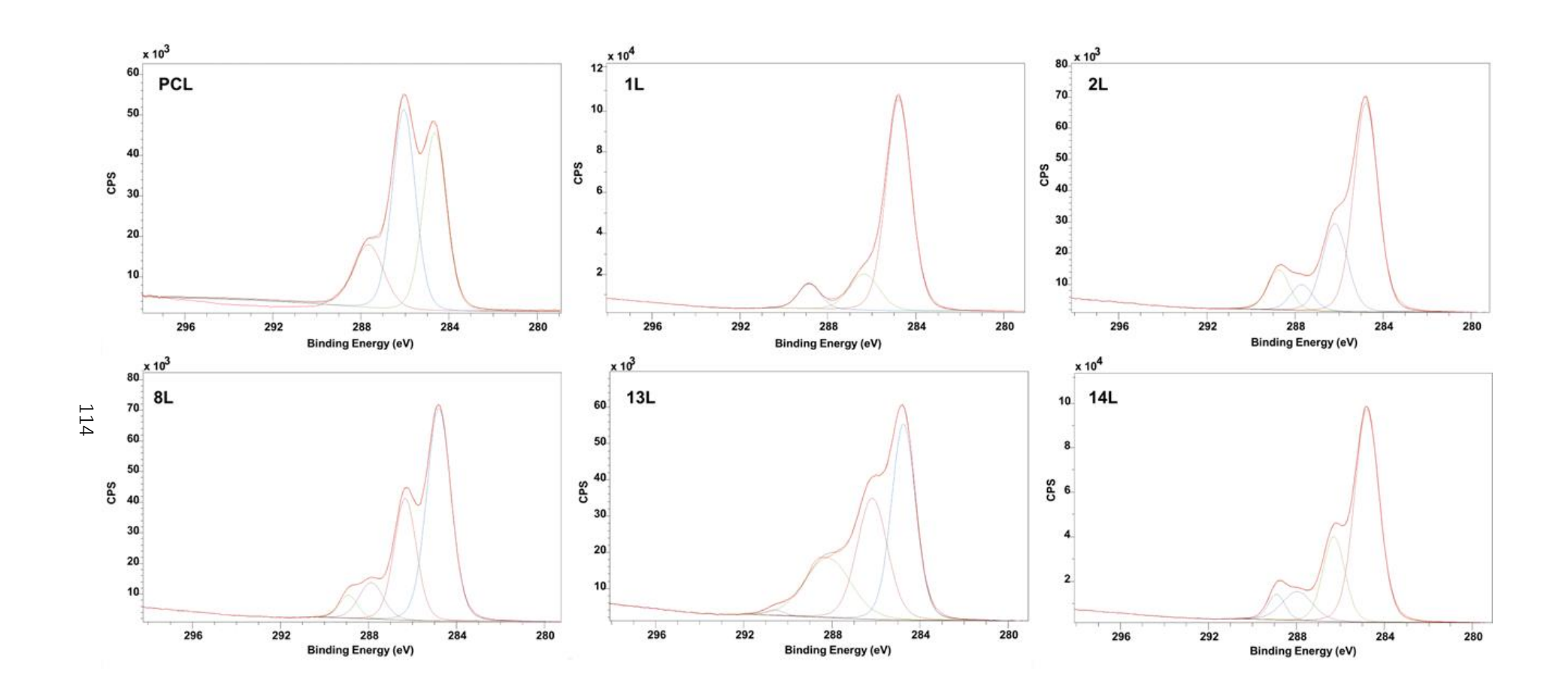


Figure 5.5. C1s high-resolution C1s spectra of the electrospun membranes before and after dip coating LbL assembly functionalization.

# **5.3.3 Scanning Electron Microscopy**

Dip coated membranes of before and after LbL assembly (8 and 14 nanolayers) were analysed by SEM. Three sections of membrane surface were chosen randomly and imaged at four magnifications, as shown in Figure 5.6.

As can be seen, as the number of nanolayers increased, the average fibre diameters increased proportionally, with pores size consistently around 1  $\mu$ m in size (Table 5.3). As the number of layers increases, honey mats the fibres together, increasing fibre diameter.

Table 5.3: Average fibre diameter (nm) measured of electrospun membranes (n = 2) before and after LbL assembly

Sample	Fibre diameter (nm)	Pore Size (nm)
0 layers (Control)	216.9±174.4	938.0±262.9
8 layers (MH550 and PAH)	379.0±60.2	1341.5±305.1
14 layers (MH550 and PAH)	402.2±92.7	1242.0±356.6

Given the average diameter of mammalian cells can be up to 100  $\mu$ m (Liu, Dahle et al. 2023), cell proliferation could occur throughout the membrane.

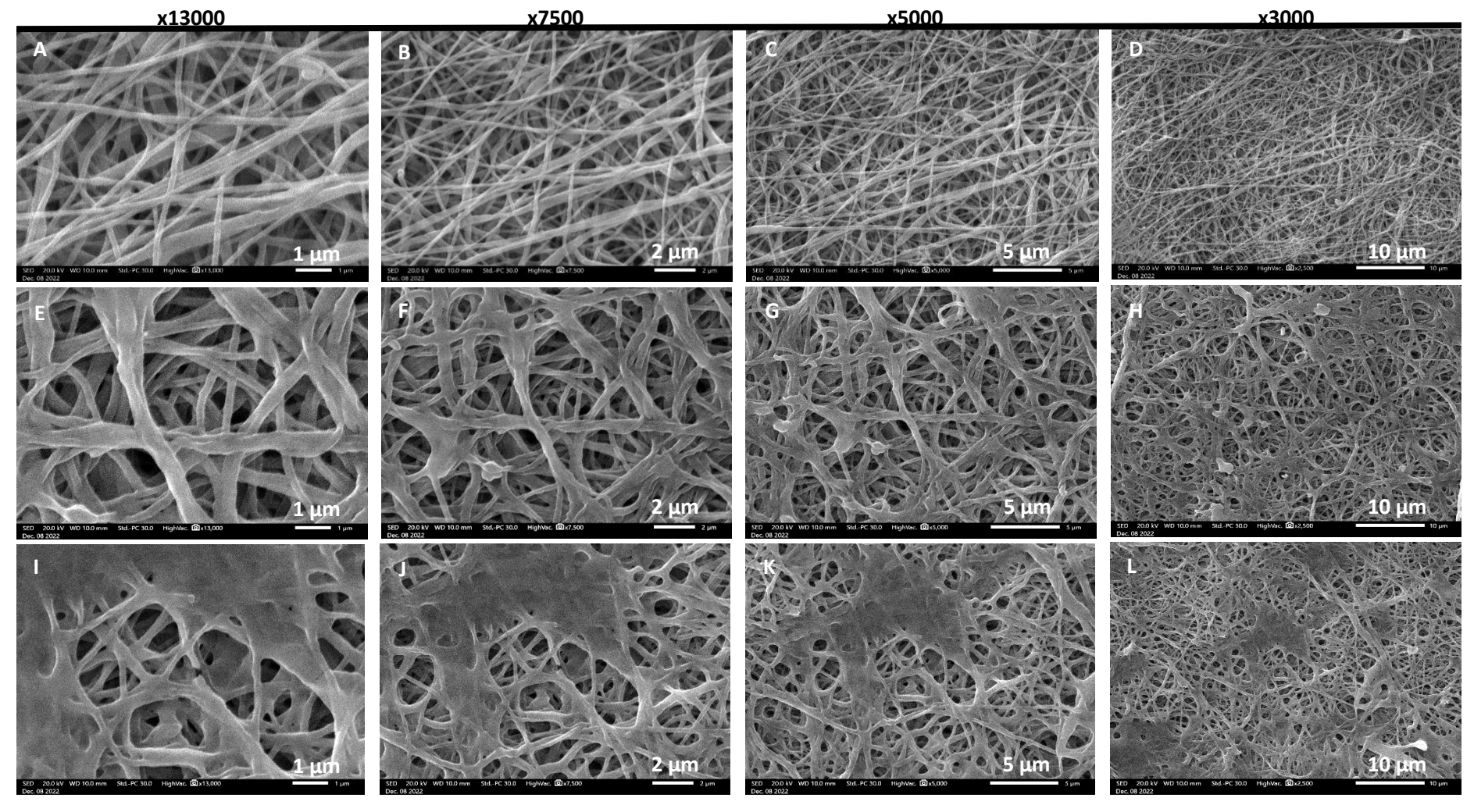


Figure 5.6: SEM images of electrospun membranes before (A, B, C, D) and after LbL assembly (8(E, F, G, H) and 14 (I, J, K, L) nanolayers). Images at 13,000x, 7500x, 5000x, and 2500x magnification.

# 5.3.4 Manuka Honey release

Functionalised 14 nanolayers-coated membranes were assessed for their Manuka Honey release over 21 days using MGO Assay Kits (see CHAPTER 3). A heat map of MGO concentrations and standard deviation are presented in Figure 5.7.

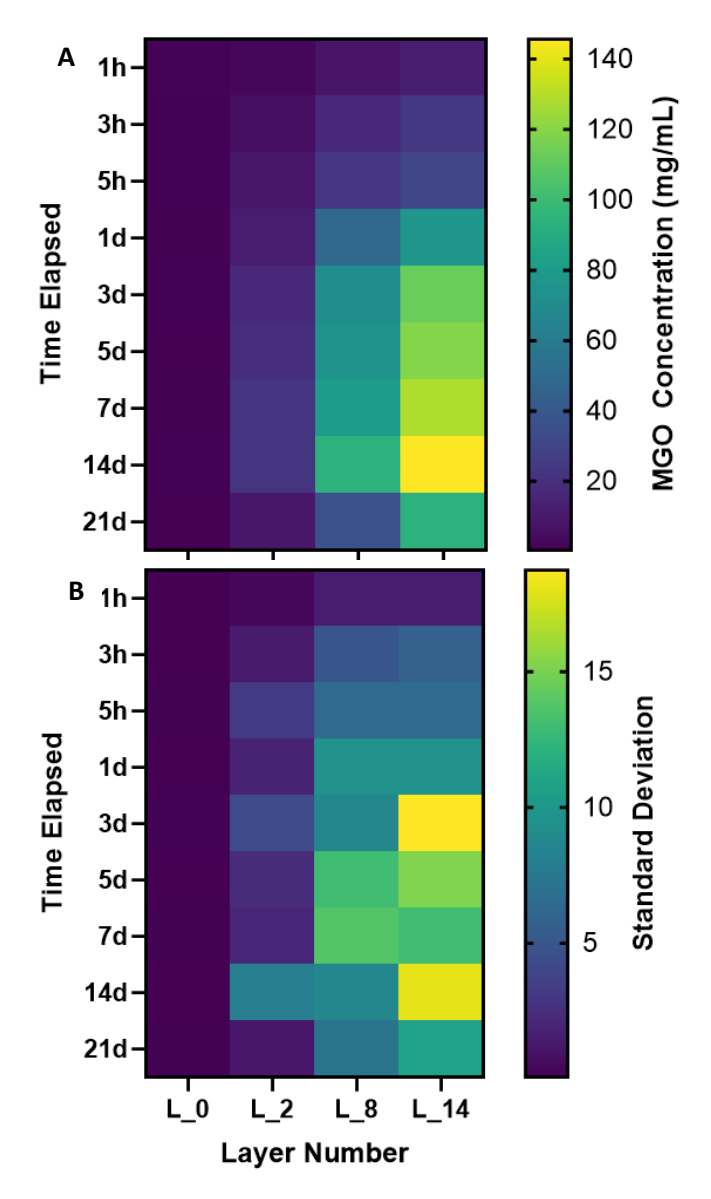


Figure 5.7: Heat map of A) Manuka Honey content (mg/mL) detected using MGO Assay Kits (n=3), and B) Standard Deviation on calculated MGO Concentration.

An increase in MGO concentration was seen up to 14 days in all layers in comparison to bare PCL membranes (PCL membranes: 0.72±0.072 mg/mL, 2 nanolayer membranes: 22.20±2.31

mg/mL, 8 nanolayer membranes: 93.68±8.65 mM, 14 nanolayer membranes: 145.57±18.02 mg/mL). By 21 days, 14 nanolayer membranes falls in MGO concentration released. This observed variation in the release activity among the MGO-loaded layers at different incubation time points strongly suggests that MGO is released from the layers in a controlled manner throughout the entire incubation period.

# 5.3.5 Antibacterial properties

Following incubation in bacterial suspensions, untreated membranes and 14 nanolayer membranes were removed and scraped using a cell scraper before performing a colony forming unit count (see CHAPTER 3).

For *S. aureus* NCTC6571, mean CFU/biofilm (n = 2) are shown in Figure 5.8. Vancomycin was used as antibiotic controls. Both membranes show reduction in CFU/biofilm (Untreated Cells:  $(6.59\pm1.18) \times 10^5$  CFU/biofilm, 0 nanolayer membranes:  $(89.17\pm3.60) \times 10^2$  CFU/biofilm, 14 nanolayer membranes:  $(70.84\pm1.05) \times 10^4$  CFU/biofilm, P  $\leq 0.01$ , \*\*), with no significant difference calculated between 0 and 14 nanolayer membranes.

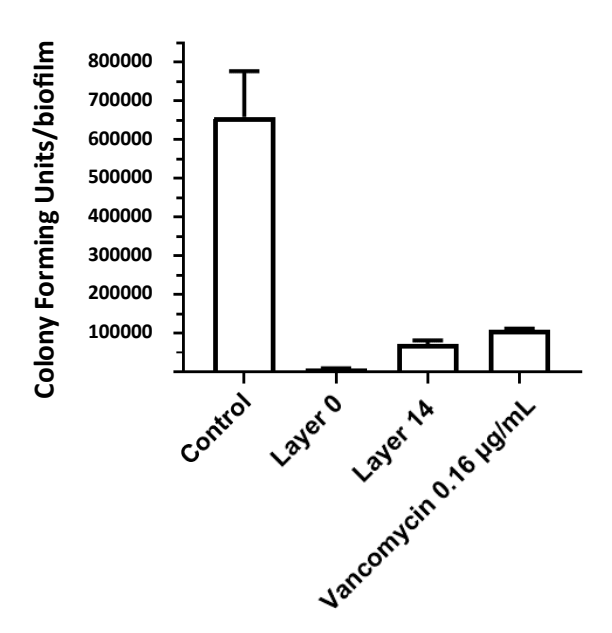


Figure 5.8: Mean Colony Forming Units/biofilm (n = 2, R=2) of *S. aureus* NCTC6571 measured after 24 hour exposure to LbL functionalised membranes

Resultant membranes were also analysed after exposure to P. gingivalis W50 in a method similar to that outlined above (see CHAPTER 3). After a further incubation period of 5 days, the number of Colony Forming Units/biofilm were counted and shown in Figure 5.9. The results from the untreated P. gingivalis W50 growth are not show here as these are magnitudes greater than other wells. In both 0 and 14 nanolayer membranes, bacterial growth is significantly reduced in comparison to antibiotic control (Untreated cells:  $14916.67\pm0.01$   $\times10^3$  CFU/biofilm, 0 nanolayer membranes:  $5.84\pm0.47$  CFU/biofilm, 14 nanolayer membranes:  $37.5\pm0.25$  CFU/biofilm, Chlorhexidine 3.2  $\mu$ g/mL:  $22500.0\pm0.36$ CFU/biofilm,  $P \le 0.0001$ , \*\*\*\*). Once again, the difference in bacterial inhibition seen in 0 and 14 nanolayer membranes were not significant.

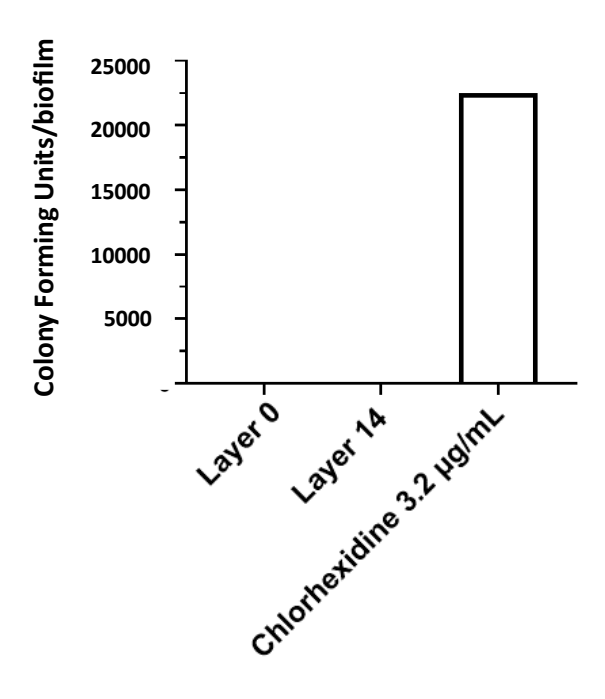


Figure 5.9: Mean Colony Forming Units/biofilm (n = 2, R=2) of *P. gingivalis* W50 measured after 5 days exposure to LbL-functionalised membranes. Positive Control too large and not shown here.

# 5.3.6 Membrane cytotoxicity

The metabolic activity of human neonatal fibroblast cells was evaluated after exposure to functionalised membranes to discern cytocompatibility (see CHAPTER 3). Following exposure and incubation (2 hours), resultant solutions were loaded in triplicate into a 96 well plate and measured at an excitation and emission of 530 nm (bandwidth 25nm) and 590 nm (bandwidth 35nm) under fluorescence. Mean and standard deviation (n = 3) relative fluorescence units (RFU) were plotted in Figure 5.10. Each mean was normalised with untreated human neonatal fibroblast cells and uncultured DMEM used as upper and lower limits respectively.

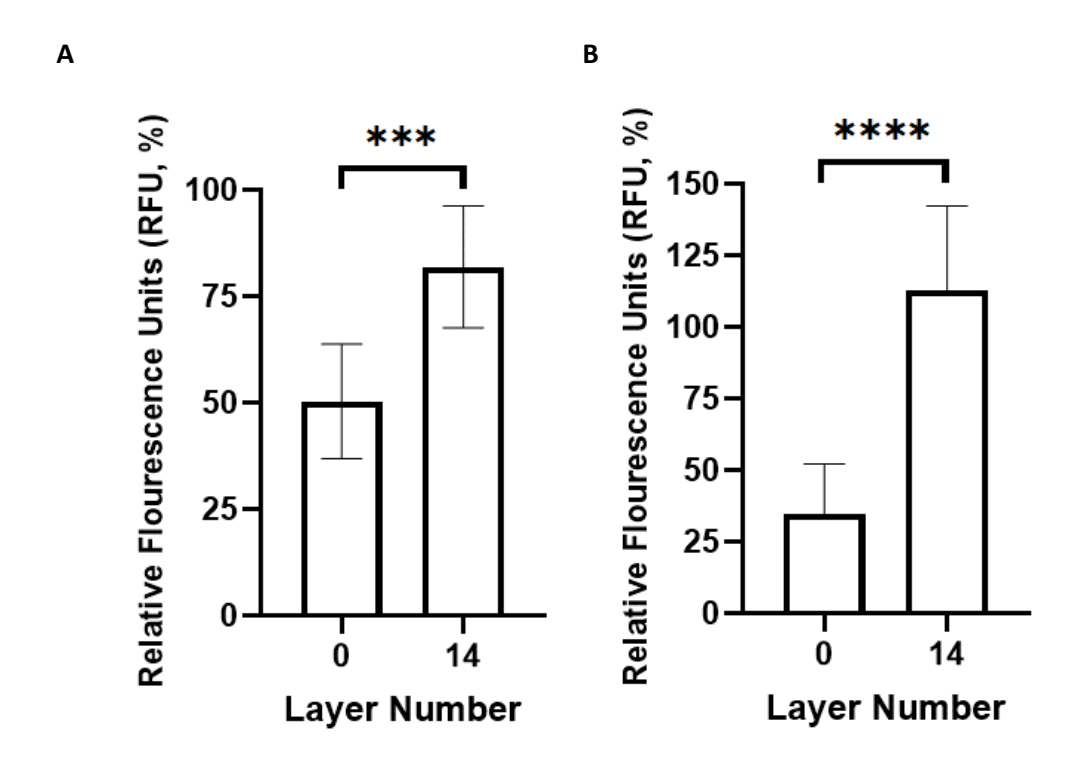


Figure 5.10: Normalised mean Relative Fluorescence Units, with standard deviation (n = 3, R=2), of fibroblast cells after exposure to 0 and 14 nanolayer functionalised membranes in microplate well. Excitation and emission of 530nm (bandwidth 25nm) and 590 nm (bandwidth 35nm) measured at 24 (A) and 48 hours (B). Untreated fibroblast cells and uncultured DMEM used as upper and lower ranges.  $P \le 0.001$  (\*\*\*),  $P \le 0.0001$  (\*\*\*\*)

The nanocoating of 14 layers evidenced an increase in the cell metabolic activity compared with the bare PCL electrospun membranes (Untreated cells:  $(4.41\pm0.0)$  x10<sup>5</sup>, 0 nanolayer membranes:  $(3.03\pm0.38)$  x10<sup>5</sup>, 14 nanolayer membranes:  $(3.91\pm0.40)$  x10<sup>5</sup>, P  $\leq$  0.001, \*\*\*\*) at 24 hours. Similar results were seen at 48 hours (Untreated cells:  $(3.81\pm0.0)$  x10<sup>5</sup>, 0 nanolayer membranes:  $(2.65\pm0.31)$  x10<sup>5</sup>, 14 nanolayer membranes:  $(4.04\pm0.52)$  x10<sup>5</sup>, P  $\leq$  0.0001, \*\*\*\*).

Cytotoxic assays were also conducted on osteoblast cells (hFOB1.19). Normalised mean and standard deviation (n = 3) relative fluorescence units (RFU) were plotted in Figure 5.11. Untreated osteoblast cells (hFOB1.19) and uncultured DMEM F-12 were used as upper and lower ranges.

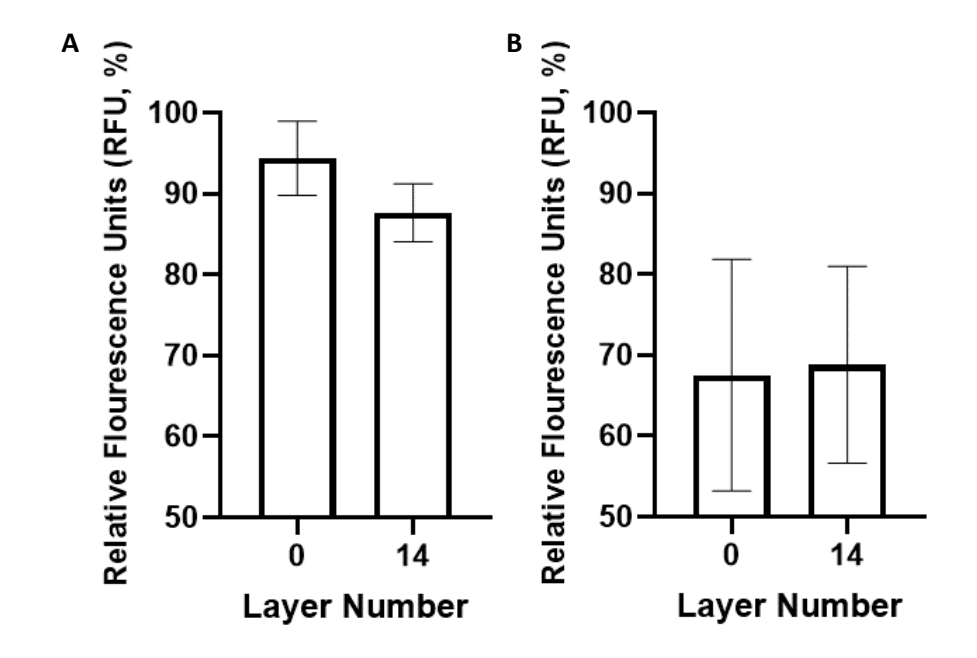


Figure 5.11: Normalised mean Relative Fluorescence Units, with standard deviation (n = 3, R=2), of osteoblast cells (hFOB 1.19) exposure to 0 and 14 nanolayer functionalised membranes in microplate well. Excitation and emission of 530nm (bandwidth 25nm) and 590 nm (bandwidth 35nm) measured at 3 (A) and 5 days (B). Untreated osteoblast cells (hFOB 1.19) and uncultured DMEM F-12 used as upper and lower ranges.

The metabolic activity of osteoblasts is not significant for 0 and 14 nanolayers in comparison to positive control wells after 3 days (Untreated cells:  $(10.93\pm0.91)$  x10<sup>2</sup>, 0 nanolayer

membranes:  $(10.47\pm0.37) \times 10^2$ , 14 nanolayer membranes:  $(9.91\pm0.29) \times 10^2$ ), however this growth is significantly reduced at Day 5 in comparison to untreated osteoblast cells (hFOB 1.19) (Untreated cells:  $(8.98\pm1.92) \times 10^3$ , 0 nanolayer membranes:  $(6.62\pm1.04) \times 10^2$ , 14 nanolayer membranes:  $(6.71\pm0.88) \times 10^3$ ).

To confirm the cytocompatibility of the obtained functionalised membranes, Live/Dead staining was performed and shown in Figure 5.12.

Whilst osteoblast cell size between 0 and 14 nanolayer membranes remains comparable, and smaller than untreated osteoblast cell growth. Cell counts were fewer across 0 nanolayer membranes than 14 nanolayer membranes.

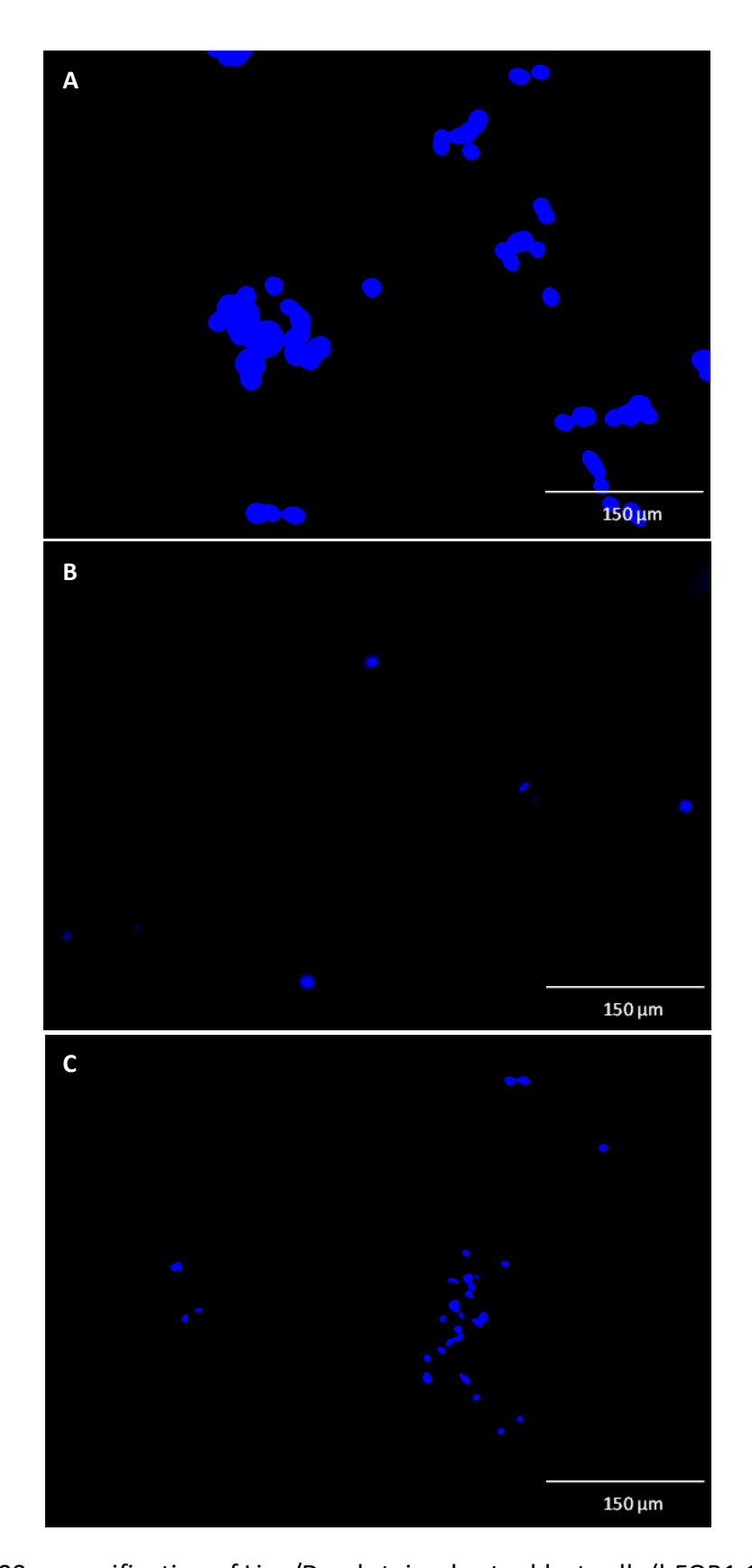


Figure 5.12: 200x magnification of Live/Dead stained osteoblast cells (hFOB1.19) after 5 days exposure to 0 (B) and 14 (C) nanolayer membranes. Untreated osteoblast cells (hFOB1.19) used as control growth (A).

#### 5.4 Discussion

Manuka Honey 400 and 550+ dilutions were analysed for their zeta potential, indicating their binding potential to membrane surface during dip coating. Both solutions showed a linear decrease in zeta potential with increasing pH.

Following dip coating layer by layer assembly of 20% wt/v Manuka Honey 550+. 2, 7, 8, 13, and 14 nanolayer membrane spectra were imaged in via FTIR-ATR. Responses show peaks at positions of 3384 cm<sup>-1</sup> (O–H), 2936 cm<sup>-1</sup> (C–H), 1637 cm<sup>-1</sup> (C=O), 1057 cm<sup>-1</sup> (C–O), 1481 cm<sup>-1</sup> (C–H), and 1570 cm<sup>-1</sup> (N-H). SEM images were also taken at 4 magnifications at 0, 8, and 14 nanolayers, with fibre diameter increasing from 216.9 $\pm$ 174.4 to 402.2 $\pm$ 92.7 with pore size not deviating from 1  $\mu$ m within error.

Functionalised 14 nanolayer membranes with 20% wt/v Manuka Honey 550+ and PAH were analysed for their MGO release. As layer number increases, increased MGO concentration was seen. In addition, after 14 days, the rate of MGO release from membranes decreases.

Functionalised 14 nanolayer membranes were exposed to *S. aureus* NCTC6571. No significant differences occurred between 14 nanolayer membranes and 0 nanolayer membranes, however both significantly reduced *S. aureus* NCTC6571 growth in comparison to untreated bacterial cells (Untreated Cells:  $(6.59\pm1.18) \times 10^5$  CFU/biofilm, 0 nanolayer membranes:  $(89.17\pm3.60) \times 10^2$  CFU/biofilm, 14 nanolayer membranes:  $(70.84\pm1.05) \times 10^4$  CFU/biofilm, P  $\leq$  0.01, \*\*).

When exposed to *P. gingivalis* W50, 0 and 14 nanolayer membranes reduced bacterial growth in comparison to untreated bacterial cells, however no significant difference occurred between 0 and 14 nanolayers (Untreated cells:  $14916.67\pm0.01 \times 10^3$  CFU/biofilm, 0 nanolayer membranes:  $5.84\pm0.47$  CFU/biofilm, 14 nanolayer membranes:  $37.5\pm0.25$  CFU/biofilm, Chlorhexidine  $3.2 \mu g/mL$ :  $22500.0\pm0.36$ CFU/biofilm,  $P \le 0.0001$ , \*\*\*\*).

To assess cytotoxicity, 0 and 14 nanolayer membranes were exposed to human neonatal fibroblast cells and assessed for metabolic activity. Following exposure, 14 nanolayers

promoted increased cell activity in comparison to 0 nanolayer membranes up to 48 hours (Untreated cells:  $(3.81\pm0.0) \times 10^5$ , 0 nanolayer membranes:  $(2.65\pm0.31) \times 10^5$ , 14 nanolayer membranes:  $(4.04\pm0.52) \times 10^5$ ).

Osteoblast cells (hFOB1.19) were also assessed for cytocompatibility. After exposure, 0 and 14 nanolayer membranes showed metabolic activity similar to untreated osteoblast cells (hFOB1.19) up to 3 days (Untreated cells:  $(10.93\pm0.91)$   $x10^2$ , 0 nanolayer membranes:  $(10.47\pm0.37)$   $x10^2$ , 14 nanolayer membranes:  $(9.91\pm0.29)$   $x10^2$ ). Live/Dead staining of resultant membranes showed smaller cell size in comparison to untreated osteoblast cells (hFOB1.19), with a larger number of cells seen in 14 nanolayer membranes than 0 nanolayer membranes.

During membrane manufacture, as the number of layers increases, the membrane began to turn a distinct shade of yellow brown colour as the honey mats the fibres together, as seen previously (Sarhan and Azzazy 2015). When surface spectra was analysed, peaks can be seen at 3384 cm<sup>-1</sup> (O–H), 2936 cm<sup>-1</sup> (C–H), 1637 cm<sup>-1</sup> (C=O), and 1057 cm<sup>-1</sup> (C–O), which has been previously shown as clear spectra of honey (Tang, Lan et al. 2019). Similarly, previously identified PAH spectra were noted at 1481 cm<sup>-1</sup> (C–H), and 1570 cm<sup>-1</sup> (N-H) (Li, Zheng et al. 2017). This displays that the Manuka Honey Zeta Potential was sufficient to allow surface bonding of Manuka Honey to membrane surface.

The MGO concentration aligns with previous work that note increase in MGO content that began to plateau by 21 days (Mancuso, Tonda-Turo et al. 2019). As MGO is a major detectable compound present within Manuka Honey, the results suggest that, within measured period, Manuka Honey is diffusing into the environment. The SEM images shown in Section 5.3.3 and the FTIR analysis shown in Section 5.3.4 confirm that Manuka Honey is adhering to membrane surface. The inference, therefore, is that conditions are suitable for Manuka Honey to detach from membrane surface into environment.

It is noted in sources that autoclaved or filter sterilised Manuka Honey causes the reduction of antibacterial efficacy and so in place of this, UV sterilisation was used (Mandal and Mandal 2011). However, in some experiments carried out here, contaminants occurred in a small number of wells of suspected *Bacillus* bacteria, which has been shown to be resistant against

many forms of sterilisation including disinfectant, and irradiation, although autoclaving is still considered to remove these agents. These results were not seen in essential oil experiments; however, this does not imply that contaminants present could not survive the UV irradiation.

It has been established that Manuka Honey at low concentrations have little to no impact on osteoblast calcification (Section 4.2.4); however, it is shown here that osteoblast activity is limited over prolonged periods suggesting that prolonged exposure could hinder osteoblast growth. This has implications on the healing period of up to six months as required (Cambridge University Hospitals 2021). The membranes used here, allowed the growth of osteoblasts across membrane surface for both 14 and 0 nanolayer samples. This suggests that osteoblasts and fibroblasts are tolerant when in presence of membrane and during surface contact. Whilst the pore size is sufficient to allow the proliferation of mammalian cells into structure, this is also true of the bacterial cells which are magnitudes smaller. Therefore, an inert membrane could act as a scaffold for human cells during GBR, but also harbour bacteria to grow and avoid the traditional efforts of dental bacteria removal as seen in certain commercial membranes (Slutzkey, Kozlovsky et al. 2015). Should the Manuka Honey not release within an appropriate time scale, bacteria will still grow across and within membrane.

Whilst fibroblast proliferation is improved in the presence of Manuka Honey coated membranes, as confirmed in published results of 10 and 20% Manuka Honey electrospun membranes (Minden-Birkenmaier, Neuhalfen et al. 2015), the presence of Manuka Honey appears negligible for osteoblast proliferation. Studies of NIH3T3 mouse fibroblasts showed up to 20% honey loaded fibres did not reduce cell viability after 24 hours (Tang, Lan et al. 2019), however no current studies consider osteoblast functionality during exposure to Manuka Honey membranes.

In output from both bacterial strains, it was seen that the 14 nanolayer membrane did not provide statistical bacterial inhibition compared to bare PCL membranes. This may be due to the polymer membranes natural hydrophobicity, making it difficult for certain bacterial strains to adhere to membrane surface (Song, Koo et al. 2015), providing a bacterial inhibition comparable to the antibacterial activity of Manuka Honey 550+. Both cases, however, show reliable inhibition in comparison to antibiotic control wells, suggesting that as a surface

adherent, bare PCL electrospun membranes in vitro, are suitable for implant protection durir	ıg
healing.	

# CHAPTER 6 MATHEMATICAL MODELLING OF BIOFILM GROWTH AND ANTIBACTERIAL ACTIVITY

### 6.1 Introduction

A mathematical model can be used to predict, confirm, and produce hypotheses in the development of medical devices (Dzianach, Dykes et al. 2019). With the introduction of a number of key parameters, a model can be developed that will allow the user to perform iterative protocols that will inform the design of an ideal membrane.

The agent-based models used in this thesis, are considering the net growth of the individual bacteria expressed as:

$$\mu_{net} = \frac{1}{X} \frac{dX}{dt}$$
 Eq 6.1

where  $\mu_{net}$  is the net growth, X is the biomass, and dX/dt is the change in biomass over time.

Whilst previous studies investigate multi-species interactions (Martin, Tamanai-Shacoori et al. 2017), inhibiting substrates, or the inclusion of an agent killing compound such as an antibiotic (Levin and Udekwu 2010), the primary focus of previously published studies was on cross sectional biofilm growth. This approach may offer a limited view when gathering qualitative comparisons to *in vitro* experimental studies which are agar-based. Currently, limited studies emulate bacterial growth on an agar plate (Rudge, Steiner et al. 2012), where nutrients do not diffuse from outside the environment. In addition, these studies do not consider the diffusion of an inhibiting bioactive compounds from the surface of an antibacterial membrane.

An adaption was undertaken of the agent-based modelling software package iDynoMiCs, developed by the Kreft Research Group developed at the University of Birmingham (Kreft Group 2015, Cockx, Foster et al. 2023), to mimic a top-down agar plate with an inhibiting reagent. The simulator was then used to test hypotheses and the results were qualitatively compared with published results for an initial validation.

### 6.2 Aims & Objectives

This chapter aims to provide a framework and proof-of-concept mathematical tool that can be used for the design of an inhibiting membrane best suited for a given application (hereafter referred to as an "ideal" membrane). Further, the model output should be qualitatively validated alongside experimental results and published resources. This refinement will be accomplished with the scope that future LbL coated membranes can be simulated *in silico* to provide the best candidates for further development. Therefore, reducing time and cost, particularly when performing experiments with multiple variables.

The model used parameters derived from literature and studies carried out within this PhD thesis (see CHAPTER 4 and CHAPTER 5) to initially model Manuka Honey 550+ diffusing into a nutrient agar that was inoculated with *P. gingivalis* in such a way as to deposit agents randomly across simulated surface.

Due to the often-diverse growth conditions required for growth of different strains of bacteria, multispecies bacteria systems can be challenging to control in a laboratory environment, such as aerobic and anaerobic bacteria that require a complex system in order to grow simultaneously (Hibbing, Fuqua et al. 2010, Salmela, Lehtinen et al. 2018). Therefore, the secondary aim of this thesis was to incorporate a two bacteria scenario that has previously been studied, and model their growth when exposed to an inhibiting membrane (Kreft, Picioreanu et al. 2001, Martin, Tamanai-Shacoori et al. 2017, Mattei, Frunzo et al. 2018).

# 6.2.1 Objectives

- 1. Modify iDynoMiCs software package to mimic top-down agar plate viewpoint of bacterial growth by changing both bacterial kinetics and nutrient flow.
- 2. Incorporate inhibiting membrane that kills any bacterial agents that make contact and diffuse into the environment at specific rates.

- 3. Derive and answer a series of hypotheses to validate the model's utility. Specifically, the following hypotheses;
  - a. The placement of an inhibiting membrane impacts the total inhibiting properties.
  - b. A higher diffusivity of an inhibiting compound will increase the overall inhibition of bacteria.
  - c. A high initial concentration of an inhibiting compound will increase the overall inhibition of bacteria.

### 6.3 Results

The model was appropriately set up as presented in CHAPTER 3. Unless otherwise stated, all simulations were run in triplicate<sup>1</sup>, and where numerical values are given, the averages of these values have been shown. Each simulation time was run for 48 hours simulation time.

At initialisation, a number of agents were randomly added to the spatial grid equal to a calculated experimental equivalent. In CHAPTER 4, a typical quantity of bacterial suspension is 100  $\mu$ L at optical density (OD<sub>595</sub>) of 0.5. An OD<sub>600</sub> of 1.0 in *E. coli* is equal to roughly 10<sup>9</sup> cells/mL, this implies the number of cells is 5 x 10<sup>8</sup> cells/mL. In 100  $\mu$ L, the number of cells is 5 x 10<sup>7</sup> in a 9 cm petri dish.

A proportional environment used is  $10^4 \, \mu m^2$ , which is smaller than the 9 cm petri dish by a magnitude of  $10^5$ . Therefore, a proportional number of 500 agents was used, randomly dispersed throughout the environment.

130

<sup>&</sup>lt;sup>1</sup> Triplicate here refers to random seeds of simulation; 1, 2, and 3. Each individual seed is initialised identically, and the average of these seeds were taken.

# 6.3.1 Assessing the influence of membrane placement on agent growth

The placement of a membrane across 9 regions detailed in Section 3.7.10 was analysed by calculating mean mass per agent (pg). A heat map of all 9 regions were at 0h, 6h, 24h, and 48h simulation time, shown in Figure 6.1. The layout of the simulated environment is provided in Figure 3.11. It is noted here the line of symmetry about the centre, which aligns with expectations of an isolated system. Due to this symmetry, whilst all cells were studied, reporting within the remainder of this chapter is limited to cells 3A, 3B, and 2B.

A distribution of inhibitor concentration was plotted at 0 and 48 hours, shown in Figure 6.2. It can be seen that little change occurred between the start and end of the simulation.

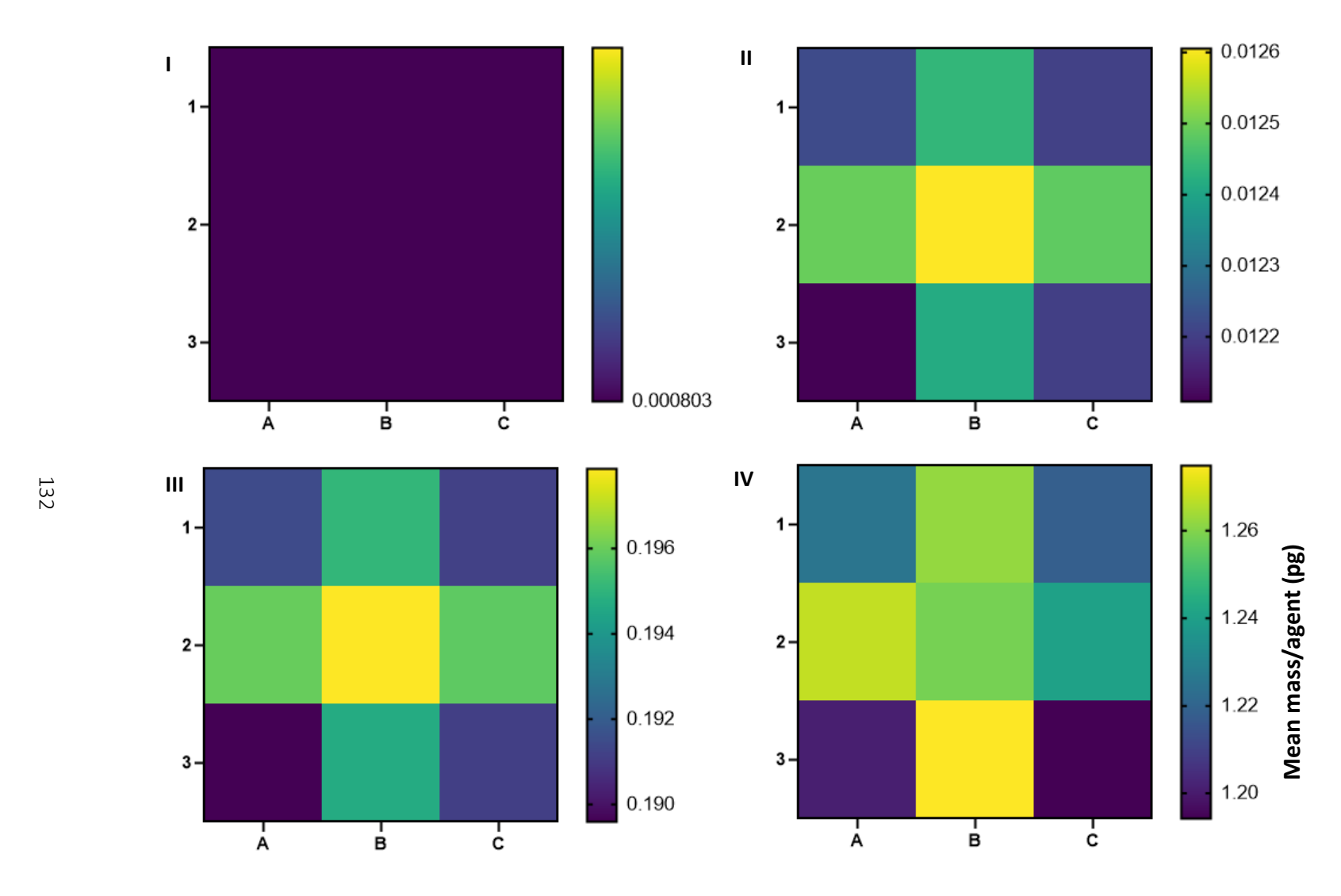


Figure 6.1: Mean mass per agent calculated for I) t=0h, II) 6h, III) 24h, IV) 48h. Each cell denotes where inhibiting component was applied at t=0, see Section 3.7.10.

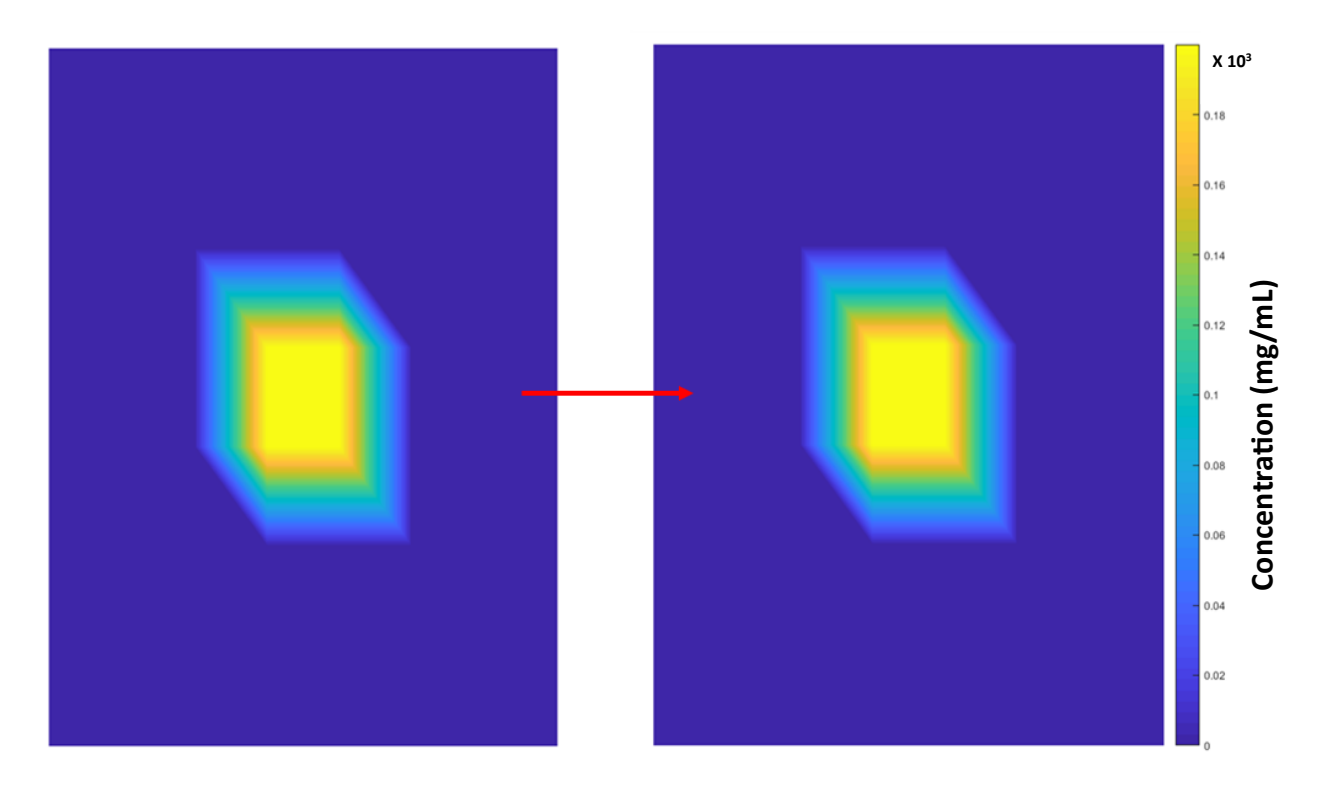


Figure 6.2: Inhibitor distribution at time, t=0h (left) and 48h (right) with D=  $1 \cdot 10^{-1}$  mg/mL per minute. Note minimal change in final concentration distribution.

# 6.3.2 Considering the influence of diffusivity in comparison to uninhibited growth

As a result of the outcome of Section 6.3.1, the diffusivity was altered and assessed for the effect on final mass per cell after 48 hours simulation time. Diffusivity ranging from 10<sup>3</sup> to 10<sup>-1</sup> mg/mL per minute were used in Regions 1, 2, and 5 (see Figure 3.11) due to the symmetrical nature of the environment as shown in Section 6.3.1, and final mean mass per cell was derived, shown in Figure 6.3. The untreated cell growth is also shown as a red dashed line representing a control simulation.

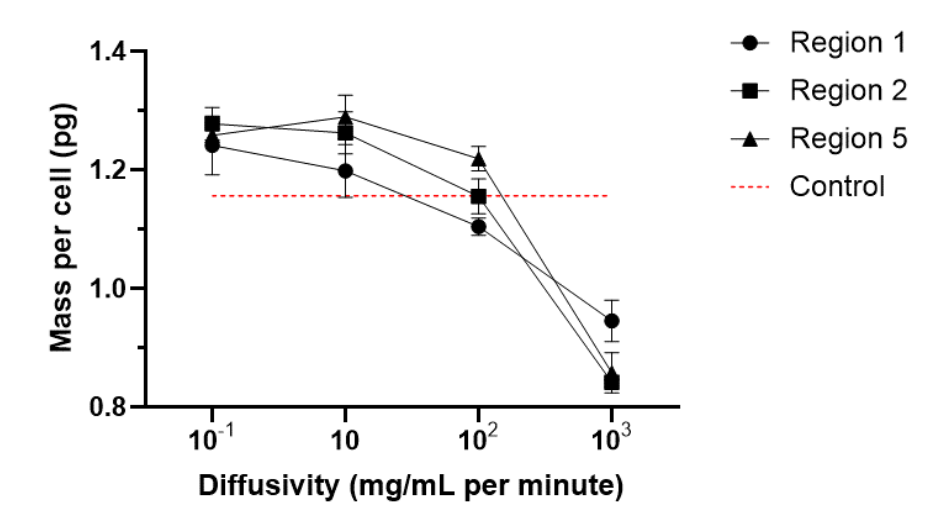


Figure 6.3: Mean mass per cell calculated at t=48 hours when subject to inhibiting reagent with variable diffusivity. Untreated *P. gingivalis* growth (Control) shown as red dashed line.

The membrane placement region appears to have minimal influence upon the mean mass per agent, with a majority of calculated p-values considered not significant (one exception at diffusivity of  $10^2$  mg/mL per minute, between Region 2:  $1.16\pm0.03$  pg, and Region 5:  $1.22\pm0.02$  pg,  $P \le 0.05$ , \*). At higher diffusivities comparable to saliva ( $D = 10^3$  mg/mL per minute), a considerable change in final mean mass per cell was noted in comparison to uninhibited agents (Control:  $1.16\pm0.02$  pg, in comparison to; Region 1:  $0.95\pm0.04$  pg,  $P \le 0.05$ , \*, Region 2:  $0.84\pm0.01$  pg,  $P \le 0.01$ , \*\*, and Region 5:  $0.86\pm0.03$  pg,  $P \le 0.0001$ , \*\*\*\*).

# 6.3.3 Influence of initial concentration on agent growth

After a simulation time of 48 hours, the average mass per cell was calculated, and plotted for Regions 1, 2, and 5 shown in Figure 6.4. The uninhibited growth (Control) is shown as a red dashed line.

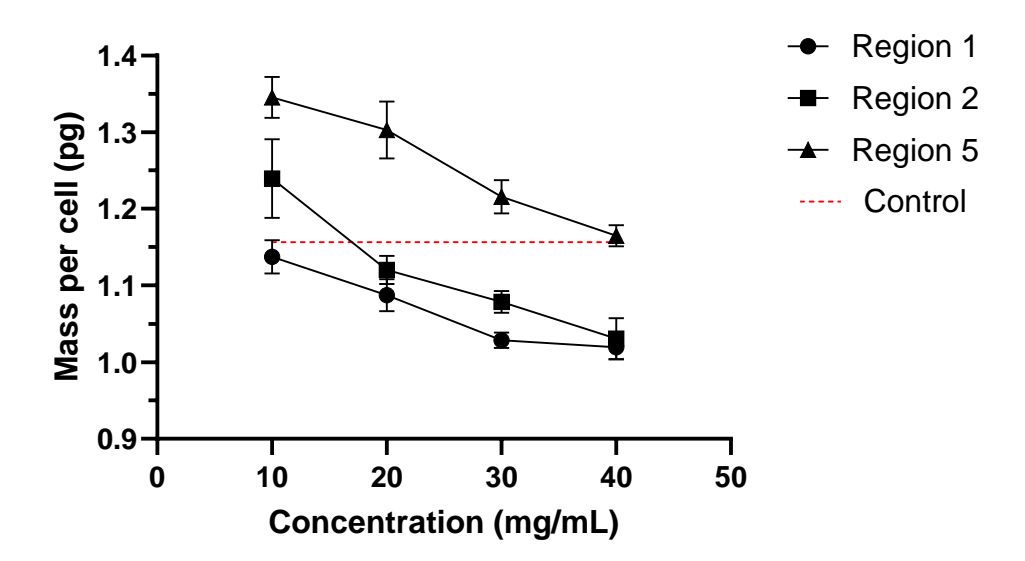


Figure 6.4: Average mass per cell calculated at t = 48 hours when subject to inhibiting reagent with variable initial concentration. Untreated *P. gingivalis* growth (Control) shown as red dashed line.

Here, a more pronounced distinction can be seen between Region 5 and Regions 1 and 2 during membrane placement, and Region 1 at a concentration of 40 mg/mL, mean values were analysed in comparison to control growth using paired t test analysis, showing significant changes (Region 1 vs. Control: P = 0.0495, \*). Region 5 had final mass per cell greater than control. A linear trend was fitted to Region 5 ( $R^2 = 0.9833$ ), and results were extrapolated to analyse when final mass per cell was significantly below control growth. Final mass per cell was reduced to 1.0 pg at a concentration of would be reduced by half when the concentration is  $\geq 65$  mg/mL.

# 6.3.4 Modelling two bacterial species in non-competitive growth in presence of inhibiting membrane

To simulate a two species system, the concentration of bacteria used was half that previously seen, leading to 250 agents in a 100  $\mu$ m<sup>2</sup> simulation space), as cumulatively the agent density at initialisation would remain the same. Therefore, in a proportional environment of 100  $\mu$ m<sup>2</sup>, and *S. aureus* and *P. gingivalis* agents equalling 250 agents per species, randomly dispersed throughout the environment. Additional parameters used for *S. aureus* are found in Table *3.2*.

.

Agent cell density; agents/  $\mu$ m<sup>3</sup>, was calculated at 6-hour intervals over 48 hours for *P. gingivalis* and *S. aureus*. In *P. gingivalis* growth shown in Figure 6.3, little distinction was seen between region placement, only Region 5 has been included for clarity. However, in comparison to control growth, the inclusion of inhibiting membranes limits the rate of growth as, by 48 hours, control growth has reached stationary phase, whereas in other environments, growth is slower and still increasing by 48 hours.

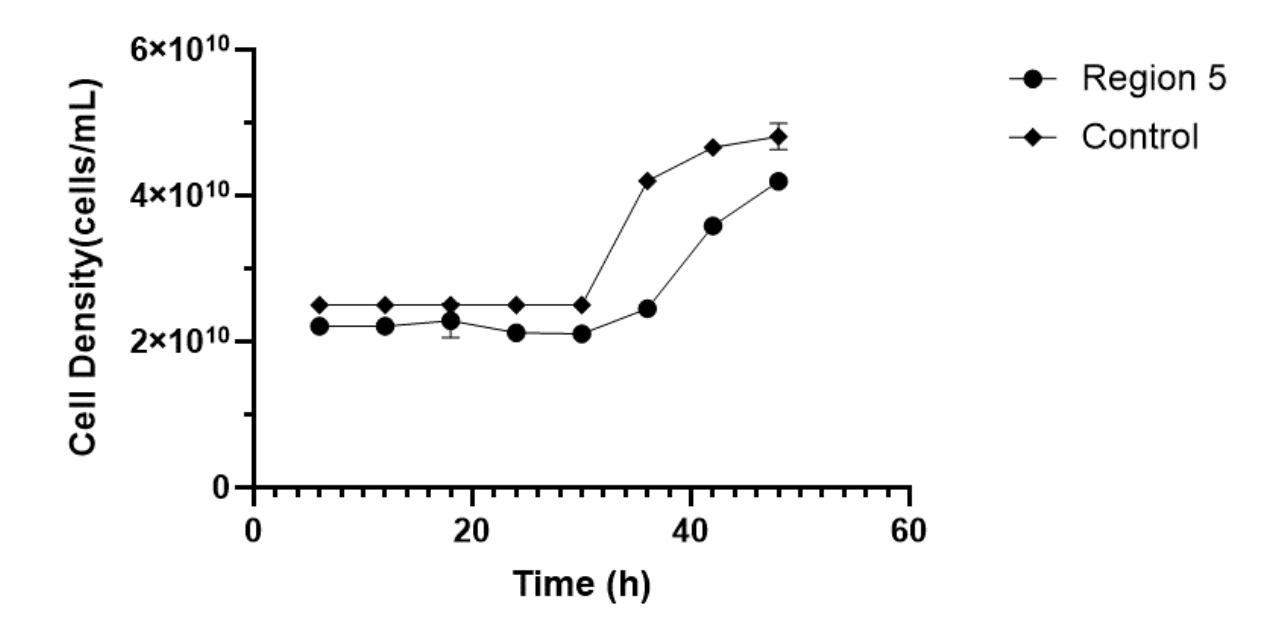


Figure 6.3: Cell density (Agents per unit mL) calculated for *P. gingivalis* agent growth in the presence of diffusing inhibiting membrane placed in three distinct regions of the environment. Growth performed alongside *S. aureus* agent growth. Control is untreated *P. gingivalis* culture.

For *S. aureus* growth (Figure 6.4), the inclusion of an inhibiting reagent allows an increasing number of agents that deviates from control at 18 hours. Although the concentration of inhibiting reagent limits growth around membrane, where membrane is placed, the agents are prevented from growth in a portion of the environment, and therefore the nutrients present here diffuse into the remainder of the environment over time, allowing for slow but steady growth. In contrast, the control environment where bacteria are uninhibited, agents rapidly consume and multiply, however a stationary phase occurs swiftly by 18 hours.

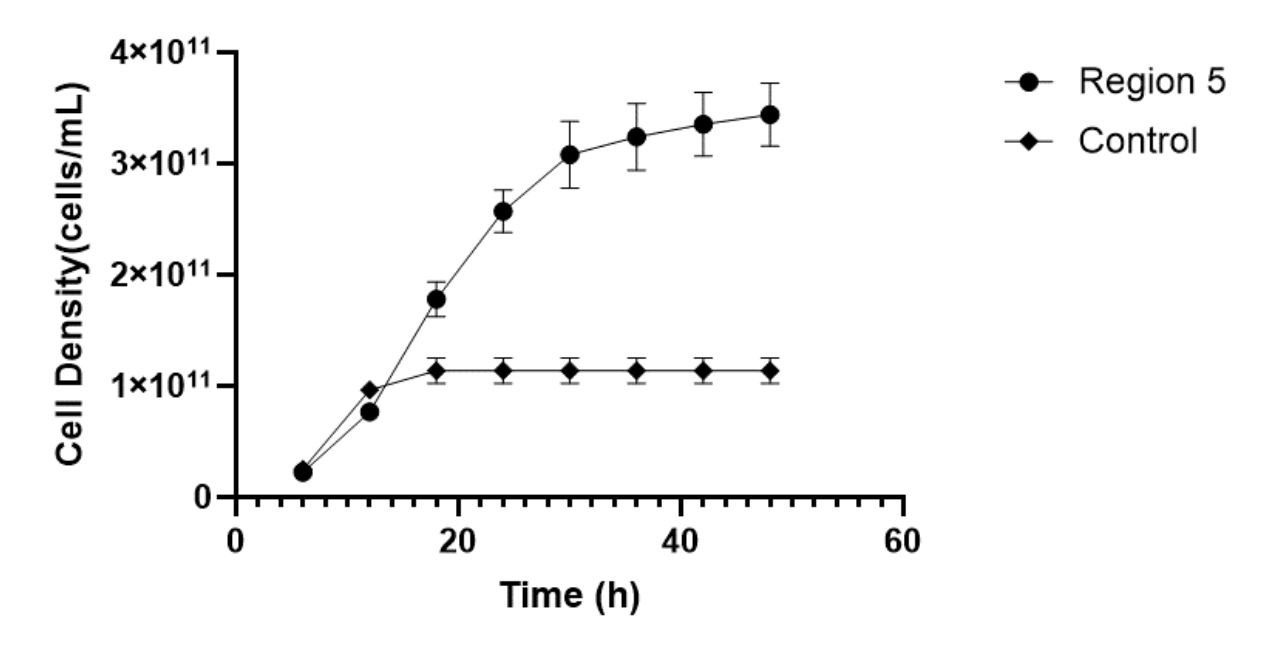


Figure 6.4: Cell density (Agents per unit mL) calculated for *S. aureus* agent growth in the presence of diffusing inhibiting membrane placed in three distinct regions of the environment. Growth performed alongside *P. gingivalis* agent growth. Control is untreated *S. aureus* culture.

Although the number of agents is increasing, when considering the mean mass per cell (APPENDIX 1), decay appears at a similar rate between simulated environments. In the context of the control well, therefore, the bacteria are starting to enter the death phase of growth.

### 6.4 Discussion

This chapter provided a framework for the design of an ideal membrane by modifying the iDynoMiCs platform, and qualitatively validated the model alongside experimental results in CHAPTER 4 and CHAPTER 5, and previously published work. The utility of such an agar plate-based model would allow users to test hypothesis that routinely occur in lab environments. In addition, it has been previously noted that thickness of a biofilm is independent of the diffusion factor, which is constant (Horn and Morgenroth 2006). Therefore, although simulations that are 1  $\mu$ m in height has been performed here, this model could include a biofilm mass of variable thickness with little change to the protocol parameters.

Validation of the model using control growth curves shows good agreement with published sources. *S. aureus* control growth showed qualitative similarities with published work, with exponential growth lasting less than 10 hours, followed by a plateau at between 12 and 18 hours (Le Marc, Valík et al. 2009, Tahi, Sousa et al. 2021). Whilst *P. gingivalis* control growth had a significantly greater lag time prior to exponential growth when compared to literature, the doubling time is still similar at 10 hours (Martin, Tamanai-Shacoori et al. 2017). In both cases, qualitatively similar growth patterns were observed during experimental work carried out during the project. As a result, the modifications made to the simulation had no fundamental change to the operation, introducing no systemic errors.

When assessing the placement of an inhibiting membrane, it was found that the diffusivity of Manuka Honey did not reduce the growth of bacteria, and analysis of the concentration distribution after 48 hours showed no change, which agrees with results presented in CHAPTER 5. Specifically, the membrane did not allow growth of bacteria on surface, but did not reduce growth in media.

Due to the low diffusivity of the reagent used ( $D_{honey}=1\cdot10^{-1}$  mL/minute), over the simulated time, the reagent did not diffuse to an extent that inhibited any significant agent growth. Agents are noted to collect in groups around the outer edge of the membrane. This would be a result of agents opportunistically feeding from the nutrients that diffused from the "AgentKill" zone, allowing these agents to grow and divide at a faster rate than other regions.

When utilised as part of layer-by-layer manufacture (see CHAPTER 5) Manuka Honey is in an undiluted state, as it deposits upon the membrane surface during drying time. When placed *in vivo*, the region would have a constant flow of saliva. Saliva would break down the polymeric surface and any inhibiting reagent would diffuse into the liquid, diluting the Manuka Honey and increasing the diffusivity. As such, validation of this model at different diffusivities would identify ideal viscosity of inhibiting reagent. Should the diffusivity be increased to an amount comparable to water, greater diffusion can be seen, and significant inhibition can be seen upon agents within 30 and 40 µm of the membrane, shown in Figure 6.7.

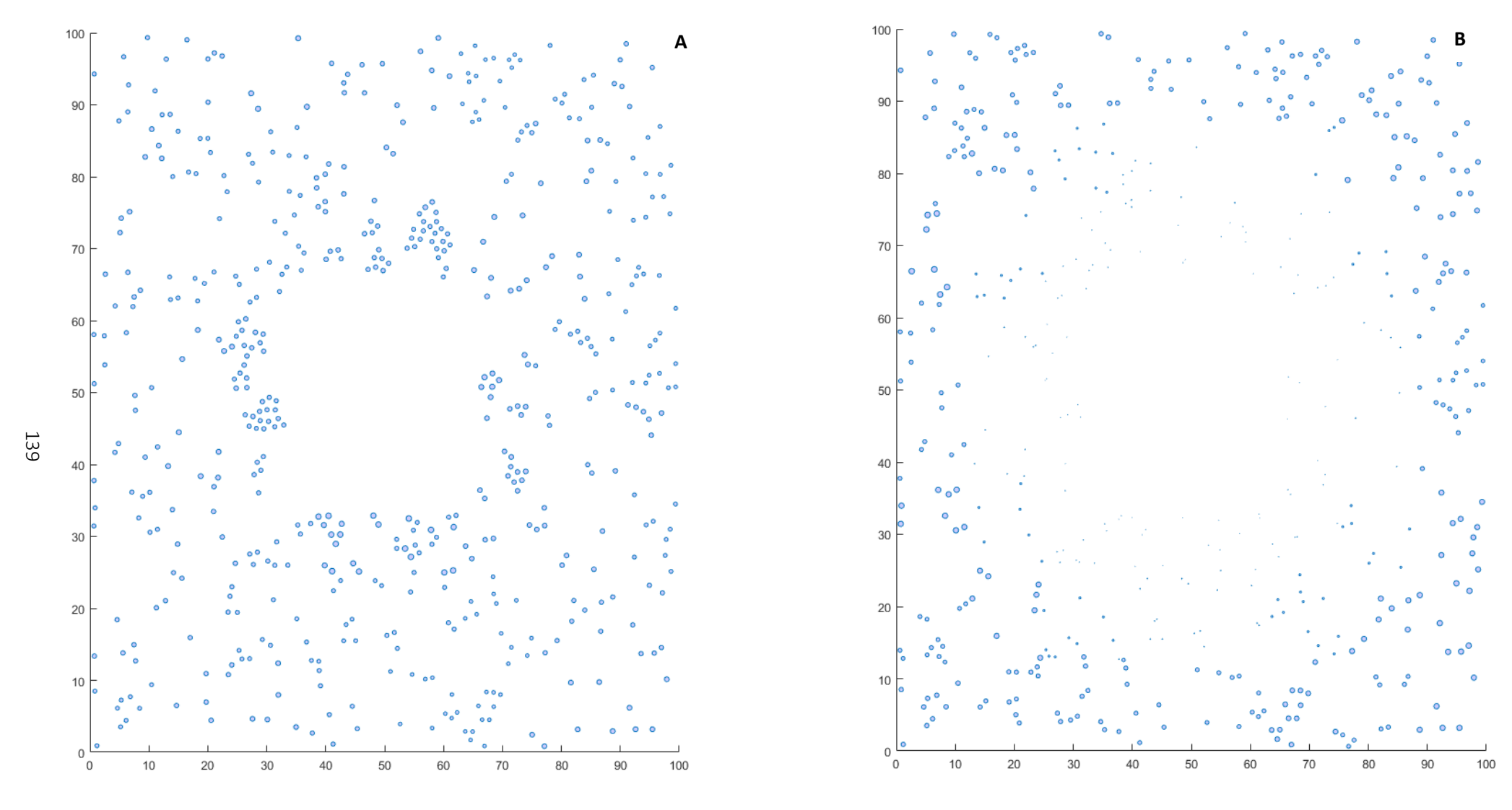


Figure 6.7: Scatter plot of agents at 48 hours for inhibiting reagent diffusivity of 10<sup>-1</sup> mL/minute (A) and 10<sup>3</sup> mL/minute (B). Size of scatter point denotes relative mass.

Increasing the diffusivity to 10<sup>3</sup> mL/minute caused a significant reduction in bacterial growth in comparison to control simulations. This is in agreement with diluted Manuka Honey shown in CHAPTER 4, which notes minimum inhibitory concentrations of 8 mg/mL, when considered diluted in media. As a solid inhibiting reagent diffuses from the membrane surface, and mixes with the saliva present in the oral surgical site, this would decrease the diffusivity to a sufficient degree as to provide a significant impact on bacterial growth.

The concentrations of the inhibiting membrane were next assessed, it was shown that inhibition of bacterial growth became significant at a Manuka Honey concentration between 40 mg/mL for *P. gingivalis*, which is greater than initially noted in CHAPTER 4, and published sources (Ahmed and Othman 2013, Safii, Tompkins et al. 2017). *P. gingivalis* is a sensitive bacteria type and, as seen in Figure 4.7, any reduction in the concentration of nutrient significantly reduces bacterial growth greater than what is proportionally expected. This inverse relationship was not considered during the development of the simulation, and may explain the discrepancy in expected inhibitory concentrations.

The concept of agar plate-based simulation is limited in recent studies. The focus primarily based on rod shaped bacteria with constant or probabilistic based growth (Granato, Smith et al. 2023, Rudge, Steiner et al. 2012). This chapter provides the framework for a novel approach for designing membranes. Examples using published sources are included here, however the addition of currently unpublished parameters would only improve the quality of output. A few considerations on specific parameters are presented here, and a summary of further improvements are made below:

 The parameters relating to growth rate of the bacteria such as the half saturation coefficient, and the maximum growth rate would benefit from individual derivation through experimentation. This would make the simulation unique for the individual used, who could tailor to fit the desired conditions (e.g. high glucose environment). 2. The rate of diffusion is assumed to be simply the diffusion coefficient of the inhibiting reagent in a 37°C, however in the case of Layer-by-Layer manufacture, the honey was diluted and deposited onto a PCL surface. The morphology (see CHAPTER 5 for further information here) is likely to have a slight variance on the diffusivity of the inhibiting reagent which would need to be analysed further.

Additionally, the assumption was made that the inhibiting reagent was deposited onto the surface at the initialisation of the simulation, however as reported in literature (Mancuso, Tonda-Turo et al. 2019), the inhibiting reagent would diffuse over a period of days. As has been seen a sufficient diffuse and highly concentrated inhibiting reagent has significant impact, however incident bacteria can occur randomly. Therefore, a more complex simulation could consider an influx of inhibiting reagent at specific times that mimic nanolayer breakdown.

Further bacterial agents could be introduced at different time steps that would model incident colonising bacteria onto the surface. For example, in Section 2.2.3, primary and secondary colonisers were introduced to indicate ideal periods when a bacterial cell would adhere to the host surface. *S. aureus* and *P. gingivalis* are examples of primary and secondary colonisers respectively, therefore their introduction into the simulation could similarly be staggered to mimic a bacterial infection more accurately.

### **CHAPTER 7 Conclusions and Recommendations**

### 7.1 General discussion

The aim of this PhD was to design and produce an ideal barrier membrane for use in the oral cavity during healing following GBR surgery. Specifically, innovative electrospun membranes were developed by functionalisation with the Layer-by-Layer assembly to incorporate natural-based antibacterial compounds. For example, the resulting electrostatic interaction created between the polyelectrolyte layers would allow a timely release of the antibacterial compounds, capable of antibacterial or bactericidal properties whilst keeping high cytocompatibility with mammalian cells. This work proposed insights for the scientific community in many different fields of research for future applications in industry as outlined below.

In CHAPTER 2, the reader was provided with the current understanding of the fields that were relevant to the research project on providing a proof-of-concept antibacterial barrier membrane from a mechanical, microbiological, and computational perspectives. This included dental implants and the risk of infection on current membranes on the market, the historic use of biofilm models and current computational augmentations, and the current study into the effectives of compounds as antibacterials. Indeed, whilst survival rate of dental implants are generally high, bacterial infection can still occur due to bacterial build up on the peri-implant tissue, which risk dental implant failure (Mombelli and Décaillet 2011, Royal College of Surgeons: Faculty of Dental Surgery and Restorative Dentistry-UK 2019).

GBR is currently employed where replacement of missing bone is required using particulate autogenous bone and/or osteoconductive material. During healing, to maintain site shape and preventing ingress of soft tissue (Budihardja 2019), barrier membranes were used. Whilst current market membranes offer physical barrier protection, previous bacterial infection of inert membranes have prompted the need for membrane augmentation to provide antibacterial relief to dental implant wound sites (Slutzkey, Kozlovsky et al. 2015,

Aprile, Letourneur et al. 2020). Different studies consider antibiotic loading into barrier membranes (Shahi 2017, Sharif 2019); however the over reliance of antibiotics has seen an exponential growth in AMR (Antimicrobial Resistance Collaborators 2022) and alternate compounds have been considered (Srikandace, Indrarti et al. 2018, Ismaila, Shamelia et al. 2019, Zhang, Liu et al. 2021).

Amongst alternative compounds such as Tea Tree Oil (Carson, Hammer et al. 2006, Yadav, Kumar et al. 2017), and Lemon Oil (Frassinetti, Caltavuturo et al. 2011, Císarová, Tančinová et al. 2016), Manuka Honey has been of interest in wound treatment applications for its anti-inflammatory properties (Mandal and Mandal 2011). Manuka Honey, in comparison to other honeys, is unique in its component of MGO, which has been linked to increased antibacterial activity (Johnston, McBride et al. 2018). An additional effect of these compounds are the effect on human tissue which at higher concentrations have produced inflammatory responses in human tissue (Minden-Birkenmaier and Bowlin 2018).

The first aim in this thesis was to parameterise selected compounds for their bactericidal and cytotoxic properties. Essential Oils were also previously reported as having effective antibacterial properties (Yadav, Kumar et al. 2017), and in this thesis, Tea Tree Oil and Lemon Oil exhibited antibacterial properties at concentrations whilst remaining cytocompatible for *S. aureus* NCTC6571; however this was not observed in *P. gingivalis* W50 assays, which required concentrations that were not deemed cytocompatible (tested using human neonatal fibroblasts and osteoblasts). Previously studied Minimum Inhibitory Concentrations for citrus oils ranged between 100 µg/mL and 250 µg/mL; however there was concern regarding the reliability of these results which relied on the use of solvents such as ethanol and DMSO which may have artificially impacted the resultant MIC (Shapiro, Meier et al. 1994, Carson, Hammer et al. 2006, Frassinetti, Caltavuturo et al. 2011, Thomsen, Hammer et al. 2013). No toxicity was found at inhibitory concentrations, agreeing with published work that noted no toxicity below 10 mg/mL (Loughlin, Gilmore et al. 2008). However, little work has currently been conducted on Lemon Oil cytotoxicity and could not be directly compared.

Furthermore, Minimum Inhibitory Concentrations for Manuka Honey 400 and 550+ were found to be around 10 mg/mL against both *S. aureus* NCTC6571 and *P. gingivalis* W50, without becoming cytotoxic to both human neonatal fibroblast and osteoblast cells. In literature it was unclear the extent at which Manuka Honey may reduce the mechanism of osteoblasts to deposit calcium, with previous studies stating reduced calcium production when exposed to Manuka Honey cryogels (Robertson, Hixon et al. 2023), and demineralise hard tissue (Safii, Tompkins et al. 2017). Within this thesis, concentrations of 10 mg/mL, Manuka Honey 400 and 550+ significantly reduced the rate of osteoblast calcification in comparison to untreated control wells.

A non-linear trend was observed in antibacterial activity of Manuka Honey against *S. aureus* NCTC6571. Moreover, high concentrations of Manuka Honey were observed to provide sufficient nutrients for bacterial growth as reported elsewhere (Mizzi, Maniscalco et al. 2020). Concentrations of Manuka Honey in membranes, therefore, should be carefully considered for *in vivo* studies, where high concentrations of Manuka Honey could lead to increased risk of infection.

Whilst essential oils should not be disregarded for their synergistic utility (Chircov, Miclea et al. 2021), Manuka Honey 400 and 550+ showed broad antibacterial properties whilst remaining cytocompatible, suggesting the most promising balance of bactericidal and non-cytotoxic properties, and were therefore used in PCL membrane functionalisation.

The second aim within this thesis sought to functionalise electrospun PCL membranes using dip coating of Manuka Honey 550+ layer-by-layer techniques. All compounds were assessed on their zeta-potential value to check if there were appropriate to be used as polyelectrolytes. A strong negative zeta-potential was noted in compounds of pH 5.5 and above. A zeta potential of ±5 mV was deemed sufficiently great to provide good adhesion to membrane surfaces, promoting the electrostatic interactions between the polyelectrolytes. A pH 5.5 was chosen as it was previously demonstrated that slightly acidic environments promoted wound healing and increased antibacterial activity *in vivo* (Nagoba, Suryawanshi et al. 2015). Further, the output spectra from FTIR-ATR showed that

characteristic PAH and Manuka Honey peaks were seen. This, combined with the SEM images, demonstrates that a pH 5.5 solution of Manuka Honey is of sufficiently high charge to build multiple nanolayers on electrospun membranes, with consistent pore size that would hypothetically allow the proliferation of mammalian cells.

Previously, it was unclear how Manuka Honey 550+ would diffuse from the surface of a membrane *in vitro* and, further, Manuka Honey 550+ adhered well to the electrospun surface. It has been shown that Manuka Honey 550+ was successfully functionalised onto electrospun membranes up to 14 nanolayers and characterised for their ability to act as an antibacterial and not cause cell cytotoxic response. In addition, a gradual measurement of MGO concentration from nanolayer membranes demonstrates the gradual release of Manuka Honey up to a period of 14 days, which plateaus by day 21.

Whilst bacterial growth was not inhibited in broth dilutions, bacteria did not attach and proliferate across the surface of membranes. The rate of Manuka Honey release from nanolayer surface as demonstrated above, did not sufficiently diffuse from the surface to provide a significant impact on bacterial growth. However, whilst 14 nanolayer MH membranes performed similarly to bare PCL membranes as an antibacterial, MH membranes showed improved cell proliferation rate as seen in previous studies on isolated Manuka Honey (Minden-Birkenmaier and Bowlin 2018).

Finally, it was the intention to incorporate the insights gleaned from the previous three chapters by incorporating our understanding into a computational model that would be able to support the selection of the selected compounds and development of membranes suitable for GBR applications. The utilisation of mathematical modelling has been used to investigate growth of bacteria (Swimberghe, Coenye et al. 2019), as a way to, for example, reduce lab times, or rapidly test hypotheses (Esser, Leveau et al. 2015). Monod kinetics provided a mathematical framework that provides insight into the dynamics of bacterial growth in the six phases of bacterial growth (Monod 1949). and has been developed for specific uses such as food safety (Le Marc, Valík et al. 2009), or wastewater treatment (Ofiţeru, Bellucci et al. 2014). At the broader scale, these models have incorporated

multiple inhibitory and nutrient diffusing sources (Andrews 1968, Esser, Leveau et al. 2015). Previous studies model multi-species interactions, inhibiting substrates, or inclusion of antibiotics (Levin and Udekwu 2010, Martin, Tamanai-Shacoori et al. 2017, Rudge, Steiner et al. 2012). However, they do not accurately portray the testing of an antibacterial membrane upon an agar plate or consider how an antibacterial would diffuse into a simulated region.

This has been shown through the manipulation of the iDynoMiCs model to simulate the effect *in vitro*. Model was validated through qualitative agreement with published work on *S. aureus* and *P. gingivalis* growth curves (Le Marc, Valík et al. 2009, Martin, Tamanai-Shacoori et al. 2017, Tahi, Sousa et al. 2021). In addition, several hypotheses were able to define the parameters of an inhibiting membrane suitable for the oral environment. From the tested hypotheses, a suitable range of diffusing inhibitor, and the initial concentration required to have significant impact on bacterial growth is shown. The opportunity to streamline experimentation has the potential to reduce lead times when used in long term projects.

# 7.2 Recommendations

Outstanding areas of interest have arisen as a result of this work that would allow for a more realised end product. These have been separated below into broad categories. However, it is worth noting generally here that peri-implant diseases are not limited to the duration of healing period, and can take years to develop, with any antimicrobial membrane only offering relatively short-term prevention (P. Andrew Norowski and Bumgardner 2009).

Whilst any implant surface and coating are being considered for long-term antibacterial benefits, the utilisation of intelligent design in antimicrobial protection could greatly benefit implant sites where longevity of membrane degradation could be tailored. This offers benefits both in the oral cavity, but also broader wound healing scenarios where size of sites can vary greatly. This may be aided using emerging biotechnologies such as

hydrogels and cryogels which could be designed to respond to different conditions, allowing for an increase of decrease in antibacterial reagent, as it has been shown that prolonged exposure could have negative impact on tissue without changing antibacterial efficacy.

# 7.2.1 Computational modelling: parameters and developments

Whilst an *in silico* model of an inhibiting membrane has been developed, it currently lacks key parameters derived through independent studies. Specifically, a single source of carbon source and kinetic parameters (e.g. half-saturation coefficient) is required, ideally in a lab environment using identical conditions and bacterial cell lines defined by the user.

In the current form, an assumption was made to deposit full concentrations of inhibiting compound at initialisation of the simulation. However in practice, the inhibiting reagent would diffuse into the environment over time. To this end, in a similar manner seen in previous studies (Head, Devine et al. 2017), a 'pulsed' concentration would mimic the effect of inhibiting release over time. This would be informed by multiple release profiles akin to those outlined within this thesis.

What has been demonstrated is a top-down view of an agar plate during bacterial growth in the presence of an inhibiting membrane. One of the assumptions was that the membrane did not interact with the environment when considering nutrient transfer and is placed only as an inhibiting bioactive compound diffusion and for agent removal. However, nutrients would permeate porous membranes dependent on the permeability of the membrane (Luis 2018). For this reason, should the intention be to model a more complex environment, consideration should be given on the effect a membrane would have on the flow of nutrients.

### 7.2.2 Membrane functionalisation

Whilst the surface composition was covered here, no work was undertaken to identify how the mechanical properties of the membrane change after LbL functionalisation, or how this could be curtailed. This mechanical change could lead to unexpected membrane breakages over longer healing periods as seen in other studies with composite membranes (Abtahi, Chen et al. 2023).

Whilst Tea Tree Oil and Lemon Oil were found be bactericidal to certain strains whilst having insignificant effect on fibroblast and osteoblast proliferation, these were not readily incorporated onto membrane surface. Preliminary work was achieved by Gallo et al. (see Acknowledgements); however, the findings were as seen in MH functionalised membrane and only exposed to bacterial strains. From this, a compositional study of how EOs are functionalised and how they interact with cell proliferation should be undertaken.

In addition, the release profile of MH membranes was assessed over time and, in a similar vein, EOs should undergo a similar protocol to analyse the diffusion of EO into the environment over time to give an indication of their long-term efficacy.

A useful concept would also be to image membranes after growth to analysis the extent of degradation to the polymeric membrane and dispersal of the Manuka Honey. In addition, over time, this hydrophobicity would decrease as the membrane took on liquid, and therefore an analysis of contact angle over time alongside the antibacterial and cytotoxic effects could give an indication on the role hydrophobic membranes play during wound healing.

As an interim stage from those outlined within this thesis, the utilisation of other studies that seek to create an artificial wound site would be a useful consideration (Vaquette, Fan et al. 2012). This would allow the user to perform membrane placement on a site and analyse effects over time without moving to *in vivo* experimentation.

# REFERENCES

Abtahi, S., et al. (2023). "Resorbable Membranes for Guided Bone Regeneration: Critical Features, Potentials, and Limitations." <u>ACS Materials</u>.

Agarwal, H., et al. (2023). "Bacterial Pigments and Their Multifaceted Roles in Contemporary Biotechnology and Pharmacological Applications." <u>Microorganisms</u> **11**(614).

Ahmed, S. and N. H. Othman (2013). "Review of the medicinal effects of tualang honey and a comparison with Manuka honey." <u>Malays J Med Sci.</u> **20**(3): 6-13.

Al-Khanati, N. M. and Y. Al-Moudallal (2019). "Effect of Intrasocket Application of Manuka Honey on Postsurgical Pain of Impacted Mandibular Third Molars Surgery: Split-Mouth Randomized Controlled Trial." J. Maxillofac. Oral Surg. 18: 147-152.

Alvarez-Suarez, J. M., et al. (2014). "The Composition and Biological Activity of Honey: A Focus on Manuka Honey." <u>Foods</u> **3**: 420-432.

Andrews, J. F. (1968). "A Mathematical Model for the Continuous Culture of Microorganisms Utilizing Inhibitory Substrates." <u>Biotechnology and Bioengineering</u> **10**: 707-723.

Anjos, O., et al. (2015). "Application of FTIR-ATR spectroscopy to the quantification of sugar in honey." <u>Food Chem.</u> **169**: 218–223.

Antimicrobial Resistance Collaborators (2022). "Global burden of bacterial antimicrobial resistance in 2019: a systematic analysis." <u>The Lancet</u> **399**(10325): 629-655.

Aprile, P., et al. (2020). "Membranes for Guided Bone Regeneration: A Road from Bench to Bedside." <u>Adv. Healthcare Mater.</u> **9**(19).

Assmanna, C. E., et al. (2018). "Tea tree oil presents in vitro antitumor acitivity on breast cancer cells without cytotoxic effects on fibroblasts and on peripheral blood mononuclear cells." Biomedicine & Pharmacotherapy **103**: 1253–1261.

Baggi, L., et al. (2008). "The influence of implant diameter and length on stress distribution of osseointegrated implants related to crestal bone geometry a three-dimensional finite element analysis." The Journal of Prosthetic Dentistry **100**(6): 422-431.

Baglivo, M. (2011). "Drug: The Effect of Tetracycline in Degradation and Permeability of Collagen Membrane." ClinicalTrials.gov identifier: NCT02057926. Retrieved 14 March 2023, from https://beta.clinicaltrials.gov/study/NCT02057926.

Berkovitch, Y., et al. (2016). Effect of natural honey treatment and external stretching on kinematics of cell migration during gap closure. <u>Computer Methods in Biomechanics and Biomedical Engineering</u>. <u>Proceedings of the 14th International Symposium CMBBE, Tel</u>
Aviv, Israel, 2016. A. Gefen and D. Weihs. Web, Springer International Publishing: 75-80.

Bethesda (MD) and National Institute of Dental and Craniofacial Research (US) (2021).

Section 3A: Oral Health Across the Lifespan: Working-Age Adults. Oral Health in America:

Advances and Challenges.

Bigham-Sadegh, A. and A. Oryan (2015). "Basic concepts regarding fracture healing and the current options and future directions in managing bone fractures." <u>International</u> Wound Journal **12**: 238–247.

Blair, S. E., et al. (2009). "The unusual antibacterial activity of medical-grade Leptospermum honey: antibacterial spectrum, resistance and transcriptome analysis." <u>Eur J Clin Microbiol Infect Dis</u> **28**: 1199–1208.

Boateng, J. and K. N. Diunase (2015). "Comparing the Antibacterial and Functional Properties of Cameroonian and Manuka Honeys for Potential Wound Healing-Have We Come Full Cycle in Dealing with Antibiotic Resistance?" Molecules **20**: 16068-16084.

Bottinoa, M. C., et al. (2012). "Recent advances in the development of GTR/GBR membranes for periodontal regeneration — A materials perspective." <u>Dental Materials</u> **28**.

Brägger, U., et al. (2005). "Economic aspects of single-tooth replacement." <u>Clin. Oral Impl.</u>
Res. **16**: 335–341.

Brah, A. S., et al. (2023). "Toxicity and therapeutic applications of citrus essential oils (CEOs): a review." <u>International Journal of Food Properties</u> **26**(1): 301-326.

British Standards Institution (2020). Susceptibility testing of infectious agents and evaluation of performance of antimicrobial susceptibility test devices Part 1: Broth microdilution reference method for testing the in vitro activity of antimicrobial agents against rapidly growing aerobic bacteria involved in infectious diseases (ISO 20776-1:2019, including Corrected version 2019-12). **BS EN ISO 20776-1:2020**.

Brudzynski, K. and C. Sjaarda (2014). "Antibacterial compounds of canadian honeys target bacterial cell wall inducing phenotype changes, growth inhibition and cell lysis that resemble action of  $\beta$ -lactam antibiotics." <u>PloS one</u> **9**(9): e106967.

Budihardja, A. S. (2019). Guided Bone Regeneration, Bone Splitting, Interpositional Osteoplastic. Bone Management in Dental Implantology. A. S. Budihardja and T. Mücke. New York, Springer.

Cambridge University Hospitals (2021). "Dental implants in restorative dentistry." 1. Retrieved 06 July 2022, from <a href="https://www.cuh.nhs.uk/patient-information/dental-implants-in-restorative-dentistry/">https://www.cuh.nhs.uk/patient-information/dental-implants-in-restorative-dentistry/</a>.

Campbell, J. and A. S. Vikulina (2020). "Layer-By-Layer Assemblies of Biopolymers: Build-Up, Mechanical Stability and Molecular Dynamics." <u>Polymers</u> **1949**(12).

Carson, C. F., et al. (2006). "Melaleuca alternifolia (Tea Tree) Oil: a Review of Antimicrobial and Other Medicinal Properties." <u>Clinical Microbiology Reviews</u> **19**(1): 50–62.

Chaturvedi, R., et al. (2008). "Evaluation of the regenerative potential of 25% doxycycline-loaded biodegradable membrane vs biodegradable membrane alone in the treatment of human periodontal infrabony defects: A clinical and radiological study." <u>Indian J Dent Res.</u> **9**(2): 116-123.

Chi, M. H., et al. (2019). "Novel Bioactive and Therapeutic Dental Polymeric Materials to Inhibit Periodontal Pathogens and Biofilms." <u>International Journal of Molecular Sciences</u> **20**(2): 29.

Chircov, C., et al. (2021). "Essential Oils for Bone Repair and Regeneration—Mechanisms and Applications." <u>Materials</u> **14**(1867).

Císarová, M., et al. (2016). "Antifungal activity of lemon, eucalyptus, thyme, oregano, sage and lavender essential oils against *Aspergillus niger* and *Aspergillus tubingensis* isolated from grapes." <u>Potravinarstvo</u> **10**(1): 83-88.

Clinical and Laboratory Standards Institute (1999). Methods for Determining Bactericidal Activity of Antimicrobial Agents; Approved Guideline. **M26-A**.

Cockx, B., et al. (2023). "Is it selfish to be filamentous in biofilms? Individual-based modeling links microbial growth strategies with morphology using the new and modular iDynoMiCS 2.0." <u>bioRxiv</u>.

Combarros-Fuertes, P., et al. (2019). "Evaluation of physiological effects induced by manuka honey upon staphylococcus aureus and escherichia coli." <u>Microorganisms</u> **7**(8): 258.

Cooper, R. A., et al. (2010). "Absence of bacterial resistance to medical-grade manuka honey." <u>Eur J Clin Microbiol Infect Dis</u> **29**: 1237–1241.

Corea-Téllez, K. S., et al. (2008). "Estimated Risks of Water and Saliva Contamination by Phthalate Diffusion from Plasticized Polyvinyl Chloride." J Environ Health **71**(3): 34–45.

Couto, R. A. S., et al. (2018). "Detection of Escherichia coli bacteria by impact electrochemistry." <u>Analyst(20)</u>.

Deyno, S., et al. (2019). "Essential oils as topical anti-infective agents: A systematic review and meta-analysis." <u>Complementary Therapies in Medicine</u> **47**: 102224.

Dimitriou, R., et al. (2012). "The role of barrier membranes for guided bone regeneration and restoration of large bone defects: current experimental and clinical evidence." <u>BMC Medicine</u> **10**(81).

Du Toit, D. F. and B. J. Page (2009). "An in vitro evaluation of the cell toxicity of honey and silver dressings." Journal of Wound Care **18**(9): 383-389.

Dzianach, P. A., et al. (2019). "Challenges of biofilm control and utilization: lessons from mathematical modelling." J. R. Soc. Interface **16**(155): 20190042.

Elzein, T., et al. (2004). "FTIR study of polycaprolactone chain organization at interfaces." Journal ofColloid and Interface Science **273**: 381–387.

English, H. K., et al. (2004). "The effects of manuka honey on plaque and gingivitis: a pilot study." J Int Acad Periodontol **6**(2): 63-67.

Esposito, M., et al. (1998). "Biological factors contributing to failures of osseointegrated oral implants, (II). Etiopathogenesis." <u>Eur J Oral Sci</u> **106**: 721–764.

Esser, D. S., et al. (2015). "Modeling microbial growth and dynamics." <u>Appl Microbiol</u> Biotechnol **99**: 8831–8846.

European Committee for Antimicrobial Susceptibility Testing (2000). Determination of minimum inhibitory concentrations (MICs) of antibacterial agents by agar dilution. <u>EUCAST Definitive Document E.Def 3.1</u>. European Society of Clinical Microbiology and Infectious Diseases. Farkasovska, J., et al. (2019). "The role of hydrogen peroxide in the antibacterial activity of different floral honeys." <u>European Food Research and Technology</u> **245**: 2739–2744.

Ferreira, A. M., et al. (2016). "Impact of Collagen/Heparin Multilayers for Regulating Bone Cellular Functions." ACS Appl Mater Interfaces **8**(44): 29923-29932.

Frassinetti, S., et al. (2011). "Antibacterial and antioxidant activity of essential oils from citrus spp." <u>Journal of Essential Oil Research</u> **23**(1): 27-31.

French, D., et al. (2021). "Long term clinical performance of 10 871 dental implants withup to 22 years of follow-up: A cohort study in 4247 patients." Clin Implant Dent Relat Res. 23: 289–297.

Galinha, C. F., et al. (2018). Chapter 6 - Membrane bioreactors. <u>Fundamental Modelling of Membrane Systems</u>. P. Luis. Oxford, Elsevier: 209-249.

Gaviria, L., et al. (2014). "Current trends in dental implants." J Korean Assoc Oral Maxillofac Surg **40**: 50-60.

Gawek, M., et al. (2021). "Energy dependent XPS measurements on thin films of a poly(vinyl methyl ether)/polystyrene blend concentration profile on a nanometer resolution to understand the behavior of nanofilms." <u>Soft Matter</u> **17**: 6985–6994.

Gentile, P., et al. (2011). "Polymeric membranes for guided bone regeneration." Biotechnol. J. **6**: 1187–1197.

Gentile, P., et al. (2017). "Multilayer Nanoscale Encapsulation of Biofunctional Peptides to Enhance Bone Tissue Regeneration In Vivo." <u>Adv. Healthcare Mater.</u> **6**: 11.

Gentile, P., et al. (2015). "Functionalised nanoscale coatings using layer-by-layer assembly for imparting antibacterial properties to polylactide-co-glycolide surfaces." <u>Acta Biomaterialia</u> **21**: 35 - 43.

Gizaw, M., et al. (2018). "Electrospun Fibers as a Dressing Material for Drug and Biological Agent Delivery in Wound Healing Applications." <u>Bioengineering</u> **5**(1).

Gokhale, S. R. and A. M. Padhye (2013). "Future prospects of systemic host modulatory agents in periodontal therapy." <u>British Dental Journal</u> **214**(9).

Golmohamadi, M., et al. (2013). "The role of charge on the diffusion of solutes and nanoparticles (silicon nanocrystals, nTiO<sub>2</sub>, nAu) in a biofilm." <u>Environ. Chem.</u> **10**: 34-41.

Gorochowski, T. E., et al. (2012). "BSim: An Agent-Based Tool for Modeling Bacterial Populations in Systems and Synthetic Biology." <u>PloS one</u> **7**(8): e42790.

Granato, E. T., et al. (2023). "Collective protection against the type VI secretion system in bacteria." The ISME Journal **17**: 1052 – 1062.

Gregory, R., et al. (2005). Computing Bacterial Evolvability Using Individual-Based Models.

Molecular Computational Models: Unconventional Approaches. M. Gheorghe. Hershey,

PA, IGI Global.

Grey, E. B., et al. (2012). "A qualitative study of patients' motivations and expectations for dental implants." <u>British Dental Journal</u> **214**.

Guazzo, R., et al. (2018). "Graphene-Based Nanomaterials for Tissue Engineering in the Dental Field." Nanomaterials **8**(5).

Gulati, M., et al. (2014). "Implant Maintenance: A Clinical Update." <u>International scholarly</u> research notices.

Gustafsson, L., et al. (2020). "Recombinant Spider Silk Forms Tough and Elastic Nanomembranes that are Protein-Permeable and Support Cell Attachment and Growth."

Adv. Funct. Mater. 30.

Güzey, D. and D. J. McClements (2006). "Influence of Environmental Stresses on O/W Emulsions Stabilized by  $\beta$ -Lactoglobulin—Pectin and  $\beta$ -Lactoglobulin—Pectin—Chitosan Membranes Produced by the Electrostatic Layer-by-Layer Deposition Technique." <u>Food Biophysics</u> **1**: 30-40.

H&R Healthcare. "L-Mesitran Hydro." Retrieved 28 September, 2021, from <a href="https://www.hrhealthcare.co.uk/portfolio/l-mesitran-hydro/">https://www.hrhealthcare.co.uk/portfolio/l-mesitran-hydro/</a>.

Hall-Stoodley, L., et al. (2012). "Towards diagnostic guidelines for biofilm-associated infections." FEMS Immunol. Med. Microbiol. **65**: 127-145.

Han, K. and O. Levenspiel (1988). "Extended Monod Kinetics for Substrate, Product, and Cell Inhibition." <u>Biotechnology and Bioengineering</u> **32**: 430-437.

Hanaor, D., et al. (2012). "The effects of carboxylic acids on the aqueous dispersion and electrophoretic deposition of ZrO<sub>2</sub>." <u>Journal of the European Ceramic Society</u> **32**: 235–244.

Hashimoto, Y., et al. (2022). "Microbial differences between active and remission peri-implantitis." <u>Scientific Reports</u> **12**(5284).

Head, D., et al. (2017). "In silico modelling to differentiate the contribution of sugar frequency *versus* total amount in driving biofilm dysbiosis in dental caries." <u>Scientific</u> Reports **7**(17413).

Head, D. A., et al. (2014). "Non-Lethal Control of the Cariogenic Potential of an Agent-Based Model for Dental Plaque." PloS one **9**(8).

Hellweger, F. L., et al. (2016). "Advancing microbial sciences by individual-based modelling." Nature Reviews. Microbiology **14**(7): 461-471.

Henriques, A. F., et al. (2010). "The intracellular effects of manuka honey on Staphylococcus aureus." <u>Eur J Clin Microbiol Infect Dis</u> **29**(1): 45–50.

Hibbing, M. E., et al. (2010). "Bacterial competition: surviving and thriving in the microbial jungle." Nat Rev Microbiol. **8**(1): 15–25.

Hixon, K. R., et al. (2019). "Investigating Manuka Honey Antibacterial Properties When Incorporated into Cryogel, Hydrogel, and Electrospun Tissue Engineering Scaffolds." <u>Gels.</u> **5**(2): 21-36.

Hixon, K. R., et al. (2019). "Mineralization and antibacterial potential of bioactive cryogel scaffolds in vitro." <a href="International Journal of Polymeric Materials">International Journal of Polymeric Materials</a> and Polymeric <a href="Biomaterials">Biomaterials</a> 68(15): 901–914.

Holmes, R. K. and M. G. Jobling (1996). Chapter 5 : Genetics. <u>Medical Microbiology</u>. S. Baron. Galveston, University of Texas Medical Branch at Galveston.

Horn, H. and E. Morgenroth (2006). "Transport of oxygen, sodium chloride, and sodium nitrate in biofilms." <u>Chemical Engineering Science</u> **61**: 1347–1356.

How, K. Y., et al. (2016). "*Porphyromonas gingivalis*: An Overview of Periodontopathic Pathogen below the Gum Line." Frontiers in microbiology **7**(53).

Iglesias-Urraca, C. (2014). Skeletal Reconstruction. <u>Complex Fractures of the Limbs:</u>

<u>Diagnosis and Management</u>. E. C. Rodríguez-Merchán and J. C. Rubio-Suárez, Springer Cham: 127-135.

Iler, R. K. (1966). "Multilayers of colloidal particles." <u>Journal of Colloid and Interface</u>
<u>Science</u> **21**(6): 569-594.

Ismaila, N. A., et al. (2019). "Antibacterial and cytotoxic effect of honey mediated copper nanoparticles synthesized using ultrasonic assistance." <u>Materials Science & Engineering C</u> **104**: 10.

Jamnongkan, T., et al. (2012). "Effect of Poly(vinyl alcohol)/Chitosan Ratio on Electrospunnanofiber Morphologies" <u>Advanced Materials Research</u> **463-464**: 734-738.

Javaid, S., et al. (2022). "Layer-By-Layer Self-Assembled Dip Coating for Antifouling Functionalized Finishing of Cotton Textile." Polymers **14**(13).

Johnston, M., et al. (2018). "Antibacterial activity of Manuka honey and its components: An overview." <u>AIMS Microbiology</u> **4**(4): 655–664.

Junqi, S., et al. (2001). "Electric Field Directed Layer-by-Layer Assembly of Highly Fluorescent CdTe Nanoparticles." <u>Journal of Nanoscience and Nanotechnology</u> **1**(2).

Kasoju, N., et al. (2018). Techniques for modifying biomaterials to improve hemocompatibility. <u>Hemocompatibility of Biomaterials for Clinical Applications</u>. C. A. Siedlecki, Woodhead Publishing.

Kate Summer, K., et al. (2022). "Out of control: The need for standardised solvent approaches and data reporting in antibiofilm assays incorporating dimethyl-sulfoxide (DMSO)." <u>Biofilm 4</u>.

Kato, Y., et al. (2019). "Dynamics of the Cellular Metabolism of Leptosperin Found in Manuka Honey." J. Agric. Food Chem. **67**: 10853–10862.

Kim, D., et al. (2011). "A Liquid Membrane as a Barrier Membrane for Guided Bone Regeneration." ISRN Dentistry **2011**.

Kokina, M., et al. (2019). "Characterization, antioxidant and antibacterial activity of essential oils and their encapsulation into biodegradable material followed by freeze drying." Food Technol. Biotechnol. **57**(2): 282-289.

Korbut, A., et al. (2021). "Three Component Composite Scaffolds Based on PCL, Hydroxyapatite, and L-Lysine Obtained in TIPS-SL: Bioactive Material for Bone Tissue Engineering." International Journal of Molecular Sciences 22.

Koshy-Chenthittayil, S., et al. (2021). "Agent Based Models of Polymicrobial Biofilms and the Microbiome—A Review." <u>Microorganisms</u> **9**.

Kreft Group (2015). "iDynoMiCS Release 1.3 (June 2015)." Retrieved 02 December 2019, from <a href="http://www.biosciences-labs.bham.ac.uk/kreftlab/idynomics/1/3/iDynomicsv1-3.html">http://www.biosciences-labs.bham.ac.uk/kreftlab/idynomics/1/3/iDynomicsv1-3.html</a>.

Kreft, J.-U., et al. (1998). "BacSim, a simulator for individual-based modelling of bacterial colony growth." <u>Microbiology</u> **144**: 3275-3287.

Kreft, J.-U., et al. (2001). "Individual-based modelling of biofilms." <u>Microbiology</u> **147**: 2897–2912.

Kruk, D., et al. (2022). "Relationship between macroscopic properties of honey and molecular dynamics – temperature effects." <u>Journal of Food Engineering</u> **314**.

Kuncic, M. K., et al. (2012). "Antibacterial and antimycotic activities of Slovenian honeys." <u>British Journal of Biomedical Science</u> **69**(4): 154-158.

Kwakman, P. H. S., et al. (2010). "How honey kills bacteria." <u>The FASEB Journal</u> **24**(7): 2576-2582.

Kwakman, P. H. S. and S. A. J. Zaat (2012). "Antibacterial Components of Honey." <u>Life</u> **64**(1): 48–55.

Lang, G. and G. Buchbauer (2012). "A review on recent research results (2008-2010) on essential oils as antimicrobials and antifungals. A review." Flavour Fragr. J. **27**: 13–39.

Lassak, E. V. and T. McCarthy (1997). Australian Medicinal Plants Victoria, Reed Books.

Le Marc, Y., et al. (2009). "Modelling the effect of the starter culture on the growth of Staphylococcus aureus in milk." <u>International Journal of Food Microbiology</u> **129**.

Lee, A. and H.-L. Wang (2010). "Biofilm Related to Dental Implants." <u>Implant Dentistry</u> **19**(5): 387-393.

Lee, D. S., et al. (2011). "Honey and wound healing: An overview." <u>Am J Clin Dermatol</u> **12**(3): 181-190.

Lee, S.-W. and S.-G. Kim (2014). "Membranes for the Guided Bone Regeneration." Maxillofac Plast Reconstr Surg **36**(6): 239-246.

Levin, B. R. and K. I. Udekwu (2010). "Population Dynamics of Antibiotic Treatment: a Mathematical Model and Hypotheses for Time-Kill and Continuous-Culture Experiments."

Antimicrobial Agents and Chemotherapy 54(8): 3414–3426.

Levin, L. (2008). "Dealing with dental implant failures." J Appl Oral Sci. 16(3): 171-175.

Li, B., et al. (2019). "NUFEB: A massively parallel simulator for individual-based modelling of microbial communities." <u>PLoS Computational Biology</u> **15**(12): e1007125.

Li, H., et al. (2017). "Non-covalent assembly of poly(allylamine hydrochloride)/triethylamine microcapsules with ionic strength-responsiveness and autofluorescence." Journal of Colloid and Interface Science **496**: 228–234.

Li, Z.-H., et al. (2019). "Antibacterial Activity and Mechanisms of Essential Oil from Citrus medica L. Var. Sarcodactylis." Molecules **24**: 1577.

Lind, J. (1753). A treatise of the scurvy. Edinburgh, Sands, Murray, and Cochran.

Liu, T., et al. (2023). "*In vitro* and *in vivo* characterization of [<sup>64</sup>Cu][Cu(elesclomol)] as a novel theranostic agent for hypoxic solid tumors." <u>European Journal of Nuclear Medicine</u> and Molecular Imaging.

Liu, W., et al. (2016). "Interspecific Bacterial Interactions are Reflected in Multispecies Biofilm Spatial Organization." <u>Frontiers</u> **7**.

Loughlin, R., et al. (2008). "Comparison of the cidal activity of tea tree oil and terpinen-4-ol against clincal bacterial skin isolates and human fibroblast cells." <u>Letters in applied</u> <u>microbiology.</u> **46**: 428–433.

Lu, W.-C., et al. (2018). "Preparation, characterization, and antimicrobial activity of nanoemulsions incorporating citral essential oil." <u>Journal of Food and Drug Analysis</u> **26**: 82-89.

Luis, P. (2018). Chapter 1 - Introduction. <u>Fundamental Modelling of Membrane Systems</u>. P. Luis. Oxford, Elsevier: 1-23.

Mailley, D., et al. (2021). "A Review on the Impact of Humidity during Electrospinning: From the Nanofiber Structure Engineering to the Applications." Macromolecular Materials and Engineering.

Maldonado, S. L., et al. (2019). "Application of a multiphase microreactor chemostat for the determination of reaction kinetics of Staphylococcus carnosus." <u>Bioprocess Biosyst</u> Eng **42**(6): 953-961.

Mancuso, E., et al. (2019). "Potential of Manuka Honey as a natural polyelectrolyte to develop biomimetic nanostructured meshes with antimicrobial properties." <u>Frontiers</u>.

Mancuso, M., et al. (2019). "Screening of antimicrobial activity of citrus essential oils against pathogenic bacteria and Candida strains." <u>Flavour Fragr J.</u> **34**: 187–200.

Mandal, M. D. and S. Mandal (2011). "Honey: Its medicinal property and antibacterial activity." <u>Asian Pac J Trop Biomed</u> **1**(2): 154-160.

Manjunath, C. and N. Mahurkar (2021). "In vitro cytotoxicity of cardamom oil, lemon oil, and jasmine oil on human skin, gastric, and brain cancer cell line." <u>Journal of Cancer</u>

<u>Research and Therapeutics</u> **17**(1): 62-68.

Martin, B., et al. (2017). "A new mathematical model of bacterial interactions in two-species oral biofilms." <u>PLOSONE</u> **12**(3).

Martin, K. J., et al. (2013). "Multidimensional modeling of biofilmdevelopment and fluid dynamics in ahydrogen-based, membrane biofilm reactor (MBfR)." <u>Water Research</u> **47**: 4739-4751.

Mason, T. G., et al. (1995). "Elasticity of Compressed Emulsions." <u>Physical Review Letters</u> **75**(10): 2051-2054.

Mattei, M. R., et al. (2018). "Continuum and discrete approach in modeling biofilm development and structure: a review." J. Math. Biol. **76**: 945–1003.

Medicines and Healthcare products Regulatory Agency. "About Us." Retrieved 03 October, 2023, from <a href="https://www.gov.uk/government/organisations/medicines-and-healthcare-products-regulatory-agency/about">https://www.gov.uk/government/organisations/medicines-and-healthcare-products-regulatory-agency/about</a>.

Miguel, M. (2010). "Antioxidant and Anti-Inflammatory Activities of Essential Oils: A Short Review." Molecules **15**: 9252-9287.

Minden-Birkenmaier, B. A. and G. L. Bowlin (2018). "Honey-Based Templates in Wound Healing and Tissue Engineering." <u>Bioengineering</u> **5**(2): 46-62.

Minden-Birkenmaier, B. A., et al. (2015). "Preliminary Investigation and Characterization of Electrospun Polycaprolactone and Manuka Honey Scaffolds for Dermal Repair." <u>Journal of Engineered Fibers and Fabrics</u> **10**(4).

Mizzi, L., et al. (2020). "Assessing the individual microbial inhibitory capacity of different sugars against pathogens commonly found in food systems." <a href="Letters in Applied"><u>Letters in Applied</u></a>
<a href="Microbiology">Microbiology</a> 71: 251-258.

Modrzyński, J., et al. (2019). "Evaluation of dimethyl sulfoxide (DMSO) as a co-solvent for toxicity testing of hydrophobic organic compounds." Ecotoxicology **28**: 1136–1141.

Mombelli, A. and F. Décaillet (2011). "The characteristics of biofilms in peri-implant disease." J Clin Periodontol **38**(11): 203–213.

Monod, J. (1949). "The growth of bacterial cultures." <u>Annual Review of Microbiology</u> **3**: 371-394.

Mount Nittany Health (2017). "Periodontal Disease Guided Tissue Regeneration GTR."

Retrieved 02 December 2019, from

<a href="https://www.mountnittany.org/articles/healthsheets/11166">https://www.mountnittany.org/articles/healthsheets/11166</a>.

Nagoba, B. S., et al. (2015). "Acidic Environment and Wound Healing: A Review." <u>Wounds</u> **27**(1): 5-11.

National Institute for Health and Care Excellence (2022). "NICE health technology evaluations: the manual." Retrieved 17 July, 2023, from <a href="https://www.nice.org.uk/process/pmg36/chapter/evidence">https://www.nice.org.uk/process/pmg36/chapter/evidence</a>.

Nešporová, K., et al. (2020). "Effects of wound dressings containing silver on skin and immune cells." <u>Scientific Reports</u> **10**.

Newcastle University (2021). "Hybrid Layer-by-Layer Deposition System for Thin Film Fabrication." Retrieved 06 September, 2022, from <a href="https://www.ncl.ac.uk/business-and-partnerships/expert-solutions/licensing/deposition-system-for-thin-film-fabrication/">https://www.ncl.ac.uk/business-and-partnerships/expert-solutions/licensing/deposition-system-for-thin-film-fabrication/</a>.

Ngouémazong, E. D., et al. (2015). "The Emulsifying and Emulsion-Stabilizing Properties of Pectin: A Review." Comprehensive Reviews in Food Science and Food Safety **14**: 705-718.

NHS England (2022). "Complementary and alternative medicine." from <a href="https://www.nhs.uk/conditions/complementary-and-alternative-medicine/">https://www.nhs.uk/conditions/complementary-and-alternative-medicine/</a>.

Niu, B., et al. (2013). "Biomimicry of quorum sensing using bacterial lifecycle model." BMC Bioinformatics **14**(Suppl 8): S8.

Nogueira, G. M., et al. (2011). "Spray-Layer-by-Layer Assembly Can More Rapidly ProduceOptical-Quality Multistack Heterostructures." <u>Langmuir</u> **27**.

Nolan, V. C., et al. (2020). "Clinical Significance of Manuka and Medical-Grade Honey for Antibiotic-Resistant Infections: A Systematic Review." <u>Antibiotics</u> **9**(766).

Ofiţeru, I. D., et al. (2014). "Multi-scale modelling of bioreactor - separator system for wastewater treatment with two-dimensional activated sludge floc dynamics." <u>Water</u> Research **50**: 382 - 395.

Oh, T.-J., et al. (2002). "The Causes of Early Implant Bone Loss: Myth or Science?" <u>J</u>

<u>Periodontol</u> **73**(3): 322-333.

Olczak, T., et al. (2005). "Iron and heme utilization in *Porphyromonas gingivalis*." <u>FEMS</u>
<u>Microbiology Reviews</u> **29**: 119–144.

Oxford Health NHS Foundation Trust (2015). Medical Honey Simplified.

P. Andrew Norowski, J. and J. D. Bumgardner (2009). "Biomaterial and antibiotic strategies for peri-implantitis." <u>Journal of Biomedical Materials Research Part B: Applied Biomaterials</u> **88**(2): 530-543.

Pajerski, W., et al. (2019). "Attachment efficiency of gold nanoparticles by Gram-positive and Gram-negative bacterial strains governed by surface charges." <u>J Nanopart Res</u> **21**(186).

Parithimarkalaignan, S. and T. V. Padmanabhan (2013). "Osseointegration: An Update." <u>J</u> <u>Indian Prosthodont Soc</u> **13**(1): 2–6. Persson, G. R. and S. Renvert (2014). "Cluster of Bacteria Associated with Peri-Implantitis." Clinical Implant Dentistry and Related Research **16**(6): 783-793.

Picart, C., et al. (2001). "Buildup Mechanism for Poly(L-lysine)Hyaluronic AcidFilms onto a Solid Surface." Langmuir **17**.

Picioreanu, C., et al. (2000). Modelling and predicting biofilm structure. <u>Community Structure and Co-operation in Biofilms</u>. D. Allison, P. Gilbert, H. Lappin-Scott and M. Wilson. Cambridge, Cambridge University Press.

Precision Periodontics (2022). "Periodontology Anatomy - Alveolar Bone." from <a href="https://www.precisioninperio.com/periodontology-anatomy-alveolar-bone/">https://www.precisioninperio.com/periodontology-anatomy-alveolar-bone/</a>.

Quirynen, M. and D. V. Steenberghe (1993). "Bacterial colonization of the internal part of two-stage implants. An in vivo study." <u>Clinical Oral Implants Research</u> **4**: 158-161.

Rabie, E., et al. (2016). "How methylglyoxal kills bacteria: An ultrastructural study." Ultrastructural Pathology **40**(2): 107–111.

Rajeshnidhi, K. R. and R. Mahesh (2019). "Antibacterial activity of tea tree oil against clinical isolates of Pseudomonas aeruginosa." <u>Drug Invention Today</u> **11**(6): 1422-1424.

Ramalingam, S., et al. (2020). Chapter 1 - Alveolar bone science: Structural characteristics and pathological changes. <u>Dental Implants and Bone Grafts</u>. H. Alghamdi and J. Jansen. Sawston, Woodhead Publishing: 1 - 22.

Richardson, J. J., et al. (2015). "Technology-driven layer-by-layer assembly of nanofilms." Science **348**(6233).

Robertson, E. M., et al. (2023). "Bioactive impact of manuka honey and bone char incorporated into gelatin and chitosan cryogels in a rat calvarial fracture model." <u>Journal of Biomedical Materials Research Part B: Applied Biomaterials</u> **111**(10): 1723-1852.

Rosen, P. S., et al. (2018). "A 1–7 year retrospective follow-up on consecutively placed 7-mm-long dental implants with an electrowetted surface." <u>International Journal of Implant Dentistry</u> **4**(1): 24.

Roshan, N., et al. (2017). "Antibacterial activity and chemical characteristics of several Western Australian honeys compared to manuka honey and pasture honey." <u>Arch</u> Microbiol **199**: 347–355.

Royal College of Surgeons: Faculty of Dental Surgery and Restorative Dentistry-UK (2019). Guidance on the standards of care for NHS-funded dental implant treatment 2019.

Rudge, T. J., et al. (2012). "Computational Modeling of Synthetic Microbial Biofilms." <u>ACS Synth. Biol.</u> 1: 345–352.

Safii, S. H., et al. (2017). "Periodontal Application of Manuka Honey: Antimicrobial and Demineralising Effects In Vitro." <u>International Journal of Dentistry</u>.

Salmela, M., et al. (2018). "Metabolic pairing of aerobic and anaerobic production in a one-pot batch cultivation." <u>Biotechnol Biofuels (2018)</u> 11:187.

Salton, M. R. J. and K.-S. Kim (1996). Chapter 2: Structure. <u>Medical Microbiology</u>. S. Baron. Galveston, University of Texas Medical Branch at Galveston.

Sarhan, W. A. and H. M. E. Azzazy (2015). "High concentration honey chitosan electrospun nanofibers: Biocompatibility and antibacterial effects." <u>Carbohydrate</u> polymers **122**: 135–143.

Sarkar, R., et al. (2018). "Repositing honey incorporated electrospun nanofiber membranes to provide anti-oxidant, anti-bacterial and anti-inflammatory microenvironment for wound regeneration." <u>Journal of Materials Science: Materials in Medicine</u> **29**(3): 31.

Schmidlin, P. R., et al. (2014). "Antibacterial potential of Manuka honey against three oral bacteria in vitro." Swiss Dental Journal **124**(9): 922-924.

Sela, J. J. and I. A. Bab (2012). Healing of Bone Fracture: General Concepts. <u>Principles of Bone Regeneration</u>. J. J. Sela and I. A. Bab. New York, Springer.

Shahi, R. G., et al. (2017). "Novel bioactive tetracycline-containing electrospun polymer fibers

as a potential antibacterial dental implant coating." Odontology 105: 354–363.

Shapiro, S., et al. (1994). "The antimicrobial activity of essential oils and essential oil components towards oral bacteria." <u>Oral Microbiology and Immunology</u> **9**: 202-208.

Sharif, F., et al. (2019). "Bioresorbable Antibacterial PCL-PLA-nHA CompositeMembranes for Oral and Maxillofacial Defects." <u>Polymer Composites</u> **40**(4): 1564-1575.

Shuler, M. L. and F. Kargi (2002). <u>Bioprocess Engineering: Basic Concepts</u>. USA, Prentice Hall PTR.

Silhavy, T. J., et al. (2010). "The Bacterial Cell Envelope." Cold Spring Harb Perspect Biol.

Siu, L. (2003). "Mass of a Bacterium - The Physics Factbook." from <a href="https://hypertextbook.com/facts/2003/LouisSiu.shtml#:~:text=A%20typical%20mass%20">https://hypertextbook.com/facts/2003/LouisSiu.shtml#:~:text=A%20typical%20mass%20</a> of%20a,a%20wide%20range%20of%20environments.

Slutzkey, S., et al. (2015). "Collagen barrier membranes may accelerate bacterial growth in vitro A potential clinical risk to regenerative procedures." <u>Quintessence International</u> **46**(1): 43-50.

Socransky, S. S. and A. D. Haffajee (2002). "Dental biofilms: difficult therapeutic targets." Periodontology 2000 **28**(1).

Song, F., et al. (2015). "Effects of material properties on bacterial adhesion and biofilm formation." <u>Journal of Dental Research</u> **94**(8): 1027 –1034.

Soukoulis, S. and R. Hirsch (2004). "The effects of a tea tree oil-containing gel on plaque and chronic gingivitis." <u>Australian Dental Journal</u> **49**(2): 78-83.

Srikandace, Y., et al. (2018). "Antibacterial activity of bacterial cellulose-based edible film incorporated with Citrus spp essential oil." <u>IOP Conf. Series: Earth and Environmental</u> Science **160**: 012004.

Styles, K. M., et al. (2021). "A Review of Using Mathematical Modeling to Improve Our Understanding of Bacteriophage, Bacteria, and Eukaryotic Interactions." <u>Frontiers in microbiology</u> **12**: 724767.

Subramanian, R., et al. (2007). "Processing of Honey: A Review." <u>International Journal of</u> Food Properties **10**(1): 127-143.

Swimberghe, R. C. D., et al. (2019). "Biofilm model systems for root canal disinfection: a literature review." International Endodontic Journal **52**: 604–628.

Tabanella, G., et al. (2009). "Clinical and Microbiological Determinants of Ailing Dental Implants." Clinical Implant Dentistry and Related Research **11**(1).

Tahi, A. A., et al. (2021). "Ultrasound and heat treatment effects on Staphylococcus aureus cell viability in orange juice." <u>Ultrasonics Sonochemistry</u> **78**.

Tahriri, M., et al. (2019). "Graphene and its derivatives: Opportunities and challenges in dentistry." <u>Materials Science & Engineering C</u> **102**: 171–185.

Tang, Y., et al. (2019). "Honey loaded alginate/PVA nanofibrous membrane as potential bioactivewound dressing." Carbohydrate polymers **219**: 113–120.

The Review on Antimicrobial Resistance (2016). Tackling drug-resistant infection globally: Final report and recommendations. H. M. Gov., O'Neill, J.

Thomsen, N. A., et al. (2013). "Effect of habituation to tea tree (Melaleuca alternifolia) oil on the subsequent susceptibility of Staphylococcus spp. to antimicrobials, triclosan, tea

tree oil, terpinen-4-ol and carvacrol." <u>International Journal of Antimicrobial Agents</u> **41**: 343–351.

Tiwari, S. K. and K. L. Bowers (2001). "Modeling biofilm growth for porous media applications." Mathematical and Computer Modelling **33**: 299-319.

Tsuchida, S. and T. Nakayama (2023). "Recent Clinical Treatment and Basic Research on the Alveolar Bone." <u>Biomedicines</u> **11**.

Valentina Gogulancea, V., et al. (2019). "Individual Based Model Links Thermodynamics, Chemical Speciation and Environmental Conditions to Microbial Growth." <u>Frontiers in microbiology</u> **10**.

Vaquette, C., et al. (2012). "A biphasic scaffold design combined with cell sheet technology for simultaneous regeneration of alveolar bone/periodontal ligament complex." <u>Biomaterials</u> **33**: 5560-5573.

Verotta, D., et al. (2017). "Mathematical Modeling of Biofilm Structures." <u>Computational</u> and <u>Mathematical Methods in Medicine</u>: 11.

Vidal, L., et al. (2020). "Reconstruction of Large Skeletal Defects: Current Clinical Therapeutic Strategies and Future Directions Using 3D Printing." <u>Frontiers in Bioengineering and Biotechnology</u> **8**(61).

Vozar, S., et al. (2009). "Automated spin-assisted layer-by-layer assembly of nanocomposites." Review of Scientific Instruments 80.

Vuuren, S. F. v., et al. (2009). "The antimicrobial activity of four commercial essential oils in combination with conventional antimicrobials." <u>Letters in applied microbiology</u>. **48**: 440–446.

Wang, B., et al. (2022). "Recent advances in biofunctional guided bone regeneration materials for repairing defective alveolar and maxillofacial bone: A review." <u>Japanese</u> <u>Dental Science Review</u> **58**: 233–248.

Wang, J., et al. (2017). "A Novel Approach to Predict the Growth of Staphylococcus aureus on Rice Cake." <u>Frontiers in microbiology</u> **8**.

Wińska, K., et al. (2019). "Essential oils as antimicrobial agents—myth or real alternative?" Molecules **24**: 2130.

Wolfram, S. (1984). "Cellular automata as models of complexity." Nature 311: 419-424.

World Health Organisation (2014). "Antimicrobial Resistance."

Wulansari, A., et al. (2017). "Studies on the formulation, physical stability, and in vitro antibacterial activity of tea tree oil (Melaleuca alternifolia) nanoemulsion gel." International Journal of Applied Pharmaceutics **9**: 135-139.

Yadav, E., et al. (2017). "Tea tree oil: a promising essential oil." <u>Journal of Essential Oil</u>

<u>Research</u> **29**(3): 201-213.

Yang, Z., et al. (2022). "Advances in Barrier Membranes for Guided Bone Regeneration Techniques." <u>Frontiers in Bioengineering and Biotechnology</u> **10**.

Yassin, S. A., et al. (2016). "Inhibition of multispecies biofilms by a fluoride-releasing dental prosthesis copolymer." <u>Journal of Dentistry</u> **48**: 62-70.

Zhang, J., et al. (2010). "Biological properties of an anti-bacterial membrane for guided bone regeneration: an experimental study in rats." <u>Clin Oral Implants Res.</u> **21**(3): 321-327.

Zhang, X., et al. (2021). "Preparation and characterization of gellan gum-chitosan polyelectrolyte complex films with the incorporation of thyme essential oil nanoemulsion." <u>Food Hydrocolloids</u> **114**: 106570.

### **APPENDIX 1**

### 1.1 Conferences

### 1.1.1 Quantitative Approaches to Antimicrobial Resistance and Microbiology 2022

Nanoemulsions incorporating essential oil as biomimetic antimicrobial biomaterials for biomedical applications

T. Honey<sup>a</sup>, C. Gallo<sup>b</sup>, C. Tonda-Turo<sup>b</sup>, I. Carmagnola<sup>b</sup>, D Ofiteru<sup>a</sup>, N Jakubovics<sup>a</sup>, P Gentile<sup>a</sup>

<sup>a</sup>Newcastle University

<sup>b</sup>Politecnico di Torino

In response to increasing global health due to AMR, naturally occurring bioactive agents which exhibit previously anecdotal antibacterial behaviour were critically considered for their use in biomedical applications. In this scenario, essential oils (EOs) are attractive antimicrobials for their potential to disrupt the permeability of the cell membrane, leading to the inhibition of normal cellular functioning and leakage of the contents from the interior of the cell.

In this work, we aimed to manufacture emulsions at the nanoscale to be used as natural biomimetic antimicrobial agents for the surface functionalisation of electrospun membranes for Guided Bone Regeneration. Preliminarily, the effect of diluted Tea Tree EOs (TTEO) oils upon neo fibroblasts cells was observed and compared to their inhibitory concentrations against strains of *S. aureus* NCTC 6571 and *P. gingivalis* W50. TTEO was observed to be cytotoxic at concentrations of 5,000  $\mu$ g/ml (0.5%w/v), and inhibitory concentrations noted above 1% w/v. Whilst direct application of TTEO is unsuitable, an incorporation into a membrane would provide indirect surface dispersion.

To create emulsions at the nanoscale, we used a Tween-80 surfactant to form TTEO-in-water nanoemulsions and attempted to optimize the formula for preparing nanoemulsions. TTEO-inwater nanoemulsions formed at EO concentration of 2 to 8% w/v and homogeniser speed of 8000 to 12000 rpm W for ~10 minutes resulted in a droplet size of < 100 nm for nanoemulsions. The observed relationship between the formulation and activity can lead to the rational design of nanoemulsion-based delivery systems for EOs in biomedical applications.

# Nanoemulsions incorporating essential oil as biomimetic antimicrobial biomaterials for biomedical applications

I. Honey<sup>a</sup>, C. Gallo<sup>b</sup>, C. Tonda-Turo<sup>b</sup>, I. Carmagnola<sup>b</sup>, D Ofiteru<sup>a</sup>, N Jakubovics<sup>a</sup>, P Gentile<sup>a</sup>

<sup>a</sup>Newcastle University, <sup>b</sup>Politecnico di Torino

aimed to manufacture emulsions at the nanoscale to be used as natural biomimetic antimicrobial agents for the surface functionalisation of electrospun mem-To combat antimicrobial resistance (AMR), tea tree essential oil (TTEO) was critically considered for their use in biomedical applications. In this work, we

Whilst TTEO was observed to be cytotoxic at lower concentrations than antibacterial, the observed relationship between the formulation and activity can lead to the rational design of nanoemulsion-based delivery systems for EOs in biomedical applications. branes for Guided Bone Regeneration.

Antimicrobial resistance is projected to result in 10 million deaths by the year 2050 [1]. Recent routes of investigation to combat has been to investigate the previously anecdotal antimicrobial essential oils (EOs), which would undergo more thorough quantitative techniques.

Here we aim to manufacture an antibacterial emulsion at nanoscale to be used in the surface functionalisation of electrospun membranes for used in Guided Bone Regeneration.

# Objective 1:

was observed and compared to their concentrations against P. gingivalis W50. TTEOs were serially The effect of diluted Tea Tree essential oils (TTEOs) upon neo fibroblasts cells strains of S. aureus NCTC 6571 and diluted in water and mixed with 50,000 neo fibroblasts cell cultures. inhibitory



TTEO. (Note: Controls in bottom corners) S. aureus after 24 hours in presence of Figure 2: MIC assays in presence of

1. World Health Organisation, Antimicrobial Resistance. 2014.

Figure 1: Cell viability of neo fibroblast cells after 24 hours in presence of TTEO (µg/ml). 0.5 1.5 Relative Fluorescence Units (RFU) (x105)

Conclusion:

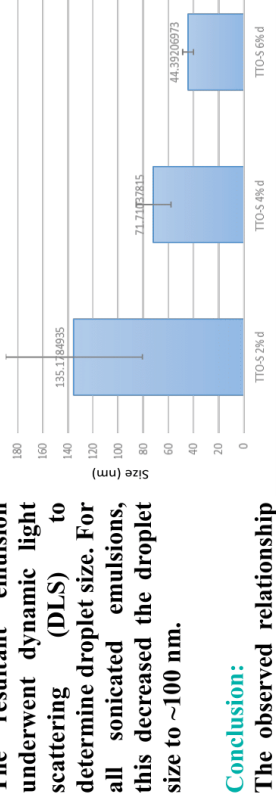
TTEO was observed to be cytotoxic at concentrations of 1,000 µg/ml (0.1%w/v), and inhibitory concentrations noted

above 10,000 µg/ml (1% w/v). Whilst direct application of TTEO is unsuitable, an incorporation into a membrane would provide indirect surface dispersion.

# Objective 2:

To create emulsions at the nanoscale, 66.7% w/w Tween-80 was used as a surfactant to form TTEO-in-water nanoemulsions, with the intention of optimising nanoemulsion protocol.

ITEO-inwater nanoemulsions were formed at EO concentration of 2 to 8% w/v, homogeniser speed of 10,000 rpm W, and sonication for ~10 minutes. 84935 135.17 180 160 (mn) əsi2 to this decreased the droplet underwent dynamic light determine droplet size. For all sonicated emulsions, The resultant emulsion (DLS) size to ~100 nm. scattering



between the formulation Figure 3: Average droplet size of TTEO-in-water and activity can lead to the nanoemulsions after sonication.

rational design of



rational

nanoemulsion-based delivery systems for EOs in biomedical applications.



### 1.1.2 Annual Conference of the European Society for Biomaterials (ESB) 2022

### Assessing the efficacy of surface functionalized Manuka Honey on Electrospun Membranes for biomedical applications

Thomas Honey<sup>1</sup>, Piergiorgio Gentile<sup>1</sup>, Nicholas Jakubovics<sup>2</sup>, Dana Ofiteru<sup>1</sup>

<sup>1</sup>School of Engineering, Newcastle University, Newcastle upon Tyne, United Kingdom

<sup>2</sup>School of Dental Sciences, Newcastle University, Newcastle upon Tyne, United Kingdom

### **INTRODUCTION**

The application of naturally occurring bioactive materials for biomedical applications is an area of recent critical interest. Most notably, due to the previously anecdotal antibacterial properties of some materials undergoing critical research and showing properties which could be readily utilised in biomedical applications1. Honey is such a material that has been used in bygone eras as a salve for its perceived protective and regenerative properties and is currently undergoing critical assessment with indications of positive utilisation within the biomedical community. The use of such biomaterials must first require appropriate characterisation and, to facilitate this transition from bygone treatment to medical device, this work aimed to assess Manuka Honey with methylglyoxal content 550 (MH) as efficient antimicrobial agent to be used as part of a medical device when functionalised upon an electrospun membrane via layer-by-layer assembly.

### **METHODS**

To assess the toxic effects of Manuka Honey 550 upon bacterial and fibroblast cells, MH was diluted in distilled water and stirred on a hotplate at 45°C for 10 minutes, yielding final concentrations of between 5 and 30% wt/v. These were added to well assays with 0.5 OD bacterial broth suspensions of *S. aureus* NCTC 6571 and *P. gingivalis* W50 and incubated for 24 hours at 37°C. The wells were then observed and compared to control wells to visually assess at which concentration bacterial inhibition occurs. To assess cytotoxicity, concentrations were added to 50,000 human neofibroblast cells and incubated for 24 hours. The resultant solution was stained with NucGreen and NucBlue and visually inspected under magnification to qualitatively identify

cytotoxic concentrations. Further quantitative analysis was achieved by adding PrestoBlue to measure fluorescence of viable cells.

To functionalise MH onto membranes, aminolysed electrospun membranes were dipped for 10 minutes into alternating charged solutions of 20% wt/v MH and Poly(allylamine hydrochloride) (PAH) which are negatively and positively charged respectively, with acetic buffer rinse stages of 5 minutes between each layer. Range of mono layers varied between 0 and 14.

The functionalised membranes were assessed using Attenuated total reflectance Fourier transform infrared spectroscopy (ATR-FTIR) over a wavenumber range 4000-500cm-1 absorbance to observe the initial surface composition and how this changes with increasing layer number. Following, membranes underwent glucose release profiles by placing membranes in phosphate buffer saline solutions at 37°C at regular time points over 4 weeks. Both of these would inform the utility of MH impregnated membranes within the biomedical community.

### **RESULTS**

Toxic effects of MH upon *S. aureus* and *P. gingivalis* were observed at concentrations of 20% w/v in both cases. This toxicity also commenced in neofibroblast assays at concentrations of 15% w/v. The implication, therefore, is that care of release should be considered when creating appropriate medical devices.

FTIR analysis of the surface shows sufficient adhesion of MH and polymer layers across full range of manufacture to membrane surface, and the release profile is sufficient for controlled release over 4 weeks.

### **CONCLUSIONS**

Manuka Honey functionalised upon an electrospun membrane has been monitored for controlled release and biocompatibility. Results showed that Manuka Honey at small concentrations exhibits both antimicrobial and cytotoxic properties. From the controlled release of Manuka Honey, however, this narrow range of toxicity can be exploited, leading to the rational design for a medical device suitable for a range of biomedical applications.

### **REFERENCES**

1. Lee, D. S., et al. (2011). "Honey and wound healing: An overview." Am J Clin Dermatol **12**(3): 181-190.

# Assessing the efficacy of surface functionalized Manuka Honey on Electrospun Membranes for biomedical applications

Thomas Honey<sup>1\*</sup>, Piergiorgio Gentile<sup>1</sup>, Nicholas Jakubovics<sup>2</sup>, Dana Ofiteru<sup>1</sup>

<sup>1</sup>School of Engineering, Newcastle University, United Kingdom,

<sup>2</sup>School of Dental Sciences, Newcastle University, United Kingdom; \*t.j.honey2@ncl.ac.uk

### Background

- Biocompatible and degradable membranes that will reduce bacteria present at a wound site have applications across the entire breadth of medical procedures where incisions are required.
- Antimicrobial Resistance (AMR) is already at a critical global health threat[1], and therefore alternatives need to be sought.
- Manuka Honey is a reagent of recent critical research, however to facilitate the
  transition from bygone treatment to medical reagent, this work aimed to assess
  Manuka Honey with methylglyoxal content 550 (MH550) as efficient antimicrobial
  agent to be used as part of a medical device when functionalised upon an
  electrospun membrane via layer-by-layer assembly.

### Methods

To functionalise MH onto membranes, aminolysed electrospun membranes were dipped for into alternating solutions of 20% wt/v MH 550 and Poly(allylamine hydrochloride) (PAH), with acetic buffer rinse stages.

Functionalised membranes assessed using **ATR-FTIR** to observe the initial surface composition and surface variance.

Toxic effects of MH550 upon bacterial and fibroblast cells via dilution from 30-5% wt/v in distilled water were assessed.

### Bacterial toxicity

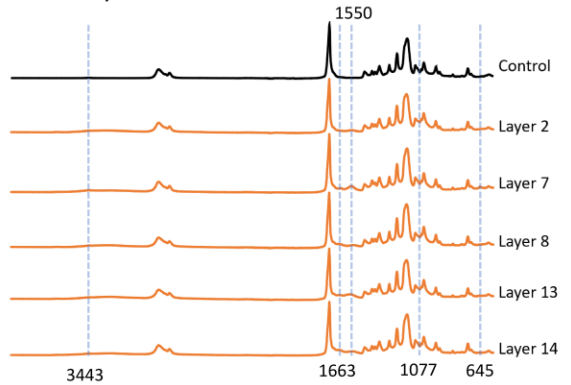
Added to 0.5 OD bacterial broth suspensions of *S. aureus* NCTC 6571 or *P. gingivalis* W50 and incubated at 37C. Inhibitory concentrations were determined visually.

### Cytotoxicity

Added to **human neofibroblast cells** and incubated. Wells were stained and assessed quantitatively and qualitatively.

### Results and Discussions

ATR-FTIR images show peaks at sugars and hydrogen peroxide present in Manuka Honey



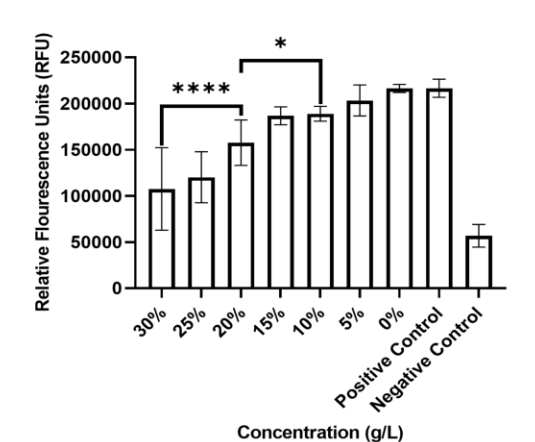
[1] World Health Organisation (2014). "Antimicrobial Resistance."

[2]Mancuso, E., et al. (2019). "Potential of Manuka Honey as a natural polyelectrolyte to develop biomimetic nanostructured meshes with antimicrobial properties." <u>Frontiers</u>.

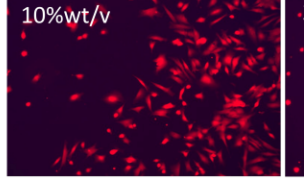
### Bacterial Inhibition response at 10-20% wt/v

Inhibitory Concentration (wt/v)	S. aureus	P. gingivalis
MH550	20%	10%

Cytotoxic response at 20-30% wt/v



# 20%wt/v



### Conclusions

- ATR-FTIR spectra show functionalised MH nanolayers on membrane surface.
- Small concentrations exhibits both antimicrobial and cytotoxic properties. Through
  controlled release of Manuka Honey, this narrow range of toxicity can be exploited
  [2].







### 1.1.3 UK Health Security Agency conference 2022

# Combatting antimicrobial resistance: essential oil nanoemulsions and their biomedical applications

**Camilla Gallo**<sup>a</sup>, **Thomas Honey**<sup>b</sup>, Chiara Tonda-Turo<sup>a</sup>, Irene Carmagnola<sup>a</sup>, Dana Ofiteru<sup>b</sup>, Nick

Jakubovics<sup>b</sup>, Piergiorgio Gentile<sup>b</sup>

<sup>a</sup> Politecnico di Torino

<sup>b</sup> Newcastle University

### 1. INTRODUCTION

Antimicrobial Resistance (AMR) - naturally occurring but strongly accelerated by the overuse and wrong use of antibiotics - is becoming a serious issue for the public health, leading to the ineffectiveness of many treatments and to a huge economic burden. Could this become the next pandemic?

To combat AMR, this study considers the use of natural compounds. Particularly, essential oils (EOs) are attractive antimicrobials for their potential to interfere with membrane enzymes and proteins, leading to an impairment in the metabolism and to a disruption of the bacterial cell wall and cytoplasmic membrane. The consequence is the leakage of contents and cell lysis.

The aim of this work is to manufacture porous biodegradable membranes for wound healing application coated with nanoemulsions of EOs and to assess their antimicrobial properties.

### 2. METHODS

Polymer membranes, based on Poly( $\epsilon$ -caprolactone), were first manufactured via electrospinning techniques, and then aminolysed in hexamethylenediamine, in order to pre-charge positively the surface to allow the further Layer-by-Layer assembly functionalisation. Then, membrane samples (size 1x1cm) were placed inside a dip-spray coating device developed at Newcastle University (WO 2021079106A1), which performed the dipping of biocompatible polyelectrolytes (chitosan as polycation and manuka honey as polyanion) and burst sprays of EO emulsions (tea tree and cinnamon oils) onto the surface of the membrane, depositing nanoscale layers (16 layers in total).

FTIR-ATR spectroscopy was used to analyse the chemical spectrum of the resulting membranes to investigate the formation and growth of the multilayered coating. EOs were taken in isolation and

as part of a membrane via agar diffusion against bacterial strains of *S. aureus* and *P. aeruginosa*. A zone of inhibition measurement was taken and compared to known antibiotics to assess efficacy in comparison to standards.

### 3. RESULTS

FTIR-ATR spectra show the presence of manuka honey and chitosan compared to the PCL control not coated, and good binding of essential oils to surface; with replicate studies showing consistent results. Multiple results highlight the formation of bonds between the polymer and essential oils.

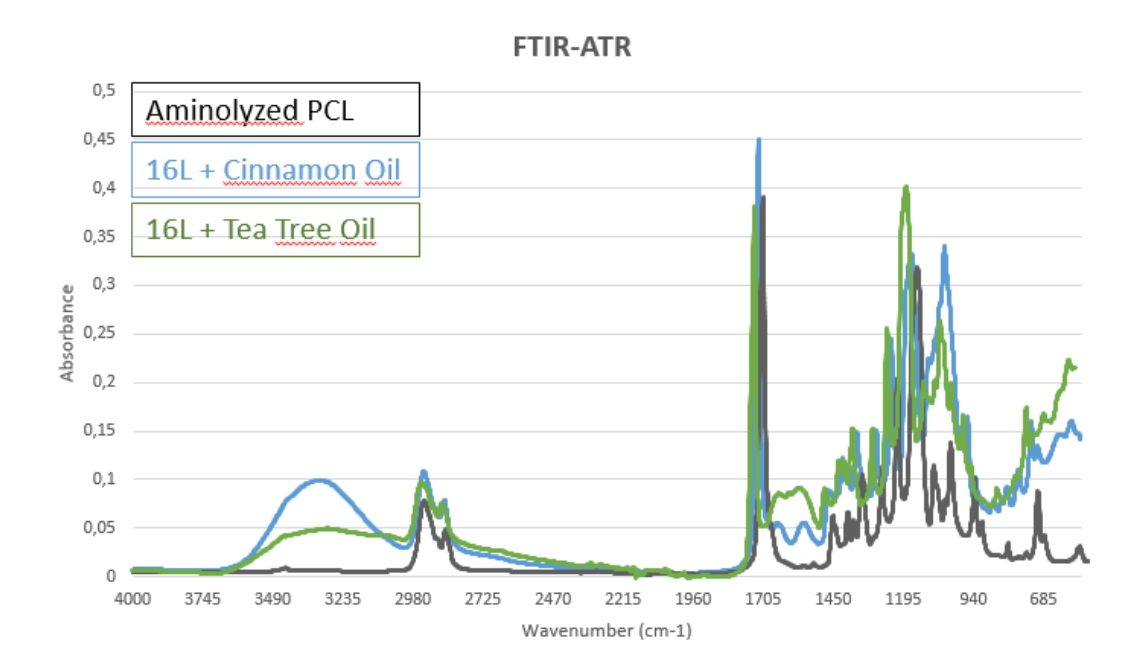


Figure 1: FTIR-ATR spectra of the functionalised membranes. Control of PCL not functionalized.

Inhibition of both Gram-positive (*S. aureus*) and -negative (*P. aeruginosa*) bacteria were shown in both oil isolates and as part of a membrane. Their comparable efficacy can be used to determine rate of diffusion from membrane.

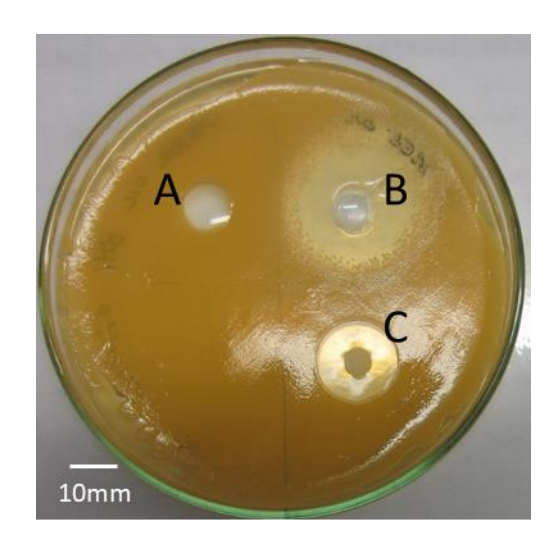


Figure 2: Agar diffusion of Tea Tree Oil (B) on overnight S. aureus culture. Vancomycin (C) used as positive control, Castor Oil (A) used as negative control.

### 4. CONCLUSIONS

This work shows the successful incorporation and effective antimicrobial properties of essential oils against both Gram-positive and -negative bacteria and their potential application in many biomedical fields. Further studies should consider the toxic potential of EOs against mammalian cells.



# Combatting antimicrobial resistance: essential oil nanoemulsions and their biomedical

**applications**Camilla Gallo °, Thomas Honey\*\*, Chiara Tonda-Turo °, Irene Carmagnola °, Irina Ofiteru <sup>b</sup>, Nick Jakubovics <sup>b</sup>, Piergiorgio Gentille <sup>b</sup>



CONTACT INFORMATION

Thomas Honey

\*t.j.honey2@ncl.ac.uk

di Torino, <sup>b</sup> Newcastle University

FTIR-ATR spectra show the presence of manuka honey and chitosan compared to the PCL control not coated, and

RESULTS

Cytotoxicity assays show good cell viability up to 7 days, and are therefore cytocompatible and not toxic. Inhibition of both gram-positive (S. aureus) and -negative (P. aeruginosa) bacteria were shown for each

compound (MH, CH, EOs) via agar test diffusion.

good binding of essential oils to surface.

# INTRODUCTION

# Antimicrobial Resistance (AMR) is strongly accelerated by the overuse AMR leads to the ineffectiveness of many treatments and to a huge and incorrect use of antibiotics.

Chitosan (CH), and essential oils (EOs) with suspected antibacterial To combat AMR, natural compounds like Manuka Honey (MH), economic burden. Could this become the next pandemic? properties have been critically considered.



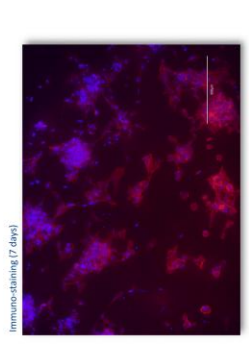
## AIM

membranes for wound healing application coated with MH, CH and nanoemulsions of EOs and to assess their antimicrobial properties. The aim of this work is to manufacture porous biodegradable



This work shows the successful incorporation and effective

SUMMARY / CONCLUSION



# antimicrobial properties of essential oils against both gram-positive Further studies should consider the diffusion rate of the layers from and -negative bacteria and their potential application in many biomedical fields. the membrane.

# **ACKNOWLEDGEMENTS**

Many thanks to EPSRC, Newcastle University, and Politecnico di Torino for their continued support to facilitate this project.

# REFERENCES

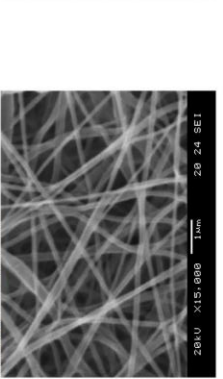
nioon, K. R., et al. (2019). "Investigating Manuka Honey Antibacterial Properties When Incorporated Into Cryogol, Hydrogel, and Electrospun Tissue Engineering Scaffolds." <u>Gels.</u> 5(2): 21-36. Carson, C. F., et al. (2006). "Melaleuca alternifolia (Tea Tree) Oil: a Review of Antim Medicinal Properties." <u>Clinical Microbiology Reviews</u> 19(1): 50–62. Vidal, L., et al. (2020).

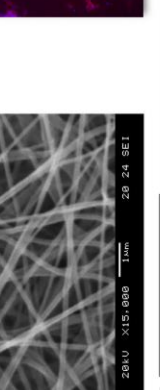
# **MATERIAL & METHODS**

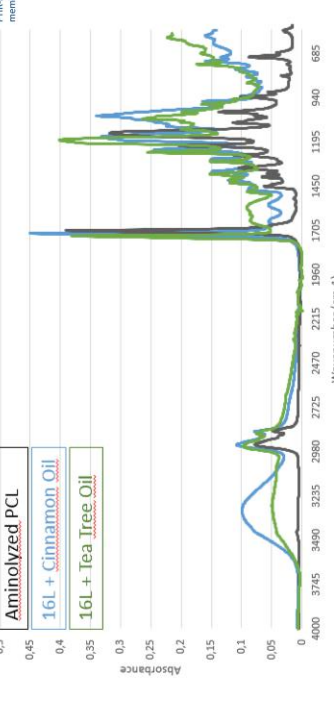
poly(e-caprolactone) membranes with nano-layers of Manuka Honey A layer-by-layer (LbL) technique was used to dip-coat electrospun cinnamon oil nanoemulsions. This utilized our in-house dip-spray 550+ and Chitosan, with final spray coatings of tea-tree, and coating device (WO 2021079106A1). resulting membranes to investigate the formation and growth of the multilayered coating.

FTIR-ATR spectroscopy analysed the chemical spectrum of the

Further, agar-diffusion tests were performed to assess the inhibition zone of the compounds against bacterial strains of S. aureus NCTC6571 and P. aeruginosa PAO1.







### 1.2 Additional Results Plots

### 1.3 TTO P. gingivalis

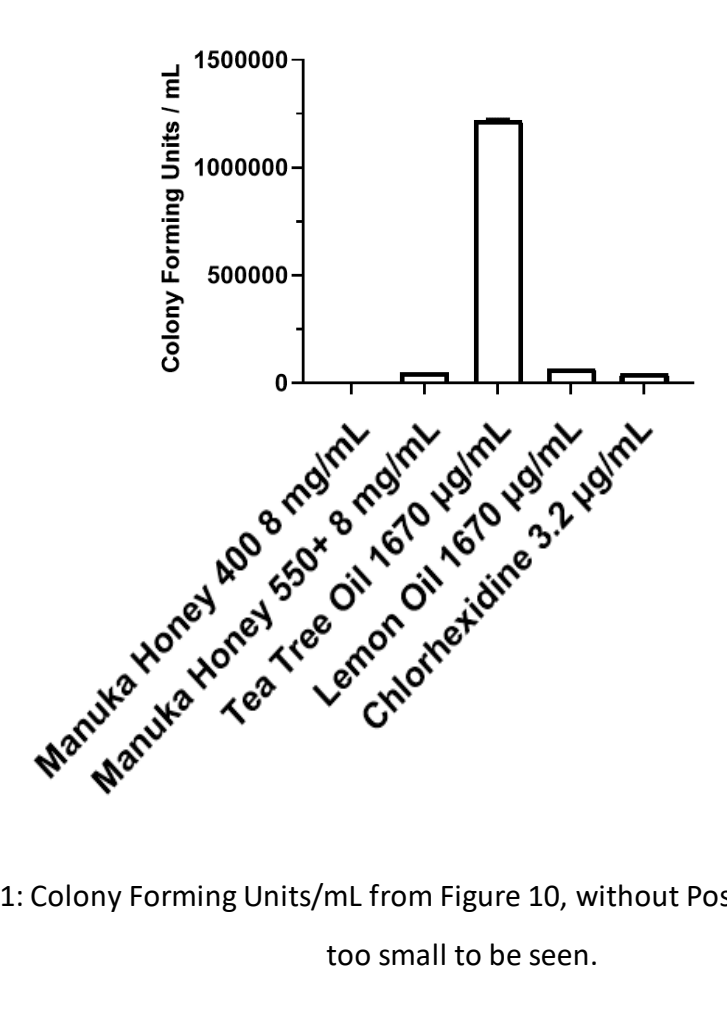


Figure 1.1: Colony Forming Units/mL from Figure 10, without Positive Control. Error bars

### 1.4 Cell Density

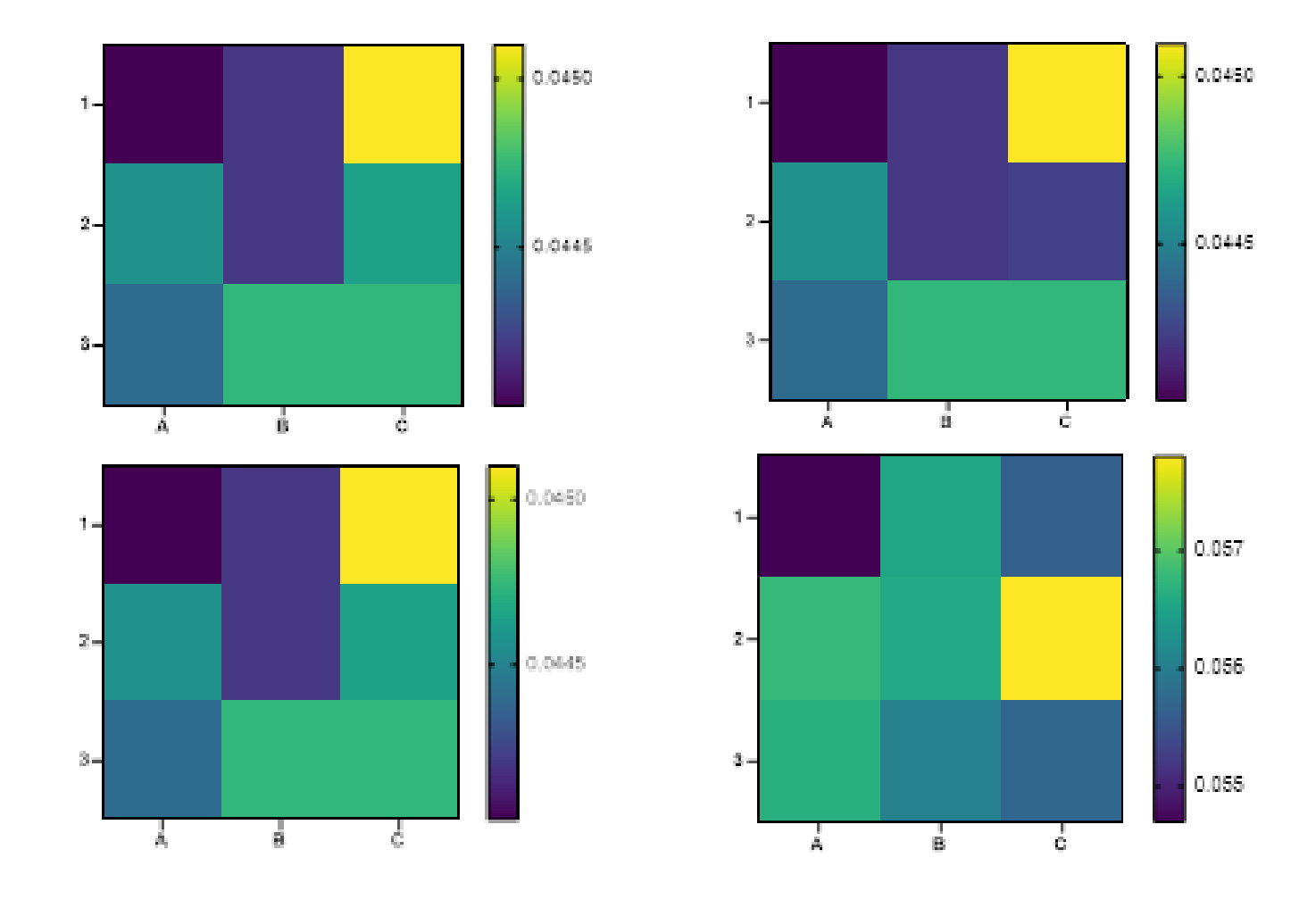


Figure 1.2: Cell density (agents/unit micrometre) calculated for A) t=0h, B) 6h, C) 24h, D) 48h. Each cell denotes where inhibiting membrane is placed.

### 1.6 Growth Curve for S. aureus

Whilst the measurements of parameters for Ks were readily available and utilised in other growth kinetics for *P. gingivalis* (Martin, Tamanai-Shacoori et al. 2017), *S. aureus* was more difficult to derive from literature directly. A comparable strain of Staphylococcus; *S. carnosus*, derived a half-saturation coefficient of  $34\cdot10^{-3}$  g/L (Maldonado, J Krull et al. 2019). To derive half-saturation coefficients for the purposes of simulation requires the use of minimal media (with a single carbon source for bacterial growth). A preliminary attempt to derive own values showed a value of Ks =  $62\cdot10^{-2}$  g/L, which is not indirectly comparable to other literature. As both cases are greater than that of *P. gingivalis*, the difference between qualitatively output is negligible.

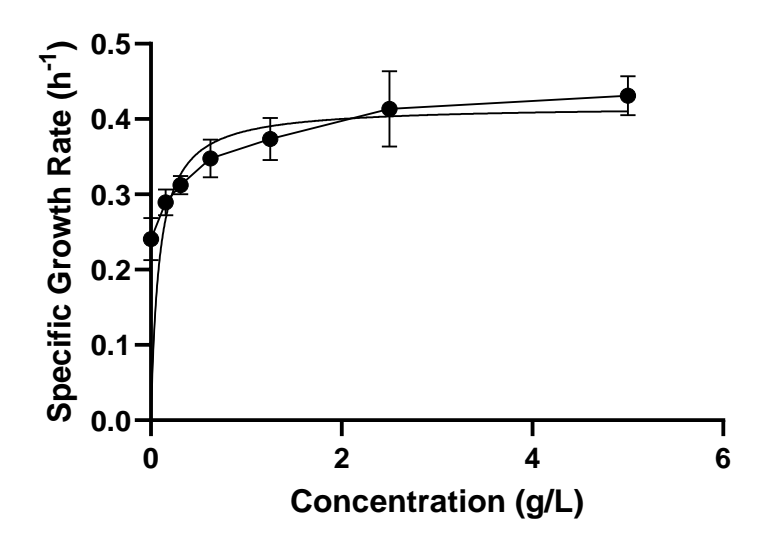


Figure 1.3: Specific Growth Rate measured at dilutions of complex media for S. aureus.